

13

# A potential vorticity component-based study of the extratropical transitions of hurricanes Danielle and Earl (1998)

A thesis submitted to

the Graduate and Postdoctoral Studies Office

of

McGill University

by

R. McTaggart-Cowan

In partial fulfillment of the requirements for the degree

of

Doctor of Philosophy

Department of Atmospheric and Oceanic Sciences

McGill University

Montréal, Québec

CANADA

©Ron McTaggart-Cowan, 2003

August 2003

August 25, 2003

15e

2022124

# Abstract

This thesis documents a study of the simultaneous North Atlantic extratropical transition (ET) and reintensification (ET/R) of ex-hurricanes Danielle and Earl (1998), with the goal of identifying the midlatitude and remnant tropical cyclone (TC) features germane to the ET/R process. Using potential vorticity (PV) based diagnostics and an extension of piecewise PV inversion techniques that accounts for atmospheric water, the initial conditions of the Mesoscale Compressible Community model are altered by the individual removal of possible forcing features. Results from ensuing sensitivity tests are compared to the control simulation and changes in the structure and/or the intensity of ET/R are diagnosed.

It is found that the existence of a trough upstream of the remnant TC is a necessary forcing for redevelopment and that larger north-south trough amplitudes result in stronger vortex reintensification. Transitions occurring in the equatorward entrance region of a baroclinic jet are likely to undergo baroclinic mode redevelopment, whereas those taking place in the poleward exit region of the jet usually take on tropical mode characteristics. Baroclinic mode storms are insensitive to the structure of the TC remnant; tropical mode redevelopments, however, rely heavily on both the circulation and the moisture associated with the ex-tropical feature.

Considered pragmatically, the results of this study amount to a list of the key ingredients necessary for the ET/R of the storms studied, which will be of use in the forecasting of similar events. A broader application of the findings in the context of current ET research yields insight into both the dynamics and thermodynamics of these extreme events.

# Resumé

Cette thèse démontre une étude de la transition extra-tropicale (TE) et ré-intensification (TE/R) simultanée Nord-Atlantique des ouragans Danielle et Earl (1998), ayant comme but d'identifier les structures des latitudes moyennes et des traces des cyclones tropicaux (CT) qui représentent les forçages essentiels pour le processus TE/R. Par l'utilisation d'un diagnostic basé sur la tourbillon potentiel (TP) et une extension des techniques fragmentées d'inversion de TP qui considèrent l'eau atmosphérique, les conditions initiales du modèle mésoéchelle compressible communautaire sont adaptées par l'enlèvement individuel d'entités de forçage. Les résultats des essais de sensibilité sont comparés aux simulations de contrôle et les changements dans la structure et/ou l'intensité du TE/R sont diagnostiqués.

Il est démontré que la présence d'un creux en amont des traces d'un CT est un forçage nécessaire pour le re-développement, et que les plus grandes amplitudes nord-sud des creux produisent de plus forte ré-intensifications des vortexes. Les transitions se retrouvant à l'entrée d'un jet barocline en remorque de l'équateur ont tendances au re-développement barocline, et celles se retrouvant à l'issue d'un jet en remorque du pôle démontrent généralement les caractéristiques d'un mode tropical. Les orages baroclines sont insensibles à la structure des traces de CT; par contre, les re-développements de mode tropical comptent de façon importante sur la circulation et l'humidité associées à l'entité ex-tropicale.

Par une considération pragmatique, les résultats de l'étude fait produire une liste d'ingrédients clés pour le processus TE/R des orages sous étude qui serviront pour la prévision d'événements similaires. Une application plus large des résultats dans

le contexte des recherches courantes au sujet de TE permettra des rendements au compréhension des dynamiques et thermodynamiques de ces événements extrêmes.

# Contributions of Authors

Chapters 2, 3, and 4 of this thesis consist of articles published in peer-reviewed journals. Chapter 5 comprises a manuscript that has been submitted for publication. As the lead author for each of these four articles, the candidate was responsible for the bulk of the research presented therein. Professors J.R. Gyakum and M.K. Yau served in their standard supervisory capacities in terms of project organization and support, and assisted in the editing of the manuscripts.

# Statement of Originality

The contributions to original knowledge of this dissertation are as follows:

- The simultaneous ET/R event of two Atlantic hurricanes (Danielle and Earl) is simulated using a state-of-the-art mesoscale model. The control simulation is verified against manually-analysed surface data, analysis data from two operational forecasting centres, and satellite imagery.
- The role of individual trough PV features upstream of ex-hurricane Earl's remnant circulation in the ET/R process is quantitatively diagnosed using piecewise PV inversion and sensitivity testing simulations.
- Potential vorticity based dynamic tropopause diagnostics are used to investigate structural differences observed between the redevelopment processes of Danielle and Earl in the control simulation. This leads to the hypothesis that there are multiple ET/R modes at work in the North Atlantic.
- Idealized initial states downstream of the remnant TC are constructed in order to test the structural sensitivity of ET/R to identifiable downstream features. The North Atlantic jet/front structure is found to modulate the tropical/baroclinic bimodality of ET/R and a conceptual model is developed to explain this sensitivity.
- An extension of piecewise PV decomposition ( $PV_{mc}$ ) is developed. The  $PV_{mc}$  field is shown to possess diagnostic qualities that highlight thermodynamically important structures in the remnant TC circulations. Further, the invertibility

of  $PV_{mc}$  is shown to be crucial to sensitivity tests involving modifications to the atmospheric moisture field.

- The importance of remnant TC structures to the reintensification phase of ET/R is diagnosed quantitatively using both dry PV and  $PV_{mc}$  inversions. The transition mode is found to be a key factor in identifying possible sensitivity to the remnant's circulation and moisture content.

# Acknowledgments

There are numerous people to whom I am indebted for their contributions both to this thesis and to the years of my life that were spent ostensibly on its completion.

Professor J.R. Gyakum provided much of the guidance and scientific support that I required during this research. Moreover, the trust that he has shown me through his willingness to provide me with a great degree of academic freedom is truly appreciated. My countless discussions with Dr. Gyakum on a wide range of topics have always encouraged me to persevere, learn, and succeed in all aspects of my life. Professor M.K. Yau has provided me with wisdom and insights into the world of research, and has always been willing and able to provide any assistance that I request. For both of their initiative and support during this project, I offer them my sincerest thanks.

I would also like to express my gratitude to others who have helped me since my arrival at McGill. Jason Milbrandt and Dr. Stephen Déry both contributed immensely to my learning experience at McGill, and their friendship has supported me throughout my time in Montreal. The patience of Dr. Badrinath Nagarajan during the initial phases of my learning process in the department is also greatly appreciated. My many scientific discussions with Dr. Yongshen Chen and Dr. Marco Carrera have further served to broaden my appreciation for the field.

Other facets of my time at McGill have also served to further my development as a scientist and as a person. My involvement with the Post-Graduate Student's Society has taught me a great deal about both the University and myself. In particular, I appreciate the friendship and guidance of Dr. Aaron Windsor, Ms. Joanne O'Malley,

Ms. Krystyna Zaluski, Mr. David Wise, Mr. Jerome Holmes, Mr. André Pierzchala, and the many others with whom I have worked during my time as President of the Society. My time with McGill Crew has also been a highlight of my stay at McGill, and I would like to thank Mr. Mark Wismer, Mr. Jacek Mysior, and Mr. Mike Modolo for their constant friendship and encouragement.

Last, but by no means least, I would like to thank those closest to both the highs and lows that I have experienced during my time at McGill. My parents have been an unending source of support and guidance for me. My father's efforts to prepare me for the world of research have served me well during this project, as have our numerous discussions and debates on my work and this field in general. My mother's unwavering support and confidence in my abilities has always helped me to persevere with my work, learning and life. My girlfriend, Sylvia Styhler, has shown me an amazing amount of love and given me incredible support throughout my presidency with the PGSS and during the final phase of this research. Her understanding, kindness, and generosity have been instrumental in my completion of this project.

Funding for this work has been provided by the Natural Sciences and Engineering Research Council, subventions from Environment Canada, the Cooperative Program for Operational Meteorology, Education and Training Program, the CMOS - Weather Research House Scholarship Supplement, and the Canadian Foundation for Climate and Atmospheric Sciences.

# Contents

Abstract	i
Resumé	ii
Contributions of Authors	iv
Statement of Originality	v
Acknowledgments	vii
Contents	ix
List of Figures	xiii
List of Tables	xxiv
<b>1 Introduction</b>	<b>1</b>
1.1 Introduction and Motivation . . . . .	1
1.2 Overview of ET Research . . . . .	4
1.3 Scientific Objectives and Manuscript Outline . . . . .	12
<b>2 The Influence of Upstream Features on ET</b>	<b>17</b>
2.1 Introduction . . . . .	19
2.2 Methods . . . . .	22
2.2.1 Model Description . . . . .	22
2.2.2 Initialization . . . . .	23

2.3	Control Simulation . . . . .	23
2.3.1	Description of Initial Fields . . . . .	23
2.3.2	Analysis of Control Simulation . . . . .	24
2.3.3	Validation . . . . .	26
2.4	PV Inversions . . . . .	26
2.5	Sensitivity Tests . . . . .	29
2.5.1	Northern Trough Removal . . . . .	29
2.5.2	Southern Trough Removal . . . . .	31
2.5.3	Upper Trough Removal . . . . .	32
2.5.4	Full Trough Removal . . . . .	33
2.5.5	Hurricane Earl Removal . . . . .	35
2.6	Summary and Discussion . . . . .	37
2.7	Appendix: Model Settings and Parameters . . . . .	41
<b>3</b>	<b>The Influence of Downstream Features on ET</b>	<b>62</b>
3.1	Introduction . . . . .	65
3.2	Model description . . . . .	68
3.3	Control simulation . . . . .	69
3.3.1	Synoptic analysis . . . . .	69
3.3.2	Potential Vorticity Analysis . . . . .	70
3.4	Sensitivity tests . . . . .	74
3.4.1	Description of the IDEALLAT test . . . . .	75
3.4.2	Description of the EXT test . . . . .	75
3.4.3	Description of the SIMJET test . . . . .	76
3.4.4	Analysis of the IDEALLAT simulation . . . . .	76
3.4.5	Analysis of the EXT simulation . . . . .	78
3.4.6	Analysis of the SIMJET simulation . . . . .	79
3.4.7	Description of modes . . . . .	79
3.5	Summary and discussion . . . . .	82

<b>4</b>	<b>Moist Component Potential Vorticity</b>	<b>105</b>
4.1	Introduction . . . . .	107
4.2	Moist component PV . . . . .	109
4.3	PV <sub>mc</sub> in an idealized model atmosphere . . . . .	112
4.3.1	Background state and moisture structure . . . . .	113
4.3.2	Introduction to PV <sub>mc</sub> in the model atmosphere . . . . .	114
4.3.3	Moist component height perturbations . . . . .	116
4.3.4	Moisture integral . . . . .	117
4.3.5	Moist component geopotential and streamfunction . . . . .	117
4.3.6	Moist component relative vorticity . . . . .	118
4.3.7	Moist component static stability . . . . .	119
4.3.8	Moist component PV . . . . .	119
4.4	Interpretation of PV <sub>mc</sub> . . . . .	121
4.5	Inversion of PV <sub>mc</sub> . . . . .	123
4.6	Summary and Discussion . . . . .	124
<b>5</b>	<b>The Influence of the Tropical Cyclone on ET</b>	<b>134</b>
5.1	Introduction . . . . .	137
5.2	Case Study and Model Description . . . . .	139
5.2.1	Case Description . . . . .	140
5.2.2	Data Sources . . . . .	142
5.2.3	Model Description . . . . .	142
5.2.4	Control Simulation . . . . .	143
5.3	Moist Component PV . . . . .	146
5.4	Sensitivity Tests . . . . .	149
5.4.1	Ex-hurricane Earl . . . . .	150
5.4.2	Ex-hurricane Danielle . . . . .	154
5.5	Summary and Discussion . . . . .	159

<b>6</b>	<b>Summary, Discussion, and Future Research</b>	<b>183</b>
6.1	Utility of PV and $PV_{mc}$	183
6.2	Case Summary	184
6.3	Upstream Features - Ex-hurricane Earl	185
6.4	Downstream Features	186
6.5	Vortex Structure	187
6.6	General Conclusions	187
6.7	Future Research Directions	188

# List of Figures

2.1	National Hurricane Center (NHC) best track for Hurricane Earl. Plotting starts 1200 UTC 31 August in the Gulf of Mexico and ends 1200 UTC 8 September in the North Atlantic. Closed and open circles indicate 0000 UTC and 1200 UTC positions respectively. . . . .	43
2.2	Comparison of storm tracks (a) and central pressures (b) with operational analyses. The pressure trace for the operational forecast is also shown in (b). Storm center locations are plotted every six hours in (a), beginning at 0000 UTC 5 September as indicated. Manual analyses were performed at the Maritimes Weather Centre in Dartmouth, Nova Scotia. . . . .	44
2.3	Time series of minimum SLP in hPa (a), 500 hPa center height in dam (b), mean winds within a 200 km radius of the storm center as defined by the central pressure minimum (c), and maximum winds in $\text{m s}^{-1}$ (d). NONTR - northern trough removal (Section 2.5.1). NOSTR - southern trough removal (Section 2.5.2). NOUSTR - upper trough removal (Section 2.5.3). NOTR - full trough removal (Section 2.5.4). NOEARL - Hurricane Earl removal (Section 2.5.5). . . . .	45

2.4	Plot of six hourly precipitation accumulations for the control (a), NOTR trough removal (b), and NOEARL Hurricane Earl removal (c) simulations. The mean accumulation is calculated within a 400 km radius of the storm - as defined by the minimum in sea level pressure - and is broken into convective, stratiform, and total (the sum of the first two) precipitation. . . . .	46
2.5	Forecast for 00 hour valid 00/05. Panel (a) shows 500 hPa height (solid) in dam, and absolute vorticity field (dashed and shaded) in $10^{-5}\text{s}^{-1}$ . Panel (b) shows surface pressure (solid) and 1000-500 hPa thickness (dashed) in dam. The 534-540 dam height interval is shaded. Panel (c) shows 700 hPa height field (solid) in dam and pressure-weighted mean relative humidity from the 850, 700, and 500 hPa levels. Unless otherwise noted, all maps are plotted using a polar stereographic projection extending from 20°N to 70°N and 30°W to 100°W with meridians and parallels plotted at 10° intervals. . . . .	47
2.6	Cross-section of equivalent potential temperature (heavy lines) at 4 K intervals, and divergence (light dotted for convergence, light solid for divergence) at $5 \times 10^{-5}\text{s}^{-1}$ intervals east-west through the storm center at 12/05 as shown in the SLP plot inset (1000, 998 and 996 hPa contours only). . . . .	48
2.7	Windspeed at 250 hPa in $\text{ms}^{-1}$ for 00/06. Location of the surface cyclone is indicated. . . . .	49
2.8	Cross-section of PV (heavy lines) valid at 12/06 in 1 PVU increments ( $1 \text{ PVU} = 10^{-6}\text{m}^2\text{K kg}^{-1}\text{s}^{-1}$ ) and specific humidity (light lines) in $1 \text{ g kg}^{-1}$ increments, east-west through the storm center as shown in the inset (968, 964, and 960 hPa contours only). . . . .	50
2.9	Forecast for 36 hours, valid 12/06. All fields as in Fig. 2.5, except for the added panel (d), which shows precipitation (solid lines and shading) in units of $\text{mm (6 h)}^{-1}$ . . . . .	51

2.10	Forecasts of 36 hour potential temperature (left column) and wind-speed (right column) at 400 (top), 700 (middle), and 850 hPa (bottom) valid 12/06. Dry bulb potential temperatures (left) are contoured at 1 K intervals with darker shading indicating higher temperatures. Windspeeds are displayed using isotachs plotted at 1 m s <sup>-1</sup> intervals, with darker shading for faster windspeeds. Following Browning et al. (1998), the LLJ encircling the warm core at 850 hPa is shown by the dotted curve, and the subpolar jet is represented using a longer dashed line at the 400 and 700 hPa levels. . . . .	52
2.11	Evolution of PV on the 325 K isentropic surface (solid lines, 1 PVU contour interval with shading for high values) and 1000-900 hPa averaged potential temperature (dashed lines, 4 K interval above 294 K). Panels (a) through (e) show the 12 hourly (from 0 through 48 hours) PV and potential temperature fields produced by the control simulation.	53
2.12	Panel (a) shows the manual analysis valid 12/06 as provided by the Maritimes Weather Centre in Dartmouth, Nova Scotia. The equivalent 36 hour control forecast is shown in panel (b). All surface pressures are shown in hPa and are contoured at 4 hPa intervals. . . . .	54
2.13	PV anomaly fields in PVU at 200 hPa (a), 400 hPa (b), and 850 hPa (c) for initial conditions of control run (00/05). The Upper trough PV anomaly is labeled A, the southern and northern trough PV anomalies are labeled B and C respectively, and Earl's <i>PV'</i> is labeled D. . . . .	55
2.14	Initial conditions following PV inversion for control and test cases as indicated. The left panel for each initialization shows the surface pressure field in hPa, and the right panel shows 500 hPa heights in dam. The areas in which PV anomaly was removed in each case are outlined at the 500 hPa level for the trough removals, and at the surface for the NOEARL run. See Table 2.1 for the precise removal parameters in each case. . . . .	56

2.15	Tracks of surface pressure minima for control simulation and sensitivity tests as indicated. Acronyms are defined in caption for Fig. 2.3. The track for the NOEARL case (indicated by the crosses and the dashed line) follows the Quebec cyclone since the hurricane has been removed from these initial conditions. . . . .	57
2.16	Geopotential height (solid lines, 6 dam intervals) and absolute vorticity (shading, units are $10^{-4} \text{ s}^{-1}$ ) at 500 hPa for (a) control, (b) NONTR, (c) NOSTR, (d) NOUSTR, (e) NOTR, and (f) NOEARL. The control plot shows the 36 hour output (valid 12/06), whereas the other panels display 45 hour (valid 21/06) prognoses, reflecting approximately the most intense period of the storm in each case. . . . .	58
2.17	Same as in Fig. 2.16 except that the fields shown are sea level pressure (solid lines, 4 hPa contour interval) and 1000-500 hPa thickness (dashed lines, 6 dam contour interval). . . . .	59
2.18	Same as in Fig. 2.11, except following the NOTR (full trough removal) initialization. . . . .	60
2.19	Same as in Fig. 2.11, except following the NOEARL (Hurricane Earl removal) initialization. . . . .	61

3.1	National Hurricane Center best track for Hurricane Danielle (a) and for Hurricane Earl (c). Minimum sea level pressure time series for the period from 0000 UTC 5 September to 0000 UTC 7 September are shown for (b) Danielle and (d) Earl for the CMC analysis, the NHC analysis (Danielle only), a manual analysis (Earl only), and the control simulation produced for this study. Plotting for Danielle’s track starts 1200 UTC 24 August in the central Atlantic and ends 0000 UTC 8 September in the North Atlantic. For Earl, tracking starts 1200 UTC 31 August in the Gulf of Mexico and ends 1200 UTC 8 September in the North Atlantic. Closed and open circles indicate 0000 UTC and 1200 UTC positions respectively in panels (a) and (c). . . . .	86
3.2	Sea level pressure (heavy solid lines, 4 hPa increments) and 1000-500 hPa thickness (dashed lines, 6 dam intervals). Fields are plotted every 12 hours for the control simulation, valid from 00/05 (a) to 00/07 (e). . . . .	87
3.3	As for Fig. 3.2, but plotting 500 hPa heights (solid lines, 6 dam intervals) and 500 hPa vorticity (shading, $10^{-5} \text{ s}^{-1}$ ). . . . .	88
3.4	Lower-level thermal advection after 36 hours of simulation in the control. Contours of advection of the 850-500 hPa mean temperature by the 700 hPa wind are plotted every $2 \times 10^{-4} \text{ K s}^{-1}$ . Locations of the low pressure centers at the surface are shown in shading. . . . .	89
3.5	Dynamic tropopause (defined as the 1.5 PVU surface) potential temperature (solid lines and shading) and winds, and 1000 hPa temperature (5 K intervals, dashed lines) from the control simulation. Plots are shown at 12 hourly forecast intervals from the initial time 00/05 (a), to the final time, 00/07 (e). . . . .	90
3.6	As for Fig. 3.5, except that plots show potential temperature at 925 hPa (solid lines at 4 K intervals) and 925-700 hPa mean PV (shading at 1 PVU increments). . . . .	91

3.7	Coupling index for 24, 36, and 48 hours of simulation for panels (a), (b), and (c). Dark shading represents CI less than 5 K, and light shading between 5 and 15 K. . . . .	92
3.8	Heavy unresolved (“convective”) 6-hourly precipitation accumulations for Earl and Danielle in the control simulation as a function of forecast hour (a). All gridpoints within approximately 875 km (25 gridpoints) of the storm centers with 6-hourly unresolved accumulations exceeding 12 mm are used to represent heavy precipitation regions. The spatial distribution of 6-hourly unresolved precipitation accumulation for forecast hours 36-42 are shown in (b) with intervals of 2,5,10,15,20, and 25 mm. Sea level pressure at 42 hours is also shown in (b) for reference, with a 4 hPa contour interval. . . . .	93
3.9	Infrared satellite imagery for (a) Earl, and (b) Danielle at 00/06. . . .	94
3.10	As for Fig. 3.5, but for the IDEALLAT member. Panels (a), (b), (c), and (d), show the 00, 24, 36, and 48 hour simulated systems, respectively.	95
3.11	As for Fig. 3.6, but for the IDEALLAT member. Panels (a), (b), (c), and (d), show the 00, 24, 36, and 48 hour simulated systems, respectively.	96
3.12	Coupling index values after 48 hours of simulation from the (a) IDEALLAT, (b) EXT, and (c) SIMJET tests. Contours are plotted at 4 K intervals with negative values dashed. . . . .	97
3.13	As for Fig. 3.10, but for the EXT member. . . . .	98
3.14	As for Fig. 3.11, but for the EXT member. . . . .	99
3.15	As for Fig. 3.10, but for the SIMJET member. . . . .	100
3.16	As for Fig. 3.11, but for the SIMJET member. . . . .	101
3.17	Lower-level thermal advection after 36 hours of simulation for (a) IDEALLAT, (b) EXT, and (c) SIMJET. Contours of advection of the 850-500 hPa mean temperature by the 700 hPa wind are plotted every $2 \times 10^{-4} \text{K s}^{-1}$ as for Fig. 3.4. . . . .	102

3.18	Cross-sections of equivalent potential temperature (dashed lines at 5 K intervals with the 325 K isopleth heavy solid) and PV (light solid lines plotted at 1 PVU intervals). Bold arrows connect similar modes of transition from the control (left column) and the sensitivity tests (right column). Sections are taken after 48 hours of simulation approximately east/west through the center of (a) Danielle in the control (tropical mode), (b) IDEALLAT (tropical mode), (c) Earl in the control (baroclinic mode), (d) EXT (baroclinic mode), and (e) SIMJET (baroclinic mode). . . . .	103
3.19	Schematic representation of a linear jet maximum. Light solid lines indicate upper-level height contours with the gradient oriented as indicated. Dashed lines represent lower-level isotherms, again with the gradient as shown. The horizontal secondary circulation at low levels generated by the jet is indicated by the heavy arrows. Two surface lows are superposed on the feature with cyclonic circulations as shown. Regions of enhanced cold and warm advection are shaded on the left and right sides of the figure, respectively. . . . .	104
4.1	Schematic representation of hydrostatic adjustment resulting from a point heat source elevated above the surface. . . . .	126
4.2	Cross-section of the water vapor mixing ratio (panel a) with 2 g kg <sup>-1</sup> contour intervals. Panel b shows profiles of the mixing ratio taken at the center (rightmost curve), $H_x$ (middle curve), and $2H_x$ (leftmost curve). . . . .	127
4.3	Relative errors of approximations for $z_{mc}$ from (4.25), light curves, and $W$ from (4.27), heavy curves. Profiles are taken at the origin (solid lines) and at $H_x$ (dashed lines) as indicated. . . . .	128

4.4	Cross-sections of the moisture integral (a), the geopotential perturbation (b), the relative vorticity perturbation (c), and $PV_{mc}$ (d). Panel a has contours plotted every $0.02 \text{ m K}^{-1}$ , panel b every $25 \text{ m}^2\text{s}^{-2}$ , panel c every $1 \times 10^7 \text{ s}^{-1}$ and panel d every $0.01 \text{ PVU}$ ( $1 \text{ PVU} = 10^{-6} \text{ m}^2\text{K kg}^{-1}\text{s}^{-1}$ ).	129
4.5	Decomposition of the $PV_{mc}$ equation (4.39). Term 1 (panel a) represents “dynamical induction”, term 2 (panel b) “stability reduction”, term 3 (panel c) the “nonlinear moist component perturbation”, and term 4 (panel d) the “nonlinear metric”. All cross sections are plotted in PVU with $0.01$ , $0.01$ , $0.0001$ , and $0.00002$ PVU contour intervals for each of a, b, c, and d respectively.	130
4.6	Schematic representation of simple moisture profiles and their resulting $PV_{mc}$ . All panels are for a local maximum in the mixing ratio in the horizontal. For a local minimum, the signs of the vorticity dominated anomalies are reversed.	131
4.7	Perturbation temperature (panel a), and height and wind fields (panel b) following the inversion of the $PV_{mc}$ anomaly shown in fig. 4.4d. Temperatures are contoured at $1 \text{ K}$ intervals, and heights at $1 \text{ dam}$ intervals. Positive wind values are entering the page, and negative values are exiting it (contours every $0.2 \text{ m s}^{-1}$ ).	132
4.8	Comparison of the original (dashed) and the retrieved (solid) mixing ratio following inversion. Contours are plotted every $2 \text{ g kg}^{-1}$ .	133

5.1	Schematic representation of a linear jet maximum. Light solid lines indicate upper-level height contours with the gradient oriented as indicated. Dashed lines represent lower-level isotherms, again with the gradient as shown. The horizontal secondary circulation at low levels generated by the jet is indicated by the heavy arrows. Two surface lows are superposed on the feature with cyclonic circulations as shown. Regions of enhanced cold and warm advection are shaded on the left and right sides of the figure, respectively. Reprinted from MGY03a. . . . .	163
5.2	Analysis (dashed) and control simulation (solid) tracks and MSLP traces (inset) with locations plotted at 6 hour intervals. . . . .	164
5.3	Left column: sea level pressure (solid, 4 hPa interval) and 1000-500 hPa thickness (dashed, 6 dam interval) in the initial conditions (panel a), and after 24 and 36 hours of simulation (panels c and e). Right column: 850 hPa height (light solid, 6 dam interval), column-integrated water vapor (precipitable water, heavy solid at 5 mm interval above 25 mm), and 250 hPa windspeed (shading for greater than 40, 50, and 60 m s <sup>-1</sup> ) in the initial conditions (panel b), and after 24 and 36 hours (panels d and f). . . . .	165
5.4	Left column: dynamic tropopause potential temperature (solid, 10 K interval) and winds in the initial conditions (panel a), and after 24 and 36 hours (panels c and e). Right column: 850 hPa potential temperature (solid, 2 K interval) and mean 1000-700 hPa PV (shading for absolute values greater than 1, 1.5, and 2 PVU) for the initial time (panel b), and after 24 and 36 hours (panels d and f). . . . .	166
5.5	Moist component PV anomaly (heavy solid, 0.1 PVU interval, dashed negative, no zero) and dry PV anomaly (light solid and shading, 0.2 PVU interval) at 700 hPa in the initial state. . . . .	167

5.6	Mean sea level pressure and 10 m windspeed intensity indicators [panel a(i) to a(vi)] within 200 km of the MSLP center for the western North Atlantic cyclone (Earl, left column) and the eastern North Atlantic cyclone (Danielle, right column) for control simulation (heavy solid), circulation removal (light solid), moisture removal (heavy dashed) and both circulation and moisture removal (light dotted). Near-core (within 400 km) 3-hourly precipitation accumulations are shown in panel b(i) to b(iv), with column and test references as for panel a. The legends shown in panels b(ii) and b(iv) apply to all plots in the figure. . . . .	168
5.7	Storm tracks for Earl simulations (panel a) and Danielle simulations (panel b). Positions are plotted at 3 hour intervals with a heavy solid line for Control simulations, a dashed line for moisture removals, a light solid line for circulation removals, and a dotted line for both removals of both circulation and moisture (as for Fig. 5.6). . . . .	169
5.8	Dry PV at 700 hPa associated with the ex-tropical feature is shown in panel a (0.1 PVU contour interval, no zero) with the balanced inverted wind field at 700 hPa. Inverted height (heavy dashed, 2 dam intervals) and wind ( $2 \text{ m s}^{-1}$ intervals) perturbation structure is shown in the inset for a cross-section as indicated by the arrow. Panel b shows potential temperature (solid, 2 K interval) and mean 1000-700 hPa PV (shading for absolute values greater than 1, 1.5, and 2 PVU) for the initial time. . . . .	170
5.9	Dynamic tropopause potential temperatures and winds (panel a) after 36 hours of simulation, as plotted in Fig. 5.4e. Potential temperature at 850 hPa and lower-level mean PV (panel b) after 36 hours plotted as in Fig. 5.4f. . . . .	171

5.10	Moist component PV and inverted winds at 700 hPa in the initial conditions, plotted as in Fig. 5.8a, are shown in panel a. Heights at 850 hPa and precipitable water contents (panel b) are plotted as in Fig. 5.3b, without windspeeds. . . . .	172
5.11	Panel a is as for Fig. 5.9a, but for EarlDry simulation. Panel b is as for Fig. 5.10, but after 36 hours of simulation. . . . .	173
5.12	Panel a is as for Fig. 5.8a, but includes both dry PV and $PV_{mc}$ anomalies. Panel b is as for Fig. 5.8b, but for the noEarlDry simulation. . .	174
5.13	Panels are as for Fig. 5.9, but for the noEarlDry simulation. . . . .	175
5.14	Panels are as for Fig. 5.8, but for the noDan simulation. . . . .	176
5.15	Panels are as for Fig. 5.9, but for the noDan simulation. . . . .	177
5.16	Panels are as for Fig. 5.10, but for the DanDry simulation. . . . .	178
5.17	Panels are as for Fig. 5.11, but for the DanDry simulation. . . . .	179
5.18	Oceanic latent heat fluxes after 3 hours in the control simulation (panel a) and DanDry sensitivity test (panel b). Contours are plotted every 50 W/m <sup>2</sup> , with shading above 300, 350, and 400 W/m <sup>2</sup> . . . . .	180
5.19	Panels are as for Fig. 5.12, but for the noDanDry simulation. . . . .	181
5.20	Panels are as for Fig. 5.13, but for the noDanDry simulation. . . . .	182

# List of Tables

2.1	Removal parameters for tests as indicated. Acronyms are defined in caption for Fig. 2.3. . . . . .	42
5.1	Summary of initial condition modifications for each test. . . . .	161
5.2	Summary of cyclogenetic sensitivity for each test. . . . .	162

# Chapter 1

## Introduction

### 1.1 Introduction and Motivation

The interaction of a tropical cyclone (TC) with the midlatitude flow, an event which usually signals the end of the tropical phase of the storm's lifecycle, can result in the production of heavy rains and high winds in coastal regions not usually affected by hurricane activity. The superposition of traditional midlatitude quasigeostrophic forcings and the latent heat and remnant vorticity contained in the lower-level tropical vortex can result in the rapid spin-up of a hybrid tropical/extratropical system during or after extratropical transition (ET). This study examines the dynamics and thermodynamics at work during the simultaneous ET and reintensification (ET/R) of ex-hurricanes Danielle and Earl on 5-7 September 1998.

A detailed description of the current understanding of the ET process will take place in the following section; however, a general description of ET will serve to ground readers not involved in this area of research. In both basins and in both hemispheres, TCs undergo lifecycles which frequently comprise both tropical and extratropical stages. DiMego and Bosart (1982a) estimate that approximately 40% of all TCs take on a significant number of extratropical characteristics at some time during their evolution. The tropical phase often begins as an equatorially trapped wave, a common trigger mechanism for TC initiation, travel westward across the equatorial Pacific or Atlantic, organizing convection and possibly resulting in TC development. The resulting storm continues to progress westward under the influence of

the trade winds until it nears the western edge of the basin. Tropical systems forming in western-basin genesis regions spin up near the eastern shores of the bounding continent, and thus join our lifecycle description at this point. A sharp anticyclonic track change marks the beginning of recurvature as the poleward component of the TC's phase speed increases. Landfalling systems may or may not complete recurvature as reduced surface heat fluxes and the shutdown of convectively-driven latent heat releases (Bosart 1981) frequently combine with increased surface friction (Montgomery et al. 2001) to result in the spin-down of the vortex. As the TC moves poleward, it begins to feel the influence of the baroclinic westerlies. Environmental shear values increase dramatically (Thorncroft and Jones 2000) and interactions between the TC's outflow and midlatitude jet/front structures can occur (Holland and Merrill 1984). Studies by Klein et al. (2000) and Hart and Evans (2001) find that 26% of North Pacific and 25% of North Atlantic TCs, respectively, undergo some form of reintensification following interaction with the midlatitude flow. The resulting storms can have catastrophic effects on the population in areas affected by the tropical rains and high windspeeds that they produce.

One of the first documented cases of western North Atlantic ET occurred in 1775, when a pair of unnamed hurricanes wreaked havoc on the American Colonies over a two week period in late August and early September. Using data gathered from a wide variety of sources, Rappaport and Ruffman (1999) suggest that the first hurricane made landfall near Cape Hatteras on 2 September, killing at least 163 people as it moved inland and weakened. A second hurricane, tracking offshore parallel to the coast, interacted with a pre-existing extratropical cyclone over Labrador on 11-12 September, resulting in high windspeeds and extreme seas which led to what is likely the largest storm-related loss of life ever in the western North Atlantic (Rappaport and Fernandez-Partagas 1997). Over 20% of the population of the French islands of St. Pierre and Miquelon, south of Newfoundland, were lost at sea during the passage of the second transitioning hurricane.

Almost a century later, the infamous "Saxby Gale" of 1869 made landfall on the

Maine-New Brunswick border (4 October), causing severe damage to the cities of St. John, Moncton, and Halifax (Ruffman 1999). In New Brunswick alone, as many as 100 people perished as the storm produced torrential rains throughout New England and the Canadian Maritimes. Parts of inland Connecticut received over 300 mm of storm-accumulated precipitation, and over 100 mm of rain fell in a 2 h period in southern New Hampshire, setting records that survive to this day (Abraham et al. 1999). This ET was made all the more legendary because of its apparent prediction by Lt. Saxby almost one year in advance of the event. Based on the tidal perigee and his own unwavering sense of infallibility, Lt. Saxby made a semi-accurate prediction of the storm, that produced record high waters (tide and storm surge combined) at the head of the Bay of Fundy (Parkes et al. 1999).

More recently, the great New England Hurricane of 1938, a classic Cape Verde storm that made landfall on Long Island (21 September), produced sustained hurricane-force winds over large parts of southern New England and is credited with the strongest winds ever recorded in the area (sustained  $54 \text{ m s}^{-1}$ , with peak gusts over  $84 \text{ m s}^{-1}$  at the Blue Hill Observatory, Milton, Massachusetts). The high windspeeds and tropical rain rates which accompanied the transitioning system resulted in 564 deaths and caused catastrophic damage to fishing fleets along the eastern seaboard where 2600 vessels were destroyed and over 3300 damaged.

Of particular Canadian interest is the 1954 ET of Hurricane Hazel, which struck southern Ontario in the early morning hours of 16 October (Knox 1955). The tropical system formed in the Lesser Antilles on 5 October and meandered northward through the Windward Islands and into the Caribbean before beginning to accelerate rapidly northward. Hurricane Hazel made landfall near Myrtle Beach, South Carolina shortly before 1200 UTC 14 October with a phase speed of over  $20 \text{ m s}^{-1}$  and maintained its intensity throughout its passage over western Washington, DC, Pennsylvania, and New York. Of particular dynamical interest, Knox (1955) describes the development of a secondary, cold core vortex that acts to continue the system's track after a jump across the Alleghenies Mountains of New York. Damage in the United States of

America totaled \$1.5 billion (1954 dollars), and 100 people were reported dead. Poor warning of the storm's heavy rains resulted in the deaths of 81 people in Toronto, mostly as a result of extensive flash flooding.

With this historical context in mind, the following section details studies of more recent ET events, and presents a snapshot of the current understanding of the complex interactions that occur during the transition process. Section 1.3 of this chapter directly addresses the research goals of this study, and provides an organizational structure for the remainder of the manuscript.

## 1.2 Overview of ET Research

The progression of tropical cyclones (TC) into the midlatitudes has always posed a threat to those living and working in coastal areas, but extensive research concerning extratropical transition (ET) has only recently begun. This review represents an attempt to consolidate and focus the study of these damaging and dangerous events, and to present a distillation of the multitude of diagnostic findings and conceptual models presented over the last two decades. The great degree of similarity between the results obtained by completely independent studies suggests that the ET research community continues to make steady progress towards the goal of understanding the complex tropical/extratropical interactions that occur during ET events.

Theories surrounding extratropical cyclogenesis have been compiled since the mid 19<sup>th</sup> century (e.g. Thomson (1852)); however, modern synoptic meteorology arose from the Bergen school's insights into the dynamics of cyclones during the development of the Norwegian cyclone model and polar front theory (Bjerknes and Solberg 1922). Baroclinic cyclones were considered to form purely as a result of the temperature gradients germane to the midlatitudes, and to decay as the potential energy contained in the troposphere-deep baroclinic zone was removed by occlusion (Charney (1947); Eady (1949)). Similarly, many studies of tropical cyclogenesis, hurricane, and typhoon development have been documented since the pioneering work of Riehl (1950) and Kleinschmidt (1951) on the subject. However, the crossover between

tropical structures and forcings and their midlatitude counterparts that occurs during the transition portion of TC lifecycles remained virtually unstudied until the New England hurricane of 1938 prompted researchers to begin investigating the processes involved in ET. Tannehill (1938) and Pierce (1939) both presented evidence for the existence of frontal structures within the system, leading to the hypothesis that a hybrid tropical-extratropical cyclone could exist. Further studies of frontal zones associated with hurricanes followed soon thereafter. Knox (1955), Hughes et al. (1955), Matano (1958), Palmen (1958), and Anthes (1990) brought their collective research efforts to bear on the study of Hurricane Hazel (1954), a devastating ET event which caused damaging winds and flooding rains as far north as Toronto, Ontario. Further studies on transitioning storms such as Tropical Storm Candy (1968) (Kornegay and Vincent 1976), Hurricane Camille (1969) (Chien and Smith 1977), Hurricane Agnes (DiMego and Bosart (1982a); DiMego and Bosart (1982c); Bosart and Bartlo (1991)), and Southern Hemisphere systems such as tropical cyclones Patsy (1986) (Sinclair 1993b) and Bola (1988) (Sinclair 1993a) greatly advanced the understanding of the complex dynamic and thermodynamic interactions that occur during ET events. Concurrent with the increased consideration of midlatitude forcings on tropical systems came an enhanced awareness of the role of physical processes in baroclinic cyclone lifecycles. Bosart (1981) investigated the impact of surface fluxes on extratropical cyclogenesis, and further studies (Gyakum 1983a,b) found that the distribution of latent heat released during convection played an important role in the rapid development of baroclinic systems. This blending of tropical and extratropical research programs acknowledges the continuous nature of atmospheric forcings and plays a leading role in modern synoptic meteorology.

The exhaustive studies of Hurricane Agnes by DiMego and Bosart (1982a) and DiMego and Bosart (1982c) hold quasigeostrophic ascent forcings [primarily cyclonic vorticity advection (CVA) and advective patterns] responsible for the focusing of tropical-intensity precipitation maxima which resulted in extreme flooding in parts of New England in 1972. With total storm damage estimated at over \$3.5 billion

(1972 dollars), the ET of Agnes remains one of the most costly flooding disasters in the history of the United States of America. DiMego and Bosart (1982a) show that much of the initial precipitation in the New England states results from convergence of the westward-flowing tropical air ahead of Agnes with a pre-existing cold air damming structure on the eastern slopes of the Appalachian Mountains. Applying the dynamical model of Krishnamurti (1968), and performing moisture, vorticity and kinetic energy budgets, DiMego and Bosart (1982c) show that the continuous cyclonic rotation of the remnant tropical vortex leads to reinforcing superposition of thermal advection, CVA, and diabatically-driven ascent forcing at different times during the storm's reintensification. With this caveat of lower-level rotation, they conclude that Agnes undergoes a nearly-classic Petterssen type B (Petterssen and Smebye 1971) redevelopment in which strong frontal waves never appear.

Studies of Southern Hemispheric TCs are rare compared to their northern counterparts; however, the division of tropical cyclone characteristics into the categories of "intensity", "size", and "strength" by Holland and Merrill (1984) and subsequent study of idealized forcings acting on a composite Southern Hemisphere storm (Holland 1983) give rise to a conceptual model which has been successfully applied in both hemispheres. Holland and Merrill (1984) find that asymmetric upper-tropospheric forcing has an influence on TC intensity, the extent of which is determined by the proximity of the forcing to the center in relation to the inertial stability of the TC outflow layer (Anthes (1972); Kitade (1980); Kurihara and Tuleya (1974), although the extent of the reduced-stability layer varies greatly from storm to storm (Alaka (1962); Black and Anthes (1971)). Outflow variability notwithstanding, this model has been applied in numerous cases, including the study of TC Patsy by Sinclair (1993b). Using traditional synoptic diagnostic procedures, the author shows how multiple trough interactions at first weakened Patsy, but later led to the rapid redevelopment of the storm as an extratropical system. Following the near-destruction of the TC in a highly sheared environment resulting from the passage of a fast-moving upper-level trough and jet streak, the outflow from the storm intensifies a down-

stream, poleward jet that in turn triggers mutually-intensifying ascent, convection, and deformation.

The study of TC David (1979) by Bosart and Lackmann (1995) signals the beginning of a movement away from traditional diagnostic frameworks, and towards more dynamically-based consideration of the ET process. Potential vorticity (PV) based dynamic tropopause analysis techniques are used to show that a relatively weak trough to the northwest of the transitioning cyclone is strengthened by the poleward advection of elevated tropopause heights associated with the diabatically-heated outflow region of the TC remnant. As described by Morgan and Nielsen-Gammon (1998), steep orography on the dynamic tropopause is indicative of upper-level jet/front structures, in this case reinforced by the TC outflow. The work of Bosart and Lackmann (1995) thereby reinforces the findings of Holland and Merrill (1984) in a dynamically significant setting and links it with physical processes through the introduction of the coupling index as a measure of bulk column stability.

One of the few observational studies of ET is presented by Browning et al. (1998) for the case of ex-hurricane Lili (1996). The authors develop a detailed conceptual model of the storm's dynamics based on data collected from mesoscale models, a mesosphere-stratosphere-troposphere radar, and satellite observations. Browning et al. (1998) are the first to demonstrate the existence and importance of a strong low-level jet that nearly encircles the core of the system just above the planetary boundary layer (PBL). This feature has more recently been observed in the study of Hurricane Michael (2000) (Jim Abraham 2000, personal communication). PV diagnostics are used by Browning et al. (1998) to highlight tropopause folds surrounding the system's core and sometimes descending to the top of the PBL. The authors categorize the storm as stage 4 of the Shapiro and Keyser (1990) model, but emphasize that the seclusion process suggested by this classification works to sustain the pre-existing warm core rather than to create it.

The ETs of hurricanes Felix and Irix (1995) (Thorncroft and Jones 2000) are again diagnosed using the "PV thinking" paradigm of Hoskins et al. (1985). Iris, a weak

TC throughout the tropical portion of its lifecycle, tracks over warm water during its eastward migration across the North Atlantic following recurvature. Strong latent heat fluxes from the ocean surface fuel continued deep convection and result in the maintenance of the warm core to significant height despite the effects of relatively strong vertical shear. The tilted PV column interacts with an upstream trough that wraps cyclonically above the remnant TC in an LC2-type baroclinic development (a full description of lifecycles can be found in Thorncroft et al. (1993)). Felix, a much stronger TC, moves over colder waters in the North Atlantic and loses its warm core structure very rapidly. Decoupling of the PBL occurs as sensible heat fluxes are directed into the ocean and the lowest layers of the atmosphere are dramatically stabilized. A combination of the weaker vertical shear and the inertial rigidity of the strong tropical vortex in this case leads to a smaller downstream tilt in the core's PV structure, and the system undergoes an exceedingly weak LC1-type development process (Thorncroft et al. 1993). Thorncroft and Jones (2000) conclude that the structure of the TC remnant plays an important role in the nature of ET, as does the location of the ex-tropical system relative to strong sea surface temperature (SST) gradients and North Atlantic jet/front structures.

Recent work on Southern Hemispheric ET has been performed by Sinclair (2002). Compiling a 28 year climatology of ET events in the southwest Pacific, the author finds only a small sensitivity to SST variability. Instead, Sinclair (2002) finds that the superposition of jet-induced regions of CVA and zones of lower-tropospheric frontogenesis (associated with isentropic ascent) are features common to the bulk of the intensifying ex-tropical cyclones in the dataset. Using a subset of 33 transitioning storms from 1980-1997, the author constructs a three-dimensional conceptual model of transition which further supports the jet-interaction hypothesis of Holland and Merrill (1984). In a simplified presentation of the original work, Sinclair (2002) describes the interaction process in three steps: 1) the jet is enhanced by TC outflow and lower-level frontogenesis; 2) absolute vorticity is lowered and inertial stability reduced on the equatorward flank of the jet; and, 3) the reduced vorticity favours

increased divergence, ascent, and convection in the warm region, which then feeds back to step 1.

Another climatological study of ET is performed by Hart and Evans (2001) for storms occurring between 1899-1996, although a subset of storms since 1950 is used to compute the bulk of the diagnostics. The authors find that 46% of Atlantic TCs progress to the transition phase of their lifecycles (here defined in four steps: tropical intensification, tropical decay, ET/R, occlusion), and that 51% of these reintensify following transition. The authors also investigate the interaction between tropical and extratropical forcings through a comparison of maximum potential intensity (Emanuel 1988) and baroclinic instability in the Eady model (Eady 1949). Further study by Hart (2003) has led to the development of a three dimensional cyclone phase space in which the onset and completion of the ET process can be objectively determined (Evans and Hart 2003). In the latter study, the climatology developed by Hart and Evans (2001) is used as a training set to develop quantitative predictors of ET evolution based on the thickness asymmetries and thermal wind indicators described by Hart (2003). The authors show that significant timing differences between model-described ET and NHC-declared transitions are reduced through the use of these objective indicators.

A climatological study of 30 western North Pacific ET cases presented by Klein et al. (2000) further attempts to provide objective indicators for transition onset and completion, this time based primarily on analysis of satellite imagery. A three-step ET process is proposed, consisting of: 1) convective shutdown in the western quadrant and dry slot appearance to the southwest of the centre; 2) convective shutoff in the western quadrant and reduced convection to the east of the centre, along with the development of a cirrus shield as jet interaction occurs; and, 3) inner-core convective shutdown, with indication of a strong warm-frontal zone and a weak cold-frontal region (Harr and Elsberry 2000a). Klein et al. (2000) claim that the model developed over the course of development of the climatology replaces that of Matano and Sekioka (1971) since it is three dimensional, generally applicable in the western North Pacific,

and dynamically-based. The climatology further reveals that only 27% of western North Pacific cyclones complete transition according to the criteria set forth by the conceptual model. Ritchie and Elsberry (2001) use the Coupled Ocean Atmosphere Mesoscale Prediction System to verify the findings of Klein et al. (2000) by initializing the model with idealized forms of the structures described by the conceptual model. The three stages of ET are modelled separately, with the only significant refinement to the model of Klein et al. (2000) coming in the third transition step. Here, Ritchie and Elsberry (2001) find that a column stabilization process acting to the west of the centre, the result of strong upper-level convergence, is responsible for the observed decrease in eyewall convection rather than the dry inflow process proposed by the original authors.

Further study of western North Pacific ET events, in this case those of typhoons David and Opal (1997), is performed by Harr and Elsberry (2000a). The authors employ decomposed vector frontogenesis diagnostics (Keyser et al. 1988) in which the scalar component is related to divergence effects, and the rotational component is associated with vortical frontogenetic influences. During ET, the rotational frontogenesis component is responsible for organizing an advective dipole that helps the remnants of Typhoon David to couple with a transient midlatitude thermal wave. A pre-existing extratropical cyclone over the central North Pacific during the ET of Typhoon Opal dominates deformation processes in the baroclinic zone so that phase locking of the ex-tropical system with the upper-level flow is impossible. Harr and Elsberry (2000a) conclude by suggesting that scalar frontogenesis could serve as yet another objective indicator of ET completion.

Two recent studies of environmental structures conducive to ET/R in the western North Pacific have been undertaken by Harr and Elsberry (2000c) and Klein et al. (2002). In the former, the authors diagnose a pair of flow regimes (“northeast” and “northwest”), based on work presented in Harr and Elsberry (2000a). In both regimes, the ex-tropical cyclone first experiences an increase in upper-level angular momentum fluxes (Molinari et al. 1995) through interaction with the midlatitude

flow. The northwest flow is subsequently conducive to increased low-level eddy heat fluxes and both barotropic and baroclinic kinetic energy production through interaction with midlatitude baroclinicity and discrete solenoidal circulations between the remnant TC and an upstream trough. In the northeast flow case, as for Typhoon Opal, a pre-existing extratropical cyclone results in a near-zonal flow and reduced interaction with the baroclinic environment. Further, Harr and Elsberry (2000a) show that there is barotropic destruction of kinetic energy as the systems approach each other. Klein et al. (2002) hypothesize that three important processes interact during ET: 1) upper- and mid-level midlatitude dynamics, especially CVA-related divergence; 2) low level thermal processes in the TC remnant; and, 3) upper level outflow characteristics. The superposition of these forcings results in environments that the authors class as “favourable”, “neutral”, or “unfavourable” for rapid extratropical redevelopment following ET. The transitions of Typhoon Bart (1999), Supertyphoon Ginger (1997), and Supertyphoon Bing (1997) are shown to have occurred in each of these environments, respectively. Relying heavily on a conceptual model virtually identical to that of Holland and Merrill (1984), Klein et al. (2002) conclude through a series of numerical model simulations that TC outflow enhancement of the downstream jet and lower-level interaction of the TC vorticity field with the associated baroclinic zone are crucial factors to ET/R.

The similarities borne between many of the conceptual models presented over the last two decades is encouraging given the wide variety of studies undertaken in efforts to develop a better understanding of ET. In particular, the use of dynamically-based diagnostics such as dynamic tropopause analyses [Bosart and Lackmann (1995), and following sections of this thesis] to reinforce theories developed under traditional synoptic frameworks (Holland and Merrill 1984) indicates that convergence on a universally-applicable model describing ET may be possible.

### 1.3 Scientific Objectives and Manuscript Outline

The scientific objective of the current study is to diagnose the relative importance of identifiable features in the midlatitude flow and remnant tropical vortices to the structure and intensity of the ET/R of ex-hurricanes Danielle and Earl (1998). As will be shown in subsequent chapters, the remnant features of both hurricanes reintensify rapidly over the period of interest (the 48 hours between 0000 UTC 5 September and 0000 UTC 7 September), Earl in the western North Atlantic and Danielle near the eastern edge of the basin. A numerical modelling study is undertaken in which a control simulation is shown to adequately replicate observations of the ET/R processes occurring over the North Atlantic from 5-7 September 1998. Sets of sensitivity tests are then employed in order to isolate and quantify the contribution of individual features to the ET/R process.

Diagnoses of most of the simulations presented in this study take place under the “PV thinking” paradigm proposed by Hoskins et al. (1985). Tropical and midlatitude features are defined using PV fields, and the piecewise PV inversion technique pioneered by Davis and Emanuel (1991) is used to isolate and modify identifiable components of the atmospheric state on 0000 UTC 5 September (hereafter 00/05), the model initialization time. Analyses of the resulting sets of sensitivity tests form a basis for the conclusions drawn from this study. The formulation of Ertel (1942) potential vorticity used in this research employs the potential temperature as its thermodynamic variable. This can be shown to be identical to the potential density-based formulation frequently applied to oceanic problems.

The ability to identify unique tropical and midlatitude features that play an important role in the ET/R process will be a valuable asset to researchers and operational meteorologists alike. Be it the presence of an intensifying upstream trough, a downstream jet/front structure, a strong remnant TC circulation, or high column-integrated water vapour (precipitable water) values in the tropical vortex, a recipe listing the key ingredients for rapid reintensification of transitioning TCs will help to

develop both a dynamical understanding of ET/R and a framework under which to enhance forecasting of these extreme events.

The role played in the ET/R process by the initial atmospheric state upstream of the transitioning TC vortex is examined in Chapter 2. This portion of the study focuses exclusively on ex-hurricane Earl. A discussion of Earl's lifecycle is followed by a description of the modelling system, updated versions of which are used throughout the manuscript (as noted). The credibility of the control simulation is established by comparison with available observations, and a sensitivity testing setup is described. The application of the piecewise PV inversion techniques developed by Davis and Emanuel (1991), and employed extensively since then (Davis 1992a,b; Huo et al. 1998; Milbrandt and Yau 2001), is described at length in Chapter 2. The amplitude and intensity of the upper-level trough initially upstream of Earl are modified, as is the strength of the lower-level vortex. It is found that the existence of the upstream trough is a necessary condition for the reintensification process, although a discussion of its sufficiency is hampered by the inability of the piecewise PV inversion methodology to modify the tropical moisture contents of the remnant vortex.

Having discovered one of the key ET/R ingredients upstream of the transitioning vortex, attention is turned to the importance of structures in the flow downstream of ex-hurricane Earl in Chapter 3. The simulation domain is necessarily expanded to include the entire North Atlantic basin so that potentially relevant features such as the North Atlantic jet/front, the system associated with ex-hurricane Danielle, and the northward extension of the Bermuda high are accurately modelled in the control integration. An introduction to the lifecycle of Hurricane Danielle is presented at the beginning of the chapter, as is a recapitulation of Earl's transformation process. The concurrent ET/R events (Danielle and Earl) are shown to possess differing structural characteristics at all levels in the control simulation, an observation borne out by comparison with satellite imagery of the mature systems. The upper-level trough studied in Chapter 2 interacts strongly with Earl throughout a classic LC2-type cyclonic roll-up of PV above the redeveloping vortex (Thorncroft et al. 1993). The

initially-weak trough upstream of Danielle at the initialization time extends rapidly southeastward and filaments to wrap around the redeveloping centre. This process is shown to entrap warm, moist tropical air advected northward and westward ahead of the remnant TC, and to create a locally-tropical environment in which the hurricane reintensifies. Since none of the initial condition modifications performed in Chapter 2 result in such differing structures of the redeveloping vortex, idealized downstream initial states (for Earl) are created to form a set of sensitivity tests used to investigate the modulation of ET/R “mode” by features in the downstream flow. It is shown that the existence of a downstream North Atlantic jet/front structure is necessary for the “baroclinic” mode transition similar to that described for Earl in the control. The absence of this feature results in “tropical” mode reintensification reminiscent of the evolution of Danielle in the control simulation. A conceptual model based on linear jet dynamics is presented as a possible explanation for the sensitivity of ET/R structure to the existence of a downstream jet/front.

The extent to which the tropical moisture contained within the remnant vortices of both Earl and Danielle aids the ET/R process remains undetermined from the investigation presented in Chapter 2. In order to address this issue, the moist component PV diagnostic ( $PV_{mc}$ ) is developed and described in Chapter 4 in order to expand the piecewise PV inversion framework to include the effects of atmospheric moisture. The variable is developed to represent the portion of the total PV field that results directly from the presence of atmospheric water, thereby amounting to the difference between the PV of a moist atmosphere and the PV of the same atmosphere with the effects of water neglected. An analytic environment is presented in which the diagnostic  $PV_{mc}$  equation becomes tractable such that its terms can be quantitatively evaluated. Thereafter, a series of hypothetical moisture distributions are examined, and the resulting  $PV_{mc}$  structures described. This portion of the study concludes with a demonstration that the numerical inversion of  $PV_{mc}$  indeed yields a solution for the moisture field that closely resembles the structure of the analytic model.

Application of both dry PV and  $PV_{mc}$  modification procedures is required for the work presented in Chapter 5. To conclusively answer the lingering question regarding the effects of tropical moisture contained within the remnant circulations, an updated version of the numerical model used throughout this study is employed for the generation of yet another control simulation. Improvements to vertical advection within the model and the application of a more realistic convective parameterization scheme increase confidence in the model's ability to accurately respond to moisture and diabatic forcings. Owing to the importance of the remnant tropical structures to this portion of the study, an enhanced description of the tropical phase of the lifecycles of ex-hurricanes Danielle and Earl is presented in this chapter. Following the validation of the control simulation against the observations presented in the previous chapters, procedures for the identification and removal of the circulation and moisture patterns associated with each transitioning TC individually are presented. It is found that the baroclinic mode cyclogenesis associated with ex-hurricane Earl in the control simulation is remarkably insensitive to the existence of the remnant tropical vortex and moisture structure. A purely extratropical surface low is found to develop beneath the intensifying upper-level trough and to intensify to virtually the same strength as Earl during reintensification. The tropical mode cyclogenesis associated with Danielle's redevelopment, however, shows a much larger sensitivity to the TC remnant. Removal of the tropical moisture field associated with the ex-hurricane results in a significantly weakened system, and removal of the remnant circulation appears to fundamentally alter both upper- and lower-level processes. It is concluded that the extent to which the tropical remnant plays a role in the ET/R process depends intrinsically on the mode of transition, with baroclinic mode transitions showing almost no dependence, and tropical mode transitions relying strongly on the ex-tropical features. The upstream trough investigated in Chapter 2 may therefore be considered both a necessary **and** sufficient condition for rapid western North Atlantic cyclogenesis only for the baroclinic mode.

A summary and discussion of the results is presented in Chapter 6 and represents

a synthesis and restatement of the conclusions presented in the discussion sections contained in each of the preceding chapters.

## Chapter 2

# The Influence of Upstream Features on ET

Since the pioneering ET studies of Tannehill (1938) and Pierce (1939), the need to develop simplified models under which to examine the complex tropical/extratropical interactions that occur during ET/R has become increasingly evident. This chapter focuses on identifying features in the initial atmospheric state upstream of Earl at 00/05 whose presence is crucial to the observed and simulated evolution of the ET/R process. A brief description of Hurricane Earl's lifecycle in Section 2.1 describes the track of the storm as it progresses northward from its genesis region in the Gulf of Mexico, across the Florida Panhandle, and off the North American continent just north of Cape Hatteras. The decaying TC's subsequent interaction with a near-coastal baroclinic zone and associated upper-level trough results in the rapid reintensification of the ex-tropical vortex. The simulation of this process over the 48 h period beginning 00/05 is documented in Sections 2.2 and 3.

As noted in the introductory chapter, the piecewise PV inversion framework of Davis and Emanuel (1991) is used throughout this study to make balanced modifications to the atmospheric state at 00/05, the initial time for all simulations. This procedure is outlined in Section 2.4, as is its application to the upstream sensitivity testing simulations presented in the remainder of the chapter. Three identifiable trough PV anomaly structures and the PV anomaly pattern associated with the remnant TC are isolated and removed individually from the initial conditions. The

resulting fields form a basis for the sensitivity testing strategy, and lead to the simulation results presented in Section 2.5. A discussion of these results and a caveat concerning the inability of the current PV inversion methodology to deal with modifications to atmospheric moisture are presented in the final section of the chapter (Section 2.6).

The following is based on McTaggart-Cowan et al. (2001), published in Monthly Weather Review, volume 129 (2001).

# Sensitivity Testing of Extratropical Transitions using Potential Vorticity Inversions to Modify Initial Conditions: Hurricane Earl Case Study

R. McTaggart-Cowan, J.R. Gyakum, and M.K. Yau

Department of Atmospheric and Oceanic Sciences, McGill University

## Abstract

This study uses the Mesoscale Compressible Community model to simulate the extratropical transition and reintensification of Hurricane Earl (1998) for the purposes of testing sensitivity to modification of the model's initial conditions. Though relatively strong "classical" cyclogenetic forcings were present in this case, operational forecasts seriously underpredicted the severity of the reintensification. Employing a piecewise PV inversion, we remove localized PV anomaly ( $PV'$ ) maxima from the initial conditions and rebalance the fields for input to the model. Several  $PV'$  structures in an upstream trough, and the  $PV'$  associated with the hurricane, are removed individually and the model rerun. Comparison of the resulting output with that of the control integration allows for a quantification of the impact of each PV anomaly on the regeneration of Earl. It is found that the existence of an upstream trough is of primary importance to the storm's reintensification, while the presence of the low-level circulation associated with the decaying hurricane plays only a secondary role.

## 2.1 Introduction

The transition of tropical cyclones (TCs) to extratropical systems is often accompanied by the reintensification of the original tropical cyclone as an extratropical

low. Approximately 40% of Atlantic and Pacific TCs progress to a transition stage according to DiMego and Bosart (1982b), and a statistical study by Klein (1997) of Pacific hurricanes shows that 26% of all TCs of tropical storm intensity or greater reintensify during the extratropical transition (ET) process. The resulting storms can be stronger than the hurricanes that spawned them. For example, one of the worst flooding events in US history occurred during the ET of Tropical Storm Agnes in June of 1972 (Carr and Bosart 1978). These storms pose a threat not only to coastal areas, fishing fleets, and shipping, but also to areas not usually affected by tropical systems. A classic example is Hurricane Hazel which struck Toronto in October, 1954.

Many features which enhance the ET and reintensification processes have been identified in the literature. These include cyclonic vorticity advection (CVA) from a polar jet streak, a baroclinic environment, an upwind trough (Petterssen and Smebye 1971), tropopause lifting, tropical airmass moisture (Bosart and Lackmann 1995), and low-level potential vorticity (PV) (Gyakum et al. 1992). Studies of Hurricane Lili (October, 1996) by Browning et al. (1998) also revealed the persistent signature of a warm core isolated from the relatively cold environment by a low-level jet (LLJ). In spite of such extensive research in the field of ET, the relative importance of each of these reintensification forcing mechanisms remains unclear. A quantification of the impact of each of the flow features mentioned above is necessary for the accurate real-time forecasting of these severe events.

The goal of this research is to assess the importance of several of these possible cyclogenetic forcings through a modeling study of Hurricane Earl (September, 1998). Identifying potentially relevant features in the initial conditions at 0000 UTC 5 September 1998 (hereafter, 00/05) allows for their removal using a PV inversion technique developed by Davis and Emanuel (1991). Each structure is removed separately from the initial fields, and the model is rerun in order to obtain a prognosis of what would have happened had that feature not been present. In this way, a quantitative analysis of the impact of the individual forcing mechanisms can be obtained

through comparison with a validated control simulation.

Hurricane Earl formed from a strong tropical wave that originated off the African west coast on 17 August. Development of the storm was suppressed by outflow from the powerful Hurricane Bonnie and intensification to tropical depression status did not occur until the wave had moved into the Gulf of Mexico at 12/31 (see NHC track map Fig. 2.1). A relatively weak hurricane, Earl reached Category 2 of the Saffir-Simpson Hurricane Scale (winds over  $40 \text{ m s}^{-1}$ ) with a central pressure of 985 hPa briefly before making landfall in Panama City, Florida at 06/03 as a Category 1 hurricane. The National Hurricane Center (NHC) declared the storm extratropical at 18/03, and Earl moved off the Virginia coast at 18/04. By the initialization time of the simulation used for this study, ex-hurricane Earl had weakened to 1004 hPa, as analyzed by the Canadian Meteorological Centre (CMC), and lay 350 km east of the New Jersey coastline.

Over the next 36 hours, Earl reintensified rapidly as it accelerated northeastward along a coastal baroclinic zone. The central pressure of the storm dropped to 960 hPa as an upstream trough began to interact with the hurricane's remnants. Winds in excess of  $38 \text{ m s}^{-1}$  appear just above the surface in the 12/06 sounding from St. John's Newfoundland (not shown). Shortly after this time, the system developed a downstream tilt and the surface circulation began to weaken while moving almost due east. After 12/08, the storm's identity became indistinguishable from that of the long-lived extratropical low that resulted from the transition of Hurricane Danielle.

The following section discusses the data set and model used for the simulation of Earl's reintensification. Section 2.3 describes the results of the control forecast and identifies the dynamically important forcing mechanisms present in this case. PV removals and inversions are described in detail in Section 2.4, and the resulting forecasts are presented in Section 2.5. The study concludes with a brief summary and a discussion of the results.

## 2.2 Methods

### 2.2.1 Model Description

All of the numerical simulations for this study are performed using Version 3.2 of the Canadian Mesoscale Compressible Community (MC2) model, a derivative of a hydrostatic limited area model developed by Robert et al. (1985). The MC2 uses semi-implicit time stepping and three dimensional semi-Lagrangian advection to solve the primitive equations on an Arakawa C-grid in the horizontal and Tokioka B-grid in the vertical. Relaxation of the hydrostatic approximation by Tanguay et al. (1990) renders the Version 3.2 governing equations fully elastic, allowing for accuracy over a wide range of scales. A summary of the MC2 parameters used in this study is provided in the appendix. For a complete description of the model dynamics, the reader is referred to Benoit et al. (1997).

Using a “successive corrections” solution method, the MC2 solves the dynamical terms of the prognostic equations first, and then begins to apply corrections from physics subroutines. The turbulent vertical diffusion scheme developed by Mailhot and Benoit (1982) uses turbulent kinetic energy to specify a diffusion-type transfer coefficient particularly important in the boundary layer. A force/restore method, as described by Benoit et al. (1997), is used for the calculation of surface heat and moisture fluxes, with sea surface temperatures prescribed by monthly means. Deep cumulus convection is parameterized using a Kuo-type scheme triggered by large-scale moisture convergence and surface evaporation in the presence of a deep layer of conditional instability. This convective scheme proved to provide the most accurate control simulation in terms of both storm intensity and structure. The Kong and Yau (1997) explicit microphysics package uses prognostic equations for water vapor, cloud water, rainwater, ice particles, and graupel to parameterize the most relevant moist processes. A complete description of the MC2 physics library can be found in Mailhot et al. (1998).

### 2.2.2 Initialization

All simulations are initialized using the 00/05 analysis generated by the regional data assimilation system at the CMC (Chouinard et al. 1994). Analyses are produced on a polar stereographic grid valid at 60°N at six hour intervals with a 35 km horizontal resolution. The MC2 interpolates linearly between analyses to obtain boundary conditions for every step.

## 2.3 Control Simulation

Before any sensitivity experiments could be undertaken, it was necessary to obtain a high-quality simulation of Earl's reintensification. This section describes the meteorological features present at 00/05 and their evolution as the control run progresses. A surface pressure trace and track map for the storm are included in Fig. 2.2. Also included on these plots are the results from several operational analyses for comparisons to be discussed in Section 2.3.3. Mean and maximum windspeeds (within 200 km of the storm center) are shown in Fig. 2.3 as the heavy solid lines in panels (b) and (c). As well, Fig. 2.4a shows the evolution of the areal-averaged precipitation within 400 km of the storm's center.

### 2.3.1 Description of Initial Fields

At 00/05, the remnants of Hurricane Earl are located 350 km east of the New Jersey coast with a minimum sea level pressure (SLP) of 1004 hPa (see Fig. 2.5). The axis of a mid-level trough centered over Quebec lies just inland of the eastern seaboard, above a coastal baroclinic zone that extends from the Carolinas to Newfoundland. Associated with this trough is a vorticity maximum initially centered over Lake Erie. A region of high relative humidity to the north of the storm (not shown) is a result of the injection of warm, moist air from the Gulf of Mexico into higher latitudes. This connection to a tropical energy source has been established by Earl itself, and results in large amounts of latent heating and convective precipitation

throughout the reintensification process.

### 2.3.2 Analysis of Control Simulation

As the simulation begins, the 500 hPa trough starts to rotate slowly eastward, with the vorticity maximum embedded in its axis. Although Earl begins too far south to interact with the trough, it is moving northeastward at  $14 \text{ m s}^{-1}$ , placing it directly downwind of the peak vorticity after 12 hours of integration. Strong cyclonic vorticity advection (CVA) at the 500 hPa level is likely responsible for much of the surface cyclone's initial deepening. Convection in the moist tropical air near the center and attendant latent heating sustains a column of high equivalent potential temperature air in the storm's core (see Fig. 2.6), which persists throughout the integration. Between 12 and 24 hours, thermal advection to the northeast of Earl begins to amplify. The reintensifying low-level circulation around the storm (mean winds have almost doubled to  $18 \text{ m s}^{-1}$  since 00/05) begins to deform the coastal baroclinic zone into a frontal wave. Precipitation accumulations reach almost  $100 \text{ mm (12 h)}^{-1}$  during the first half of the simulation, and are primarily located off the coast where a sharp humidity front lies along the cold frontal slope. The mean precipitation near the storm's center (within 400 km of the pressure minimum) reaches a maximum of almost  $13 \text{ mm (6 h)}^{-1}$  after 24 hours (Fig. 2.4a). Although the primary precipitation type is still convective, the stratiform accumulations continue to increase owing to the large-scale ascent forced by both the approaching trough and a pair of jet streaks. Figure 2.7 shows the location of the 250 hPa jets at 00/06, along with the location of the storm's center. In the control simulation, the system lies between two maxima in the polar jet - just poleward of the exit of one, and equatorward of the entrance of the other - leading to strong quasigeostrophic forcing for ascent near the center at 24 hours.

As phase lock is established between the surface vortex and the 500 hPa trough, the latter begins to intensify rapidly as shown in Fig. 2.3b. This is a result of the subsidence of the tropopause in the trough, which injects high-PV air into the middle

troposphere (see Fig. 2.8). The surface center remains fixed just north of Newfoundland until accelerating eastward during the last six hours of the integration. The stationary storm's circulation continues to deform the baroclinic zone, and kinking of the surface isobars across the fronts becomes more noticeable by 12/06 (Fig. 2.9). By 36 hours, a hook structure has emerged in the humidity field as dry stratospheric air begins to wrap in towards the center of the system. The warm core structure of the storm is evident in Fig. 2.10, as is a low-level jet encircling the storm's core. Browning et al. (1998) suggest that this jet acts essentially as a material surface to separate the warm air of the core from the cooler environment. The system reaches its peak intensity at 15/06 (39 hours into the integration) with a surface pressure of 956 hPa and maximum winds over  $32 \text{ m s}^{-1}$ . The primary precipitation process is now stable lifting, although some convection is still present near the core. Precipitation accumulations have decreased throughout the last half of the simulation as convective activity gradually slows down. The mid-level trough continues to move rapidly eastward, and a downshear tilt develops during the last six hours of the integration. Having lost much of its upper-level support, the storm begins to fill and the baroclinic wave becomes detached from the center. According to NHC tracking, the system continues to weaken and move slowly eastward until it is absorbed by the remnants of Hurricane Danielle on 8 September off the coast of England.

Another perspective on the evolution of the system is shown in Fig. 2.11. This set of panels consists of 12 hourly snapshots of PV on the 325 K surface in conjunction with low-level (1000-900 hPa mean) potential temperature. At 00/05 (panel (a)), a strong PV maximum of over 7 PVU is located over Quebec, with a "trough" of high PV air extending southwards over New York. At this level (approximately 400 hPa in mid-latitudes), the remnants of Earl can be seen as the 1 PVU closed contour just off the US east coast. As time progresses, the large PV maximum initially over Quebec advects eastward and begins to wrap cyclonically as the system intensifies rapidly. This development is very similar to the generation stage of the LC2 baroclinic lifecycle discussed by Thorncroft et al. (1993), and observed by Thorncroft and Jones (2000)

during the extratropical transition and reintensification of Hurricane Iris (1995).

### 2.3.3 Validation

The surface pressure trace and track of the modelled storm are compared to various analyses in Fig. 2.2. As mentioned in Section 2.2.2, the CMC analysis represents an amalgamation of the global forecast and observations. Likewise, the NHC analysis is comprised of an ensemble of global forecasts combined with selected observations. It has been noted (Gyakum 1983a) that assimilated analyses such as these can seriously underpredict the intensity of deep storm centers when observations are sparse near the core. Therefore, the fact that the comparison between the control and both the CMC and NHC analyses is very good until Earl crosses the north coast of Newfoundland is encouraging. Similarly, the correlation of intensity and structure between the simulation and operational manual analyses performed at the Maritimes Weather Centre (Atmospheric Environment Service) is excellent (Fig. 2.12). Precise tracking of the storm center in Fig. 2.2a was made difficult by the formation of several secondary vortices during the first 24 hours of the simulation; the manual analyses show up to three centers on 5 September. Although there seems to be an eastward bias in the model over that period, the tracks converge as the cyclone intensifies. The Canadian operational forecast initialized at 00/05 poorly predicted the intensity of Earl's redevelopment as seen in Fig. 2.2b.

## 2.4 PV Inversions

The utility of PV as a meteorological variable has long been known (Rossby 1939). The two main principles behind its usefulness are described in detail by Hoskins et al. (1985). The first is the conservation of PV on isentropic surfaces provided that adiabatic effects dominate over frictional and diabatic processes. This allows PV to be used as a “tracer” in the flow as well as a diagnostic variable with strong links to cyclogenesis. The second principle is that of PV “invertability”, which remains valid even when friction and diabatic effects are important. The practical limitations of

PV inversion arise from the need for a balance equation which, in general, does not account for these processes.

Hurricane Earl, as a meso- $\alpha$  scale feature, is best described using Ertel (1942) PV defined as

$$q = \frac{1}{\rho} \eta \cdot \nabla \theta, \quad (2.1)$$

because of the attractive quality that it is conserved in the absence of frictional and diabatic processes. Here  $\rho$  is air density,  $\eta$  is the absolute vorticity vector, and  $\theta$  is the potential temperature. Charney's nonlinear balance equation (Charney 1955) is used to relate the geopotential ( $\phi$ ) to the streamfunction ( $\psi$ ) and assumes only that the irrotational component of the wind is small compared to the non-divergent part:

$$\nabla^2 \phi = \nabla \cdot f \nabla \psi + 2 \left[ \frac{\partial^2 \psi}{\partial x^2} \frac{\partial^2 \psi}{\partial y^2} - \left( \frac{\partial^2 \psi}{\partial x \partial y} \right)^2 \right]. \quad (2.2)$$

Here  $\nabla$  is a two-dimensional (horizontal) operator. In the initial conditions for these simulations, the absolute vorticity is at least an order or magnitude greater than the divergence throughout the domain. This suggests that the neglect of the irrotational wind component is a reasonable approximation in this case. Replacing the horizontal velocities in Equation 2.1 with the non-divergent wind and assuming hydrostatic balance allows for a recasting of (2.1) in terms of  $\phi$  and  $\psi$ :

$$q = \frac{g\kappa\pi}{p} \left[ (f + \nabla^2 \psi) \frac{\partial^2 \phi}{\partial \pi^2} - \frac{\partial^2 \psi}{\partial \pi \partial x} \frac{\partial^2 \phi}{\partial \pi \partial x} - \frac{\partial^2 \psi}{\partial \pi \partial y} \frac{\partial^2 \phi}{\partial \pi \partial y} \right]. \quad (2.3)$$

Here  $\kappa = \frac{R_d}{c_p}$  and  $\pi = c_p \left( \frac{p}{p_o} \right)^\kappa$  is the Exner function which serves as the vertical coordinate. Given a field of Ertel's PV (hereafter referred to as PV unless otherwise noted), (2.2) and (2.3) now form a system of equations for  $\phi$  and  $\psi$ . The resulting system of differential equations is elliptical so long as PV is everywhere positive; Dirichlet conditions are used on the lateral boundaries, and Neumann conditions of the form

$$\frac{\partial \phi}{\partial \pi} = f_o \frac{\partial \psi}{\partial \pi} = -\theta \quad (\pi = \pi_o; \pi = \pi_T), \quad (2.4)$$

provide values on the top and bottom boundaries ( $\pi_T$  is the upper boundary). The nonlinearity of the system makes the solutions non-unique for perturbations and

piecewise inversion of the PV anomaly ( $PV'$ ) difficult. For a full description of the solution technique, the reader is referred to Appendix A of Davis and Emanuel (1991). Separate inversions are performed for the mean and perturbation fields, the results of which are additive. An 18 day mean background flow taken between 00/28 and 00/14 is specified in this case, from which the mean PV and  $PV'$  are computed.

In this study, the invertability principle was employed in creating balanced fields of height, wind, and temperature for the model's initial conditions. PV was calculated for all levels at the initial time (00/05). Figure 2.13 shows the 850 hPa, 400 hPa, and 250 hPa  $PV'$  fields. Four separate PV maxima were identified as described in Table 2.1: an upper trough anomaly (A) above 250 hPa (panel a); a southern trough anomaly (B) from 500 to 250 hPa (panel b); a northern trough anomaly (C) from 400 to 250 hPa (panel b); and Hurricane Earl's anomaly (D) from the surface to 500 hPa (panel c). Each of these anomalies was removed separately from the PV field, and an inversion applied in order to obtain the corresponding meteorological inputs for the model initialization. The horizontal extent of each removal is shown in Figs. 2.13 and 2.14. The resulting model prognoses were compared with the control run output to examine the sensitivity of Earl's reintensification to the flow feature removed. The results from these experiments are presented in the following section. Further tests were undertaken in which both the horizontal and vertical extents of the removals were changed (by approximately 100 km and 100 hPa respectively) in order to examine the sensitivity of the results to the precise removal parameters shown in Table 2.1. These simulations (not shown) indicate that the results discussed in the following section are insensitive to changes in the  $PV'$  removal areas to the extent that the same conclusions would have been arrived at had alternative, equally reasonable, removal volumes been selected. The larger horizontal removal resulted in an unchanged central pressure following reintensification, and the deeper removal (up to 400 hPa) resulted in a 1 hPa deeper low. Another simulation was performed in which the initial fields were simply balanced using the PV inversion (no anomaly removals), in order to test the sensitivity of the results to the balancing process itself.

The results from this run (not shown) are very similar to those of the control, with the resulting storm intensity, structure, and location essentially unchanged.

## 2.5 Sensitivity Tests

As outlined in the introduction, sensitivity testing in this case consists of modifying the initial fields using the PV inversion methods outlined in Section 2.4. Once new initial conditions have been obtained, the model is rerun to produce predictions of what might have happened had the particular  $PV'$  maximum been absent. Comparison of simulation results from five such  $PV'$  removal tests are presented here. Initial surface and 500 hPa conditions for each case are shown in Fig. 2.14. Time series of SLP, 500 hPa heights, mean winds, and maximum winds are shown in Fig. 2.3. Figure 2.4 shows the evolution of the areal-averaged precipitation within 400 km of the storm center for the control simulation and two selected tests (analyzed in Sections 2.5.4 and 2.5.5).

### 2.5.1 Northern Trough Removal

The mid-level trough contains two separate  $PV'$  maxima (Fig. 2.13b). For the initial conditions in this test, the more northerly anomaly (C) is removed using the parameters listed in Table 2.1. The inverted results of this modification can be seen in Fig. 2.14. The center in the 500 hPa trough is the feature which undergoes the greatest change in this case; its height rises 12 dam to a value of 564 dam. However, the north-south amplitude of the 500 hPa wave remains relatively unaffected. Because this “filling” implies the addition of mass at upper levels, surface pressures are increased. Earl’s SLP rises to 1008 hPa, but other low-level fields such as relative humidity and temperature remain almost unchanged. The results from this test compared to the control can thus be viewed as the sensitivity of the reintensification process to the initial depth of the center in the upwind trough.

The first major difference between this test and the control simulation occurs between 12 and 24 hours, when the center fails to accelerate northeastward and instead

slows down (Fig. 2.15). This results in a 24 hour position that is almost 500 km southeast of the control storm's location. This places the surface cyclone directly beneath the same 250 hPa jet streak that enhanced the control run intensification when the low center was located below the favorable left exit region (Fig. 2.7). The warm core structure of the storm is similar to the control until 18 hours into the simulation; however, strong vertical wind shear associated with the jet aloft acts to tilt the core downstream. Before the midpoint of the integration, the strong upper level flow has entirely sheared off the top of the storm. This results in a deep layer of potential instability as the cold air in the jet overlies the tropical air retained at low levels. Although the release of this potential instability by large-scale vertical motion contributes to development, the weakened upper-level forcing produces a central pressure drop to only 990 hPa after 24 hours, as opposed to 976 hPa in the control. The resulting weak low-level circulation (mean winds are below  $14 \text{ m s}^{-1}$ ) produces significantly less deformation in the baroclinic zone and much poorer organization of the regenerating system.

The surface cyclone continues to move too slowly northeastward after the midpoint of the integration. However the trough, whose wavelength has not been altered, maintains the same phase speed as in the control. This leads to an interaction between the surface center and the trough that is similar to the control, but delayed by six hours. As a result, the storm does not reach its peak intensity until 45 hours into the simulation (Figs. 2.16b and 2.17b). The system never develops a well-defined warm core and the LLJ is weaker, allowing for more interaction between the storm center and its environment. The position of the cyclone near the left exit of a southwesterly 250 hPa jet at 42 hours (not shown) enhances its intensification at later stages. The lack of effective phase-lock with the trough, as evidenced by the reduced deepening at 500 hPa (Fig. 2.3b), is enough to reduce the maximum intensity of the storm to a SLP of only 967 hPa. However, the storm does produce peak winds of over  $35 \text{ m s}^{-1}$  at the surface, stronger than those observed in the control (Fig. 2.3d).

The weakened center in the upper level trough combined with the delayed move-

ment of the surface vortex to produce a less intense storm than in the control. Although a warm core developed, it was short-lived as penetration from the cooler surroundings were not suppressed at low levels and strong vertical shear acted to destroy its structure. The delay in trough interaction and the lack of phase-lock resulted in a weakened reintensification that occurred six hours later than in the control. Although the depth of the center in the 500 hPa trough influenced the structure and timing of the regeneration, it played only a secondary role in determining the final intensity of the system, which was only 12 hPa weaker than that observed in the control and contained very strong winds.

### 2.5.2 Southern Trough Removal

Table 2.1 gives details of how the southern trough anomaly shown in Fig. 2.13b (labeled B) was removed from the initial conditions. The resulting inversion has a greater effect on Earl and its surroundings than did the modifications in the previous case (see Fig. 2.14). The surface pressure of the hurricane's remnants increases from 1004 to 1010 hPa, and the baroclinic zone is weakened, particularly at high latitudes. The amplitude of the 500 hPa trough is significantly reduced while its center rises only 6 dam. The results from this initialization may thus be interpreted as a prognosis of what would have occurred had the amplitude of the 500 hPa wave been significantly smaller.

A secondary surface vortex appears during the first three hours of the integration, spinning up 700 km east-northeast of Earl, similar to the secondary cyclogenesis observed by Carrera et al. (1999). As in the previous case, the progression of Earl's center is slowed, an effect which is enhanced by the low-level circulation induced by the developing secondary cyclone. After 18 hours, three separate vortices are present, aligned northeast-southwest along the track of the storm in the control. The hurricane's remnants form the southern center, but it is the northern one that experiences the strongest cyclogenesis. After 24 hours, the location of the secondary system is almost identical to that of the control storm, and the same favorable jet

structure as shown in Fig. 2.7 plays an active role in its intensification. A warm core is found to be present over the first 24 hours, but its location directly beneath the jet maximum results in the destruction of the center's structure by a similar mechanism to that discussed in the previous section. By 24 hours, the mean winds around the cyclone reach only  $12 \text{ m s}^{-1}$ , significantly weaker than the  $17 \text{ m s}^{-1}$  surface winds observed in the control.

The 500 hPa center, which deepened only 5 dam over the first 24 hours, continues to intensify slowly during the last half of the integration. The weak low level circulation results in reduced deformation of the baroclinic zone, less frontogenesis, and the virtual non-existence of any hook structure or dry slot. Again, the surface cyclone is displaced to the east of its position in the control, leading to a delay in deepening as described in the previous case. The system reaches its maximum intensity at 45 hours (Figs. 2.16c, and 2.17c), with a central pressure of 977 hPa and maximum windspeeds of  $29 \text{ m s}^{-1}$ .

The reintensification of the storm in this case was very different from that of the control simulation. A secondary vortex was favored for cyclogenesis as the hurricane's remnants were destroyed by strong vertical wind shear. With a lowest SLP of 977 hPa and a reduced extratropical structure, the storm in this case was significantly weaker than in the control. We conclude that the amplitude of the 500 hPa wave played an important role in determining the nature of Earl's redevelopment.

### 2.5.3 Upper Trough Removal

The  $PV'$  maximum removed from the initial conditions in this case appears only above 250 hPa (Fig. 2.13a). Table 2.1 summarizes the removal parameters. The impact of the inversion is the smallest of any of the tests; however, it is enough to raise Earl's SLP 4 hPa to 1008 hPa, and the trough's central height 4 dam to 556 dam (Fig. 2.14). This test may be interpreted as the prognosis for an atmosphere that does not contain unusually large PV above the 500 hPa trough. It must be emphasized that it is only the  $PV'$  that is removed, so the stratosphere may still act as a PV

source in this case.

The reduced PV aloft decreases both the intensity and the deepening rate of the 500 hPa trough during the first half of the integration. The resulting weak mid-level flow may thus be responsible for the retardation of Earl along its track. This slowed movement of the surface cyclone results in a 24 hour position that is 250 km south of the storm's location in the control simulation. Thus, the jet arrangement, which is similar to that of the control, does not appreciably enhance the reintensification of the system. As a result, the storm at 24 hours is poorly organized and the temperature gradients across the fronts are reduced.

The trough begins its intensification three to six hours later than in the control, probably due to the reduced stratospheric PV source. The storm in this case continues along a northeastward track at a relatively constant speed as opposed to the system in the control which slows appreciably north of Newfoundland. The result is again a six hour delay in maximum intensity, represented by a minimum SLP of 962 hPa at 45 hours (Figs. 2.16d, and 2.17d), with maximum winds of  $33 \text{ m s}^{-1}$  near the surface.

The removal of the anomalous upper-level PV resulted in a slightly weaker 500 hPa center and a decreased mid-level flow intensity. This reduced the propagation speed of the surface cyclone and delayed phase-lock by six hours. Other than this delay, the resulting system was very similar to that produced in the control simulation.

#### 2.5.4 Full Trough Removal

This section examines the results obtained following the removal of all  $PV'$  associated with the 500 hPa trough over Quebec. All three anomalies discussed previously are deleted from the initial conditions (see Table 2.1 and Fig. 2.13 for details). This results in a primarily zonal flow aloft, although a weak trough persists due to its presence in the 18 day mean. Surface pressures are significantly increased because of the large amounts of mass added at upper levels. For example, Earl's minimum SLP rises to 1014 hPa in the initialization for this case (Fig. 2.14).

The westerly flow above the hurricane's remnants results in the slow propagation

of the center along a significantly more easterly track than in the control. A secondary cyclone appears 500 km east-northeast of Earl after six hours. The modifications to the upper level flow result in a single, weak jet maximum overlying both surface centers at 24 hours which has a negative impact on their intensification. By 24 hours, the tropical cyclone has a SLP of 1000 hPa, while the secondary (northern) center has deepened to 1001 hPa. The mean windspeeds near the surface have increased by only  $1 \text{ m s}^{-1}$  since the initialization (Fig. 2.3). No organized structures can be attributed to either vortex.

The surface signature of the secondary cyclone persists until 33 hours, at which time it weakens and leaves a single center elongated in a northeasterly direction. Deformation of the baroclinic zone is minimal owing to the weak flow at low levels (maximum winds never reach  $20 \text{ m s}^{-1}$ ) and no hook structure or dry intrusion is seen at any stage. After 45 hours of simulation, Earl's central pressure is only 990 hPa (Fig. 2.17e), and little indication of further deepening is observed. Mean precipitation accumulations have leveled off at just over  $2 \text{ mm (6 h)}^{-1}$ , with stratiform and convective sources contributing about equally to this value (Fig. 2.4b). No significant regeneration of the 500 hPa trough is noted (Fig. 2.16e), and the final location of the surface cyclone is 600 km south of its position in the control run.

Without the support of the trough's cyclogenetic forcing in this case, Earl never developed into an organized extratropical system. We therefore conclude that the existence of the upstream trough was critical for Earl's reintensification.

A series of plots showing PV on the 325 K surface (Fig. 2.18) highlight the difference in the evolution of this case as compared to the control (Fig. 2.11). Instead of a reduction in the meridional extent of the PV "trough" and its eventual cyclonic wrapping, this simulation produces an increase in the north-south amplitude of the remaining PV maximum. Panel (d) of Fig. 2.18 shows the beginnings of anticyclonic rotation in the base of the PV "trough" as it moves to the equatorward side of the jet. Unfortunately, boundary contamination influences the PV maximum in the 48 hour output; however, the development in this case is similar to the LC1 type baroclinic

generation proposed by Thorncroft et al. (1993) in which anticyclonic Rossby wave breaking and a cutoff PV maximum lead to weak cyclogenesis over the time-scales considered in this study.

### 2.5.5 Hurricane Earl Removal

Removal of Earl's dynamical structure from the initial conditions allows for a quantification of the importance of the dynamics of the hurricane's remnants to cyclogenesis ahead of the upstream trough. The results of the previous section hint that the mid-level trough is a necessary condition for deepening, and an ideal sensitivity test would determine whether it also represents a sufficient condition. This conclusion would result from the generation of an intense storm in spite of the complete removal (dynamic and thermodynamic) of Hurricane Earl's remnants from the initial conditions. Since the PV inversion that we employ for the removal modifies only the dry dynamical variables, the interpretation of this test is somewhat complicated. This simulation can at most lead to the conclusion that the trough is a sufficient condition given the pool of moist air left over from the vortex removal, which may play a role in rapid intensification (Bosart and Lackmann 1995). As noted in Section 2.6, we are currently working on a way to deconvolve the influences of these features through dynamically consistent water vapour removal. Removal of the  $PV'$  field associated with Earl was undertaken as outlined in Table 2.1 and Fig. 2.13c. Fig. 2.14 shows the initial conditions for this test. No sign of the ex-hurricane's dynamics remains, and yet the depth and amplitude of the 500 hPa trough remain almost unchanged.

A surface pressure minimum initially over central Quebec builds slowly eastward ahead of the 500 hPa trough axis during the first 24 hours of the simulation. Upper level CVA appears to be the primary cyclogenetic forcing over the period although the surface cyclone remains weak, reaching a SLP of 997 hPa at 24 hours. Mean winds, however, have increased dramatically from under  $4 \text{ m s}^{-1}$  in the initialization to almost  $13 \text{ m s}^{-1}$  (Fig. 2.3). The storm's position at this time is almost identical to that of the center in the control, placing it in the favored ascent region of 250 hPa jets

very similar to those of Fig. 2.7. The trough does not deepen between 18 and 24 hours (Fig. 2.3b) as it did in the control, presumably because it depends on interaction with Earl's high values of lower-tropospheric PV for such rapid intensification. Although the surface cyclone remains relatively weak until 24 hours, deformation of the baroclinic zone and increasing precipitation accumulations (Fig. 2.4c) indicate that it is beginning to tap into the same moisture source that enhanced Earl's reintensification.

Latent heat release fuels an increase in PV near the cyclone center as convective precipitation reaches its maximum shortly after 00/06. Although weak LLJ structures emerge near the end of the integration, the core's circulation never becomes as active as in the control case. However, the increase in low level PV seems to initiate a slight deepening in the 500 hPa trough which then feeds back to the surface cyclone in the form of enhanced vorticity advection. The surface center stalls 400 km off the east coast of Newfoundland after 36 hours, initially leading to a favorable upstream tilt in the system. Intensification continues until 45 hours, when the trough overruns the cyclone to produce a downshear tilt. The structure of the system at 45 hours is shown in Figs. 2.16f and 2.17f, and is similar to that of the storm in the control, though less intense. The maximum windspeeds in the storm are  $27 \text{ m s}^{-1}$ , compared with just over  $33 \text{ m s}^{-1}$  in the control (Fig. 2.3d). A hook structure is observed (not shown), and the 500 hPa vorticity wraps almost completely around the center at mid-levels.

The evolution of PV on the 325 K surface (Fig. 2.19) in this case is very similar to that of the control simulation (Fig. 2.11). The PV maximum, slightly reduced due to the PV' removal and inversion, moves eastward from Quebec (panels (a) through (c)) and wraps cyclonically over the surface low pressure center between 36 and 48 hours (panels (d) and (e)). The low level baroclinicity of the system is slightly weakened from that of the control, and the wrapping is delayed by 6 hours; however, the dynamics of the development in this simulation are very similar to those of the control.

With the low level circulation of the hurricane's remnants removed, a surface center from Quebec built eastward ahead of the trough to lie in the same favorable

jet-forced ascent region as Earl did in the control. Through condensation, low level PV was generated during the latter half of the integration and produced a coupling with the PV in the 500 hPa wave. A relatively structured and intense storm was induced in a location very similar to that of Earl in the control. We can therefore conclude that the dry dynamics of Hurricane Earl are not crucial to the development of an intense storm over Newfoundland on 6-7 September 1998. To consider the mid-level trough alone to be a sufficient condition for cyclogenesis would be somewhat of an overstatement. The cyclogenetic forcings of the trough and of the moist pool left over from the vortex removal must be individually quantified before such a conclusion may be drawn. However, the results presented here suggest that the hurricane circulation plays only a secondary role in reintensification in this case.

## 2.6 Summary and Discussion

A modeling study of the extratropical transition of Hurricane Earl (September, 1998) is carried out with the objective of determining the sensitivity of the reintensification process to the modification of initial conditions. In particular, it is hoped that a quantification of the relative importance of individual PV features in the initial fields will aid in the operational forecasting of these potentially dangerous and damaging events.

The MC2 model is initialized at 00/05 as ex-hurricane Earl is weakening 350 km off the New Jersey coast. Prominent synoptic features in the initial conditions include a large-amplitude 500 hPa trough containing a local height minimum over Quebec, and a strong baroclinic zone along the eastern seaboard. CVA at upper levels initiates the reintensification process and interaction with the baroclinic zone results in warm advection and large-scale ascent throughout the regenerating system. The energy contained within the moist tropical air near the cyclone's center is released through convection and allows Earl to maintain its warm core structure. Rapid deepening of the 500 hPa height minimum indicates the establishment of phase-lock with the low-level PV maximum as the system reaches its most intense state at 15/06 with a

SLP of 956 hPa and maximum surface winds over  $33 \text{ ms}^{-1}$ . Although the large-scale structure of the storm is purely extratropical, the persistent warm core testifies to its tropical origin as do its large convective precipitation accumulations. Similar results were obtained by Browning et al. (1998) in their study of ex-hurricane Lili. From a PV-theta perspective, the evolution of the storm is reminiscent of the LC2 type baroclinic development proposed by Thorncroft et al. (1993) in which the cyclonic wrapping of PV leads to the rapid development of an intense surface cyclone.

Using a piecewise PV inversion scheme developed by Davis (1992b), we modify the initial conditions and rebalance the fields. Four separate  $PV'$  maxima were identified in the 00/05 analysis: two in the mid level trough over Quebec, one near the tropopause in the same area, and one at low levels associated with the hurricane's remnants. Each of these is eliminated in turn, the fields rebalanced, and the model rerun to assess the impact of the removed feature on the storm's reintensification.

Removal of the northern trough PV anomaly results in a weakened center in the 500 hPa trough. The decreased speed of the mid level flow slows Earl's propagation and positions it beneath a 250 hPa jet maximum midway through the integration. The top of the warm core is sheared off by the strong winds, resulting in a deep layer of conditional instability. CVA from the upstream trough forces enough ascent to trigger convection, resulting in a minimum SLP of 967 hPa.

A significantly reduced amplitude of the 500 hPa wave is the result of the southern trough anomaly's removal. The zonal flow enhances Earl's eastward propagation and a secondary vortex appears northeast of the tropical center almost immediately. By 00/06, Earl is positioned below the same 250 hPa jet as in the previous case, but the secondary cyclone is located in its favorable left exit region. Rapid cyclogenesis follows and the formation of a warm core is observed in the secondary center. The central pressure of the newly formed system drops to 977 hPa after 45 hours of simulation.

Removal of the upper trough anomaly has very little effect on the reintensification, except to delay the deepening of the 500 hPa center. With decreased upper level

support, the minimum surface pressure in this case is 962 hPa.

When all three trough  $PV'$  anomalies are removed simultaneously, the result is a weak, zonal flow at middle and upper levels. Without CVA forcing, the cyclone's reintensification is driven by interaction with the baroclinic zone and latent heat release. However, deformation is minimal because of the weak winds (always less than  $20 \text{ m s}^{-1}$ ) around the cyclone, and frontal features are almost nonexistent. No regeneration of the 500 hPa trough is observed, and the minimum SLP of the system is only 989 hPa in this case.

Removing the  $PV'$  associated with the hurricane's remnants results in a very different scenario. A small surface cyclone initially over Quebec propagates eastward in front of the trough to lie in a 00/06 position which is almost identical to the location of Earl in the control simulation. Tapping into the moisture that remains in the initial conditions, the storm deepens rapidly over the last 24 hours of the integration. In spite of the removal of the hurricane's dynamics, the SLP of the system at 00/07 is 975 hPa, and winds of almost  $27 \text{ m s}^{-1}$  develop. Work is currently in progress that will provide a means for the consistent removal of the moisture associated with the hurricane's remnant. This will allow for an investigation into the relative importance of the decaying storm's dynamics and thermodynamics to the generation of a system during the integration, and will be the subject of a future paper.

These results serve as an indication of what might have occurred had the removed  $PV'$  maxima - and associated flow characteristics - not been present in the initial conditions. Comparison of the resulting simulations yields insight into the influence of each anomaly on the reintensification process. The presence of the 500 hPa trough seems to be of primary importance to the redevelopment, and its amplitude plays a significant role in determining the strength of the resulting storm. The depth of the 500 hPa center is of secondary importance, while the existence of an upper level (above 250 hPa)  $PV'$  maximum is of minimal consequence. Most surprising, perhaps, is the result that the lower-level dynamics of the hurricane itself are not crucial to the intensification. These results may serve as intuitive guidelines to improve the

predictability of future extratropical transition and reintensification events.

## **Acknowledgments**

We thank the members of the Mesoscale Research Group (McGill University) for their guidance and support throughout the course of this research. As well, we thank the Sarah Jones and the two other anonymous reviewers for their help in preparing this paper for publication. This work has been supported by Natural Sciences and Engineering Research Council grants and by subventions from the Meteorological Service of Canada.

## 2.7 Appendix: Model Settings and Parameters

The settings used for the MC2 integrations are as follows:

- polar stereographic projection valid at 60°N;
- 150 × 175 gridpoint domain with 35 km resolution as shown in figures;
- 35 Gal-Chen and Sommerville (1975) evenly-spaced computational levels with a rigid lid at 35 km;
- 10 gridpoint nesting in the horizontal and a 7 km sponge at the top boundary;
- 360 s timestep with no dynamic initialization; and,
- radiation evaluated every 1800 s.

t Name	Shape	Center Coordinates		Semi-Axis Length		Levels (hPa)
		Latitude	Longitude	$x$ (km)	$y$ (km)	
NTR	semi-ellipse	59°N	63°W	1225	1400	400 → 250
STR	circle	44°N	75°W	525	525	500 → 250
UTR	ellipse	50°N	71°W	560	770	250 → 50
TR	semi-ellipse	59°N	63°W	1225	1400	400 → 250
	circle	44°N	75°W	525	525	500 → 250
	ellipse	50°N	71°W	560	770	250 → 50
EARL	ellipse	35°N	70°W	910	1225	925 → 500

Figure 2.1: Removal parameters for tests as indicated. Acronyms are defined in caption for Fig. 2.3.

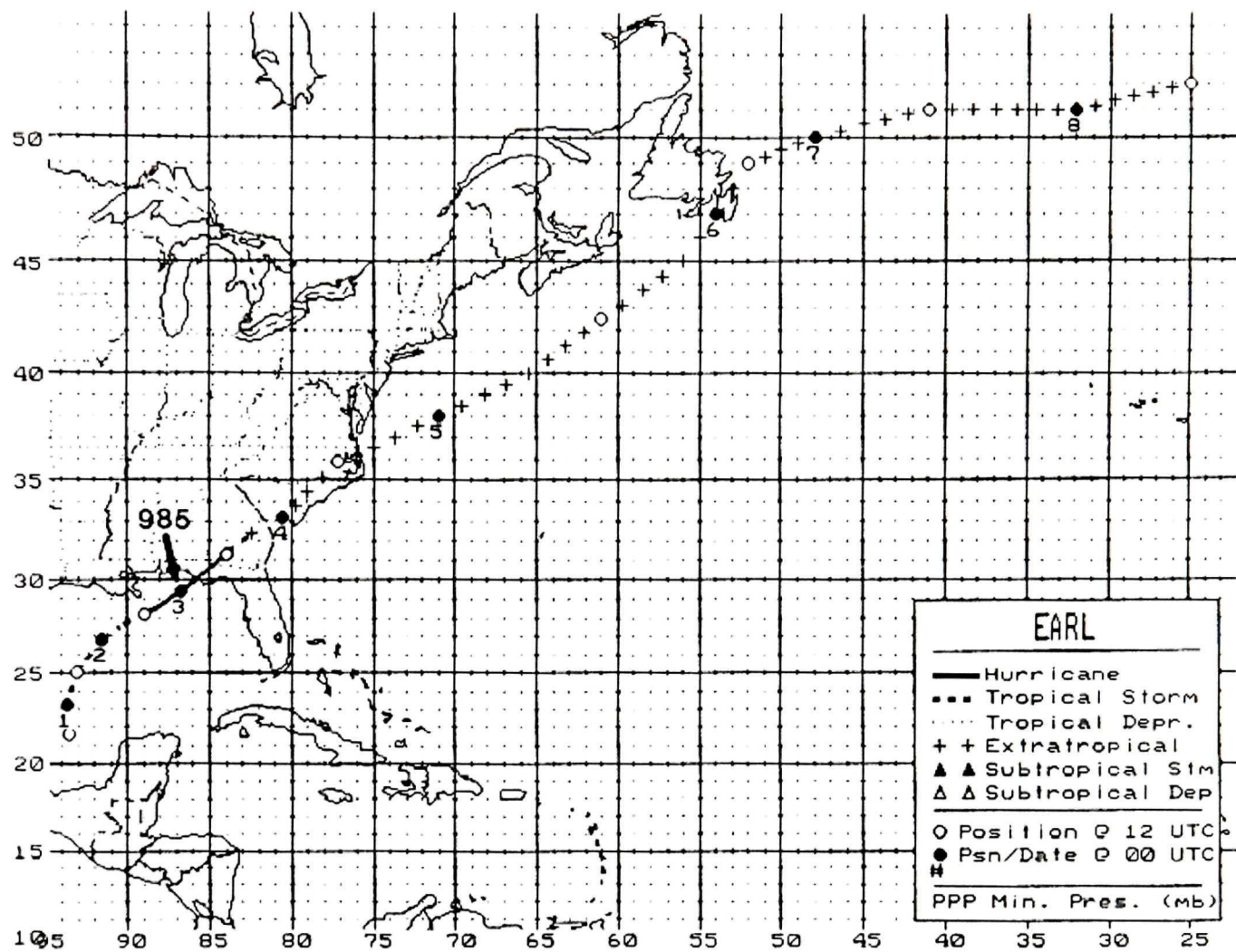


Figure 2.1: National Hurricane Center (NHC) best track for Hurricane Earl. Plotting starts 1200 UTC 31 August in the Gulf of Mexico and ends 1200 UTC 8 September in the North Atlantic. Closed and open circles indicate 0000 UTC and 1200 UTC positions respectively.

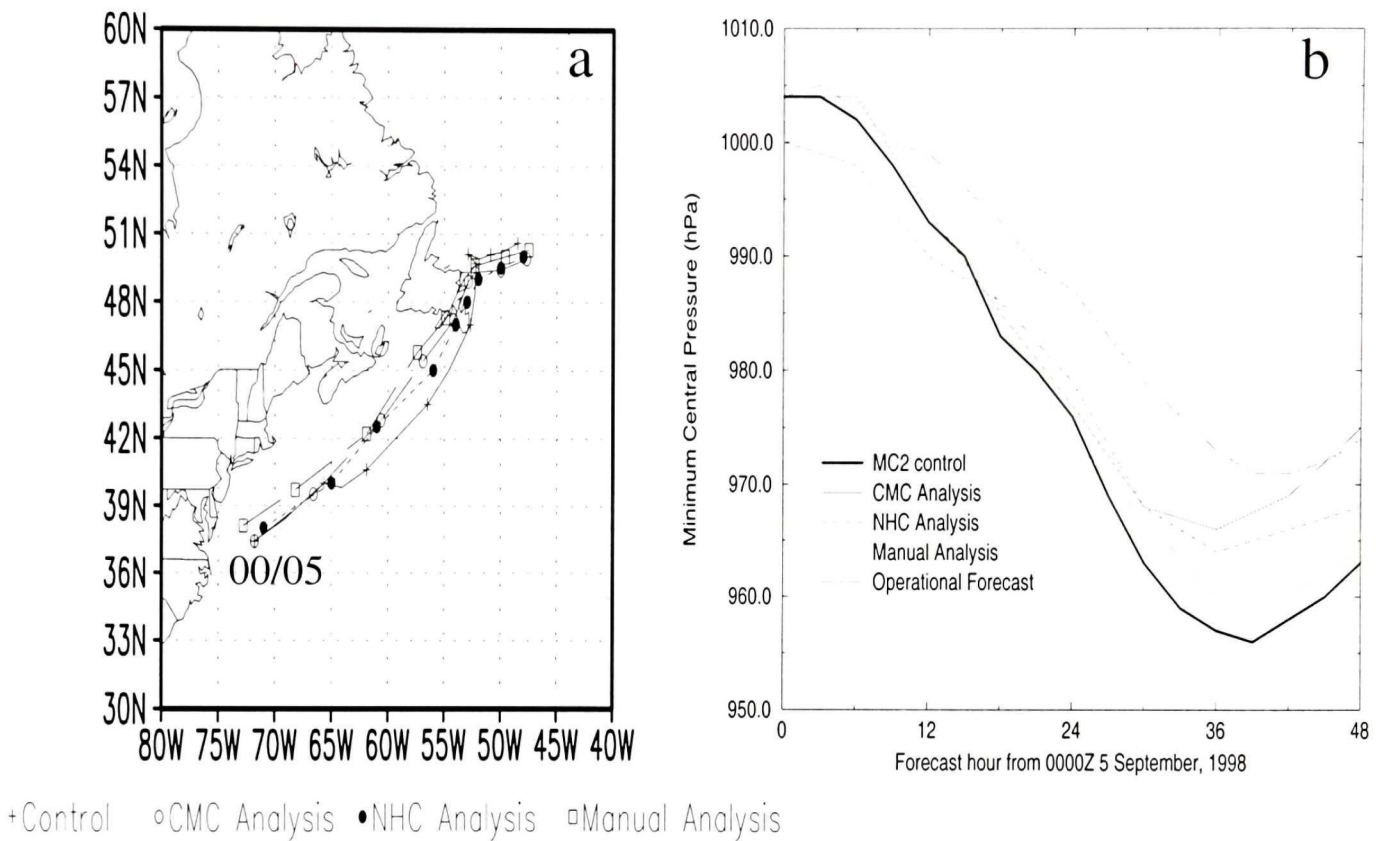


Figure 2.2: Comparison of storm tracks (a) and central pressures (b) with operational analyses. The pressure trace for the operational forecast is also shown in (b). Storm center locations are plotted every six hours in (a), beginning at 0000 UTC 5 September as indicated. Manual analyses were performed at the Maritimes Weather Centre in Dartmouth, Nova Scotia.

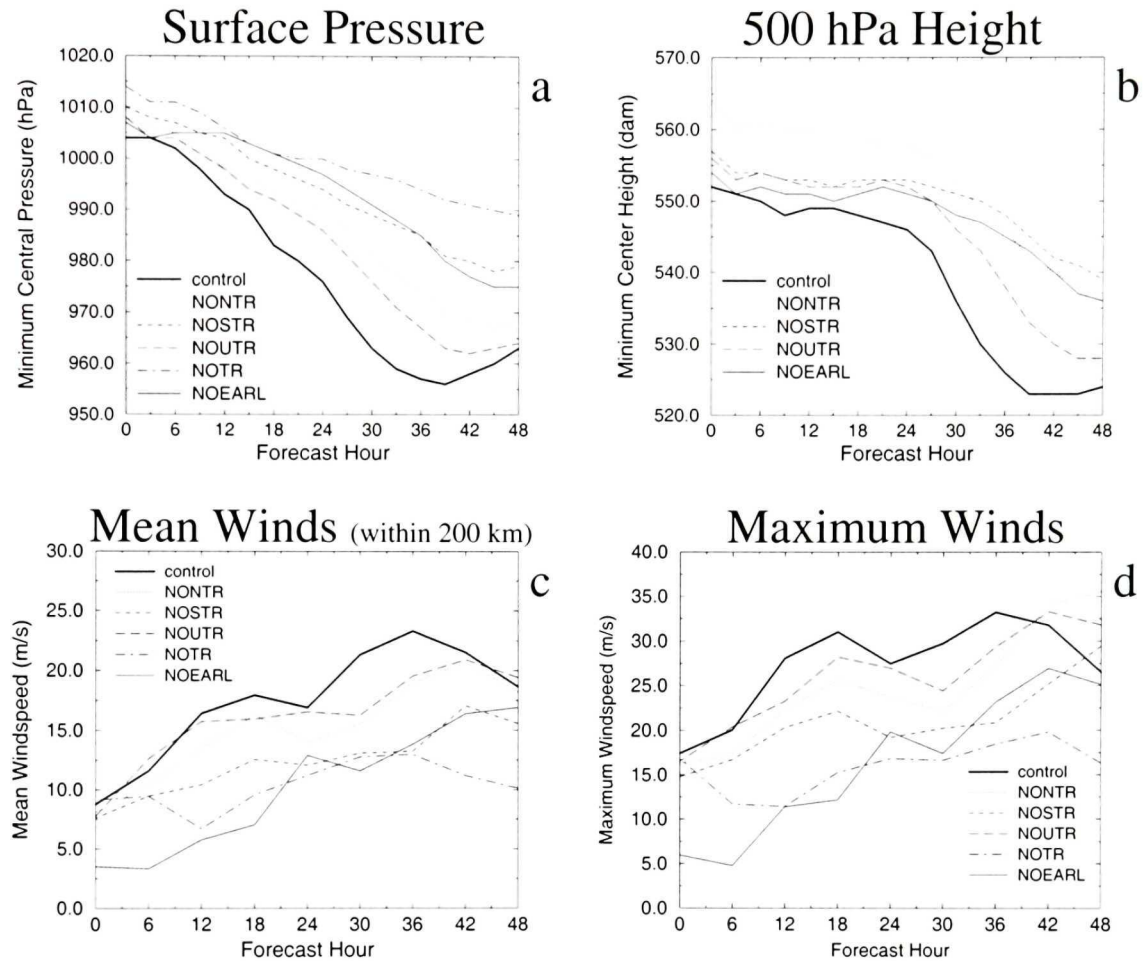


Figure 2.3: Time series of minimum SLP in hPa (a), 500 hPa center height in dam (b), mean winds within a 200 km radius of the storm center as defined by the central pressure minimum (c), and maximum winds in  $\text{m s}^{-1}$  (d). NONTR - northern trough removal (Section 2.5.1). NOSTR - southern trough removal (Section 2.5.2). NOUTR - upper trough removal (Section 2.5.3). NOTR - full trough removal (Section 2.5.4). NOEARL - Hurricane Earl removal (Section 2.5.5).

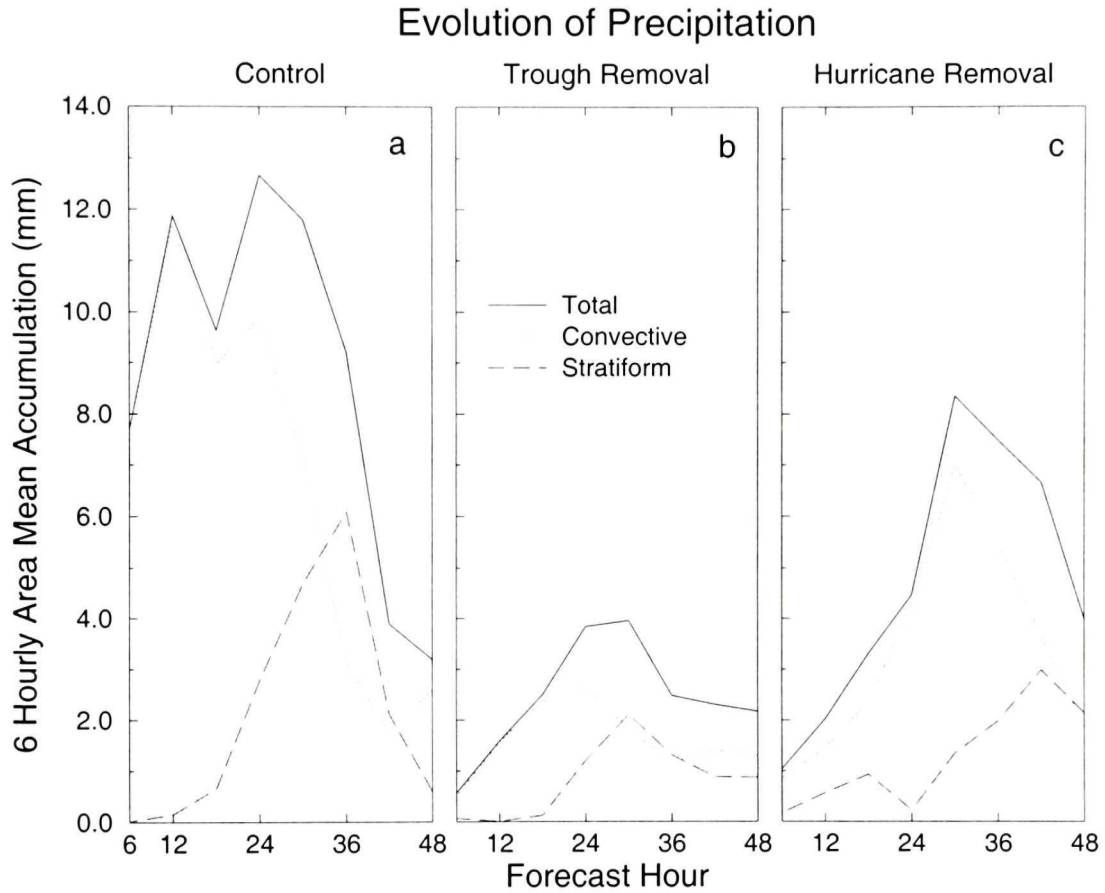


Figure 2.4: Plot of six hourly precipitation accumulations for the control (a), NOTR trough removal (b), and NOEARL Hurricane Earl removal (c) simulations. The mean accumulation is calculated within a 400 km radius of the storm - as defined by the minimum in sea level pressure - and is broken into convective, stratiform, and total (the sum of the first two) precipitation.

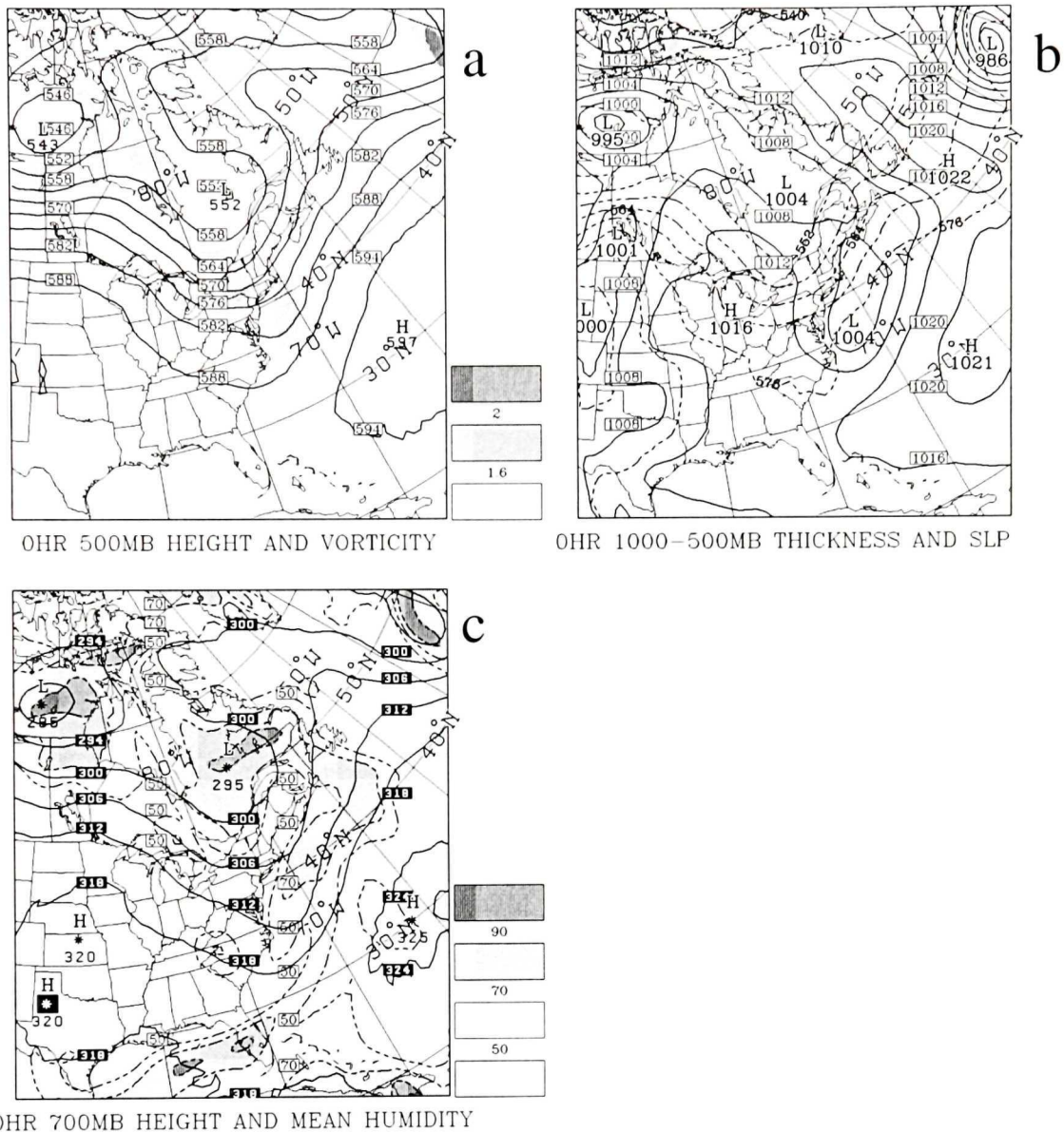


Figure 2.5: Forecast for 00 hour valid 00/05. Panel (a) shows 500 hPa height (solid) in dam, and absolute vorticity field (dashed and shaded) in  $10^{-5} s^{-1}$ . Panel (b) shows surface pressure (solid) and 1000-500 hPa thickness (dashed) in dam. The 534-540 dam height interval is shaded. Panel (c) shows 700 hPa height field (solid) in dam and pressure-weighted mean relative humidity from the 850, 700, and 500 hPa levels. Unless otherwise noted, all maps are plotted using a polar stereographic projection extending from 20°N to 70°N and 30°W to 100°W with meridians and parallels plotted at 10° intervals.

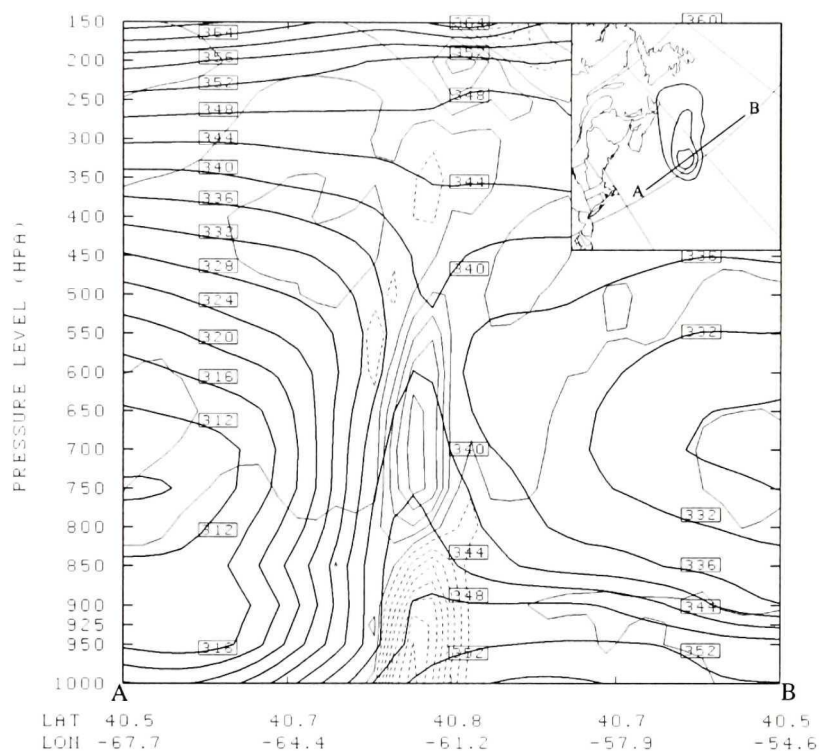


Figure 2.6: Cross-section of equivalent potential temperature (heavy lines) at 4 K intervals, and divergence (light dotted for convergence, light solid for divergence) at  $5 \times 10^{-5} \text{s}^{-1}$  intervals east-west through the storm center at 12/05 as shown in the SLP plot inset (1000, 998 and 996 hPa contours only).

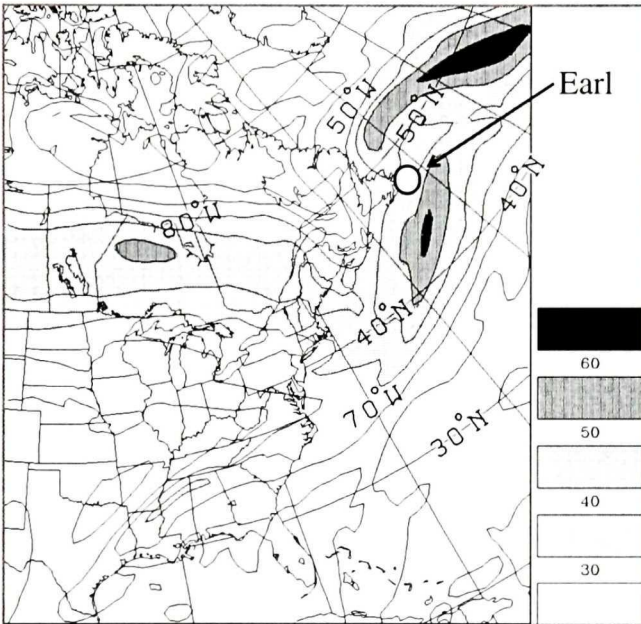


Figure 2.7: Windspeed at 250 hPa in  $\text{m s}^{-1}$  for 00/06. Location of the surface cyclone is indicated.

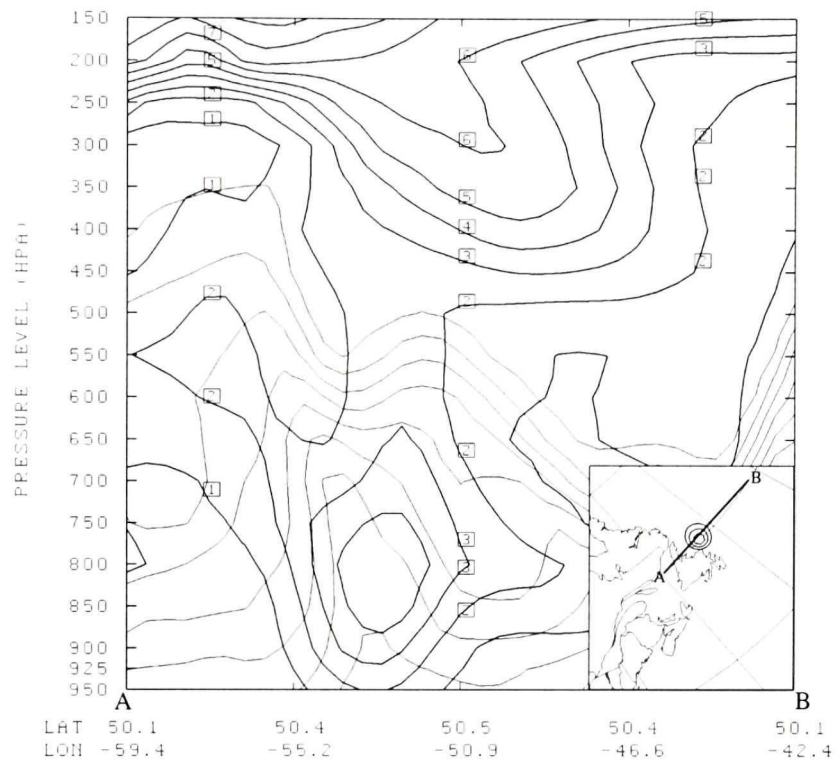


Figure 2.8: Cross-section of PV (heavy lines) valid at 12/06 in 1 PVU increments ( $1 \text{ PVU} = 10^{-6} \text{m}^2 \text{K kg}^{-1} \text{s}^{-1}$ ) and specific humidity (light lines) in  $1 \text{ g kg}^{-1}$  increments, east-west through the storm center as shown in the inset (968, 964, and 960 hPa contours only).

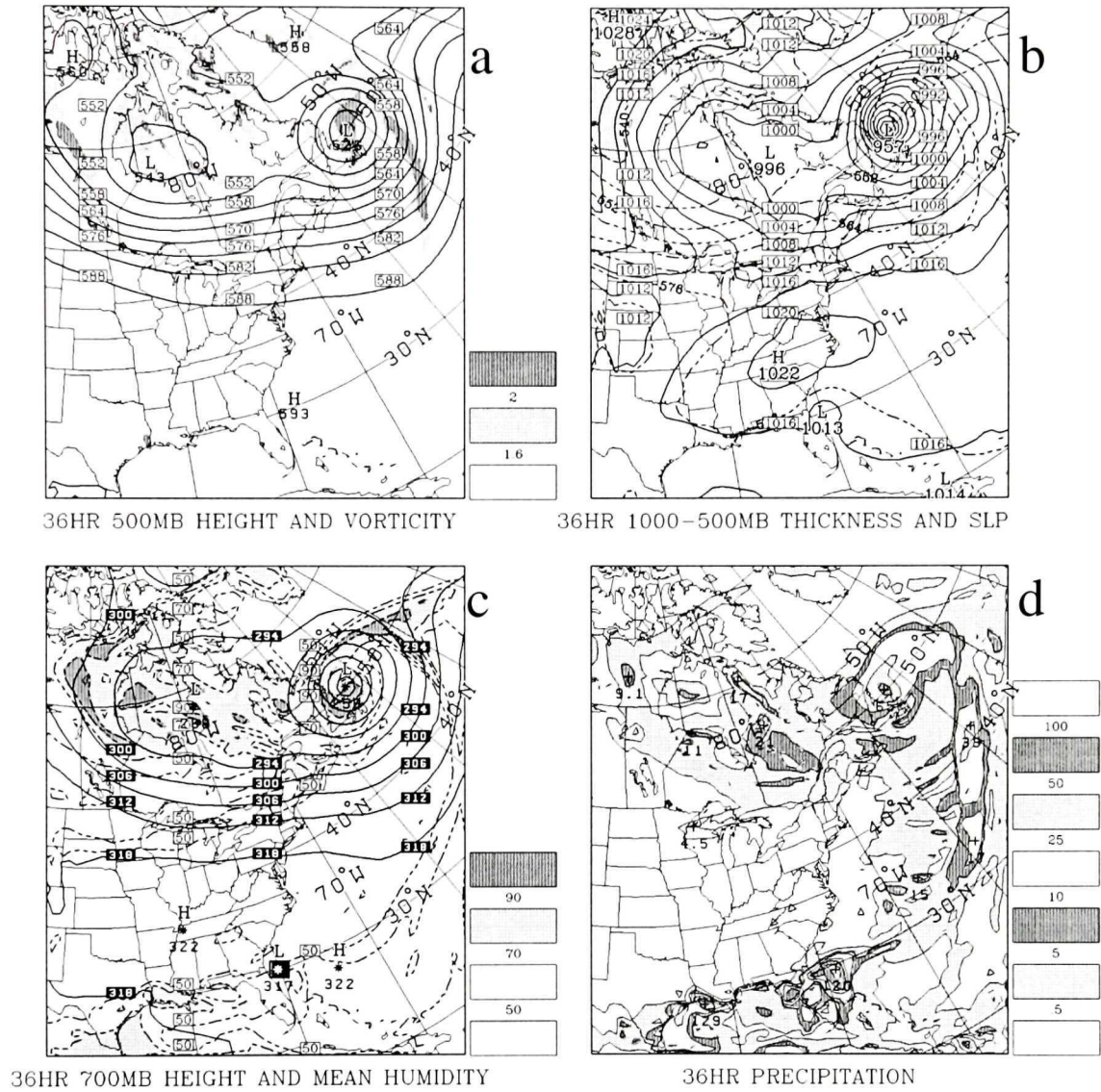


Figure 2.9: Forecast for 36 hours, valid 12/06. All fields as in Fig. 2.5, except for the added panel (d), which shows precipitation (solid lines and shading) in units of  $\text{mm} (6 \text{ h})^{-1}$ .

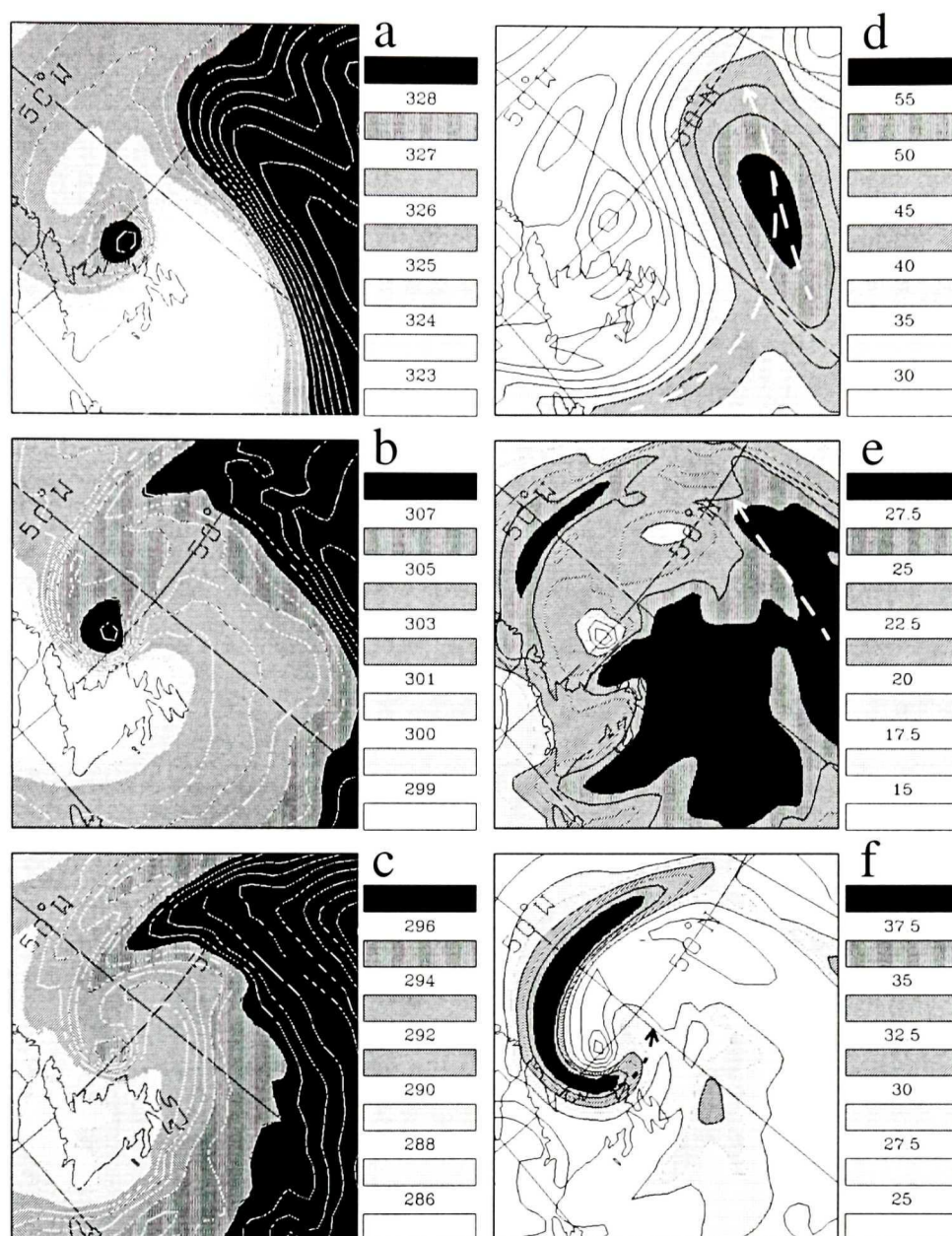


Figure 2.10: Forecasts of 36 hour potential temperature (left column) and windspeed (right column) at 400 (top), 700 (middle), and 850 hPa (bottom) valid 12/06. Dry bulb potential temperatures (left) are contoured at 1 K intervals with darker shading indicating higher temperatures. Windspeeds are displayed using isotachs plotted at  $1 \text{ m s}^{-1}$  intervals, with darker shading for faster windspeeds. Following Browning et al. (1998), the LLJ encircling the warm core at 850 hPa is shown by the dotted curve, and the subpolar jet is represented using a longer dashed line at the 400 and 700 hPa levels.

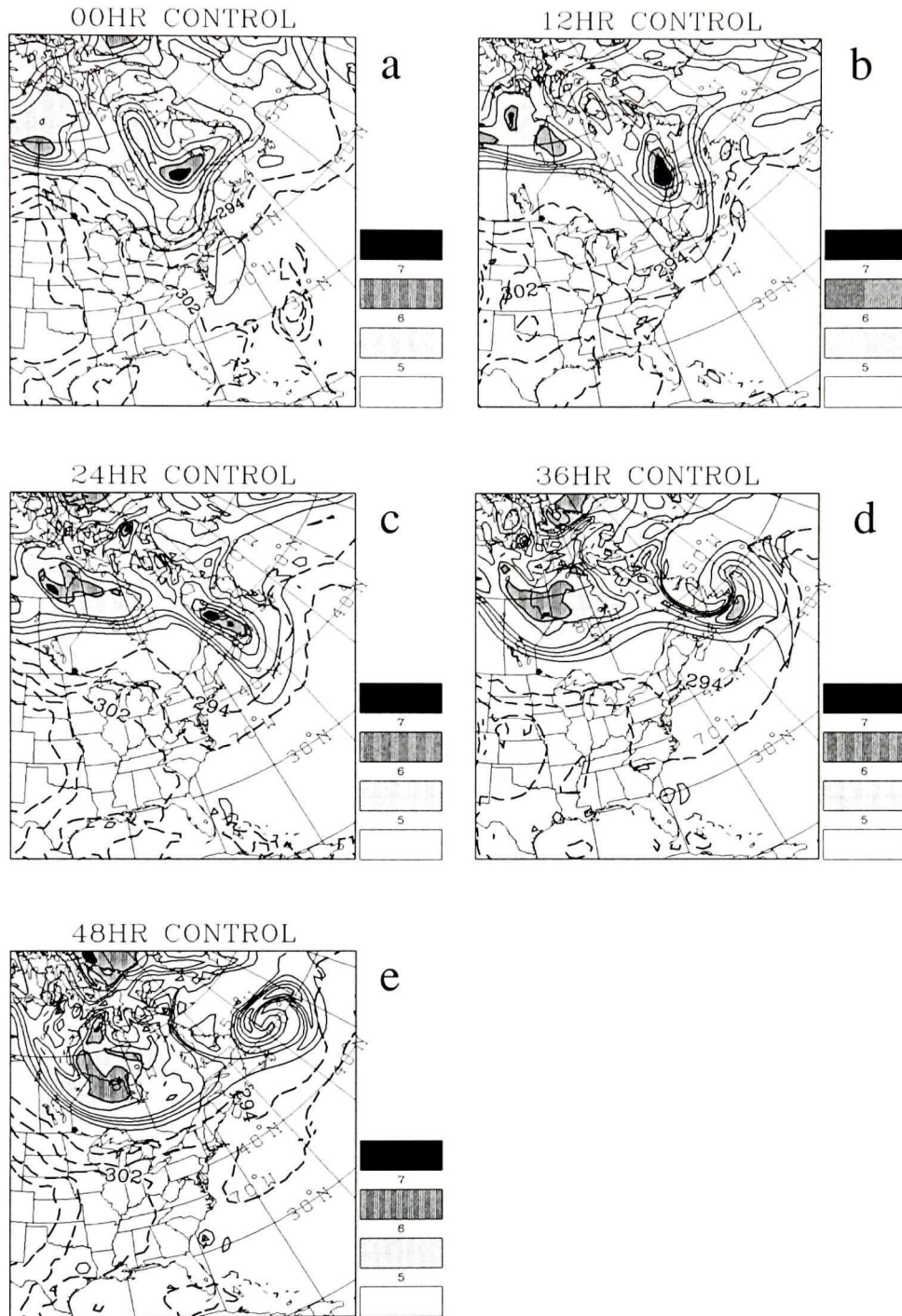


Figure 2.11: Evolution of PV on the 325 K isentropic surface (solid lines, 1 PVU contour interval with shading for high values) and 1000-900 hPa averaged potential temperature (dashed lines, 4 K interval above 294 K). Panels (a) through (e) show the 12 hourly (from 0 through 48 hours) PV and potential temperature fields produced by the control simulation.

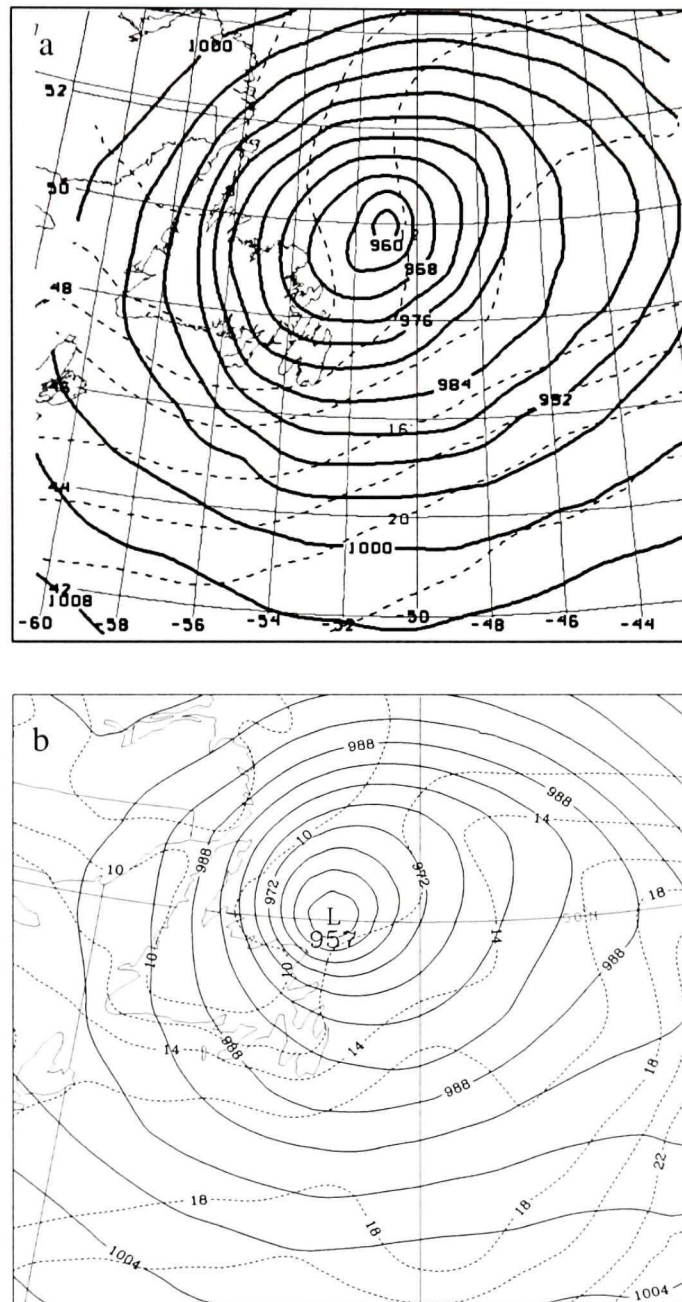


Figure 2.12: Panel (a) shows the manual analysis valid 12/06 as provided by the Maritimes Weather Centre in Dartmouth, Nova Scotia. The equivalent 36 hour control forecast is shown in panel (b). All surface pressures are shown in hPa and are contoured at 4 hPa intervals.

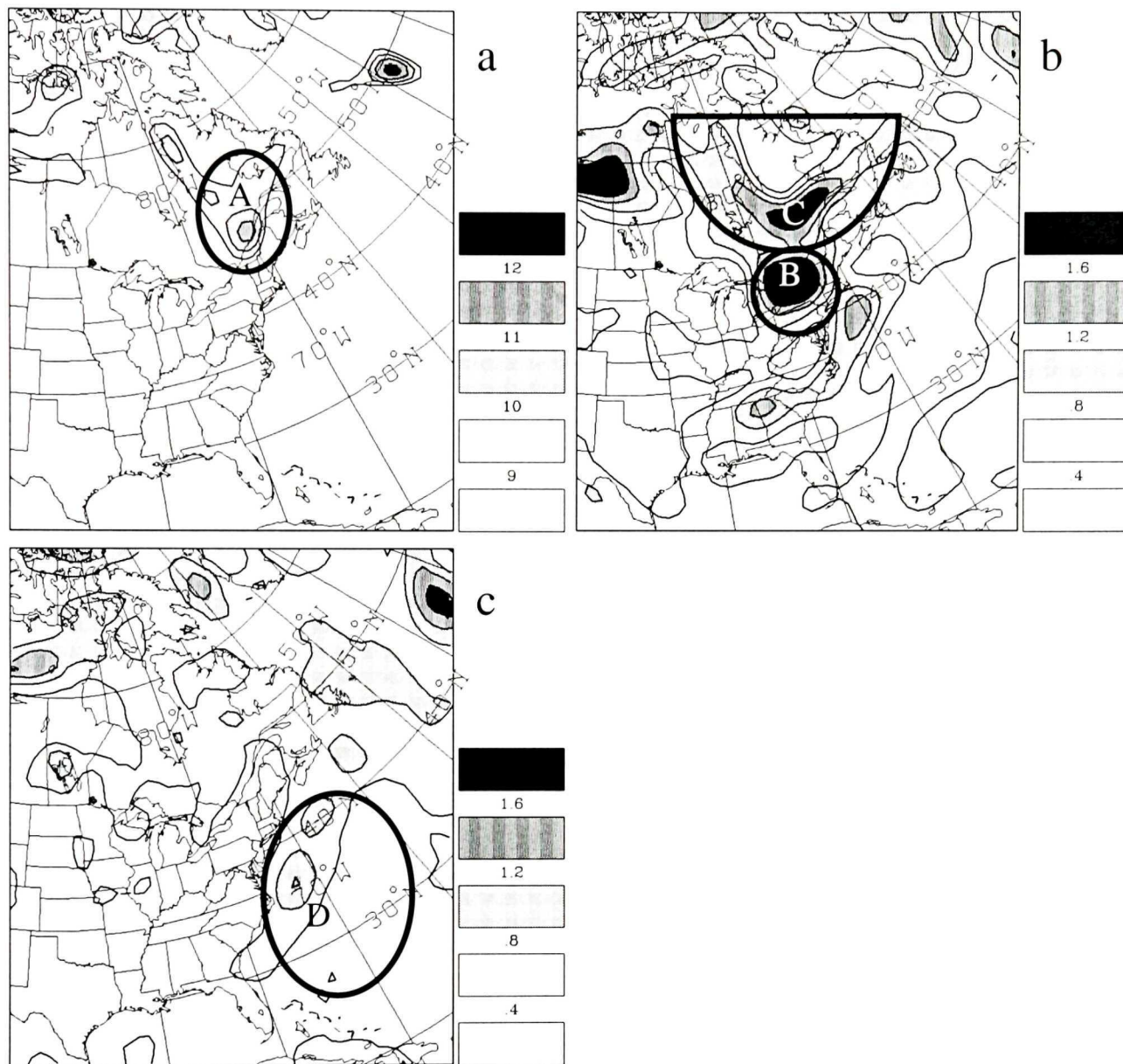


Figure 2.13: PV anomaly fields in PVU at 200 hPa (a), 400 hPa (b), and 850 hPa (c) for initial conditions of control run (00/05). The Upper trough PV anomaly is labeled A, the southern and northern trough PV anomalies are labeled B and C respectively, and Earl's  $PV'$  is labeled D.



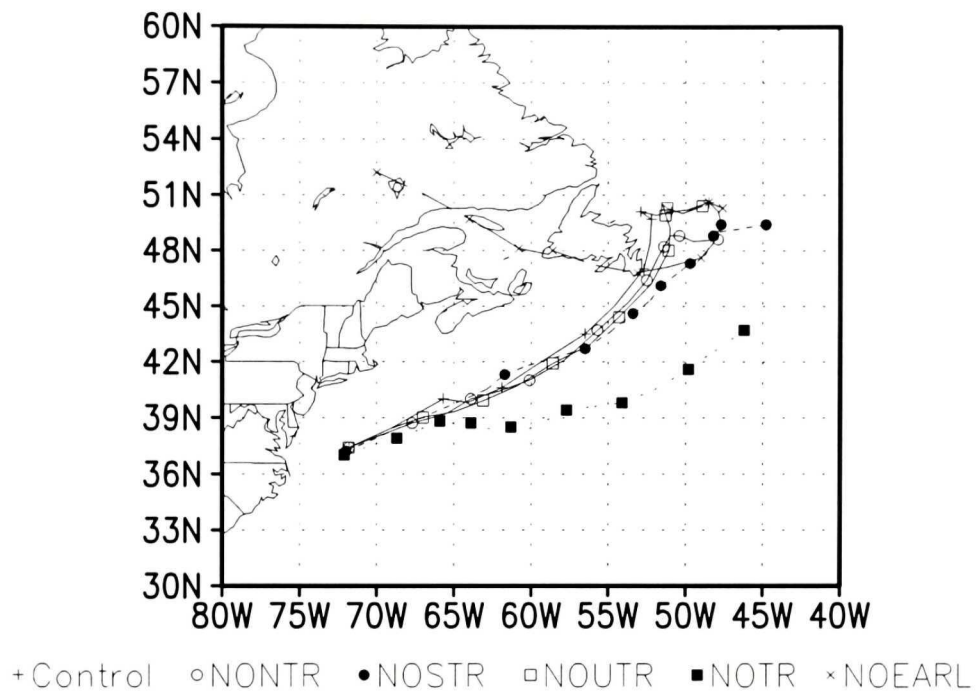


Figure 2.15: Tracks of surface pressure minima for control simulation and sensitivity tests as indicated. Acronyms are defined in caption for Fig. 2.3. The track for the NOEARL case (indicated by the crosses and the dashed line) follows the Quebec cyclone since the hurricane has been removed from these initial conditions.

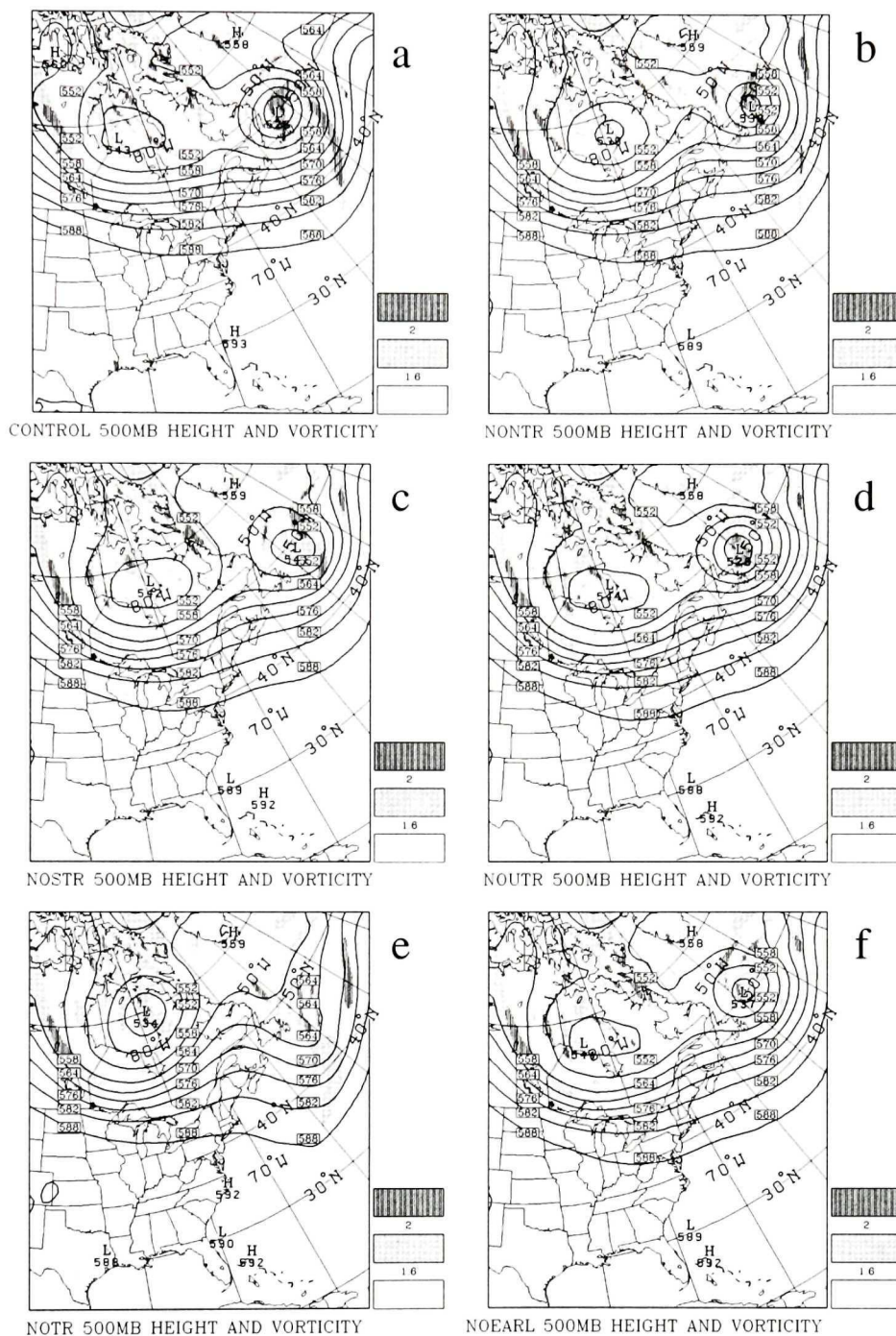


Figure 2.16: Geopotential height (solid lines, 6 dam intervals) and absolute vorticity (shading, units are  $10^{-4} \text{ s}^{-1}$ ) at 500 hPa for (a) control, (b) NONTR, (c) NOSTR, (d) NOUTR, (e) NOTR, and (f) NOEARL. The control plot shows the 36 hour output (valid 12/06), whereas the other panels display 45 hour (valid 21/06) prognoses, reflecting approximately the most intense period of the storm in each case.

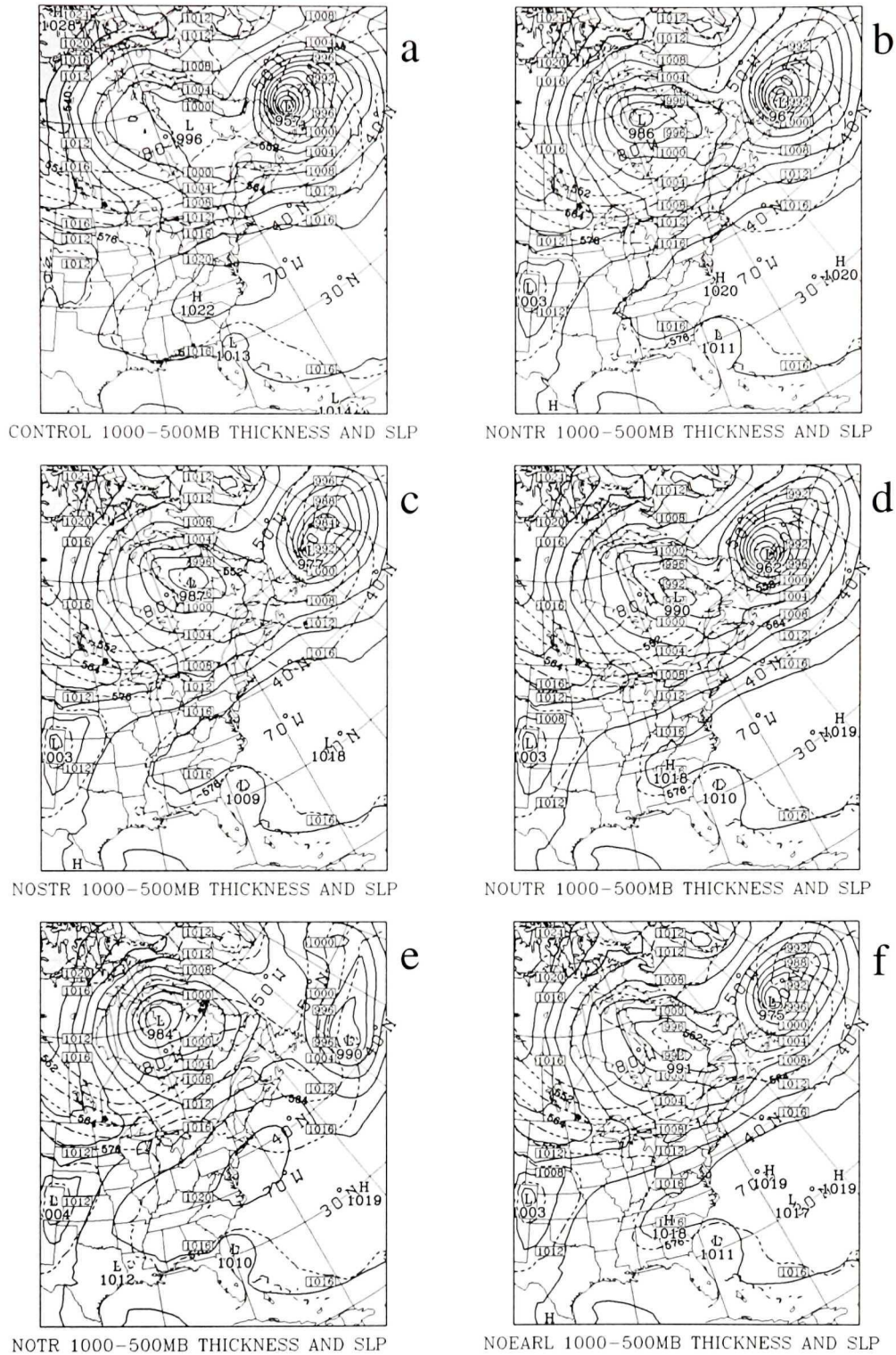


Figure 2.17: Same as in Fig. 2.16 except that the fields shown are sea level pressure (solid lines, 4 hPa contour interval) and 1000-500 hPa thickness (dashed lines, 6 dam contour interval).

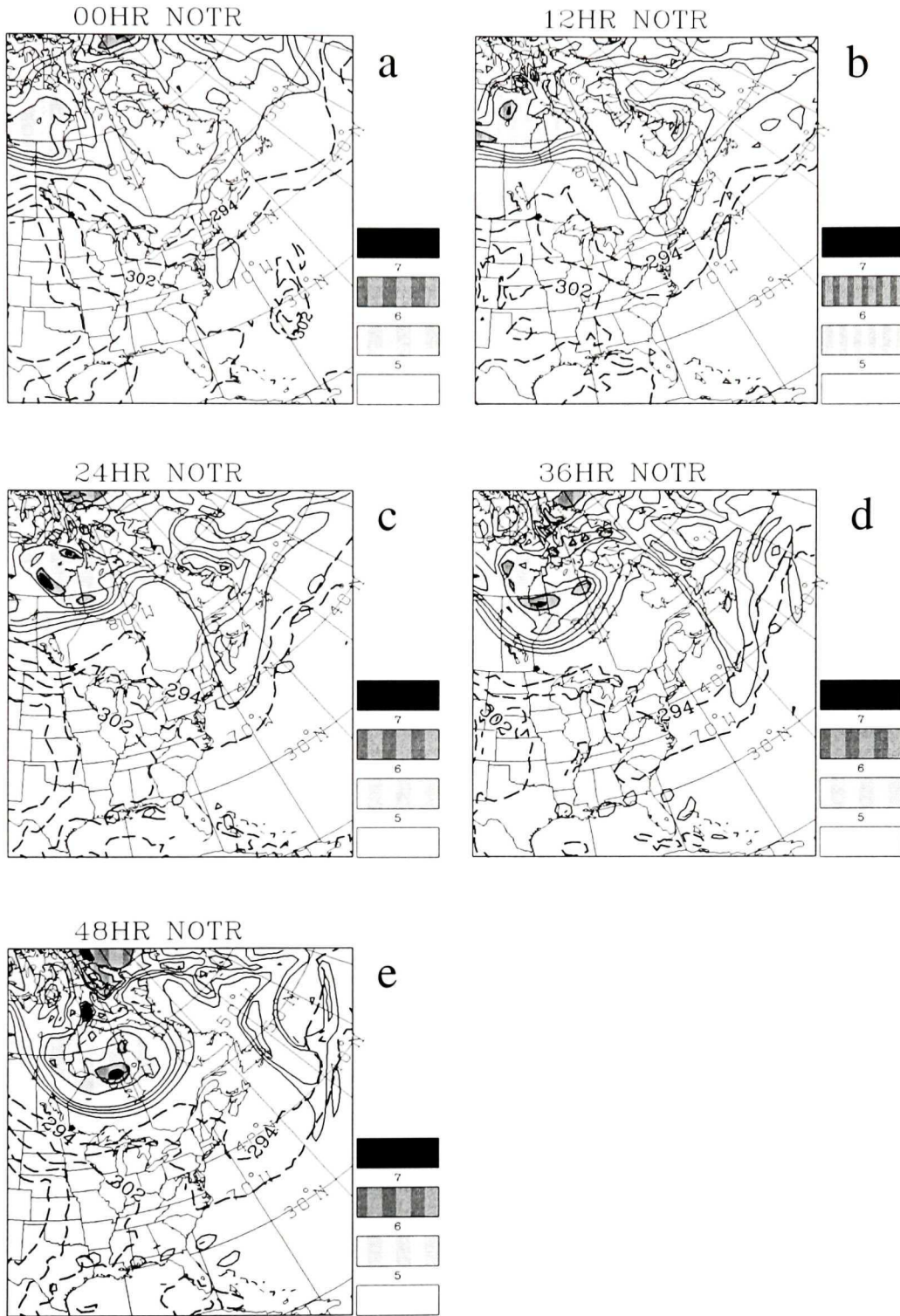


Figure 2.18: Same as in Fig. 2.11, except following the NOTR (full trough removal) initialization.

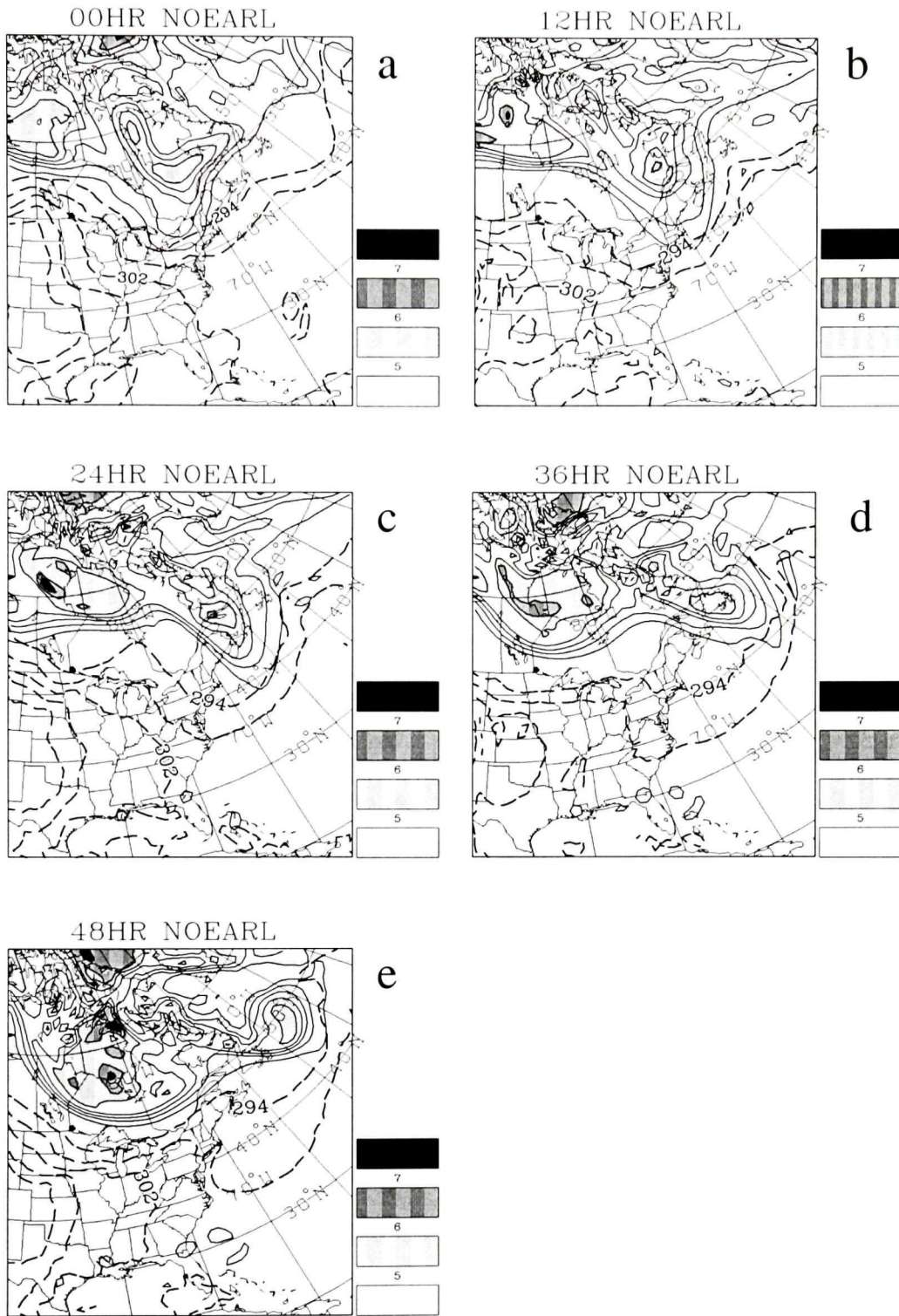


Figure 2.19: Same as in Fig. 2.11, except following the NOEARL (Hurricane Earl removal) initialization.

## Chapter 3

# The Influence of Downstream Features on ET

The findings presented by McTaggart-Cowan et al. (2001) (Chapter 2) indicate that the trough upstream of ex-hurricane Earl at 00/05 plays a vital role in the ensuing redevelopment of the TC remnant. However, the qualitative structure of the ET/R process is not modified, except in the NOTR case (Section 2.5) in which the entire trough anomaly is removed. In this chapter, the eastward extension of the domain across the entire North Atlantic basin reveals a second, simultaneous ET/R event associated with ex-hurricane Danielle whose evolution is dramatically different from that of Earl. Danielle, a classic Cape Verde hurricane which experiences multiple intensity fluctuations resulting from outflow interactions with Hurricane Bonnie, re-curves well east of the North American continent and slows almost to a standstill by 00/05 in the central North Atlantic as described in Section 3.1. As observed and simulated (Sections 3.2 and 3.3) Danielle subsequently undergoes 30 h of reintensification as the upper-level trough upstream of the remnant TC extends southwards, filaments, and wraps cyclonically around the perimeter of the developing troposphere-deep circulation, entrapping warm, moist tropical air near the storm's core.

The striking developmental differences between the two ET/R events in the control simulation lead to the hypothesis that at least two modes of transition exist in the North Atlantic. To explore this theory, and given that the upstream modifications of McTaggart-Cowan et al. (2001) did little to alter the structure of the system, a series

of idealized downstream state initializations are used to develop a set of sensitivity testing simulations described in Section 3.4. Further refinement of the theory of bimodal ET/R is described in Section 3.4g, and a simple jet-based conceptual model is suggested. This portion of the study concludes with a discussion of the findings in Section 3.5.

The following is based on McTaggart-Cowan et al. (2003a), in press with Monthly Weather Review.

# The influence of the downstream state on extratropical transition: Hurricane Earl (1998) case study

R. McTaggart-Cowan, J.R. Gyakum, and M.K. Yau

Department of Atmospheric and Oceanic Sciences, McGill University

## Abstract

The multitude of tropical/extratropical interactions that occur during an extratropical transition (ET) complicate the prediction and diagnosis of these extreme events. This study focuses on the analysis of a double ET and reintensification event that took place between 5 and 7 September 1998. Ex-hurricanes Earl and Danielle reintensified rapidly over the western and eastern North Atlantic, respectively. Using a set of idealizations for a numerical model's initial and boundary conditions downstream of ex-hurricane Earl, we run a set of simulations designed to test the sensitivity of Earl's ET to features in the downstream state. Dynamic tropopause analyses and the "PV thinking" paradigm applied under the Eady model highlight important developmental and structural differences between the tests.

In fact, two distinct solution modes are diagnosed both in the control and in the sensitivity tests. Earl's ET proceeds according to a "baroclinic mode" of redevelopment, whereas Danielle displays distinct "tropical mode" ET signatures throughout the period of investigation. The presence of a strong zonal jet immediately downstream of the transitioning cyclone is found to be sufficient to induce a baroclinic mode of redevelopment characterized by cyclonic potential vorticity rollup and strong near-surface frontogenesis. Under the influence of an upstream jet in isolation, the reintensification takes on distinctly tropical characteristics as the enhanced northward intrusion of warm, moist air ahead of the system creates a local environment favorable for a tropical mode of redevelopment. A description of the dynamics as-

sociated with these two distinct redevelopment modes may aid in the understanding and prediction of these events.

### 3.1 Introduction

The extratropical transition (ET) of Atlantic hurricanes off the east coast of North America forms an excellent test-bed for the study of tropical-extratropical interactions. Approximately 50% of Atlantic tropical cyclones undergo ET, and 50% of these redevelop during the process (Hart and Evans 2001). These events pose a very real threat to the inhabitants of the eastern seaboard since the moisture contained within the tropical system is often released as heavy precipitation over a very short period of time. One of the worst flooding events in United States history occurred during the ET and reintensification (ET/R) of Hurricane Agnes in 1972 (Carr and Bosart 1978; DiMego and Bosart 1982a,c). In 1954, Hurricane Hazel's track across Pennsylvania, New York, and Ontario resulted in over 180 deaths (Knox 1955). In October 2000, Hurricane Michael struck Newfoundland with sustained winds of  $35 \text{ m s}^{-1}$  and gusts in excess of  $45 \text{ m s}^{-1}$ . Despite significant research efforts, the complex interactions involved in ET/R make these extreme events very difficult to forecast.

The effects of middle-latitude forcings on cyclogenesis are generally well understood. Similarly, much effort has been devoted to the understanding of hurricane dynamics and thermodynamics. However, the interaction between a moist tropical vortex and standard quasigeostrophic forcings presents a unique problem in both a prognostic and a diagnostic sense. Bosart and Lackmann (1995) employ a "potential vorticity thinking" (Hoskins et al. 1985) approach to their study the ET/R of Hurricane David (September, 1979). Tropical Cyclone Patsy (December, 1986) was described under a more traditional synoptic framework by Sinclair (1993b). Thorncroft and Jones (2000) (hereafter TJ) study the influence of background shear and atmospheric stability on the lifecycles of hurricanes Felix and Iris in 1995. A review of the sensitivities of Hurricane Earl's (September, 1998) ET/R to the existence and intensity of an upstream trough and to the strength of the low-level tropical vortex

is given by McTaggart-Cowan et al. (2001) (hereafter MGY).

This study represents a continuation of the research presented by MGY, with the objective of determining the sensitivity of Earl's reintensification to the downstream conditions present at the time of the ET. While the upstream trough was found to control the intensity of the ET/R (in fact, complete removal of the trough resulted in almost no reintensification), the structure of the resulting storm was remarkably similar in all of the sensitivity tests, including one involving the removal of the remnant hurricane dynamics. This result suggests that baroclinic forcing provided a significant amount of the energy required for the ET/R process. Upon investigation of the simultaneous ET/R of ex-hurricanes Earl and Danielle we found marked differences in the structures of the resulting systems. Since modifications to the upstream initial state had not yielded changes to Earl's appearance, we decided to investigate the possibility that the downstream state plays a role in modulating the ET/R process. This paper presents the results from our study, beginning with a brief description of the case to be investigated. For a more comprehensive analysis of Hurricane Earl's ET/R, the reader is referred to MGY.

Hurricane Earl began as a tropical wave over the Cape Verde Islands in mid-August 1998. As the wave traveled westward over the equatorial Pacific, its development was suppressed by the outflow from the large and long-lived Hurricane Bonnie. As a result, Earl did not reach tropical depression status until 1200 UTC 31 August in the Gulf of Mexico. Tracking northeastward, Earl reached Category 2 on the Saffir-Simpson Hurricane Scale (surface windspeeds in excess of  $48 \text{ m s}^{-1}$ ) briefly before making landfall in Panama City, Florida at 0600 UTC 3 September (hereafter 06/03) as a nominal Category 1 hurricane, although observed winds never exceeded  $31 \text{ m s}^{-1}$ . After landfall, Earl was rapidly downgraded to a tropical depression, and was declared extratropical by the National Hurricane Center (NHC) at 18/03. Earl continued to track northeastward and to fill until 00/05. At that time, used as the initial time for all of the simulations to be presented in this paper, Earl lay 350 km east of the New Jersey coast with a central pressure of 1004 hPa as analyzed by the

Canadian Meteorological Centre (CMC).

At the same time, ex-hurricane Danielle, declared extratropical by the NHC at 00/04, was still an intense system with  $33 \text{ m s}^{-1}$  sustained winds and was located near  $46^\circ\text{N}$ ,  $33^\circ\text{W}$  midway across the North Atlantic. The best track produced by the NHC (Fig. 3.1a) shows an unusually slow progression across the Atlantic following recurvature. By 00/05, the phase speed of the cyclone had slowed to between 1 and  $3 \text{ m s}^{-1}$ . A sharp ridge had built in behind Danielle as an extension of the Bermuda high.

The 36 hours following 00/05 saw Earl's central pressure drop from 1004 hPa to 960 hPa (Fig. 3.1d) as the remnants of the tropical cyclone interacted with the coastal baroclinic zone and a strong upper level trough. As shown in Fig. 3.1c, Earl crossed Newfoundland's Avalon Peninsula at 00/06, then made a sharp anticyclonic track change to complete recurvature by 12/06. Danielle also underwent marked reintensification over the same period. Although there are large discrepancies between the CMC and the NHC analyses, it appears as though Danielle's central pressure fell from 985 to 965 hPa (Fig. 3.1b). Despite its increased intensity, Danielle's phase speed continued to be a slow  $1\text{-}2 \text{ m s}^{-1}$ .

Earl maintained a forward speed of nearly  $10 \text{ m s}^{-1}$  following recurvature. The proximity of the two cyclones had a dramatic impact on the strength of the ridge between them. As the scale<sup>1</sup> over the North Atlantic contracted, the ridge was pinched off at all levels, resulting in a zonal background flow with two embedded, mature systems by 00/07. Analyses suggest that Earl merged with ex-hurricane Danielle around 00/09 as the two became indistinguishable on satellite imagery (not shown).

The following section describes the model and dataset employed in this study. An analysis of the control simulation is presented in section 3.3. Section 3.4 describes the set of sensitivity experiments used to a quantify the influence of the downstream

---

<sup>1</sup>The scale length is here defined according to Nielsen and Dole (1992) as the distance between the low center and the downstream col (saddle point) in the reduced sea level pressure field.

state on Earl's ET. An investigation of two modes of reintensification observed during the sensitivity study comprises section 3.43.4.7. The study concludes with a brief summary and a discussion of the results.

## 3.2 Model description

All of the results presented in this paper are obtained using version 3.2 of the non-hydrostatic Canadian Mesoscale Compressible Community (MC2) model. Semi-implicit time-stepping and semi-Lagrangian advection ensure the model's numerical stability over a wide range of scales. A 35 km horizontal grid spacing is employed for all simulations. In the vertical, 25 terrain-following Gal-Chen levels are distributed logarithmically beneath a 25 km rigid lid. A fixed condition with a ten point blending zone is used at the lateral boundaries. Further details concerning the model dynamics are described by Benoit et al. (1997).

A Kuo-type convective parameterization (Kuo 1974) and the Kong and Yau five-category explicit microphysics scheme (Kong and Yau 1997) are used to simulate moist processes. A Kain-Fritsch convective parameterization Kain and Fritsch (1990) was also employed for both the control simulation and the sensitivity tests. No structural differences were evident between simulations using the differing schemes; however, the storm intensities in the runs using the Kain-Fritsch scheme were somewhat weaker than observed. A turbulent kinetic energy boundary layer closure and a force-restore lower boundary condition are employed at lower levels. Sea surface temperatures are fixed at their initial values, but land temperatures are allowed to evolve. A more complete description of the model setup can be found in MGY. For a comprehensive review of the MC2 physical package, the reader is referred to Mailhot et al. (1998).

Six-hourly analyses from the CMC (Chouinard et al. 1994) are used as the initial and boundary conditions for the control simulation. The analyses are archived on a northern hemispheric polar stereographic grid with a 35 km grid spacing at 60°N. All runs are initialized on 00/05 at 12 pressure levels. The domain used for the

integrations presented here (for example, the domain in Fig. 3.2) is much larger than that employed by MGY to allow for the simultaneous simulation of both Earl and Danielle. The differences in Earl’s track and intensity for the two domains are minimal (not shown) with less than 50 km and 2 hPa of difference at all times.

### 3.3 Control simulation

A complete description and validation of ex-hurricane Earl’s ET/R is provided by MGY; a summary of the event is reproduced here for continuity. A description of ex-hurricane Danielle’s reintensification is presented concurrently.

#### 3.3.1 Synoptic analysis

At 00/05, Earl lies 350 km off the east coast of New Jersey (Fig. 3.2). The ex-hurricane has a central pressure of 1004 hPa, and only a weak circulation at all levels. Danielle is located in the eastern North Atlantic, with a more defined circulation and a central pressure of 986 hPa. A strong baroclinic zone runs parallel to the eastern seaboard of North America, and extends eastward above a northward protrusion of the Bermuda high. The associated North Atlantic jet has embedded windspeed maxima which exceed  $55 \text{ m s}^{-1}$  at 250 hPa. A strong mid-level trough upstream of Earl has been shown to be necessary for the reintensification of the ex-hurricane (MGY). A weak trough also exists upstream of Danielle.

Over the first 24 hours of the simulation, the trough upstream of Earl intensifies slowly and rotates eastward (Fig. 3.3). Earl itself accelerates along the baroclinic zone, and intensifies to 979 hPa. Since Danielle is nearly stationary over this period, the scale length in the North Atlantic decreases significantly, resulting in the pinching of the ridge between the two cyclones. The highest surface pressure between the cyclones decreases from 1022 hPa at 00/05 to 1008 hPa by 00/06. The mid-level vorticity associated with Danielle shows well organized cyclonic wrapping after 24 hours of simulation, indicative of a nearly-mature system. There is no sign of a coherent cyclonic vortex roll-up associated with Earl at this time.

The subsequent 12 hours of simulation (from 00/06 to 12/06) result in the rapid spin-up of ex-hurricane Earl. The storm reaches its peak intensity after 36 hours of simulation, with a lowest sea level pressure (SLP) of 964 hPa and winds in excess of  $32 \text{ m s}^{-1}$ . Shortly thereafter, Earl breaks from its northerly track to move almost due east. This further reduces the scale length between the newly-matured cyclone and slow-moving Danielle, which is still over the eastern North Atlantic. The frontal wave (as seen in the thickness fields in Fig. 3.2) produced by Earl's deformation of the baroclinic zone has moved well ahead of the surface center by the end of the simulation, thus completing an LC2-type development and indicating that the cyclonic branch of the system's three-dimensional circulation is dominant. (For a complete analysis of cyclone lifecycle characteristics, the reader is referred to Thorncroft et al. (1993).) Earl's rapid spin-up is also evident at mid-levels, where heights in the 500 hPa trough fall from 547 to 534 dam above the remnant tropical vortex. Although Danielle's mid-level circulation does not intensify significantly over the period, the expansion of both systems results in the pinching of the ridge and the virtual elimination of the background meridional geostrophic flow. The frontal signatures around Danielle are weak at all times, although the SLP of the system dips to 961 hPa 30 hours into the simulation. The lower-level temperature advection field after 36 hours of simulation (Fig 3.4) illustrates the drastically differing thermodynamic structures of the two systems. Strong warm advection to the south and east of Earl, and strong cold advection in the region of the system's "dry slot", are contrasted against the almost non-existent advective patterns associated with Danielle. This suggests that baroclinic conversion is much more important to Earl's ET/R than it is to Danielle's. By the end of the simulation (00/07), the two low centers dominate the North Atlantic map, with the ridging between them virtually non-existent.

### 3.3.2 Potential Vorticity Analysis

Morgan and Nielsen-Gammon (1998) suggest that plots of the potential temperature and winds on the dynamic tropopause (here defined as the 1.5 PVU surface,

1 PVU= $10^{-6}\text{m}^2\text{K kg}^{-1}\text{s}^{-1}$ ) can be coupled with maps of the potential temperature at the top of the boundary layer and lower-tropospheric Ertel potential vorticity (PV) to give a complete view of the atmosphere under the constraints of the Eady model (Eady 1949). Figures 3.5 and 3.6 show sequential plots of these quantities for the control simulation and form the basis of our PV analysis.

At 00/05, a broad zone of low potential temperatures representing the upper-level trough lies over Quebec and the New England states (Fig. 3.5). A much smaller disturbance can be seen over the central North Atlantic upstream of Danielle, and a third is visible over Great Britain. A strong zonal jet (approximately  $55\text{ m s}^{-1}$ ) runs along the steeply tilted tropopause to the south and east of the disturbance upstream of Earl. Near the surface, the cold advection behind Danielle is evidenced by the cooled boundary layer temperatures east of the Canadian Maritimes (Fig. 3.6). The low-level PV associated with Danielle (a result of condensational warming at mid-levels) is much broader in extent than that of Earl, and an intensification of the baroclinic zone can be seen to the north and west of Danielle's center.

Over the first 24 hours of simulation, the trough upstream of Earl rotates across the coast and develops a strong tropopause fold along its downstream edge. This process injects high PV air into mid-levels, and tends to convectively destabilize the region since drying at mid-levels modifies the equivalent potential temperature sounding and lowers the coupling index (CI). The CI is a column-based bulk stability variable defined as the potential temperature on the dynamic tropopause minus the equivalent potential temperature at the top of the planetary boundary layer. A lower CI indicates greater conditional instability and increased atmospheric coupling.

The CI has the very attractive quality that it provides a link between the system's dynamic and thermodynamic structures. A low (including negative) CI occurs in regions where either the dynamic tropopause is lowered and/or the equivalent potential temperature at the top of the planetary boundary layer (PBL) is elevated. In the first case, a strong cyclonic circulation is implied throughout the column (as is a large thermal vorticity), and advection will result in vigorous ascent as the region

of lowered CI approaches. In the second case, convective instability is likely, due to the elevated equivalent potential temperature layer at low levels, often generated by strong surface fluxes of sensible and latent heat.

In this paper, we use the CI as a quantity by which to compare the results of this simulation with studies by TJ and Browning et al. (1998). In the former, the authors explore the impact of strong surface heat fluxes on the evolution of two storms in the North Atlantic (Felix and Iris) through a series of cross-sections. In the latter, the authors study the dynamics of PV streamers which inject dry, high-PV air into the near-core circulation of ex-hurricane Lili. Both of these processes are visible in the CI fields shown in fig. 3.7. The trough feature interacting with Earl's circulation is clearly seen as a negative (black) CI region over the Canadian Maritimes. The filamenting PV maximum above Danielle is evident wrapping round the center of the lower-level vortex in the eastern North Atlantic. Earl's developing "warm sector" is evidenced by a broad area of weak CI (0-10 K) to the south of the system after 24 hours of simulation. The large region of reduced CI surrounding Danielle's center is a result of elevated PBL equivalent potential temperatures, which are themselves a result of both strong low-level warm advection ahead of the system and strong sensible and latent heat fluxes from the ocean. The relative importance of upper-level PV forcing (as described by Browning et al. (1998)) and lower-level destabilization (as investigated by TJ) can therefore be at least qualitatively deduced by an inspection of the regions dominated by each process.

The jet bows northward during the first 24 hours of simulation, developing more anticyclonic curvature, and intensifies. The trough above Danielle filaments and curls cyclonically around the surface cyclone (Fig. 3.5c). This leads to the decreased zonal flow velocity on the dynamic tropopause that may be responsible for the remarkably slow phase speed of the system. There is a dramatic spin-up of lower-tropospheric PV in both systems as latent heating becomes important. Figure 3.8a, a time series of unresolved precipitation accumulation for each storm, shows that parameterized convection is a maximum over this period. The front northwest of Danielle initially

intensifies, then weakens slightly by 24 hours into the simulation. Meanwhile, both cold and warm fronts are clearly visible to the south and east of Earl, indicating a typical baroclinic development for that system (Fig. 3.6c).

The final 24 hours of the simulation highlight crucial differences in the development of the two systems. Danielle continues to spin warm, moist tropical air into its core region from west of northern Africa. This warm air is almost completely surrounded by an intense tropopause fold after 36 hours (Fig. 3.5d). The entire region enclosed by the descending PV streamers has reduced CI values because of both its tropical origins and the continuous surface heat fluxes (Fig. 3.7b, c). The trough upstream of Earl wraps cyclonically without the filamentation seen above Danielle. The near-surface potential temperatures are much colder near Earl's core (supporting elevated CI values), suggesting a common baroclinic development process (Fig. 3.6d).

The bullseye of low dynamic tropopause potential temperatures in Earl's circulation (Fig. 3.5d, e) is the result of three distinct processes: advection of a localized tropopause depression around the base of the digging trough (traceable throughout the Fig. 3.5 time series); a burst of near-core convection in the early stages of the simulation (Fig. 3.8a); and, a strengthening frontal occlusion over the latter half of the simulation. Harr and Elsberry (2000a) observe a similar tropopause folding process associated with a strong frontolytic region and potential "frontal fracture" (Browning et al. 1997) in their examination of Typhoon David (1997). That storm, like Earl (seen in its mature stage in Fig. 3.9a), underwent rapid redevelopment as a baroclinic extratropical cyclone. In Danielle's case, the development of the central bullseye structure is related to the effects of convection alone. As shown in Fig. 3.8a, the heavy unresolved precipitation accumulations in the vicinity of Danielle do not drop off nearly as sharply as those for Earl. In fact, the differences in the convective intensities of the storms may be even larger than is suggested in this time series. Figure 3.8b shows the 36-42 hour unresolved precipitation accumulation for the two storms and highlights striking structural differences. Firstly, the strong, broad frontal features associated with Earl, classed as "convective" at a gridspac-

ing of 35 km, would be handled primarily explicitly as “stratiform” precipitation at higher resolution. However, the coherent convective patterns near Danielle’s core are consistent with the deep convective signature present in satellite imagery (Fig. 3.9b). Secondly, the vast majority of the true convection associated with Earl serves as a frontogenetic forcing away from the core of the system; conversely, much of the convection in Danielle’s vicinity is organized near the storm’s core and beneath the PV streamers encircling it. Thus, the direct impacts of convection are more focused in Danielle’s case than they are in Earl’s. The structural differences resulting from these differing forcing mechanisms are manifest throughout the depth of the troposphere.

The divergence in the evolution of the near-surface fields is equally dramatic. The near-surface potential temperatures around Earl in Fig. 3.6e show clear frontal boundaries, as do elevated lower-tropospheric PV values which run in bands along the regions of enhanced baroclinicity. Conversely, the local region around Danielle is very warm and virtually isothermal. The storm’s low-level PV structure is nearly perfectly symmetric. We suggest that the entrainment of tropical air around Danielle’s core has resulted in a mode of redevelopment which is fundamentally different from that experienced by Earl during its reintensification. This hypothesis will be discussed in detail in section 3.5.

### 3.4 Sensitivity tests

The purpose of the set of sensitivity tests described here is to quantify the potential impacts of the downstream state on Earl’s ET/R as described in the previous section. The tests differ only in their initial conditions over the North Atlantic, downstream of Earl at 00/05, and subsequent boundary updates. In all cases, geostrophic balance is used to obtain the flow field from an idealized hydrostatic mass field in the modified region. The lack of curvature in any of the idealized initial states allows for this simplified balancing procedure which results in a nearly non-divergent initial state (latitudinal variations of the Coriolis force introduce a negligible divergent component to the wind field). An analytic solution of the vorticity tendency equation

with divergence forcing ( $\frac{\partial \xi}{\partial t} = -\delta [\xi + f]$ ) can be used to estimate a timescale for the development of a realistic divergent wind field. This timescale (approximately one hour at mid-latitudes) is less than the typical spin-up time of a mesoscale model such as the MC2. Thus, by the time that the model's convective precipitation fields are expected to become meaningful, a fully-developed large-scale divergent wind field has long been in place. Lateral boundary conditions are updated with fields modified in a manner similar to the initial conditions. The underlying sea surface temperature field in each sensitivity test is modified in the same way as the atmospheric temperature field in order to minimize the possibility of spurious surface fluxes during model spin-up. Indeed, initial sensible and latent heat fluxes are larger in the unmodified region upstream of Earl than they are in the idealized downstream area for all of the sensitivity tests. A description of the modifications made to the initial and boundary conditions for each test is presented in subsections 3.4.1-3.4.3, and the simulations are analyzed in subsections 3.4.4-3.4.6.

### 3.4.1 Description of the IDEALLAT test

This sensitivity test is intended to determine the upper bound of the sensitivity of ex-hurricane Earl's ET/R to the initial downstream atmospheric state. In this case, the mean northern and southern boundary temperatures are used at their respective lateral boundaries and the north-south temperature gradient at all interior points downstream of the system is minimized. As a result, the initial state in this case contains no meridional structure downstream of the storm and the wind field is purely zonal and exceedingly weak. The differences between Earl's ET/R in this simulation and that in the control will yield an estimate of the maximum possible response of the case to the initial downstream atmospheric state.

### 3.4.2 Description of the EXT test

The initial and boundary conditions for this simulation are designed to test the sensitivity of ex-hurricane Earl's ET/R to the initial far-downstream atmospheric state.

We define “far-downstream” as any point beyond one Rossby radius<sup>2</sup> ( $\sim 1000$  km) east of the storm. The far-downstream state in the initial conditions and in each of the boundary updates is idealized by extending the mean “near-downstream” (within one Rossby radius of the ex-hurricane) state latitudinally. Thus, the meridional near-system structure is reproduced without curvature across the North Atlantic. If Earl’s ET/R in this simulation is similar to that of the control, then we can conclude that at least one of the features present in the near-downstream field is germane to the structure and intensity of the ET/R process, or that the case is insensitive to downstream conditions.

### 3.4.3 Description of the SIMJET test

This test is designed to quantify the sensitivity of ex-hurricane Earl’s ET/R to all downstream features not directly associated with an idealized representation of the observed North Atlantic jet/front structure. As for the IDEALLAT modifications presented in subsection 3.4.1, the mean temperatures at the northern and southern boundaries are employed as the lateral boundary values in the initial and boundary conditions. In the interior, and at the eastern boundary, a zonal baroclinic zone is established beneath the location of the North Atlantic jet in the control simulation ( $\sim 45^\circ\text{N}$ ). The idealized jet intensity at 250 hPa is  $57 \text{ m s}^{-1}$ , almost exactly the same as that observed in the control ( $58 \text{ m s}^{-1}$  maximum). Differences between this run and the control simulation highlight the sensitivity of Earl’s ET/R to downstream features such as ex-hurricane Danielle’s system and the ridging between the two tropical cyclones.

### 3.4.4 Analysis of the IDEALLAT simulation

This simulation, initialized with an almost quiescent atmosphere downstream of ex-hurricane Earl, shows the largest deviation from the control simulation of any of the

---

<sup>2</sup> $L_R = \frac{NH}{f_o}$  where the Brunt-Väisälä frequency,  $N = \sqrt{\frac{g}{\theta} \frac{\partial \theta}{\partial z}} \approx 0.01 \text{ s}^{-1}$ , the scale height  $H = 10^4 \text{ m}$ , and  $f_o = 10^{-4} \text{ s}^{-1}$

sensitivity tests, with the storm's minimum SLP dipping to 938 hPa after 48 hours of simulation (not shown). More striking than the intensity difference, however, is the change in the structural evolution of the system, best viewed using dynamic tropopause analyses.

An analysis of the tropopause maps provided in Fig. 3.10 suggests that Earl's reintensification in this simulation is fundamentally different from that of the control storm. By 24 hours, the meridional extent of the tropopause fold ahead of the cyclone suggests that warm, moist tropical air is being funneled into the system ahead of its passage. The destruction of the upper-level PV surrounding the cyclone's core between 24 and 48 hours is the result of mid-level latent heat release (not shown) and demonstrates the importance of convection to the rapid development of the system. After 48 hours of simulation, the tropical air has become isolated in an elliptical pool surrounding the core of the storm. PV streamers dip to as low as 500 hPa around the edge of the tropical air, and act as barriers to mixing with the cooler environment. The near-surface potential temperature field (Fig. 3.11) is nearly an isothermal 298 K for the entire enclosed tropical region. The CI (Fig. 3.12a) highlights both the stratospheric intrusions wrapping around the perimeter of the system, and the large region of reduced stability representing the moist, tropical PBL surrounding the core of the storm. Both of these features are reminiscent of those observed during ex-hurricane Danielle's ET/R in the control simulation. Similarly, no typical baroclinic frontal features are visible except for an enhanced baroclinic zone to the north and west of the storm. The lower-tropospheric mean PV field also shows no sign of frontal development; rather, a nearly-symmetric monopole structure prevails.

The development and final state of the storm in the IDEALLAT simulation are far more reminiscent of Danielle in the control run than they are of Earl. We suggest that this is because both this storm and Danielle undergo a tropical mode of redevelopment rather than a baroclinic one.

### 3.4.5 Analysis of the EXT simulation

The purpose of this simulation is to determine the influence of features in the far-downstream ( $> L_R \approx 1000$  km) region. Despite the aggressive idealization downstream of ex-hurricane Earl, the storm's ET/R in this simulation proceeds in a manner similar to that analyzed in the control. This suggests that the near-downstream state is much more important to the ET/R structure than are the intuitively important far-downstream features, including ex-hurricane Danielle.

The EXT simulation yields results very similar to those of the control. The minimum SLP of the storm dips to 975 hPa after 36 hours of simulation. Given the somewhat drastic nature of the initial idealization, this results suggests that the sensitivity of Earl's ET/R to the far-downstream flow is quite weak. The dynamic tropopause and near-surface plots shown in Figs. 3.13 and 3.14 both illustrate a mature extratropical cyclone that has undergone rapid vortex roll-up at upper levels. Figure 3.13 suggests that a warm core (nonexistent in the initial state at 00/05) may have reformed in part due to latent heat release over the period of reintensification. However, the presence of strong frontal features near the surface may indicate that a frontal occlusion process (Keyser and Shapiro 1986) is additionally responsible for the warm air near the center of the cyclone. The CI in this case (Fig. 3.12b) shows vividly the cyclonic PV rollup at upper levels; however, the inflow air nearing the storm's core contains CI values in excess of 14 K, indicating fairly high bulk stability and a relatively cool PBL unfavorable for deep convection. All of these signs suggest that this is a baroclinic system very similar to Earl in the control simulation.

The results of the EXT member suggest that the near-downstream state is much more important to the nature of Earl's redevelopment than are the features in the far-downstream field. The primary component of the near-downstream flow is the right entrance to the relatively linear North Atlantic zonal jet and its associated baroclinic zone. The results of the replacement of this feature and subsequent model integration are discussed in the next subsection.

### 3.4.6 Analysis of the SIMJET simulation

This simulation is designed to test the sensitivity of ex-hurricane Earl's ET/R to a single feature in the initial downstream state at 00/05, namely the North Atlantic jet/front. A redevelopment similar to that of the control storm (and therefore fundamentally different from that observed in the IDEALLAT test described in subsection 3.4.4) would indicate that the presence of this feature plays a crucial role in the structure of Earl's ET/R.

The dynamic tropopause analysis shown in Fig. 3.15 suggests that the system does indeed undergo strong baroclinic redevelopment very similar to that displayed by Earl in the control. The filamenting trough continues to roll cyclonically throughout the simulation rather than encircle the tropical air as it does for Danielle in the control, and in the IDEALLAT simulation (subsection 3.4.4). Strong frontal features are seen in both the near-surface potential temperature and lower-tropospheric PV fields (Fig. 3.16). The CI pattern after 48 hours of simulation (Fig. 3.12c) resembles that of the system in the EXT test (Fig. 3.12b) and Earl in the control (Fig. 3.7). The negative CI values corresponding to regions of strong upper-level PV wrap cyclonically in the system's core, while the inflowing air is relatively stable with CI values greater than 14 K. All of these factors suggest strongly that the presence of the zonal jet is indeed sufficient to induce the baroclinic mode of ET/R.

In spite of the highly idealized downstream initial conditions used for this simulation, the resulting system is very similar to ex-hurricane Earl in the control. This result implies that the downstream jet is important in determining the mode of ET/R.

### 3.4.7 Description of modes

The two modes of ET/R identified in the previous sections (baroclinic and tropical) have been shown to possess very different dynamical properties. The baroclinic mode exhibits an LC2-type upper-level PV vortex rollup (Thorncroft et al. 1993). Strong fronts form rapidly near the surface and the system matures quickly. The tropical mode is characterized by enhanced northward and westward advection of warm, hu-

mid tropical air in advance of the system. Upper level PV encircles a large region of the tropical air and acts as a barrier to mixing with the cooler environment. Differing transition characteristics have also been presented in previous studies such as TJ. The discussion in that paper focuses on the influences of environmental shear and stability structures on a pair of ET/R events. The results of this research follow similar lines, suggesting that the case studies are indeed complimentary. This of course leads to a more robust conclusion set.

As it nears maturity, a system undergoing the tropical mode of reintensification creates its own local environment. This is displayed vividly both in the lower-level advective fields (Fig. 3.17) and in a set of cross-sections from the sensitivity tests shown in Fig. 3.18. The mature cyclones in Fig. 3.17 (and Fig. 3.4 for the control) display dramatically differing lower-level thermal advection patterns. The mature tropical mode storms (Danielle in Fig. 3.4 and the system in Fig. 3.17a) support little temperature advection, with a weakly-organized, north-south oriented dipole implying a slow northward translation of the warm system. Baroclinic mode systems (Earl in Fig. 3.4 and the storms shown in panels b and c of Fig. 3.17) are associated with thermal advection patterns which display the effects of “dry slot” formation and evolving frontal structures (Harr and Elsberry 2000a). The strengthened thermal gradients associated with baroclinic mode systems are clearly much more important to this mode of ET/R than they are to tropical mode storms. The vertical structure of these systems is also remarkably different. The left hand panels in Fig. 3.18 show sections of equivalent potential temperature and PV in the control run for Danielle (panel a) and Earl (panel c). Those tests whose ET/R is described as baroclinic mode (EXT and SIMJET) are shown beside Earl, while the IDEALLAT tests, in which the storm underwent tropical mode reintensification is shown next to Danielle. Clearly, the differences between the sensitivity tests in each of the groups is much smaller than the differences between the groups. The convective stability of the near-storm environment thus shows marked differences between the modes. The tropical mode ET/R plots (Fig. 3.18a, b) show columns of weak convective stability as evidenced

by the vertical orientation of the highlighted 325 K isopleth of equivalent potential temperature. The baroclinic mode systems shown in Fig. 3.18c, d, and e contain a convectively stable structure. Perhaps even more striking, however, is comparison between the results presented here with those contained in TJ (summarized below).

Ex-hurricane Iris (1995) developed in a manner remarkably similar to Danielle in the control simulation. The slow phase speed of the system in the North Atlantic (TJ Fig. 1), the location of the system relative to the North Atlantic jet (TJ Fig. 4), the filamentation of the upper level PV structure, the lack of baroclinicity and frontal structures in the lower-level thermal field (TJ Fig. 5), and the stability structure shown in TJ Fig. 7d are all consistent with a tropical mode ET/R process. Similarly, ex-hurricane Felix (1995) possesses characteristics suggesting that it underwent a baroclinic mode ET/R. The zonal acceleration of the system (TJ Fig. 8), the location of the system in the basin (TJ Fig. 11), the upper-level PV distribution, the lower-level frontal structures (TJ Fig. 12), and the convective stability of the storm (TJ Fig. 13d) all support this conclusion.

The fact that some form of strong zonal jet exists downstream of the reintensifying system in each of the baroclinic mode simulations, and is not present in the initial state downstream of cyclones whose ET/R is tropical in nature, suggests that this jet is the deciding factor as to how the evolution of the ET will occur. We advance the following explanation as to the sensitivity of the ET process, based solely on the simple theory of linear jet streak dynamics and superposition arguments (Fig. 3.19). Arguably, a more complicated theory could be applied which would essentially describe the same characteristics as those presented here. Given the linear structure of the North Atlantic jet present in these simulations we will confine our statements to this simple jet model.

Linear jet dynamics can be used to show that the right entrance and left exit regions of a jet streak are favorable regions for ascent and cyclogenesis. Subsidence occurs across the axis of the jet. This vertical motion couplet sets up a lower-level secondary circulation around the jet as shown by the dark arrows in Fig 3.19. In

this figure, a linear jet exists at upper levels as evidenced by a strong geopotential gradient. The associated frontal structure is shown at lower levels. Superposed on this jet streak is a pair of cyclones, each represented by an “L”. The circulation around each cyclone in isolation is shown by the smaller arrows. In terms of this case study, the low in the right entrance of the jet represents Earl, and that in the left exit, Danielle. Regions in which the flow around the cyclone and secondary circulation around the jet streak are in phase are shaded. Owing to the necessary existence of the temperature gradient at lower levels by the thermal wind relation, these shaded regions also represent areas of enhanced thermal advection. As observed in the baroclinic mode of the control, this simple model suggests that “Earl” will wrap cold air around its center and will move further into the baroclinic zone. “Danielle”, however, will pull warm air from the south ahead of itself, resulting in an immediate environment which is almost tropical in nature.

We suggest that it is the location of the reintensifying cyclone relative to the zonal jet that determines which of the development modes will dominate. The baroclinic mode will occur preferentially in the right entrance, and the tropical mode in the left exit region. TJ also cites the jet-relative location as an important component of the ET/R process for ex-hurricanes Felix and Iris. Klein et al. (2002) find that upper-level outflow from systems undergoing ET in the western North Pacific enhances the downstream jet and induces a positive feedback on baroclinic mode reintensification. This suggests that the findings presented in this paper may be equally applicable in other basins. This surprisingly simple superposition argument based on linear jet dynamics has been borne out by all of the sensitivity tests and provides a reasonable framework by which to describe each of the baroclinic and tropical ET/R modes.

### 3.5 Summary and discussion

The understanding and prediction of ET/R events in the North Atlantic have proven to be challenging problems for both researchers and operational meteorologists. This work focuses on a description of the influence of the downstream state (i.e. the flow

over the North Atlantic) on rapid ex-tropical cyclone redevelopment. In particular, we investigate a case of double rapid cyclogenesis that occurred on 5 to 8 September 1998. Over this period, ex-hurricane Danielle deepens rapidly over the eastern half of the basin while ex-hurricane Earl intensifies explosively just off the east coast of North America.

In a previous study, MGY found that the strength and existence of a trough upstream of ex-hurricane Earl at 00/05 played a crucial role in determining the strength and structure of the storm's ET/R process. The system's interaction with its upstream environment was thus determined to be of significant importance. In this study, we investigate the role of interactions between Earl and its downstream environment. To assess the sensitivity of Earl's ET/R to the presence of identifiable features in the downstream flow (Danielle, a strong ridge between the two systems, and the subpolar jet) a set of sensitivity tests was employed, each with a different idealized state downstream of Earl at the initial time. A testing framework was developed to aid in the interpretation of the resulting simulations. Upon analysis, the tests indicate that two distinct modes of ex-hurricane ET/R exist in the North Atlantic. Baroclinic mode redevelopments (which include the control simulation Earl) are characterized by a baroclinic wave that separates from the cyclone center as the system matures, a typical structure for an LC2 development (Thorncroft et al. 1993). A tropical mode of redevelopment is observed in the absence of a strong downstream jet (e.g. the control simulation Danielle) and is identifiable due to the large northward intrusion of warm, moist tropical air in advance of the system. This flow wraps westward around the cyclone and eventually becomes the storm's local environment, reinforced by vertical PV bands separating the tropical air from the cooler extratropical surroundings. These transition modes are also evident in the cases of Felix and Iris as diagnosed in TJ. As discussed in section 3.43.4.7, many of the quantities investigated in that study can be used to strengthen the conclusions presented here.

A qualitative investigation of the partitioning between the effects of the upper-level PV features (such as those studied by Browning et al. (1998) for Lili) and

lower-level convective destabilization (as described by TJ for Felix and Iris) can be made by studying the CI fields from the simulations. The systems undergoing a baroclinic mode of ET/R show negative CI values (associated with depressions on the dynamic tropopause) wrapping cyclonically above the near-surface circulation, with relatively stable (CI greater than 14 K) air in the warm inflow region. Tropical mode ET/R cases display wrapping of the negative CI values around the perimeter of the near-cyclone circulation, and low CI (representing reduced bulk convective stability) values in the warm, tropical inflow region.

The IDEALLAT simulation displays distinctly tropical characteristics, indicating that the ET/R mode is indeed determined by the downstream state. The EXT member, in which Earl’s local downstream environment is extended across the domain, shows a very similar evolution (baroclinic mode) to the control. This suggests that the feature modulating the mode of the solution lies physically close to the cyclone. The SIMJET simulation shows that the existence of a zonal jet downstream of the developing system is crucial to the baroclinic development mode. The control run reintensification is well reproduced using an idealized version of the North Atlantic jet/front structure as the only downstream perturbation. We suggest that the key to understanding this sensitivity lies in the superposition of the cyclonic circulation near the surface low and the secondary circulation around the jet maximum. In the right entrance region of a linear jet streak, these flows are in phase behind the cyclone and lead to the cyclonic LC2-type rollup as observed for Earl in the control (Thorncroft et al. 1993). However, if the cyclone lies in the left exit region of the jet streak, warm advection ahead of the cyclone is enhanced and eventually creates a warm, moist local environment in which the cyclone undergoes a tropical mode of redevelopment.

The fundamental structural differences between the baroclinic and tropical ET/R modes result in differing storm dynamics. We hope to continue this study by simulating several ET/R events of each type in order to build more powerful conceptual models and/or to gather statistical information on the “weather” produced by each mode. As well, the extent to which the moisture in the air surrounding the cyclone

in the tropical mode effects the final intensity of the system is as yet unknown. A future paper employing methods developed by McTaggart-Cowan et al. (2003b) will address the issue of the influence of subsaturated moisture both within the reintensifying ex-hurricane and its local environment.

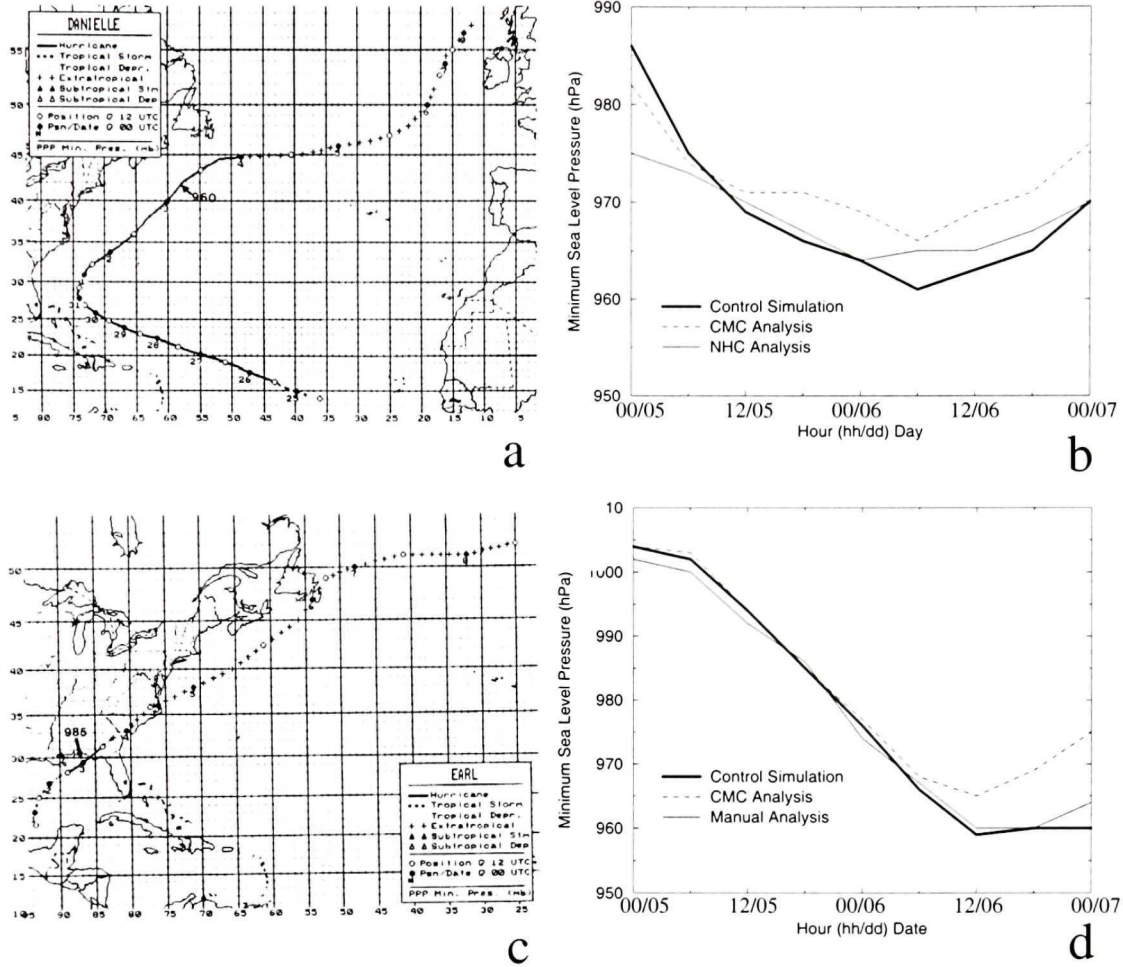


Figure 3.1: National Hurricane Center best track for Hurricane Danielle (a) and for Hurricane Earl (c). Minimum sea level pressure time series for the period from 0000 UTC 5 September to 0000 UTC 7 September are shown for (b) Danielle and (d) Earl for the CMC analysis, the NHC analysis (Danielle only), a manual analysis (Earl only), and the control simulation produced for this study. Plotting for Danielle’s track starts 1200 UTC 24 August in the central Atlantic and ends 0000 UTC 8 September in the North Atlantic. For Earl, tracking starts 1200 UTC 31 August in the Gulf of Mexico and ends 1200 UTC 8 September in the North Atlantic. Closed and open circles indicate 0000 UTC and 1200 UTC positions respectively in panels (a) and (c).

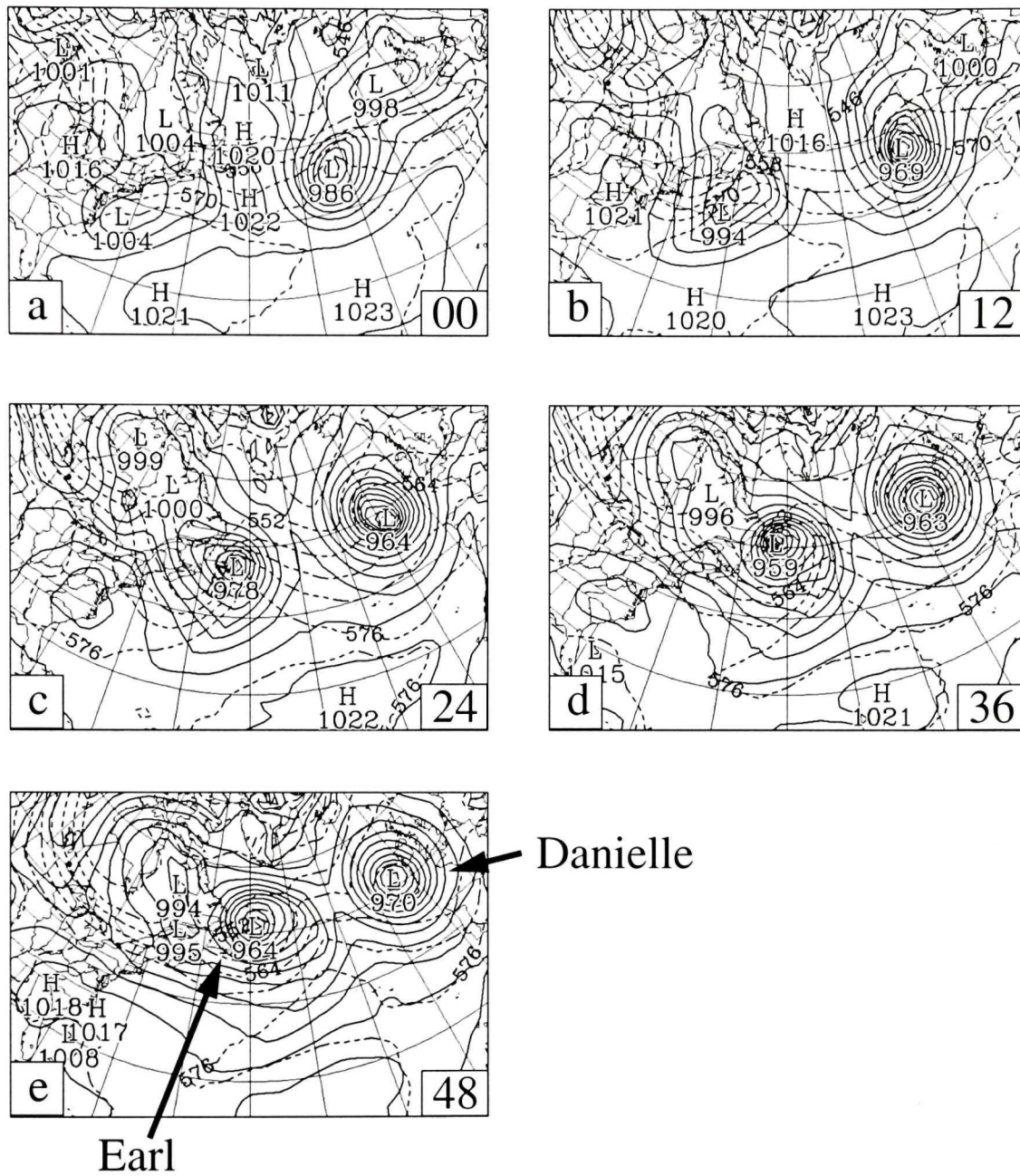


Figure 3.2: Sea level pressure (heavy solid lines, 4 hPa increments) and 1000-500 hPa thickness (dashed lines, 6 dam intervals). Fields are plotted every 12 hours for the control simulation, valid from 00/05 (a) to 00/07 (e).

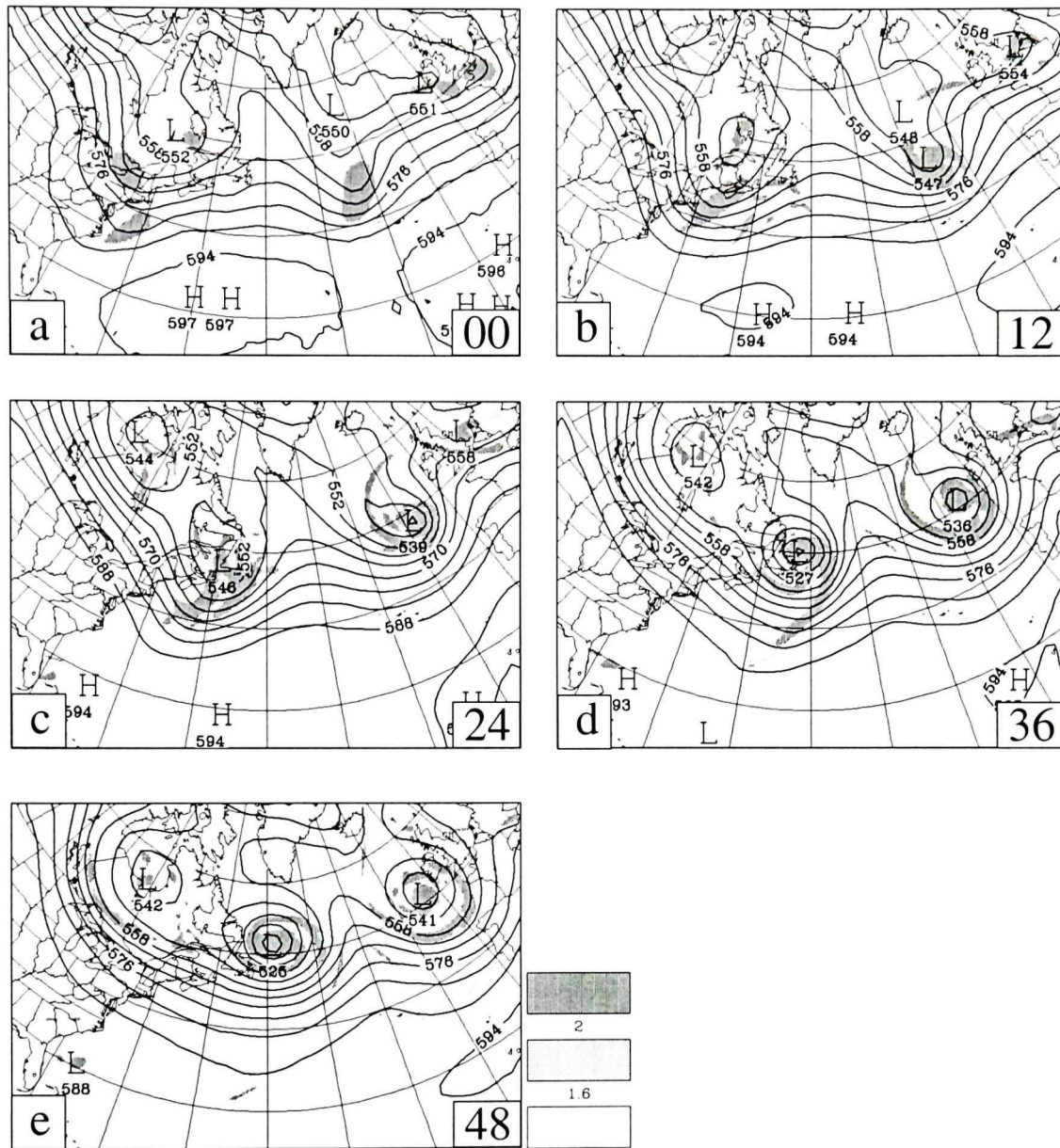


Figure 3.3: As for Fig. 3.2, but plotting 500 hPa heights (solid lines, 6 dam intervals) and 500 hPa vorticity (shading,  $10^{-5} \text{ s}^{-1}$ ).

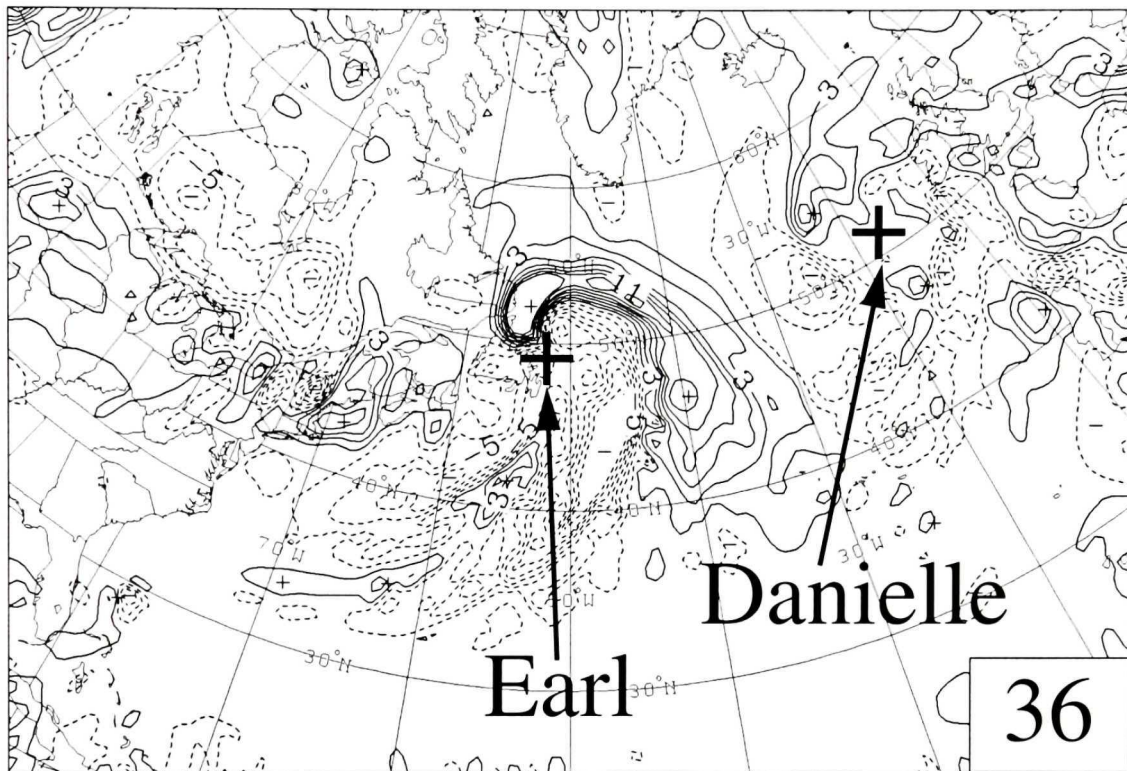


Figure 3.4: Lower-level thermal advection after 36 hours of simulation in the control. Contours of advection of the 850-500 hPa mean temperature by the 700 hPa wind are plotted every  $2 \times 10^{-4} \text{K s}^{-1}$ . Locations of the low pressure centers at the surface are shown in shading.

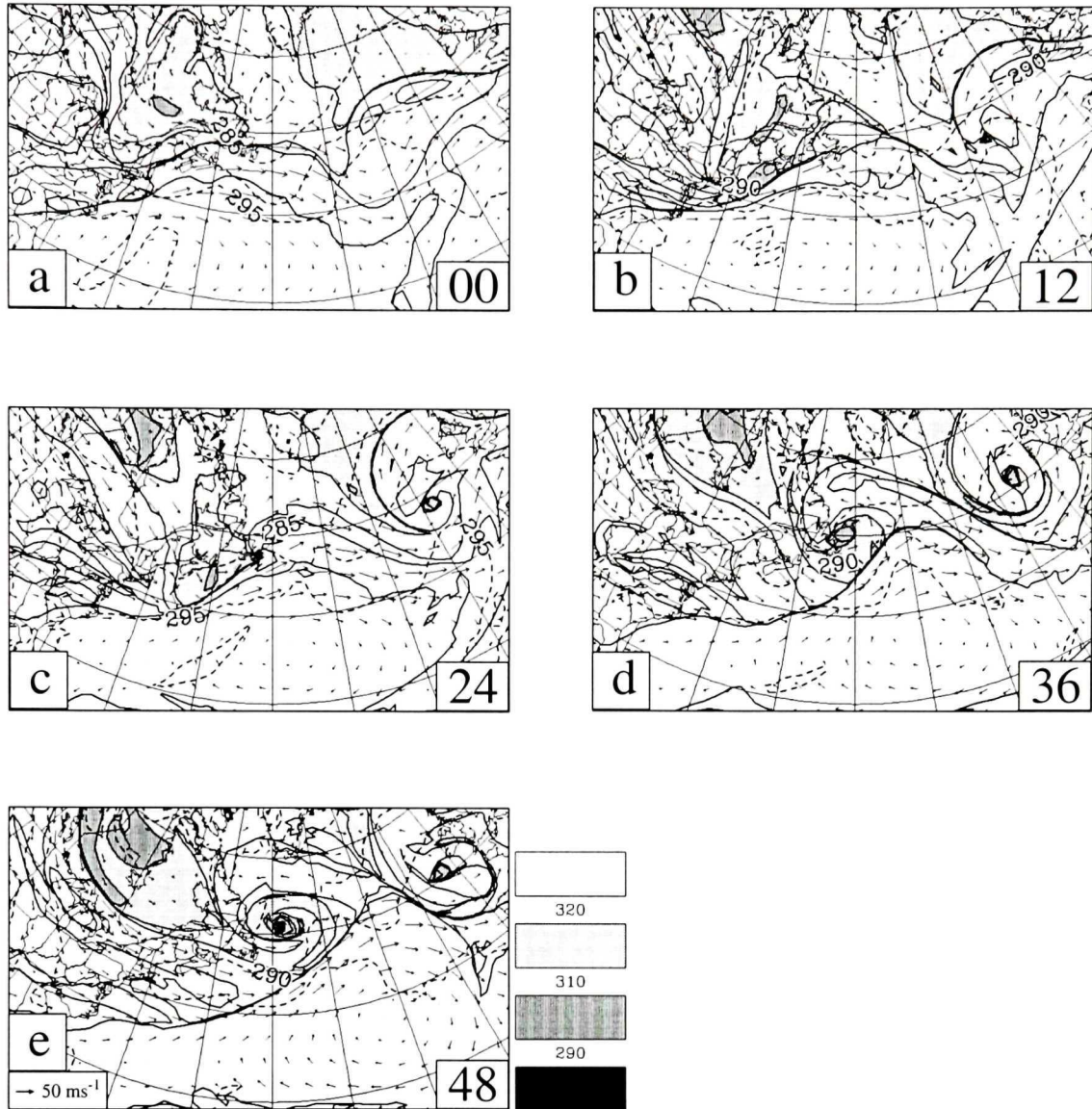


Figure 3.5: Dynamic tropopause (defined as the 1.5 PVU surface) potential temperature (solid lines and shading) and winds, and 1000 hPa temperature (5 K intervals, dashed lines) from the control simulation. Plots are shown at 12 hourly forecast intervals from the initial time 00/05 (a), to the final time, 00/07 (e).

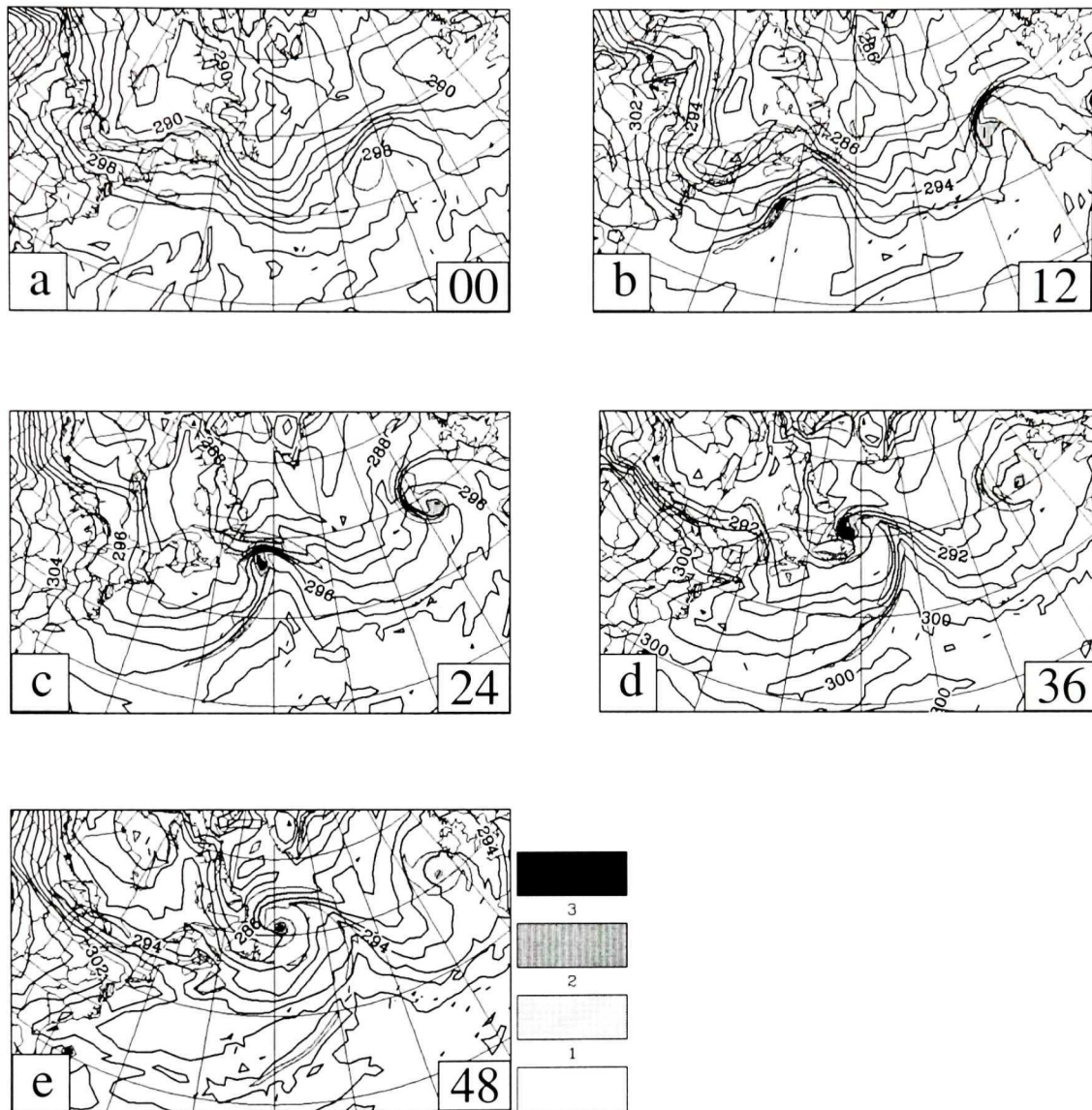


Figure 3.6: As for Fig. 3.5, except that plots show potential temperature at 925 hPa (solid lines at 4 K intervals) and 925-700 hPa mean PV (shading at 1 PVU increments).

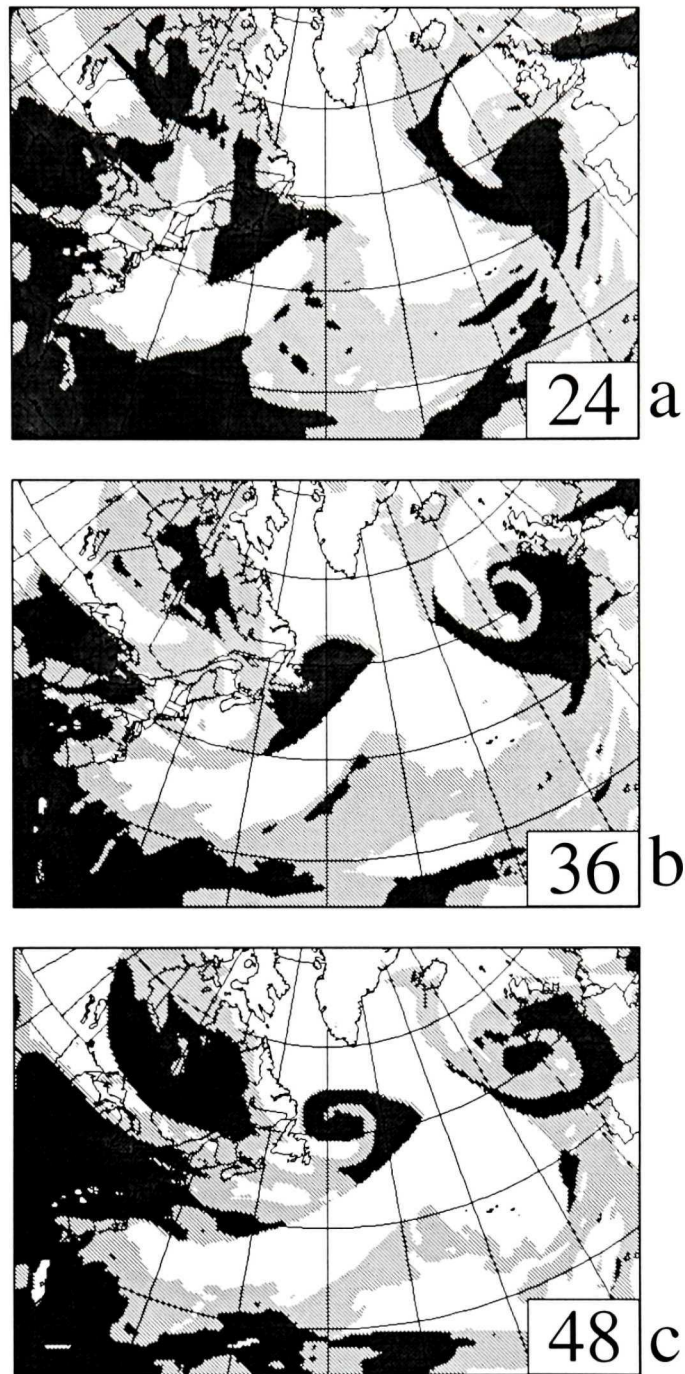


Figure 3.7: Coupling index for 24, 36, and 48 hours of simulation for panels (a), (b), and (c). Dark shading represents CI less than 5 K, and light shading between 5 and 15 K.

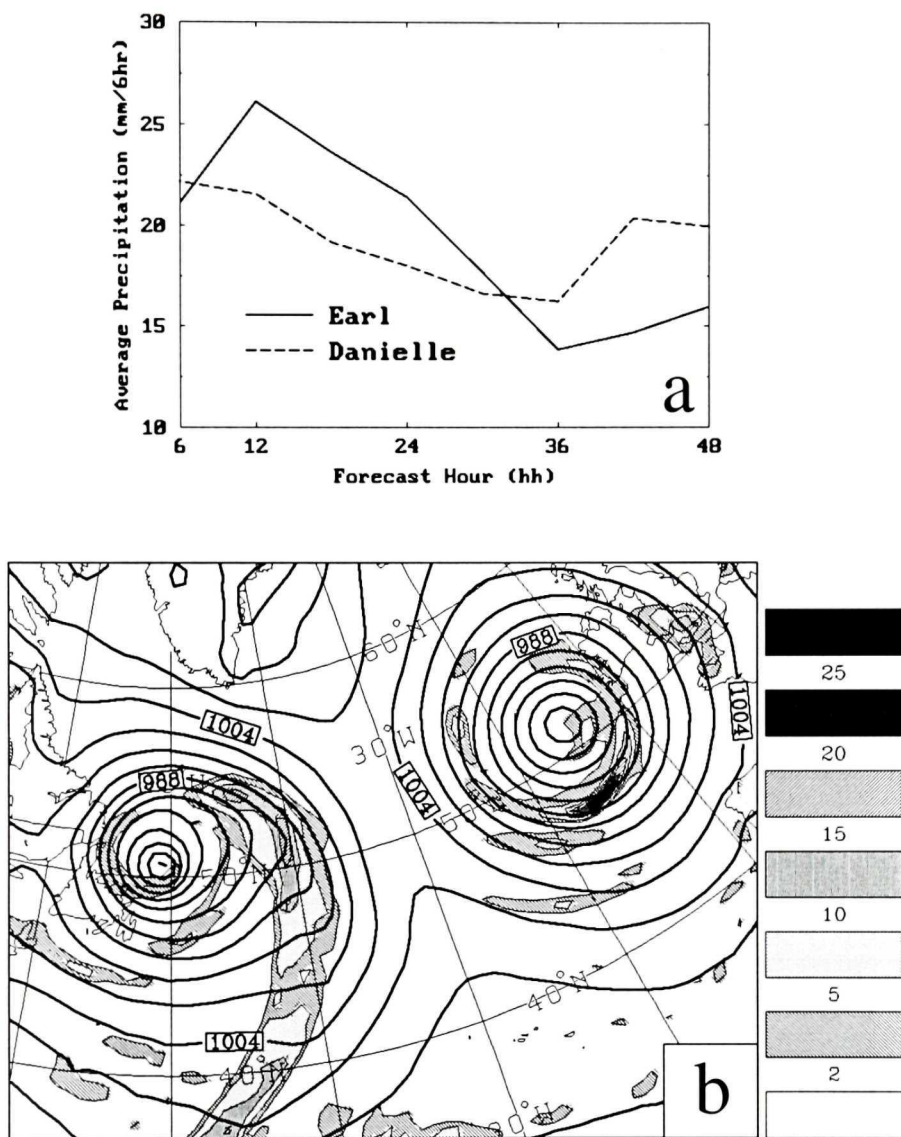


Figure 3.8: Heavy unresolved (“convective”) 6-hourly precipitation accumulations for Earl and Danielle in the control simulation as a function of forecast hour (a). All gridpoints within approximately 875 km (25 gridpoints) of the storm centers with 6-hourly unresolved accumulations exceeding 12 mm are used to represent heavy precipitation regions. The spatial distribution of 6-hourly unresolved precipitation accumulation for forecast hours 36-42 are shown in (b) with intervals of 2,5,10,15,20, and 25 mm. Sea level pressure at 42 hours is also shown in (b) for reference, with a 4 hPa contour interval.

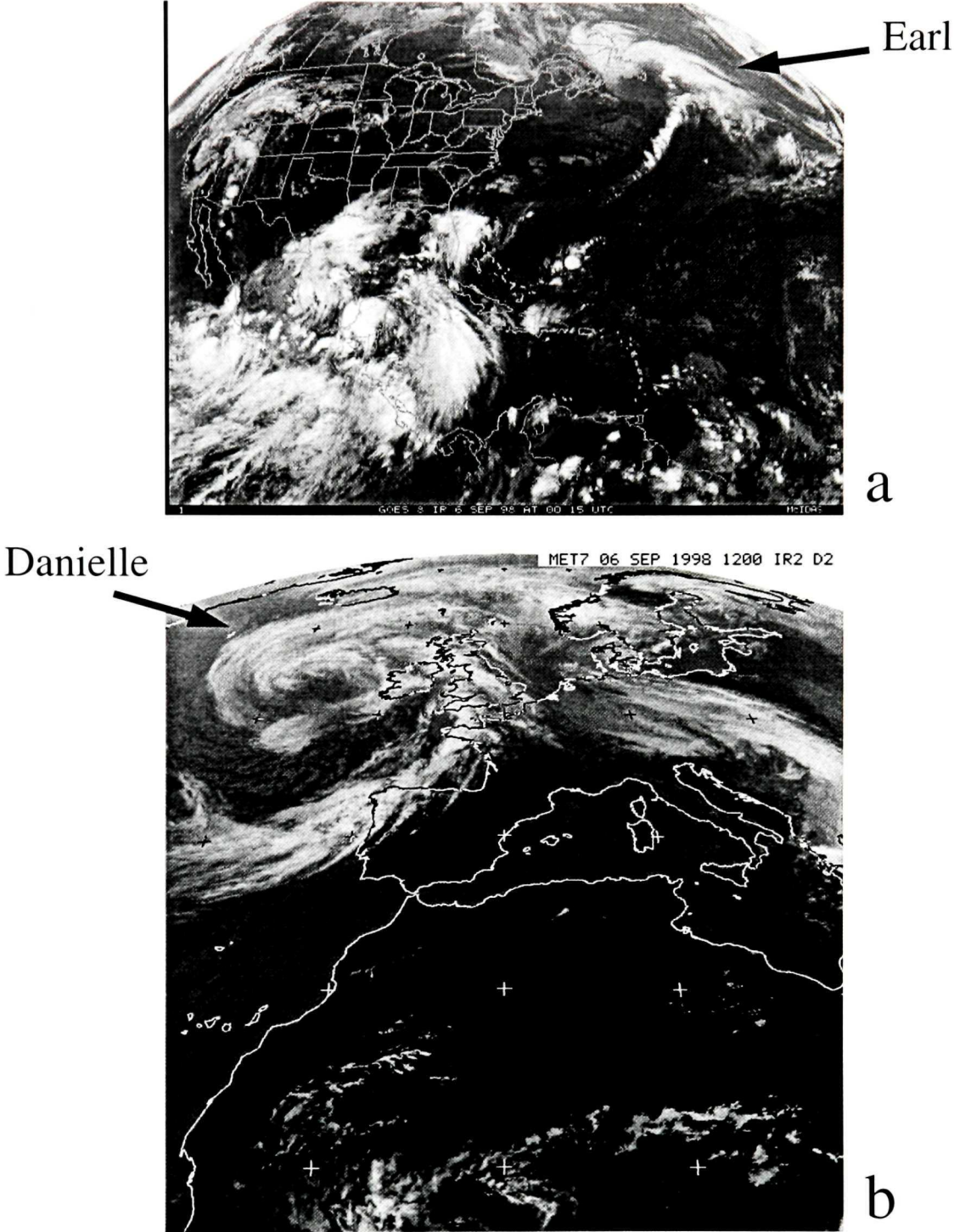


Figure 3.9: Infrared satellite imagery for (a) Earl, and (b) Danielle at 00/06.

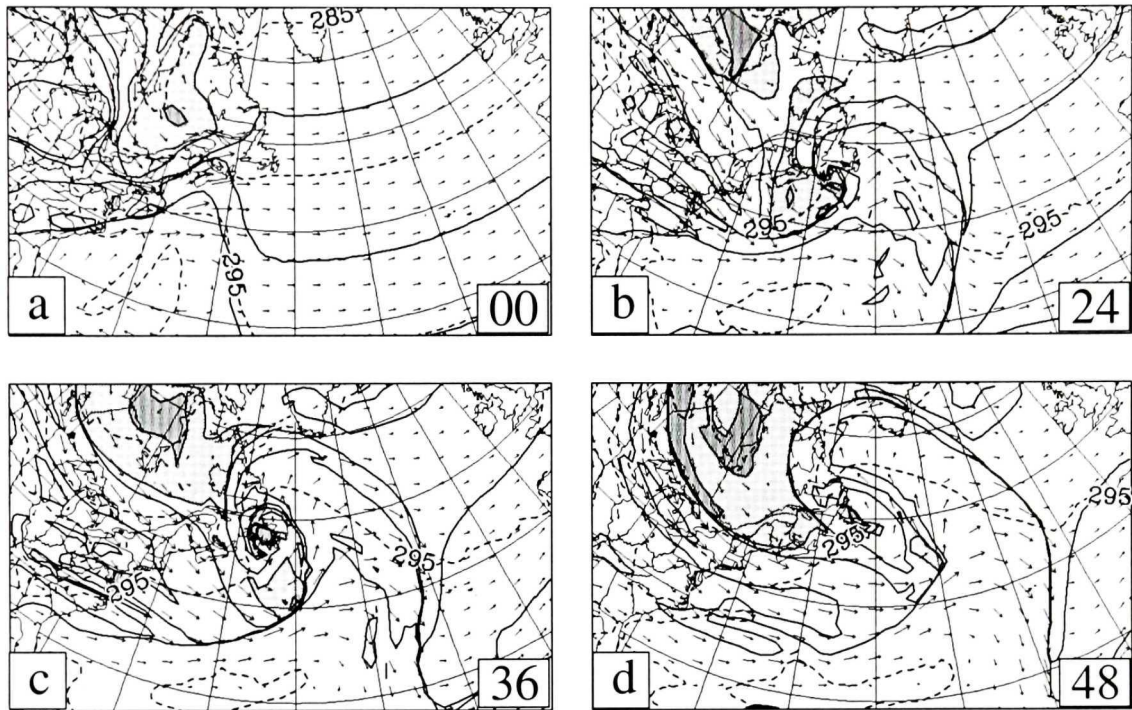


Figure 3.10: As for Fig. 3.5, but for the IDEALLAT member. Panels (a), (b), (c), and (d), show the 00, 24, 36, and 48 hour simulated systems, respectively.

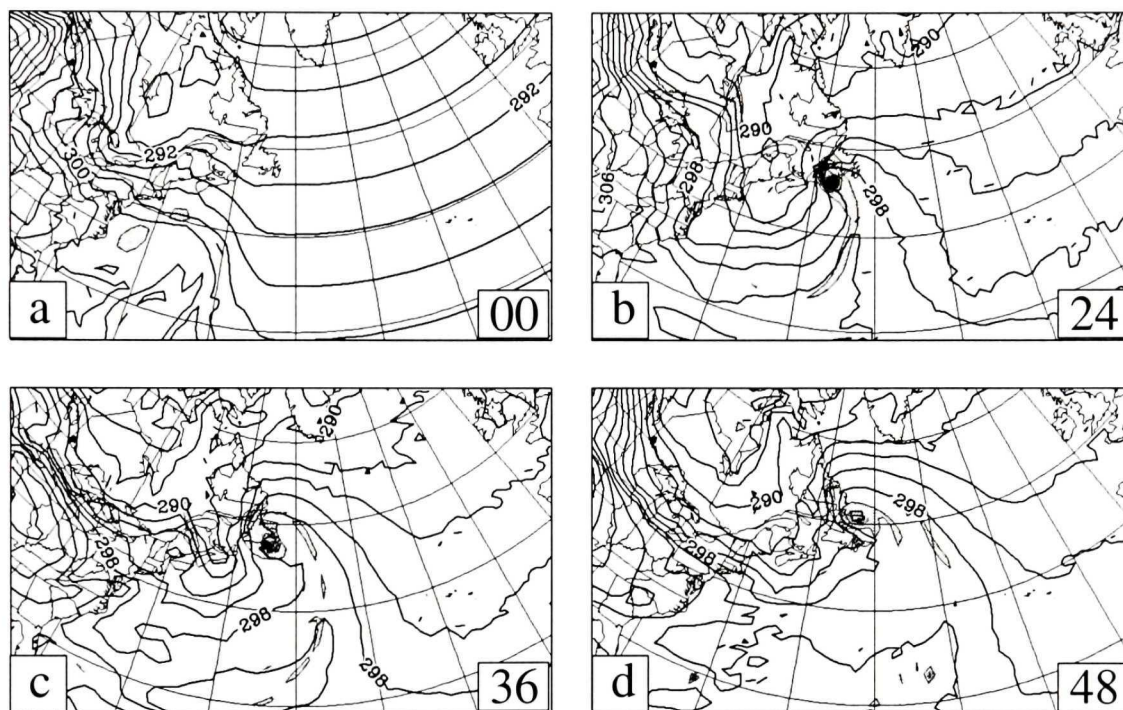


Figure 3.11: As for Fig. 3.6, but for the IDEALLAT member. Panels (a), (b), (c), and (d), show the 00, 24, 36, and 48 hour simulated systems, respectively.

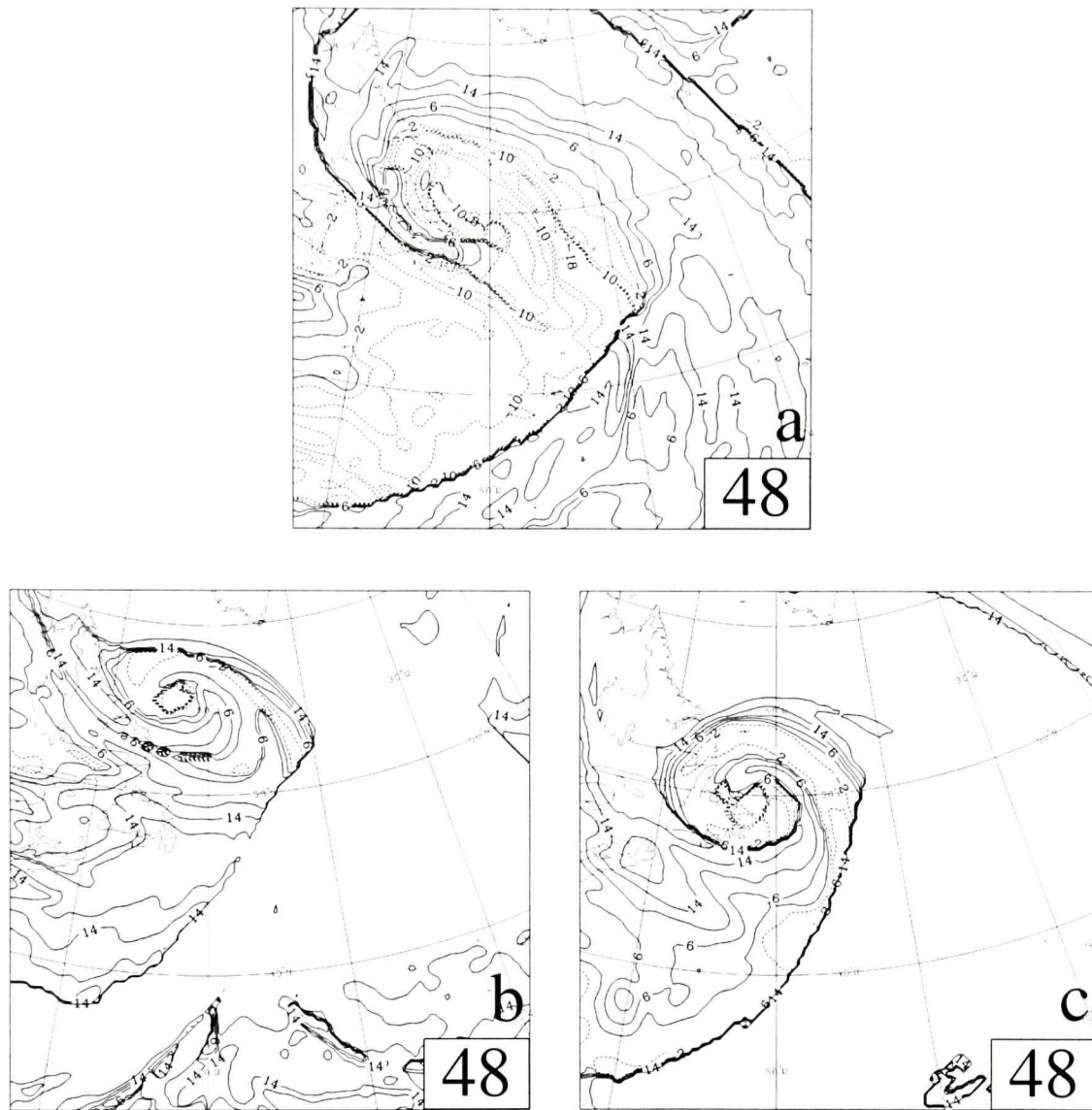


Figure 3.12: Coupling index values after 48 hours of simulation from the (a) IDEAL-LAT, (b) EXT, and (c) SIMJET tests. Contours are plotted at 4 K intervals with negative values dashed.

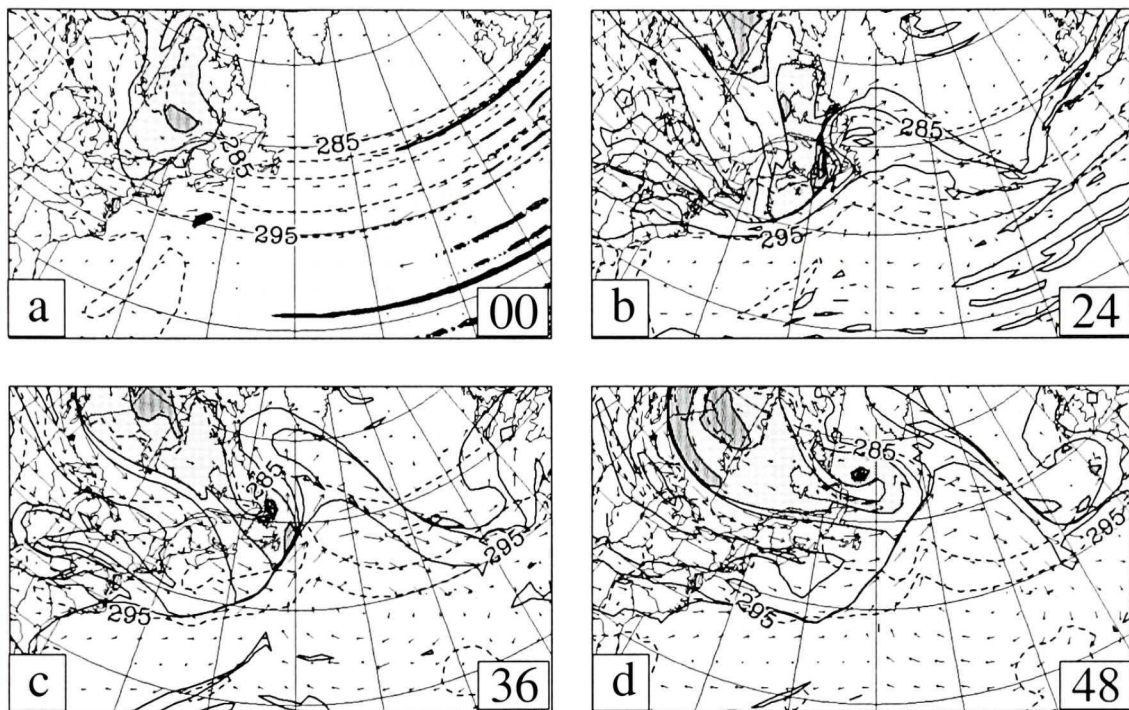


Figure 3.13: As for Fig. 3.10, but for the EXT member.

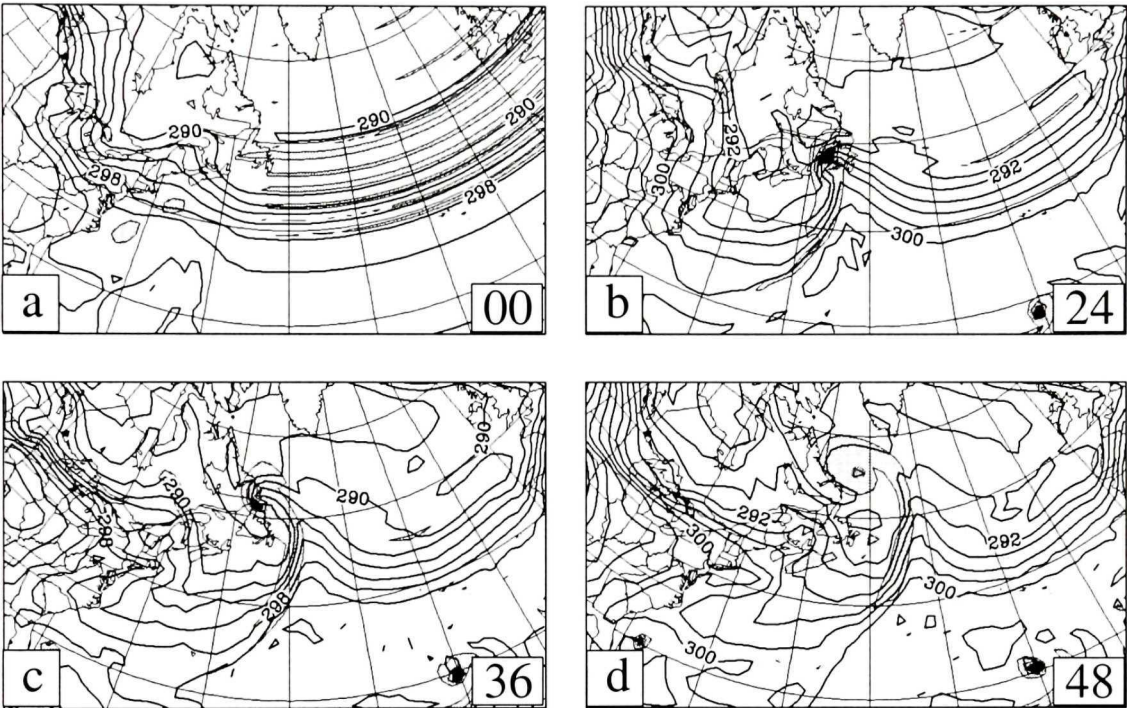


Figure 3.14: As for Fig. 3.11, but for the EXT member.

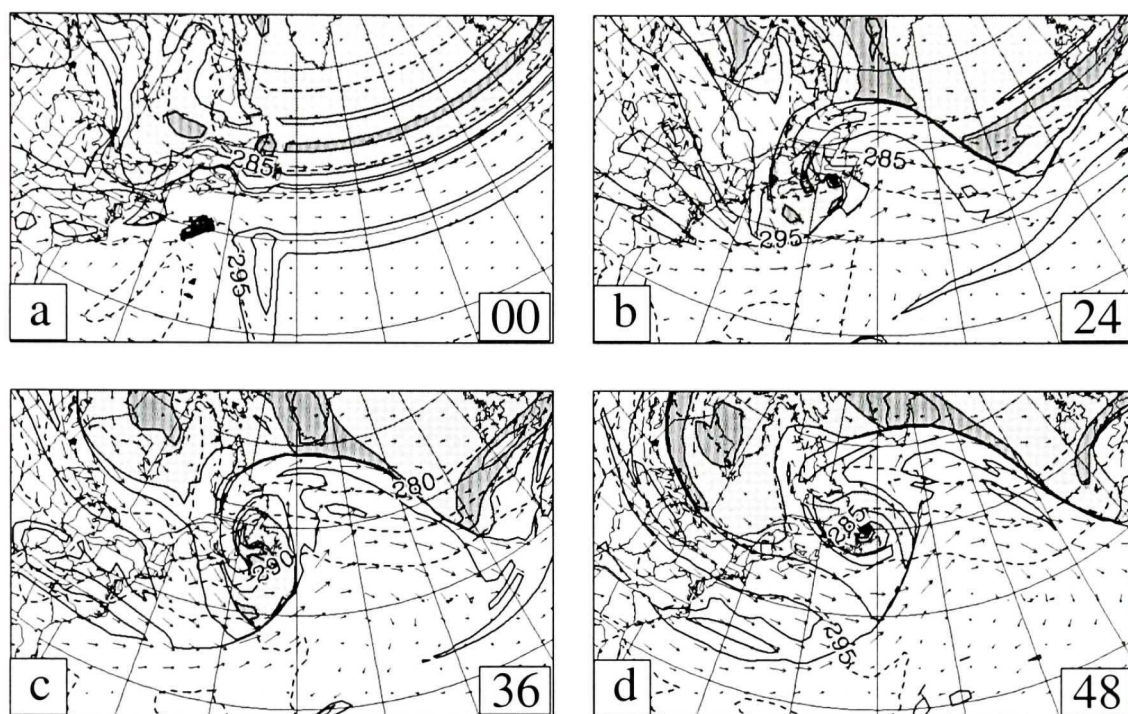


Figure 3.15: As for Fig. 3.10, but for the SIMJET member.

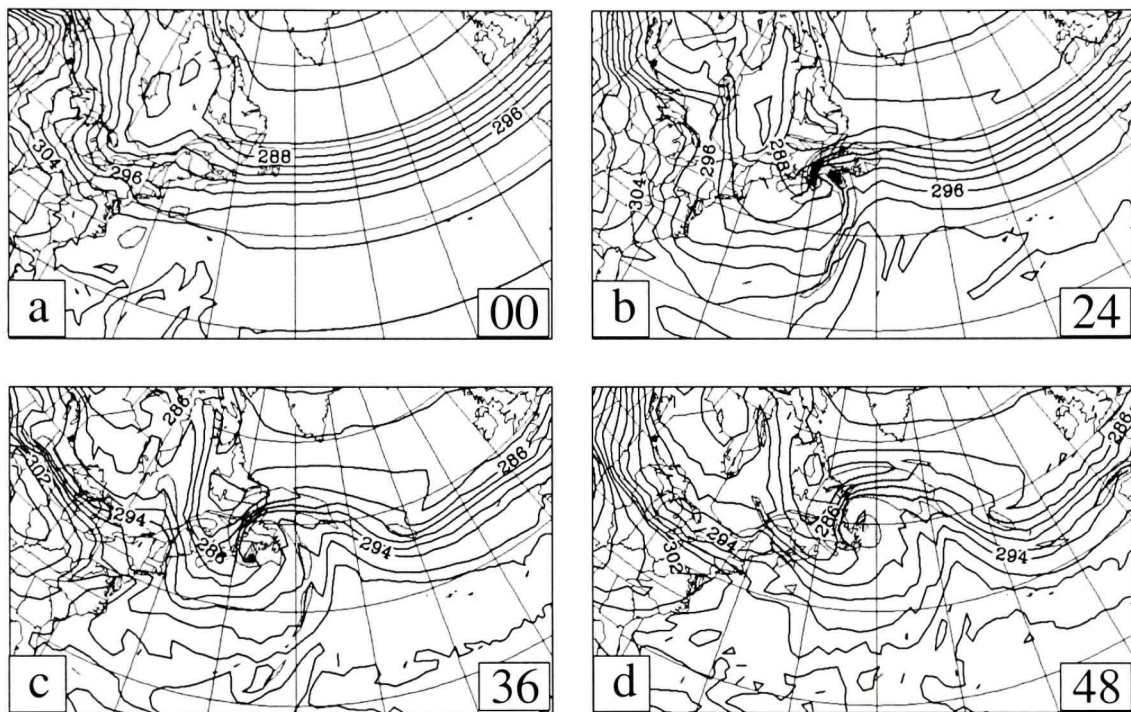


Figure 3.16: As for Fig. 3.11, but for the SIMJET member.

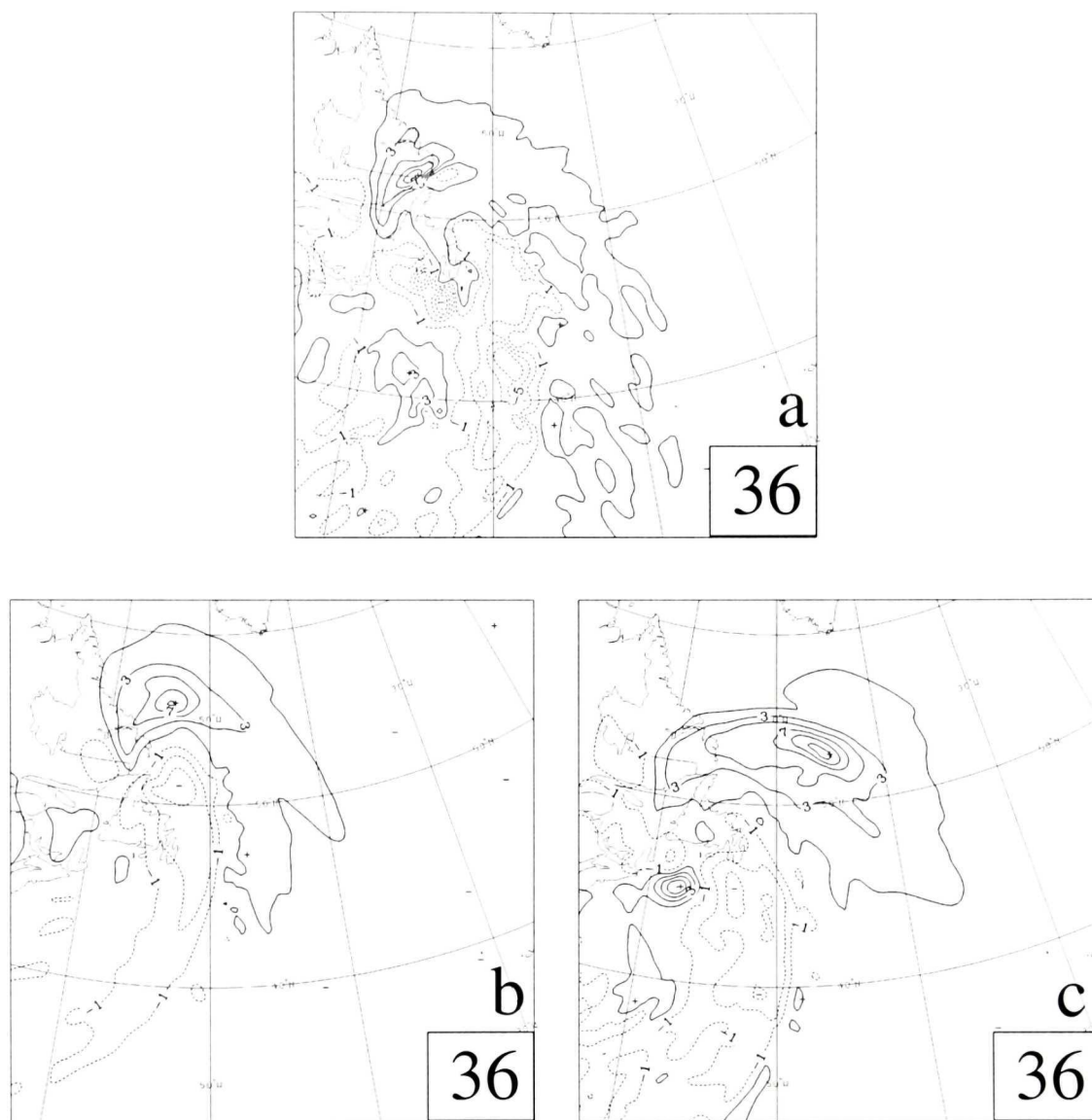


Figure 3.17: Lower-level thermal advection after 36 hours of simulation for (a) IDE-ALLAT, (b) EXT, and (c) SIMJET. Contours of advection of the 850-500 hPa mean temperature by the 700 hPa wind are plotted every  $2 \times 10^{-4} \text{K s}^{-1}$  as for Fig. 3.4.

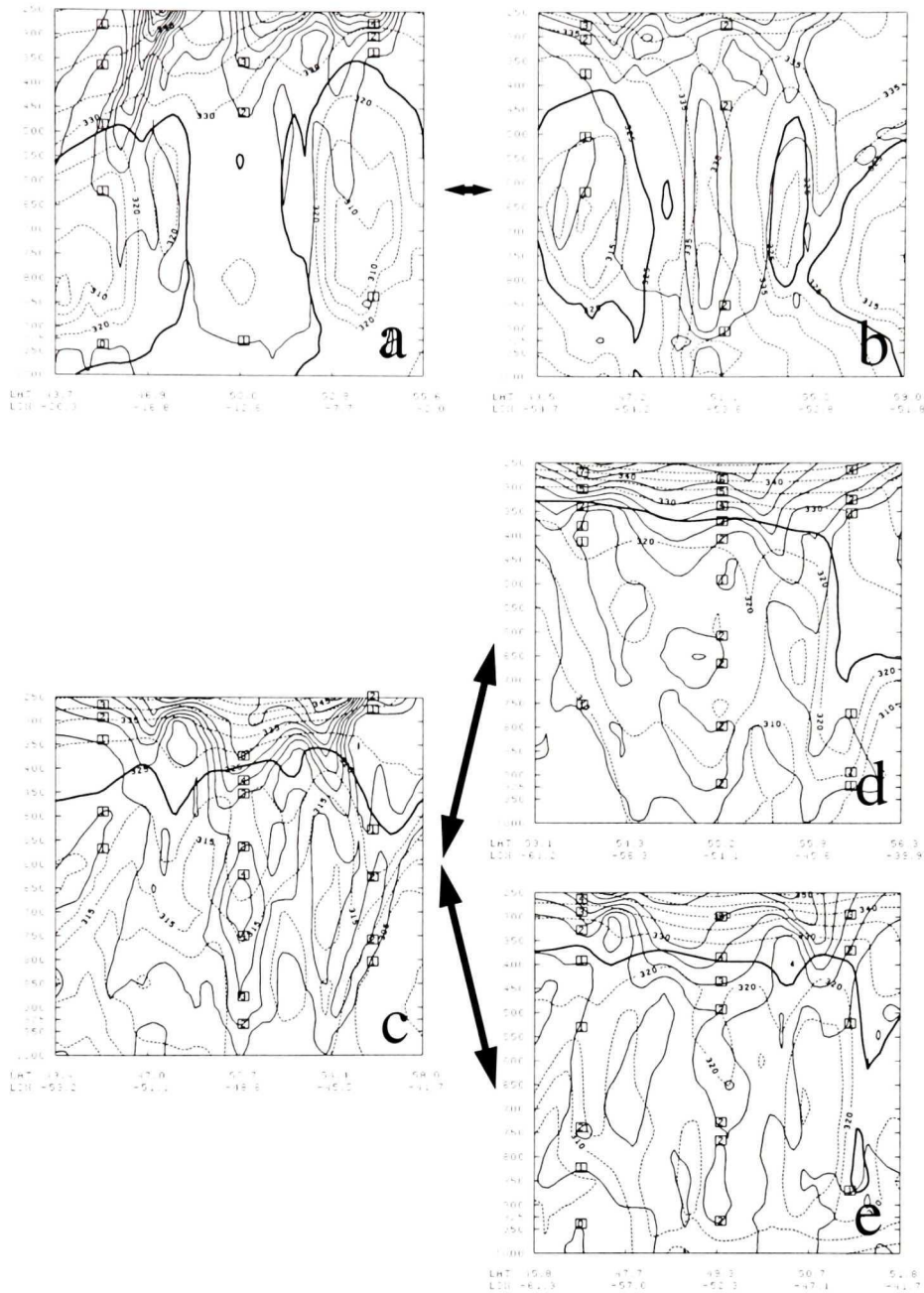


Figure 3.18: Cross-sections of equivalent potential temperature (dashed lines at 5 K intervals with the 325 K isopleth heavy solid) and PV (light solid lines plotted at 1 PVU intervals). Bold arrows connect similar modes of transition from the control (left column) and the sensitivity tests (right column). Sections are taken after 48 hours of simulation approximately east/west through the center of (a) Danielle in the control (tropical mode), (b) IDEALLAT (tropical mode), (c) Earl in the control (baroclinic mode), (d) EXT (baroclinic mode), and (e) SIMJET (baroclinic mode).

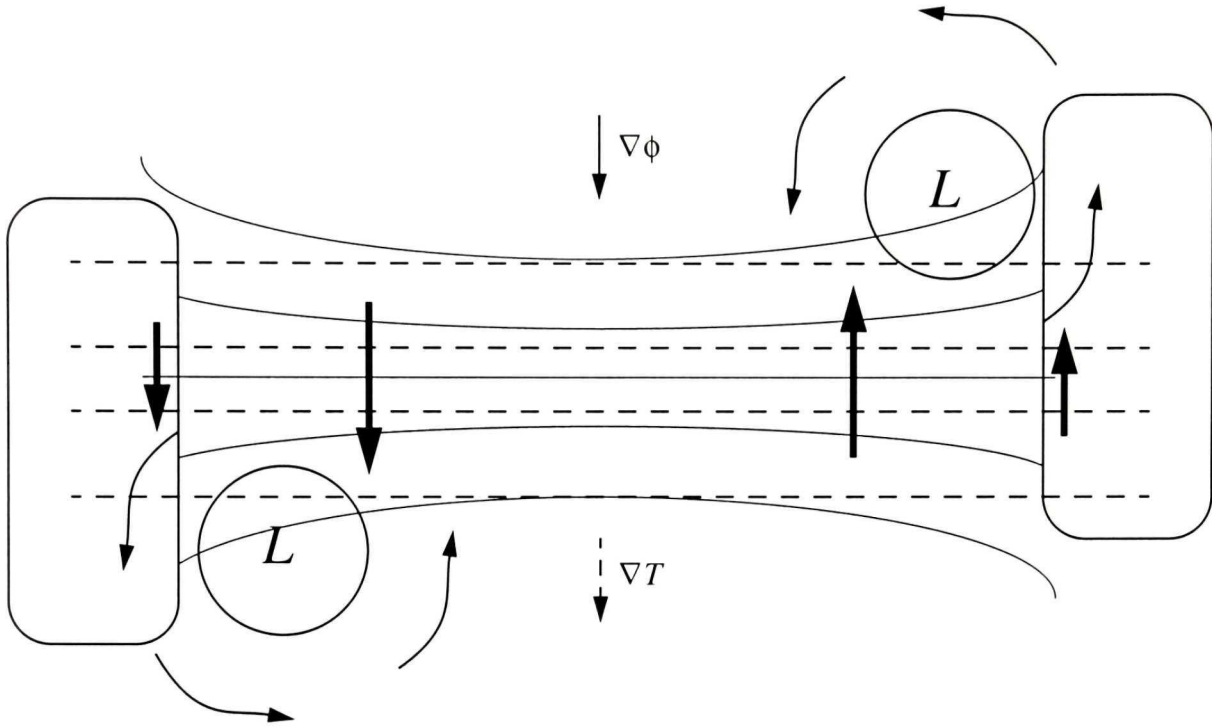


Figure 3.19: Schematic representation of a linear jet maximum. Light solid lines indicate upper-level height contours with the gradient oriented as indicated. Dashed lines represent lower-level isotherms, again with the gradient as shown. The horizontal secondary circulation at low levels generated by the jet is indicated by the heavy arrows. Two surface lows are superposed on the feature with cyclonic circulations as shown. Regions of enhanced cold and warm advection are shaded on the left and right sides of the figure, respectively.

# Chapter 4

## Moist Component Potential Vorticity

As noted in the discussion of McTaggart-Cowan et al. (2001) (Chapter 2.6), the utility of the piecewise PV inversion framework is limited by its inability to explicitly deal with atmospheric moisture. In the context of this study, any meaningful test of the remnant TC's impact on ET/R will necessarily involve the removal of both the tropical vortex dynamics and the moisture associated with the decaying storm. Chapter 4 introduces the  $PV_{mc}$  diagnostic, a variable which extends the piecewise PV decomposition strategy to include the effects of all forms of atmospheric water (Section 4.1). A general definition of  $PV_{mc}$  is developed in Section 4.2, and amounts to a statement that  $PV_{mc}$  represents the portion of the total PV field that arises directly from the presence of atmospheric water.

An idealized atmosphere is described in Section 4.3 in which the diagnostic  $PV_{mc}$  equation becomes tractable. This is valuable in that it allows for an explicit evaluation of the leading terms of the equation and for the development of physical interpretations thereof in Section 4.4. While the  $PV_{mc}$  field itself is useful in identifying thermodynamically significant regions of the flow, it is the invertibility of the quantity which will be most directly applicable to the current study. The results of a sample  $PV_{mc}$  inversion are presented in Section 4.5 and indicate that the dynamically-significant, balanced removal of moisture will have a small but non-negligible effect on the structure of the remnant TCs. A summary and discussion of

potential applications for  $PV_{mc}$  and  $PV_{mc}$  inversions is presented in Section 4.6.

The following is based on McTaggart-Cowan et al. (2003b), published in the *Journal of the Atmospheric Sciences*, volume 60 (2003).

# Moist Component Potential Vorticity

R. McTaggart-Cowan, J.R. Gyakum, and M.K. Yau

Department of Atmospheric and Oceanic Sciences, McGill University

## Abstract

The role that atmospheric water, in both its liquid and vapor phases, plays in cyclogenesis is difficult to determine because of the complex interactions between dynamic and thermodynamic forcings. From a potential vorticity (PV) perspective, it is possible to decompose the atmospheric state into a set of superposed PV anomalies. The modification of these anomalies allows for sensitivity testing using numerical models. Although this approach allows for the determination of cyclogenetic contributions from individual PV features, its application has not accounted for the dynamically consistent modification of the moisture field. This paper develops a PV-based variable that describes the effects of water vapor, cloud, and rainwater on balanced dynamics. A special-case analytic form of this “moist component” PV is developed and interpreted using an idealized model of the atmosphere. The application of the moist component methodology developed here provides the basis for future work, which includes sensitivity tests designed to separate the impacts of dynamics and thermodynamics on cyclogenesis.

## 4.1 Introduction

A method for quantitatively assessing the relative importance of dynamics and thermodynamics to cyclogenesis would be a valuable asset to operational and research meteorologists alike. This paper presents the development of a potential vorticity (PV) based variable that describes the balanced dynamics associated with the atmospheric moisture field. An idealized model atmosphere is used as a testbed to

simplify the interpretation of the variable. We suggest how this “moist component” methodology may be used in sensitivity studies to evaluate quantitatively the impacts of dynamics and thermodynamics on cyclogenesis.

The utility of PV as a diagnostic variable for atmospheric motion has been recognized since its inception by Rossby (1939). Two properties make the PV variable of particular interest. The first is the Lagrangian conservation principle, which states that the PV of a parcel of air does not change in frictionless, adiabatic flow. The second important property of PV is invertibility, which remains conceptually valid even when frictional and diabatic effects are important. The “invertibility principle” states that given a PV field and a balance condition, the state of the atmosphere can be uniquely diagnosed (for further description of PV attributes, the reader is referred to Hoskins et al., 1985). It is this second quality of PV that will prove most valuable to the current research. In particular, a piecewise casting of the invertibility principle using Ertel PV (Ertel 1942) and the nonlinear balance equation (Charney 1955) developed by Davis and Emanuel (1991) (hereafter DE91) will act as a framework for the proposed moist component developments.

A typical application of the piecewise PV procedure as proposed by DE91 involves the decomposition of the flow into a set of recognizable PV anomalies defined relative to a time mean. A subsequent inversion allows for the diagnosis of the balanced flow associated with each feature (Davis (1992a), Davis (1992b), Davis et al. (1996)). Some authors, including Huo et al. (1998) and McTaggart-Cowan et al. (2001), have performed sensitivity experiments based on the modification of these PV anomalies in model initial conditions. Such modifications have the advantage of being consistent since dynamical balance is enforced by the inversion process. The effects of subsaturated moisture on the atmospheric balance may or may not be included in this process, depending on the form of hydrostatic balance employed in the model or analysis cycle used to obtain the initial conditions. The research presented here focuses on the explicit calculation of the impact of water vapor, cloud, and rainwater on balanced dynamics by developing a set of idealized moist component perturba-

tion equations which fit into the piecewise PV framework. Modification of the moist component member of the set of PV anomalies will allow for the dynamically consistent modification of the atmospheric moisture field. Such changes in moisture could be used to test the sensitivity of cyclogenesis to the water vapor field of a model's initial state, and could be used to add an extra degree of freedom to ensemble forecasts. As well, they could provide the basis for an assessment of water vapor analysis uncertainty and its impact on operational forecasting.

The following section presents a derivation of the general form of the moist component PV ( $PV_{mc}$ ). A description of the analytic model's background state and humidity structure is given in section 4.3.1. The remainder of section 4.3 provides a set of analytic descriptions for the moist component variables. Physical interpretation of  $PV_{mc}$  is presented in section 4.4. Section 4.5 describes the result of a piecewise inversion of  $PV_{mc}$ . The study concludes with a brief summary and a discussion of the potential for the application of  $PV_{mc}$  to the real atmosphere.

## 4.2 Moist component PV

A general definition of  $PV_{mc}$  can be given as “the portion of the full PV field that is directly attributable to the presence of water in the atmosphere”. To formalize this statement mathematically, we begin with the definition of PV for a moist atmosphere, as given by Schubert et al. (2001):

$$\mathcal{P} = \frac{1}{\rho} \overline{\eta} \cdot \nabla \theta_v. \quad (4.1)$$

Here,  $\overline{\eta}$  is the absolute vorticity and  $\theta_v$  is the virtual potential temperature given by  $\theta_v = T_v \left( \frac{p_0}{p} \right)^\kappa$ , where  $T_v = \frac{p_a + p_v}{(\rho_a + \rho_m + \rho_r) R_a}$  is the virtual temperature and  $\kappa = \frac{R_a}{c_{p_a}}$ .  $p_a$  and  $p_v$  are the dry air and water vapor partial pressures, respectively ( $p = p_a + p_v$ ),  $\rho_a$  is the dry air density,  $\rho_m$  is the summed water vapor and cloud water density,  $\rho_r$  is the rainwater density ( $\rho = \rho_a + \rho_m + \rho_r$ ),  $R_a$  is the gas constant for dry air, and  $c_{p_a}$  is the specific heat at constant pressure for dry air. As noted by Schubert et al. (2001), the PV described by (4.1) retains the properties of conservation and invertibility for

an atmosphere which contains moisture. Assuming hydrostatic balance yields,

$$\mathcal{P} = -g \left( f \hat{k} + \vec{\xi} \right) \cdot \nabla_p \theta_v, \quad (4.2)$$

where  $\vec{\xi} = \nabla_p \times \vec{v}$  is the three dimensional relative vorticity. Equation 4.2 is similar to that of Hoskins et al. (1985), except that the virtual potential temperature replaces the potential temperature. This is the isobaric form of PV for a moist atmosphere and  $\nabla_p$  is the three dimensional gradient operator in isobaric coordinates. In this derivation,  $\xi = \hat{k} \cdot \vec{\xi}$  (the vertical component of the  $\vec{\xi}$ ) is computed diagnostically from the mass field through a balance equation and therefore varies with a changing moisture field. Expanding (4.2) into components,

$$\mathcal{P} = -g \left[ (f + \xi) \frac{\partial \theta_v}{\partial p} + \frac{\partial u}{\partial p} \frac{\partial \theta_v}{\partial y} - \frac{\partial v}{\partial p} \frac{\partial \theta_v}{\partial x} \right], \quad (4.3)$$

and converting to an Exner function ( $\pi = c_{p_a} \left( \frac{p}{p_0} \right)^\kappa$ ) vertical coordinate,

$$\mathcal{P} = -\frac{g\kappa\pi}{p} \left[ (f + \xi) \frac{\partial \theta_v}{\partial \pi} + \frac{\partial u}{\partial \pi} \frac{\partial \theta_v}{\partial y} - \frac{\partial v}{\partial \pi} \frac{\partial \theta_v}{\partial x} \right]. \quad (4.4)$$

We note that  $\frac{\partial \phi}{\partial \pi} = -\theta_v$ ,  $\frac{\partial \psi}{\partial y} = -u$ , and  $\frac{\partial \psi}{\partial x} = v$ , where  $\phi$  is the geopotential calculated hypsometrically using  $T_v$ , and  $\psi$  is the corresponding balanced streamfunction. Substitution of these expressions into (4.4) yields,

$$\mathcal{P} = \frac{g\kappa\pi}{p} \left[ (f + \nabla^2 \psi) \frac{\partial^2 \phi}{\partial \pi^2} - \frac{\partial^2 \psi}{\partial x \partial \pi} \frac{\partial^2 \phi}{\partial x \partial \pi} - \frac{\partial^2 \psi}{\partial y \partial \pi} \frac{\partial^2 \phi}{\partial y \partial \pi} \right], \quad (4.5)$$

the PV equation for a moist atmosphere cast in terms of the geopotential and balanced streamfunction.

For the case of a completely dry atmosphere ( $[\rho_m, \rho_r] \rightarrow 0$ ), we start again with the definition of PV,

$$\mathcal{P}_d = \frac{1}{\rho_a} \vec{\xi}_d \cdot \nabla \theta, \quad (4.6)$$

which is identical to (4.1) except that  $\theta_v$ ,  $\rho$ , and  $\vec{\xi}$  have reduced to  $\theta = T \left( \frac{p_0}{p_a} \right)^\kappa$ ,  $\rho_a$ , and  $\vec{\xi}_d$  for the dry case. Employment of the same approximations that yielded (4.2) results in the isobaric form of the dry PV,

$$\mathcal{P}_d = -g \left( f \hat{k} + \vec{\xi}_d \right) \cdot \nabla_p \theta, \quad (4.7)$$

where  $\vec{\xi}_d$  is the three-dimensional dry balanced vorticity vector calculated from the dry mass field. The derivation of the dry form of the PV equation continues exactly as outlined above for the moist case except that all of the moisture-dependent variables in (4.1) to (4.5) are replaced by their dry counterparts. Thus,

$$\mathcal{P}_d = \frac{g\kappa\pi}{p} \left[ (f + \nabla^2\psi_d) \frac{\partial^2\phi_d}{\partial\pi^2} - \frac{\partial^2\psi_d}{\partial x\partial\pi} \frac{\partial^2\phi_d}{\partial x\partial\pi} - \frac{\partial^2\psi_d}{\partial y\partial\pi} \frac{\partial^2\phi_d}{\partial y\partial\pi} \right], \quad (4.8)$$

is the PV equation for a dry atmosphere, where the  $d$  subscripts indicate that the variables are computed for the dry state. Again,  $\psi_d$  is related to  $\phi_d$  through an appropriate balance equation. As noted by Schubert et al. (2001), this is in fact the form of PV that is generally, but incorrectly, used in calculations. The difference between this dry PV and the full PV given by (4.5) forms the basis of  $\text{PV}_{\text{mc}}$  since it represents the effects on the PV field of the inclusion of water vapor.

The moist component PV is itself simply defined as the difference between the full (moist) and dry PV fields of a balanced atmosphere,

$$\mathcal{P}_{\text{mc}} \equiv \mathcal{P} - \mathcal{P}_d. \quad (4.9)$$

This expression could be employed directly given a knowledge of the dry and moist atmospheric states. In fact, the inversion of  $\text{PV}_{\text{mc}}$  calculated from (4.9) would yield the moist component streamfunction and geopotential fields. However, a diagnostic expression for  $\text{PV}_{\text{mc}}$  is desirable for two reasons. Firstly, the signal-to-noise ratio of (4.9) is very small, and secondly, very little physical insight is gained from this simple expression. Accordingly, we begin by expanding the full geopotential and balanced streamfunction fields of (4.5) in a Maclaurin series around the dry ( $\rho = \rho_a$ ) state and introduce the total mixing ratio ( $w$ ) as the independent moisture variable,

$$\phi = \phi_{(w=0)} + \left. \frac{\partial\phi}{\partial w} \right|_{w=0} w + \frac{1}{2} \left. \frac{\partial^2\phi}{\partial w^2} \right|_{w=0} w^2 + \dots \quad (4.10)$$

$$\psi = \psi_{(w=0)} + \left. \frac{\partial\psi}{\partial w} \right|_{w=0} w + \frac{1}{2} \left. \frac{\partial^2\psi}{\partial w^2} \right|_{w=0} w^2 + \dots \quad (4.11)$$

Here,  $w = w_m + w_r$ , where  $w_m = \frac{\rho_m}{\rho_a}$  is the summed water vapor and cloud water mixing ratio, and  $w_r = \frac{\rho_r}{\rho_a}$  is the rainwater mixing ratio. We note that  $\phi_{(w=0)} = \phi_d$

and  $\psi_{(w=0)} = \psi_d$  and retain only the zeroth and first order terms to obtain,

$$\phi = \phi_d + \phi_{\text{mc}}, \quad \text{and}, \quad (4.12)$$

$$\psi = \psi_d + \psi_{\text{mc}}, \quad (4.13)$$

where  $\phi_{\text{mc}} = \frac{\partial \phi}{\partial w} \Big|_{w=0} w$  is the moist component geopotential and  $\psi_{\text{mc}} = \frac{\partial \psi}{\partial w} \Big|_{w=0} w$  is the corresponding balanced moist component streamfunction. Substitution of the expressions in (4.13) into (4.5) and subtraction of (4.8) yields an expression for  $\text{PV}_{\text{mc}}$

$$\mathcal{P}_{\text{mc}} = \frac{g\kappa\pi}{p} \left[ (f + \nabla^2 \psi_d) \frac{\partial^2 \phi_{\text{mc}}}{\partial \pi^2} + \nabla^2 \psi_{\text{mc}} \frac{\partial^2 \phi_d}{\partial \pi^2} + \nabla^2 \psi_{\text{mc}} \frac{\partial^2 \phi_{\text{mc}}}{\partial \pi^2} - \mathcal{L}(\phi_d, \psi_{\text{mc}}) - \mathcal{L}(\psi_d, \phi_{\text{mc}}) - \mathcal{L}(\psi_{\text{mc}}, \phi_{\text{mc}}) \right], \quad (4.14)$$

$$\text{where, } \mathcal{L}(A, B) = \frac{\partial^2 A}{\partial x \partial \pi} \frac{\partial^2 B}{\partial x \partial \pi} + \frac{\partial^2 A}{\partial y \partial \pi} \frac{\partial^2 B}{\partial y \partial \pi}$$

as defined by (4.9). Not suprisingly, the form of this equation is similar to that of the piecewise decomposition of DE91. In this case however, instead of expanding the perturbations around a background mean, the anomalies are defined relative to the instantaneous dry state. As well, the nonlinear terms in (4.14) are explicitly retained rather than hidden in the nonconstant coefficients of the linear differential operator. Equation 4.14 represents a definition of the portion of the PV field directly attributable to the presence of water in the atmosphere. We will now test the applicability of this expression using an idealized atmosphere and balance condition to ease interpretation of the results.

### 4.3 $\text{PV}_{\text{mc}}$ in an idealized model atmosphere

The complexity of (4.14) makes the interpretation of  $\text{PV}_{\text{mc}}$  a daunting task. It is therefore instructive to consider the distribution of  $\text{PV}_{\text{mc}}$  under a set of simplifying conditions that make (4.14) tractable. We begin in section 4.3.1 with a description of the idealized model to be employed in developing an analytic expression for  $\text{PV}_{\text{mc}}$ . Section 4.3.2 outlines the steps required for the calculation of  $\text{PV}_{\text{mc}}$ , and calculations for each item are presented in sections 4.3.3 through 4.3.8.

### 4.3.1 Background state and moisture structure

For the purposes of defining a simple framework under which to develop and interpret the moist component variables, a simplified atmospheric structure is assumed. The dry atmosphere is defined to be isothermal (dry bulb temperature constant everywhere) and motionless. “Dry-balanced” implies that the vertical structure of the model atmosphere is described by a hypsometric relation of the form,

$$\ln \left( \frac{p_{od}}{p_d} \right) = \frac{g}{RT} \int_{z_{od}}^{z_d} dZ, \quad (4.15)$$

where all of the symbols have their standard meanings and subscript “o” refers to surface values. The “moist-balanced” atmosphere is one in which the dry bulb temperature in (4.15) is replaced by an approximate form of the virtual temperature,

$$T_v \approx T(1 + 0.6w_v), \quad (4.16)$$

and the dry subscripts are removed. For the remainder of the paper, we consider only subsaturated water vapor by redefining  $w \equiv w_v$ , the mixing ratio, in units of  $\text{kg}_{(\text{water vapor})} \text{kg}_{(\text{dry air})}^{-1}$ . Thus, (4.16) becomes  $T_v = T(1 + 0.6w)$ . This simplified form of the virtual temperature is used because of its linear dependence on the moisture field that makes an analytic description of  $PV_{\text{mc}}$  possible. In calculations for the real atmosphere, a generalized form of the virtual temperature which includes the effects of cloud and rainwater should be used (Schubert et al. 2001). Since the mixing ratio will be allowed to vary with height,  $T_v$  cannot be removed from the integral as in (4.15). Consequently, the hypsometric equation for a moist-balanced atmosphere takes the form,

$$\ln \left( \frac{p_o}{p} \right) = \frac{g}{R} \int_{z_o}^z \frac{dZ}{T_v}. \quad (4.17)$$

The Coriolis parameter ( $f_o$ ) is assumed to be a constant of  $10^{-4}\text{s}^{-1}$  everywhere and results in a non-zero dry-balanced absolute vorticity, in spite of the motionless constraint in the dry case. The differences in the heights which serve as the upper bounds of the integration in (4.15) and (4.17) ( $z_d$  versus  $z$ ) will form the basis of the moist component perturbations. The height differences follow directly from the fact

that the density of water vapor is less than that of air. Thus, the inclusion of water vapor in a hydrostatically balanced column will result in increased thicknesses.

The profile of moisture in the model atmosphere is described by an exponential function of the form,

$$w(z_d) = w_o e^{-\frac{z_d}{H_z}}, \quad (4.18)$$

where  $w_o$  is the mixing ratio at the surface, and  $H_z$  is the e-folding height of the profile. The dry vertical coordinate ( $z_d$ ) is used since it is independent of the mixing ratio. The moisture variation in the horizontal is axi-symmetric and therefore best described in cylindrical coordinates. In the following equations,  $r$  and  $\lambda$  represent the radial and azimuthal directions respectively. Since the moisture field is azimuthally invariant, the full three dimensional structure of the mixing ratio is given by,

$$w(r, z_d) = w_o e^{-\left(\frac{r^2}{H_x^2} + \frac{z_d}{H_z}\right)}, \quad (4.19)$$

where  $H_x$  is the horizontal length scale of the moisture “bubble”. The structure of the mixing ratio field is shown in fig. 4.2.

### 4.3.2 Introduction to $PV_{mc}$ in the model atmosphere

A brief outline of the method used to obtain the moist component perturbation variables is contained in this subsection. The steps described here will be presented in greater detail throughout the remainder of the section. Everywhere here, moist component perturbations (denoted by a subscript “mc”) are defined relative to the dry state as described by (4.15). The first step consists of diagnosing the height change of a pressure surface by differencing (4.15) and (4.17). As a lower boundary condition, we assume that the dry surface pressure is the same as the moist surface pressure,

$$p_{od}(z_d=0) = p_o(z=0), \quad (4.20)$$

since analyses of surface pressure are reasonably accurate. This is equivalent to assuming that for each unit mass of water vapor present in the moist column, an equivalent mass of dry air is absent.

Another reasonable, though more complicated, choice of boundary condition involves the use of the height of the humidity maximum in the column ( $z_{w_{max}}$ ). In this case, we set,

$$p_d(z_d=z_{w_{max}}) = p(z=z_{w_{max}}), \quad (4.21)$$

so that surface pressure perturbations are restricted to be non-positive. The physical meaning of (4.21) is best described by use of a simple thought exercise (fig. 4.1). A motionless point heat source located between discrete pressure levels  $p^+$  and  $p^-$  will lead to a hydrostatically increased separation distance ( $\delta p > \delta p_o$ ). Since the heating is confined by the extent of the source (the effects of diffusion are ignored in this exercise) the temperatures in the layers below  $p^+$  and above  $p^-$  are unchanged. Thus, the thicknesses  $\delta p^+$  and  $\delta p^-$  are constant and the height perturbations experienced by the  $p^+$  and  $p^-$  surfaces are translated hydrostatically to all levels below and above  $p$ , respectively. This choice of boundary condition is characterized by null geopotential perturbations at  $z_{w_{max}}$ , as evinced by (4.21), and contains the intuitive advantage that the surface pressure need not be fixed. In the simplified atmosphere described here, and indeed in general for the real atmosphere, the maximum water vapor mixing ratio occurs at the lowest level, so that (4.21) reduces exactly to (4.20). Even for cases in which  $z_{w_{max}}$  is slightly elevated above the lowest level, (4.21) likely remains approximately true and surface pressure perturbations will be small.

With the lowest height (surface pressure) fixed, any non-zero specific humidity will result in higher virtual temperatures in the column and thus larger thicknesses in the moist atmosphere. These differences in the geopotential heights of each pressure level in the moist atmosphere can be related to differences in the streamfunction through a balance equation. In the interests of obtaining an analytic result, geostrophic balance is assumed. A higher order balance equation (e.g., Charney, 1955) might be more applicable for the real atmosphere, especially given the fine-scale structure of typical moisture features. The Laplacian of this moist component streamfunction yields the moist component relative vorticity, which appears in two of the terms in the  $PV_{mc}$  equation (4.14). The changes to the static stability of the column are obtained by

considering the difference between the vertical gradients of dry ( $\theta$ ) and virtual ( $\theta_v$ ) potential temperatures.

### 4.3.3 Moist component height perturbations

In order to track the height change of a pressure level,  $p_d$  and  $p$  in (4.15) and (4.17) are set equal, and the perturbation  $z_{mc} = z - z_d$  is obtained. Differencing (4.15) and (4.17) and employing the condition described by (4.20) yields,

$$\int_0^z \frac{dZ}{T_v} = \int_0^{z_d} \frac{dZ}{T}, \quad (4.22)$$

which may be rearranged to produce,

$$\int_{z_d}^z \frac{dZ}{T_v} = 0.6W, \quad \text{where,} \quad (4.23)$$

$$W = \int_0^{z_d} \frac{w}{T_v} dZ, \quad (4.24)$$

is the moisture integral. In the simplified model atmosphere considered here, the integral in (4.24) can be expressed analytically. Solving for the height perturbation yields,

$$z_{mc} = 0.6WT + H_z \ln \left[ 1 - 0.6w \left( e^{-\frac{0.6WT}{H_z}} - 1 \right) \right]. \quad (4.25)$$

To a good approximation,  $T_v$  may be considered constant for small height changes ( $z_{mc}$ ), so virtual temperature can be brought outside the integral in (4.23) to yield an approximation for  $z_{mc}$ ,

$$z_{mc} \approx 0.6WT_v. \quad (4.26)$$

For our simplified atmosphere, it is found that (4.26) predicts height perturbations whose values are within 1% of those given by (4.25) (fig. 4.3). We will therefore use (4.26) to diagnose moist component height perturbations in an effort to keep the subsequent analytic solutions as simple as possible without an appreciable loss of accuracy.

### 4.3.4 Moisture integral

Using the idealized exponential profile of humidity given by (4.19), it is possible to integrate (4.24) using partial fractions. The complete form of the integral yields,

$$W = \frac{H_z}{0.6T} \ln \left( \frac{1 + 0.6w_o A}{1 + 0.6w} \right), \quad (4.27)$$

$$\text{where } A = e^{-\frac{r^2}{H_x^2}}, \quad \text{and } \alpha = e^{\frac{z_d}{H_z}}.$$

A highly simplified result is obtained if we assume that  $T_v \rightarrow T$  in the denominator of (4.24). This approximation results in,

$$W \approx \frac{H_z w_o A}{T} \left( 1 - \frac{1}{\alpha} \right), \quad (4.28)$$

which is accurate to within 1% for tropical moisture profiles (fig. 4.3). A cross-section of  $W$  through the center of the moisture maximum is shown in fig. 4.4a. The free parameters  $H_z$  and  $H_x$  are set to 3000 m and 3000 km respectively for all of the calculations in this study. Equation (4.28) will be used to describe the moisture integral for the remainder of the paper.

### 4.3.5 Moist component geopotential and streamfunction

From (4.26), the expression for the moist component geopotential ( $\phi_{\text{mc}} = gz_{\text{mc}}$ ) is simply,

$$\phi_{\text{mc}}(r, z_d) = 0.6gT_v(r, z_d)W(r, z_d). \quad (4.29)$$

Using the approximate form of the moisture integral (4.28), the moist component geopotential can be expressed as,

$$\phi_{\text{mc}} = 0.6gH_z w_o A (1 + 0.6w) \left( 1 - \frac{1}{\alpha} \right), \quad (4.30)$$

and is displayed in fig. 4.4b. Assuming that the perturbations are geostrophically balanced, the moist component streamfunction is trivially derived as,

$$\psi_{\text{mc}} = \frac{0.6gH_z w_o}{f_o} A (1 + 0.6w) \left( 1 - \frac{1}{\alpha} \right). \quad (4.31)$$

Equations (4.30) and (4.31) describe the difference in the geopotential and streamfunction fields between a dry balanced atmosphere (4.15) and a moist balanced atmosphere (4.17). As evidenced by fig. 4.4b, the largest perturbations in the geopotential and streamfunction fields occur at upper levels directly above the moisture maximum. Although this result may initially seem somewhat counter-intuitive since the humidity maximum occurs at the surface, it is a necessary consequence of the lower boundary condition for the moisture integral given by (4.20). The height of the column base is fixed and the perturbations are sign-definite and positive; therefore, the moisture integral (and thus the moist component geopotential and streamfunction profiles) are monotonic increasing functions of height. This leads directly to the result shown in fig. 4.4b.

### 4.3.6 Moist component relative vorticity

The qualitative differences in the vorticity structures of the dry and moist hydrostatically balanced states is evident from the thickness analysis described in the outline of this section. Since the lowest level heights and surface pressures are not allowed to change, the consideration of moisture results in increased heights everywhere above the ground. Near the origin, where the specific humidity is largest, this effect will be most pronounced. We thus end up with a “dome” of higher heights and attendant anticyclonic flow at upper levels in the vicinity of the humidity maximum. This leads to a predominantly negative moist component relative vorticity, which can be expressed as,

$$\begin{aligned}
 \xi_{\text{mc}} &= \nabla^2 \psi_{\text{mc}} \\
 &= \frac{1}{r} \frac{\partial}{\partial r} \left( r \frac{\partial \psi}{\partial r} \right) \quad (\text{in the axisymmetric model employed here}) \\
 &= -\frac{2.4gw_o}{f_o} \frac{H_z}{H_x^2} \left( 1 - \frac{1}{\alpha} \right) A \left[ (1 + 1.2w) \left( 1 - \frac{r^2}{H_x^2} \right) - 1.2 \frac{r^2}{H_x^2} w \right]. \quad (4.32)
 \end{aligned}$$

For the idealized moisture distribution described by (4.19), the value of  $\xi_{\text{mc}}$  is generally negative (fig. 4.4c) for  $r < H_x$  and positive for  $r > H_x$ . This is because the curvature component of the vorticity (considered in a natural coordinate system)

dominates inside  $H_x$  and the shear component dominates at larger radii. For a local minimum in the moisture field, the moist component relative vorticity would be positive near the center, and negative beyond  $H_x$ .

### 4.3.7 Moist component static stability

Absolute vorticity plays an important role in the calculation of PV; however, so does the static stability,  $\frac{\partial\theta}{\partial p}$ . For consistency with (4.14), we will employ an alternative form containing the geopotential in Exner function coordinates,

$$\frac{\partial^2\phi}{\partial\pi^2} = -\frac{p}{\kappa\pi} \frac{\partial\theta_v}{\partial p}. \quad (4.33)$$

Using the simplifying qualities of the current model,

$$\theta_{\text{mc}} = 0.6w\theta, \quad \text{and,} \quad \frac{\partial^2\phi_d}{\partial\pi^2} = \frac{\theta}{\pi}, \quad (4.34)$$

expansion of the static stability into dry and moist component parts results in a moist component static stability term,

$$\frac{\partial^2\phi_{\text{mc}}}{\partial\pi^2} = -0.6w\theta \left( \frac{\theta}{gH_z} - \frac{1}{\pi} \right), \quad (4.35)$$

which is negative for all reasonable  $H_z$ . The form of (4.35) depends strongly on the vertical gradient of  $w$ ; in fact, if  $w$  were to *increase* exponentially with height, the sign of the (dominant) first bracketed term in (4.35) would reverse.

### 4.3.8 Moist component PV

Moist component PV is derived in Cartesian coordinates as (4.14). The cylindrical coordinate form of the diagnostic  $PV_{\text{mc}}$  equation is,

$$\mathcal{P}_{\text{mc}} = \frac{g\kappa\pi}{p} \left[ (f + \nabla^2\psi_d) \frac{\partial^2\phi_{\text{mc}}}{\partial\pi^2} + \nabla^2\psi_{\text{mc}} \frac{\partial^2\phi_d}{\partial\pi^2} + \nabla^2\psi_{\text{mc}} \frac{\partial^2\phi_{\text{mc}}}{\partial\pi^2} - \mathcal{L}(\phi_d, \psi_{\text{mc}}) - \mathcal{L}(\psi_d, \phi_{\text{mc}}) - \mathcal{L}(\psi_{\text{mc}}, \phi_{\text{mc}}) \right], \quad (4.36)$$

$$\text{where,} \quad \mathcal{L}(A, B) = \frac{\partial^2 A}{\partial r \partial \pi} \frac{\partial^2 B}{\partial r \partial \pi} + \frac{1}{r^2} \frac{\partial^2 A}{\partial \lambda \partial \pi} \frac{\partial^2 B}{\partial \lambda \partial \pi},$$

$$\text{and,} \quad \nabla^2 = \frac{1}{r} \frac{\partial}{\partial r} \left( r \frac{\partial}{\partial r} \right) + \frac{1}{r^2} \frac{\partial^2}{\partial \lambda^2}.$$

Employing the simplifying assumptions of our model (isothermal, motionless dry state, f-plane), (4.36) reduces to,

$$\mathcal{P}_{\text{mc}} = \frac{g\kappa\pi}{p} \left[ \underbrace{\xi_{\text{mc}} \frac{\partial^2 \phi_d}{\partial \pi^2}}_{\text{term 1}} + \underbrace{f_{\circ} \frac{\partial^2 \phi_{\text{mc}}}{\partial \pi^2}}_{\text{term 2}} + \underbrace{\xi_{\text{mc}} \frac{\partial^2 \phi_{\text{mc}}}{\partial \pi^2}}_{\text{term 3}} - \underbrace{\mathcal{L}(\psi_{\text{mc}}, \phi_{\text{mc}})}_{\text{term 4}} \right]. \quad (4.37)$$

The analytic form of the nonlinear metric term (term 4) in (4.37) is easily derived as,

$$\mathcal{L}(\psi_{\text{mc}}, \phi_{\text{mc}}) = \frac{1}{f_{\circ}} \left( \frac{1.2w\theta_{dr}}{H_x^2} \right)^2, \quad (4.38)$$

from our knowledge of the three dimensional distribution of  $\phi_{\text{mc}}$  and the balance equation. Thus, the full analytic form of the  $\text{PV}_{\text{mc}}$  equation for the simplified model atmosphere is given by,

$$\mathcal{P}_{\text{mc}} = \frac{g\kappa\pi}{p} \left\{ \underbrace{-\frac{2.4gw_{\circ}\theta}{f_{\circ}\pi} \frac{H_z}{H_x^2} \left(1 - \frac{1}{\alpha}\right) A \left[ (1 + 1.2w) \left(1 - \frac{r^2}{H_x^2}\right) - 1.2 \frac{r^2}{H_x^2} w \right]}_{\text{term 1: dynamical induction}} \right. \\ \underbrace{-0.6f_{\circ}w\theta \left( \frac{\theta}{gH_z} - \frac{1}{\pi} \right)}_{\text{term 2: stability reduction}} \\ \underbrace{+ \frac{1.44gw_{\circ}\theta w}{f_{\circ}} \frac{H_z}{H_x^2} \left(1 - \frac{1}{\alpha}\right) A \left[ (1 + 1.2w) \left(1 - \frac{r^2}{H_x^2}\right) - 1.2 \frac{r^2}{H_x^2} w \right] \left( \frac{\theta}{gH_z} - \frac{1}{\pi} \right)}_{\text{term 3: nonlinear moist component perturbation}} \\ \left. \underbrace{-\frac{1}{f_{\circ}} \left( \frac{1.2w\theta_{dr}}{H_x^2} \right)^2}_{\text{term 4: nonlinear metric}} \right\}. \quad (4.39)$$

An investigation of each of the terms of (4.39) will be presented in section 4.4. Radius-height plots of the individual terms appear in fig. 4.5 and a cross-section of  $\text{PV}_{\text{mc}}$  is shown in fig. 4.4d. Calculations are performed only up to 300 hPa since the static stability ( $\frac{\partial^2 \phi}{\partial \pi^2}$ ) at that level exceeds  $0.6 \text{ K}^2 \text{ s}^3 \text{ m}^{-2}$ , a typical value for the tropopause. Above this level lies the idealized model's "stratosphere" - although the tropopause in the model is not defined by a sharp gradient in stability due to the isothermal state - in which we do not consider the effects of water vapor due to its negligible quantities at such high altitudes.

Like (4.9), (4.39) describes the  $PV_{mc}$  field - the PV that is present in the atmosphere solely as a result of the presence of subsaturated water vapor. It is conceptually the same as an individual component of the decomposed PV field of the type described by DE91. The moist component PV computed from (4.39) is therefore an ideal candidate for a piecewise PV inversion. Such an inversion would yield the balanced perturbation geopotential and streamfunction fields associated with subsaturated moisture. In this way, the dynamical influence of individual humidity structures, generally considered to be relatively passive until saturation, can be directly evaluated. This link between PV and atmospheric water is crucial for the type of sensitivity studies proposed by McTaggart-Cowan et al. (2001), which involve modifications to the moisture field.

## 4.4 Interpretation of $PV_{mc}$

The utility of  $PV_{mc}$  stems from its ability to describe the balanced portion of the dynamics directly associated with the atmospheric moisture field. Although the analytic model presented here deals only with subsaturated moisture, (4.9) is a general equation which can include the effects of both cloud and rainwater. Local maxima in the moisture field generally correspond to negative  $PV_{mc}$  whereas local minima lead to positive  $PV_{mc}$ . The vertical gradient of humidity also plays an important role in determining the sign of  $PV_{mc}$ . An investigation of the individual terms in (4.39) yields insight into how these anomalies are created.

Term 1 of (4.39), the “dynamical induction” term, describes the role that subsaturated moisture plays in modifying balanced atmospheric dynamics. The generation of a height “dome” centered above the humidity maximum results in balanced anticyclonic flow around the origin. As noted in section 4.3.6, the competing contributions of curvature and shear vorticity result in a sign switch at  $r \approx H_x$  for the dynamical induction term. In the analytic model, the influence of curvature is greater for  $r \lesssim H_x$  and results in the expected anticyclonic vorticity near the center. For  $r \gtrsim H_x$ , this term becomes positive; however, its values are so small beyond  $H_x$  as to be negligible

(fig. 4.5a).

The “stability reduction” term (term 2) in (4.39) describes the effects of the moisture-modified static stability on PV. Any monotonically decreasing function of  $w$  with  $z$  will have the effect of reducing the atmosphere’s static stability as virtual temperatures below rise more than those aloft. This will necessarily decrease the magnitude of PV everywhere, but most notably where the vertical gradient of  $w$  is the largest. In the model,  $w$  decreases exponentially with height, so this term is a maximum near the surface as shown in fig. 4.5b. In the model troposphere, this is the dominant term of the  $PV_{mc}$  equation.

Terms 3 (the “nonlinear moist component perturbation”) and 4 (the “nonlinear metric”) are two orders of magnitude smaller than the leading terms (1 and 2) as would be expected of perturbation correlations. As shown in fig. 4.5c, the nonlinear moist component perturbation is largest in the region where both the dynamical induction and the stability reduction terms are of significant magnitude. The nonlinear metric (fig. 4.5d) is identically zero at the origin in the analytic model, and reaches a maximum near the surface inside  $H_x$ . As noted by DE91, these nonlinear terms must be retained in order to ensure the additive nature of the component perturbations under the piecewise PV framework.

Schematics of the leading  $PV_{mc}$  terms for several moisture profiles are shown in fig. 4.6. All of the conceptual models presented here are valid for a local moisture maximum in the horizontal. For a local minimum in humidity, the sign of the  $PV_{mc}$  anomalies labelled “vorticity” in fig. 4.6 (term 1 in the description above) should be reversed. Figure 4.6a summarizes the case presented in this paper. Humidity decreases monotonically with height, leading to destabilization primarily at lower levels and a negative  $PV_{mc}$  anomaly. The moisture integral is of moderate magnitude, and leads to a negative  $PV_{mc}$  anomaly at higher levels. A constant mixing ratio with height, as shown in fig. 4.6b, results in slightly increased static stabilities at all levels and a weak positive  $PV_{mc}$  anomaly. At upper levels, the large moisture integral will lead to a strong negative anomaly, the effects of which will outweigh those of

the stability reduction term (term 2). In another unusual case in which the mixing ratio increases monotonically with height (fig. 4.6c), the increased static stability at middle and upper levels will tend to produce a positive anomaly. However, the continually-increasing moisture integral leads to a negative  $PV_{mc}$  anomaly. The sign of the resulting  $PV_{mc}$  is case-dependent. Figure 4.6d shows the  $PV_{mc}$  structure associated with a mid-level moisture maximum. In this case, static stabilities below the maximum are increased while those above it are decreased, leading to an opposite-signed couplet in the  $PV_{mc}$  field centered on the humidity peak. At upper levels, the moderately-large moisture integral produces moist component geopotentials which result in an upper level negative  $PV_{mc}$  anomaly. Although the list of possible states presented here is by no means exhaustive, the schematics of fig. 4.6 will hopefully serve as a starting point from which to address more complicated situations.

## 4.5 Inversion of $PV_{mc}$

As described in section 4.34.3.8,  $PV_{mc}$  represents a component perturbation on the background (dry) state (4.9). It is thus possible to retrieve the balanced wind and mass fields resulting from the presence of subsaturated water vapor using a piecewise PV inversion scheme such as that described by DE91. Such an inversion of the  $PV_{mc}$  field (fig. 4.4d) yields the balanced wind, temperature, and height anomalies shown in fig. 4.7. The temperature perturbations arising from the  $PV_{mc}$  anomalies should be exactly those given by the virtual temperature, allowing for the retrieval of the mixing ratio through rearrangement of (4.16),

$$w = \frac{\delta T}{0.6T} \quad , \quad (4.40)$$

where  $\delta T$  is the inverted temperature perturbation and  $T$  is the dry bulb temperature of the (dry) background state. The results of this retrieval are shown in fig. 4.8. The small differences between the original and retrieved mixing ratio values near the surface reflect the errors associated with the geostrophic balance assumption applied during the derivation of  $PV_{mc}$  for the purposes of obtaining analytic solutions for

this idealized case.

The calculation of  $PV_{mc}$  for more realistic atmospheres will involve the use higher-order balance equations, and may proceed in one of two ways. The simplest approach employs (4.9), and consists of calculating  $\phi_d$  from (4.15), and  $\psi_d$  from a balance equation. Having obtained these values, the calculation of  $\mathcal{P}_d$  from (4.8) is simple, as is the solution of (4.9) for  $PV_{mc}$  ( $\mathcal{P}_{mc}$ ). Alternatively,  $PV_{mc}$  can be calculated directly from (4.14) using (4.23) to compute  $\phi_{mc}$ , and a balance equation to determine  $\psi_{mc}$ . The geopotential and streamfunction values for the dry atmosphere are again calculated from (4.15) and a balance equation, respectively. Both of these techniques result in three-dimensional  $PV_{mc}$  fields which can be inverted using a piecewise PV inversion. For the case presented here (fig. 4.8) the piecewise inversion of  $PV_{mc}$  calculated directly from (4.14) (and hence (4.39) for our simple atmosphere) serves to quantify the role that subsaturated moisture plays in adjusting the dynamics of the atmosphere. A local maximum (minimum) in the moisture integral results in anticyclonic (cyclonic) flow and increased (decreased) heights.

## 4.6 Summary and Discussion

A PV-based variable ( $PV_{mc}$ ) describing the effects of water vapor, cloud, and rain-water on balanced atmospheric dynamics was derived using the moist PV definition of Schubert et al. (2001) and the piecewise decomposition framework of DE91. The complexity of the full equation (4.14) for  $PV_{mc}$  makes interpretation difficult for a realistic atmosphere. To simplify the problem, we focused on describing the dynamical influence of subsaturated water vapor using an idealized atmospheric model. Using two forms of the hypsometric equation, (4.15) and (4.17), which assume dry and moist hydrostatic balance respectively, perturbation equations for the geopotential, streamfunction, relative vorticity, static stability, and PV were developed. When viewed as a component anomaly, the  $PV_{mc}$  field described by (4.36) is an excellent candidate for PV inversion. The resulting mass and wind fields describe the direct effect of the presence of atmospheric water on the dynamics of the atmosphere. It is

also possible to retrieve the original specific humidity field through (4.40).

A potential application of this moist component methodology is to the problem of sensitivity testing as outlined by McTaggart-Cowan et al. (2001). The sensitivity of the extratropical transition and reintensification of Hurricane Earl (1998) to PV anomalies in the initial conditions was investigated using PV removal and inversion. However, as noted in that paper, it is very difficult to assess the impact of the moisture field on the rapid redevelopment of the storm. The research presented here suggests that a link between the PV field and the moisture field exists through the  $PV_{mc}$  variable. For example, the removal of the moisture, and balanced mass and wind fields associated with temporally anomalous  $PV_{mc}$  could be coupled with the removal of the dry PV anomaly associated with ex-hurricane Earl to completely remove the remnant hurricane from the initial conditions of a simulation. Such a sensitivity case study will be the topic of a future paper. The results from such research may elucidate the role of the near-surface tropical features in rapid cyclogenesis. In such a way, we hope that  $PV_{mc}$  will allow for a quantitative assessment of the relative importance of dynamics and thermodynamics in developing systems.

## Acknowledgments

We thank the members of the Mesoscale Research Group (McGill University) for their guidance and support throughout the course of this research. As well, we thank the three anonymous reviewers for their help in preparing this paper for publication. This work has been supported by Natural Sciences and Engineering Research Council grants and by subventions from the Meteorological Service of Canada.

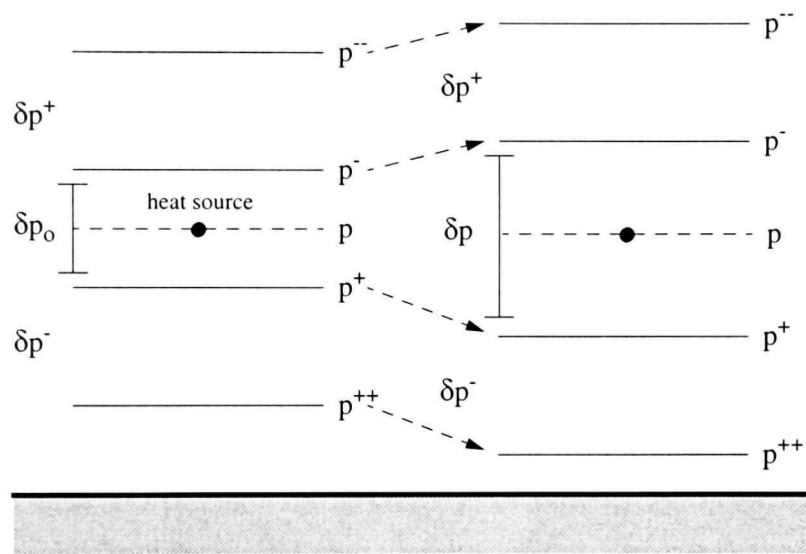


Figure 4.1: Schematic representation of hydrostatic adjustment resulting from a point heat source elevated above the surface.

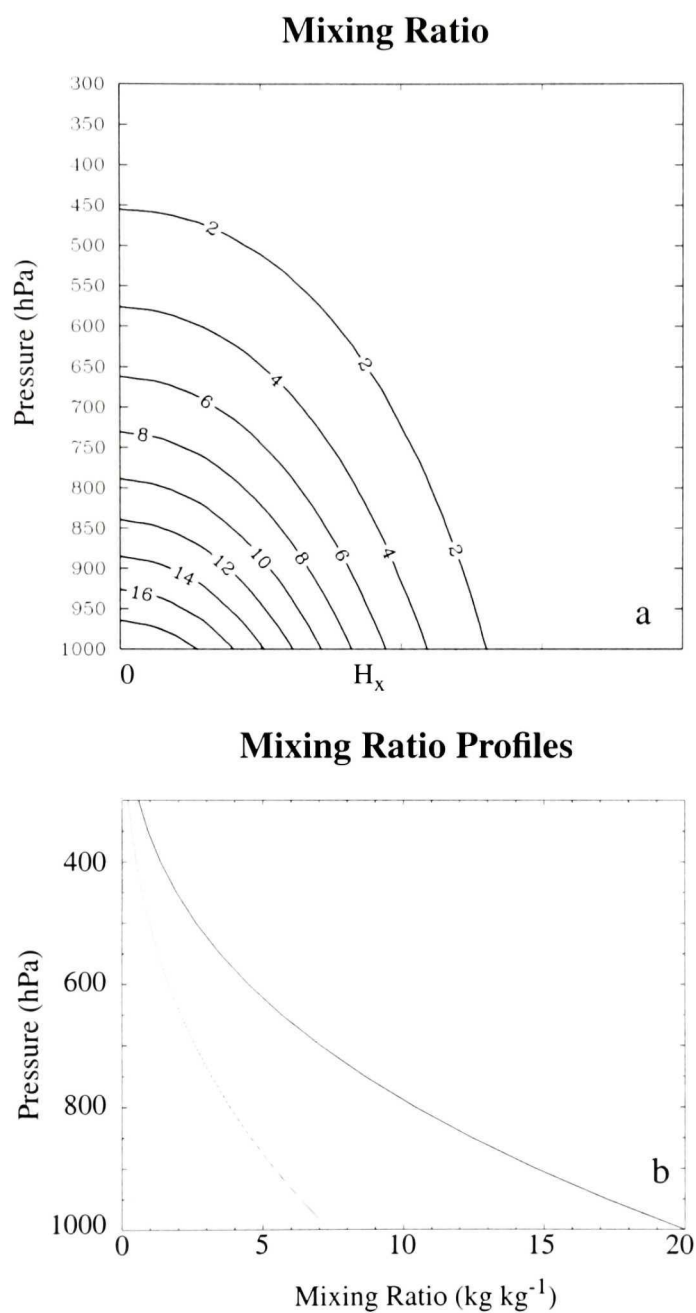


Figure 4.2: Cross-section of the water vapor mixing ratio (panel a) with 2  $\text{g kg}^{-1}$  contour intervals. Panel b shows profiles of the mixing ratio taken at the center (rightmost curve),  $H_x$  (middle curve), and  $2H_x$  (leftmost curve).

## Relative Errors for Approximations

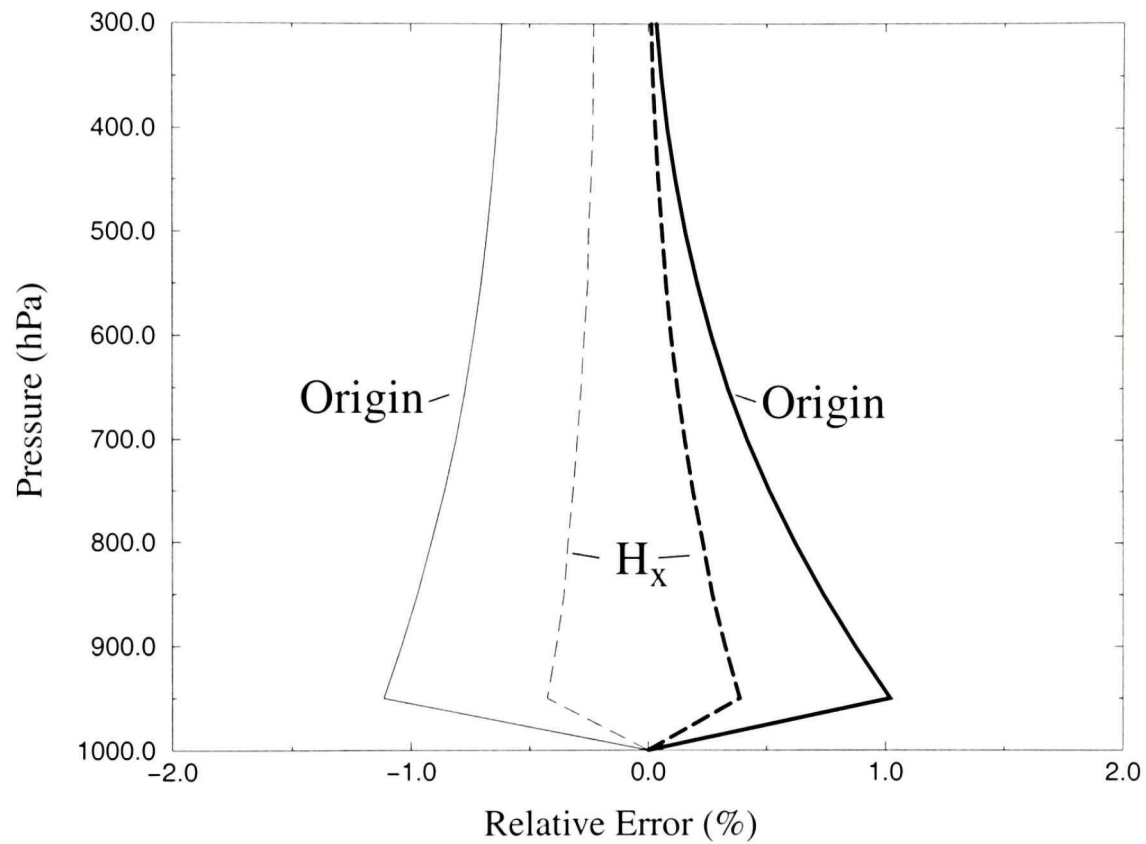


Figure 4.3: Relative errors of approximations for  $z_{mc}$  from (4.25), light curves, and  $W$  from (4.27), heavy curves. Profiles are taken at the origin (solid lines) and at  $H_x$  (dashed lines) as indicated.

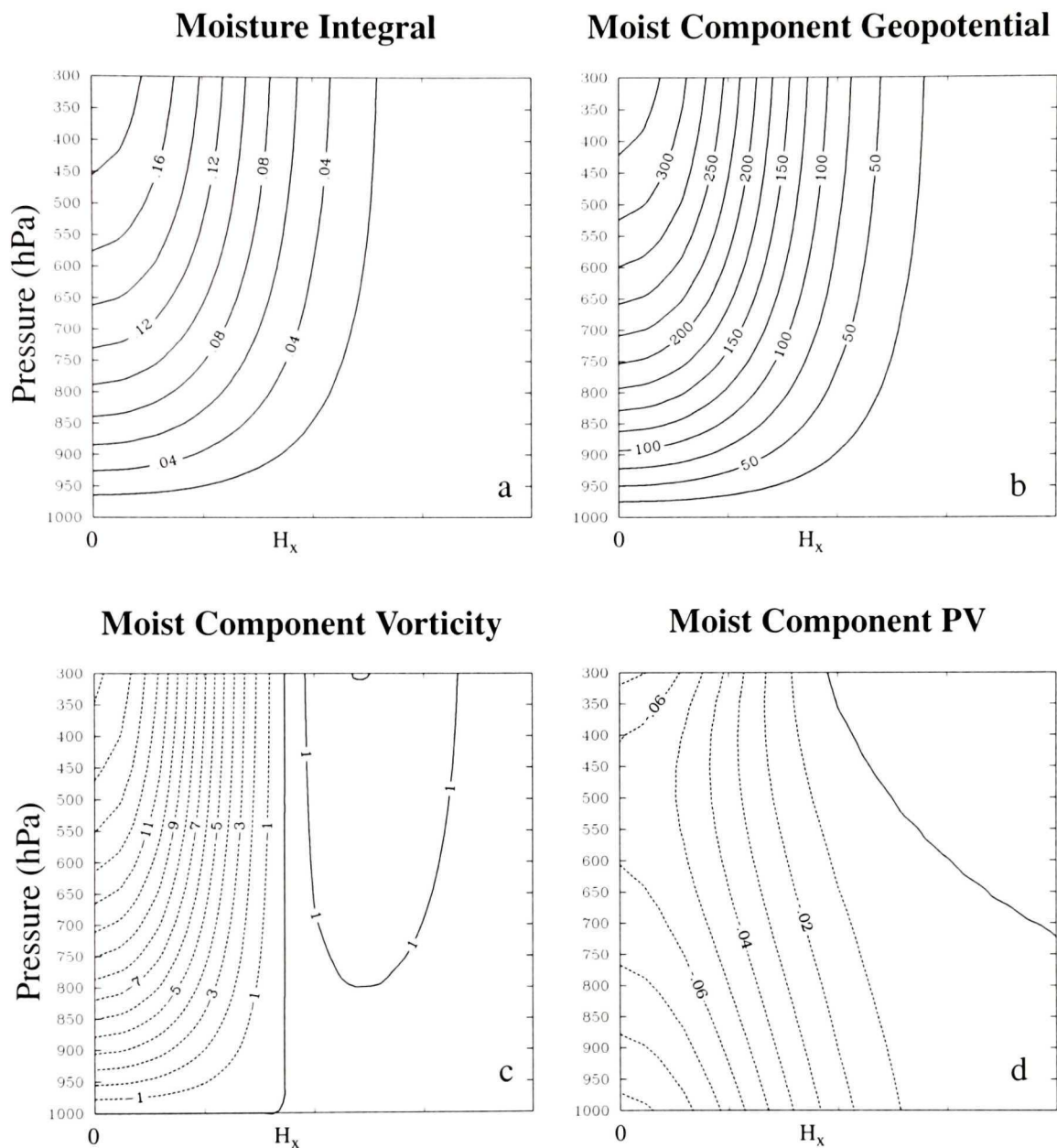


Figure 4.4: Cross-sections of the moisture integral (a), the geopotential perturbation (b), the relative vorticity perturbation (c), and  $PV_{mc}$  (d). Panel a has contours plotted every  $0.02 \text{ m K}^{-1}$ , panel b every  $25 \text{ m}^2 \text{ s}^{-2}$ , panel c every  $1 \times 10^7 \text{ s}^{-1}$  and panel d every  $0.01 \text{ PVU}$  ( $1 \text{ PVU} = 10^{-6} \text{ m}^2 \text{ K kg}^{-1} \text{ s}^{-1}$ ).

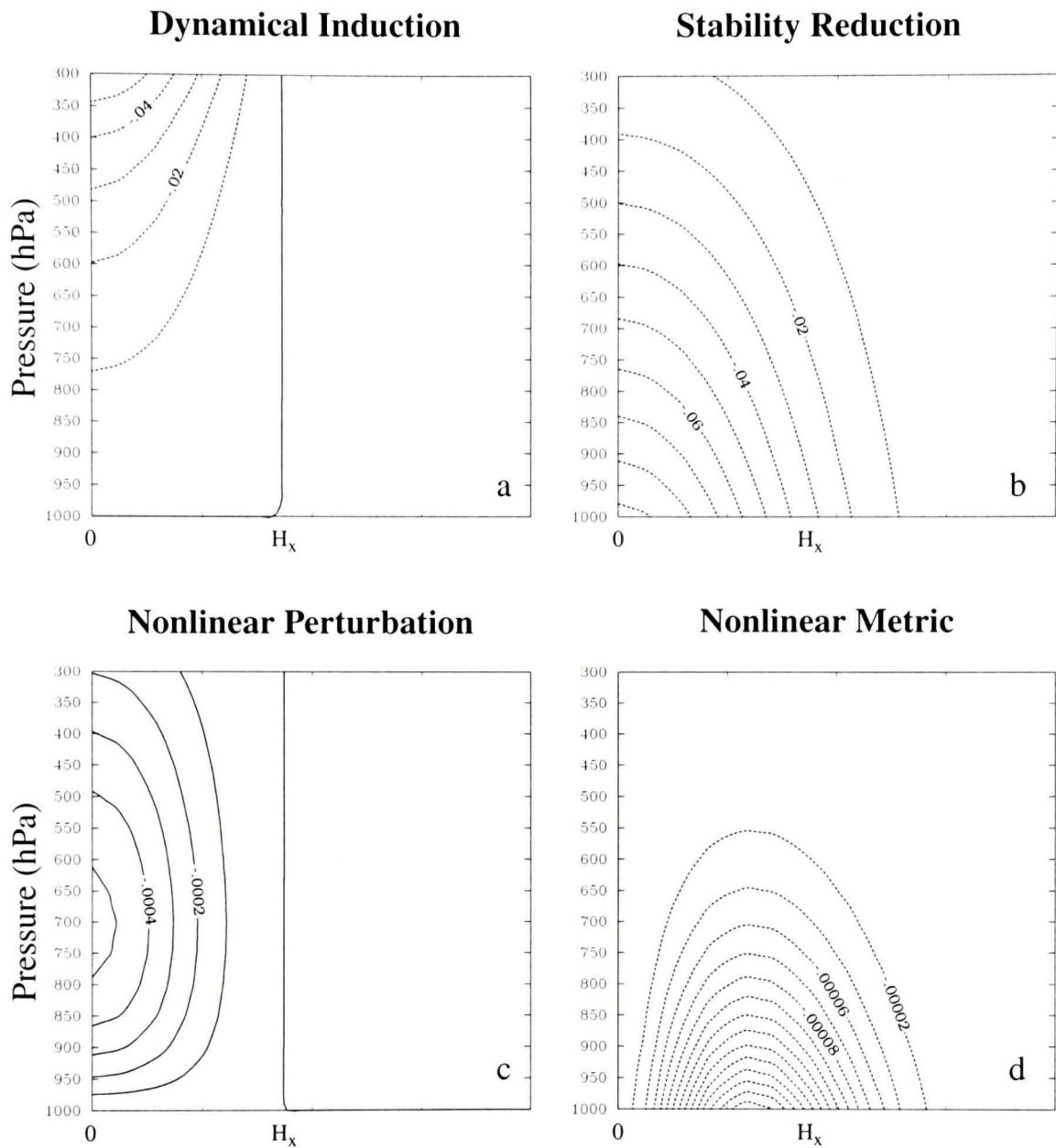


Figure 4.5: Decomposition of the  $PV_{mc}$  equation (4.39). Term 1 (panel a) represents “dynamical induction”, term 2 (panel b) “stability reduction”, term 3 (panel c) the “nonlinear moist component perturbation”, and term 4 (panel d) the “nonlinear metric”. All cross sections are plotted in PVU with 0.01, 0.01, 0.0001, and 0.00002 PVU contour intervals for each of a, b, c, and d respectively.

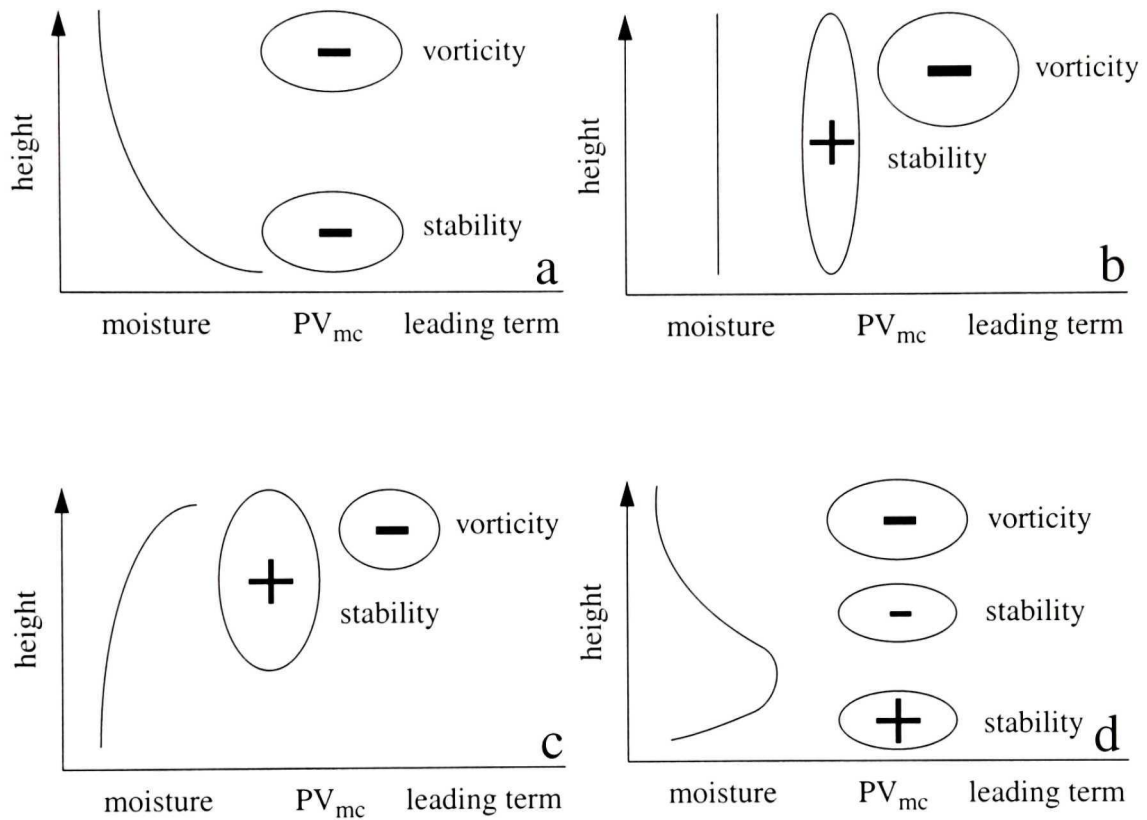


Figure 4.6: Schematic representation of simple moisture profiles and their resulting  $PV_{mc}$ . All panels are for a local maximum in the mixing ratio in the horizontal. For a local minimum, the signs of the vorticity dominated anomalies are reversed.

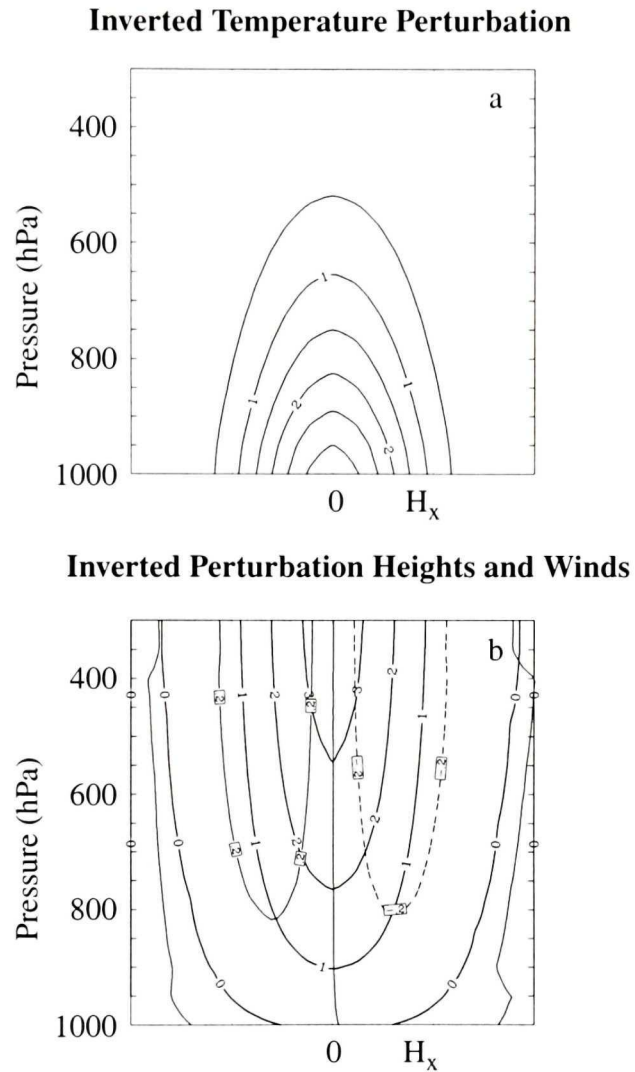


Figure 4.7: Perturbation temperature (panel a), and height and wind fields (panel b) following the inversion of the  $PV_{MC}$  anomaly shown in fig. 4.4d. Temperatures are contoured at 1 K intervals, and heights at 1 dam intervals. Positive wind values are entering the page, and negative values are exiting it (contours every  $0.2 \text{ m s}^{-1}$ ).

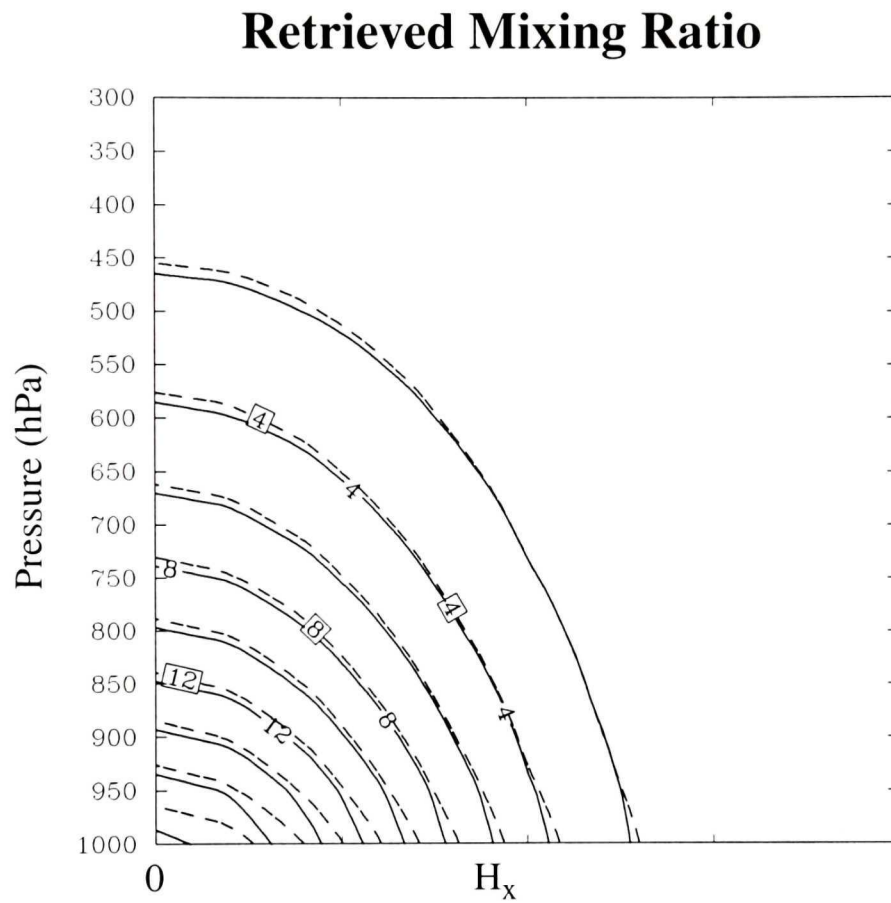


Figure 4.8: Comparison of the original (dashed) and the retrieved (solid) mixing ratio following inversion. Contours are plotted every  $2 \text{ g kg}^{-1}$ .

# Chapter 5

## The Influence of the Tropical Cyclone on ET

The final set of sensitivity tests address the issue of TC remnant importance to the ET/R process. As noted by McTaggart-Cowan et al. (2001) and McTaggart-Cowan et al. (2003b), the NOEARL test presented in Chapter 2 is incomplete owing to the persistence of the tropical moisture values in the region of the removed vortex. The development of  $PV_{mc}$  (Chapter 4) as a tool with which to diagnose the dynamical influence of atmospheric water now allows for the balanced removal of both the dry ex-hurricane dynamics (PV anomaly) and the moisture associated with the tropical vortex ( $PV_{mc}$  anomaly). Chapter 5 is placed in context with previous studies of ex-hurricanes Danielle and Earl in Section 5.1. An extended description of the tropical lifecycles of the hurricanes is presented in Section 5.2, emphasizing the still-tropical nature of the decaying storms at 00/05. The  $PV_{mc}$  variable is reintroduced in Section 5.3, and its applicability to the work presented in this chapter is discussed.

Circulation and moisture removal sensitivity tests employing dry PV and  $PV_{mc}$  modification and inversion procedures are presented in Section 5.4, and their results discussed in the context of the bimodality of ET/R suggested by McTaggart-Cowan et al. (2003a). Marked differences are found in the tropical and baroclinic mode responses to the remnant TC structures. This portion of the study concludes with a summary of the findings in Section 5.5.

The following is based on a manuscript submitted to Monthly Weather Review,

May 2003.

# The impact of tropical remnants on extratropical cyclogenesis: case study of hurricanes Danielle and Earl (1998)

R. McTaggart-Cowan, J.R. Gyakum, and M.K. Yau

Department of Atmospheric and Oceanic Sciences, McGill University

## Abstract

The importance of remnant tropical cyclone (TC) circulation and moisture structures is investigated for a simultaneous extratropical transition (ET) event involving ex-hurricanes Danielle and Earl (September 1998). Although both storms undergo prolonged periods of reintensification following ET, the forcings involved in each of their redevelopment processes differ fundamentally. A review of the tropical and baroclinic ET modes in the North Atlantic stresses the importance of jet/front structures to the nature of the reintensification process. Ex-hurricane Danielle begins to redevelop in the eastern half of the basin in the downstream, poleward sector of an intensifying polar jet. The system undergoes a tropical mode of reintensification, resulting in a troposphere-deep warm environment surrounding the storm, devoid of near-surface fronts and maintained by strong tropopause folds at its periphery. Ex-hurricane Earl reintensifies near the eastern seaboard according to a baroclinic mode, under the influence of an up-shear upper-level trough. A rapid cyclonic rollup of upper-level potential vorticity over the reintensifying low-level center results in a strong baroclinic system with well-defined frontal boundaries.

The two elements of the remnant TCs considered here are circulation and moisture. Potential vorticity-based modifications are made to the initial atmospheric state of the Mesoscale Compressible Community model in order to remove either one or both of these possible cyclogenetic forcings. The resulting set of sensitivity tests is analyzed in terms of system intensity and structure. It is found that the tropical

mode reintensification (ex-hurricane Danielle) process requires the presence of the remnant's circulation and moisture for rapid redevelopment. However, the baroclinic mode transition studied (ex-hurricane Earl) is remarkably insensitive to the removal of the ex-tropical vorticity and moisture structures of the TC remnant.

## 5.1 Introduction

The progression of tropical features into the extratropics poses diagnostic and forecasting challenges in both ocean basins and both hemispheres. The study of particularly severe events of tropical-extratropical interaction known as extratropical transitions (ET) has recently gained momentum, although few research efforts have focused on the importance of the tropical remnant<sup>1</sup> during the reintensification phase of ET (Ritchie and Elsberry 2001; McTaggart-Cowan et al. 2001; Klein et al. 2002). As a tropical cyclone (TC) moves poleward, it becomes increasingly influenced by the baroclinic westerly flow, and begins to lose important tropical characteristics such as axisymmetry, banding structures, and widespread deep convection (Klein et al. 2000; Harr and Elsberry 2000b,c; Evans and Hart 2003). The increasing shear at higher latitudes has been shown to induce tilting in the tropopause-deep vortex (Thorncroft and Jones 2000), and thermal advection patterns lead to the shutdown of convection in the southwest quadrant of the storm as a dry-slot forms (Sinclair and Revell 2000; Sinclair 2002; Klein et al. 2000). Low-level frontogenesis is particularly active in the warm-frontal region, as warm, moist tropical air is wrapped rapidly northwards ahead of the accelerating remnant TC.

Approximately 25% of the TCs completing ET undergo some form of extratropical reintensification (DiMego and Bosart 1982b; Klein et al. 2000; Hart and Evans 2001). This reintensification may occur during or after the transition process, and has been found to be strongly dependent on the structure of the mid-latitude flow (Klein et al. 2002; Hart and Evans 2001; McTaggart-Cowan et al. 2001). An upper-level

---

<sup>1</sup>The tropical remnant (or remnant tropical cyclone) comprises the three-dimensional circulation and moisture fields associated with the ex-hurricane as it progresses into the midlatitudes.

trough upstream of the transitioning TC plays a crucial role in coupling traditional quasigeostrophic forcings with the tropical moisture and heat associated with the remnant vortex. Both Thorncroft and Jones (2000) and McTaggart-Cowan et al. (2003a) (hereafter MGY03a) find that the relative location of the tropical feature to windspeed maxima in the polar jet modulates the structure of the ET.

In a study of the same case examined here, the authors observe a bimodality in the reintensification process. Employing quasi-idealized simulations, MGY03a define “tropical” and “baroclinic” ET and reintensification (ET/R) modes to occur in the left entrance and right exit regions of the North Atlantic jet, respectively. The authors suggest that the superposition of the secondary circulation around the jet maximum and the flow associated with the surface cyclones leads to enhanced advective patterns in the jet entrance and exit regions as shown in Fig. 5.1. Strengthened advection to the west of the cyclone occupying the equatorward entrance region of the jet leads to enhanced cold environmental inflow and the development of the marked dry slot and frontal features observed in strongly-baroclinic ET processes (Klein et al. 2000). Conversely, the reinforcement of warm advection ahead of a cyclone lying beneath the poleward exit region of the jet results in the preconditioning of the storm’s environment for a tropical mode of reintensification. Systems redeveloping in this area display weak frontal patterns and maintain deep near-core convection.

The role that the properties of the remnant TC vortex plays in the ET process (and particularly in reintensification, should it occur) remains unclear. McTaggart-Cowan et al. (2001) (hereafter MGY01) find that the removal of the remnant dynamics of ex-hurricane Earl do not have a great impact on the final intensity of the system which forms beneath the upper-level trough. A weak surface cyclone, initially located in central Quebec, progresses southeastward below upper-level trough forcing and intensifies rapidly as it reaches the Grand Banks to the east of Newfoundland. They conclude that the dynamics of the remnant TC are not of primary importance to cyclogenesis in this case. The question that remains, however, is to what extent the tropical moisture values, still present following the removal of the vortex dynamics,

influence the storm's intensification through the release of latent heat.

The development of the moist component potential vorticity ( $PV_{mc}$ ) diagnostic by McTaggart-Cowan et al. (2003b) (hereafter MGY03b) makes sensitivity tests involving modifications to the remnants' moisture contents possible. This extension of the potential vorticity [PV, Ertel (1942)] based piecewise decomposition framework established by Davis and Emanuel (1991) allows for the dynamically-consistent diagnosis and balanced modification of atmospheric water fields. Application of  $PV_{mc}$  inversion procedures will allow this paper to extend the work of MGY01 by investigating the unresolved issues surrounding the influence of remnant tropical moisture on the ET/R process.

In order to investigate the impact of both the dynamical and thermodynamical properties of the remnant TC vortex on ET/R, a series of sensitivity testing simulations are undertaken for initial atmospheric states in which the dynamics and/or the moisture of each of the systems has been removed. Large differences between the control simulation and a sensitivity test indicate that the modified quantity has a significant impact on the evolution of the ET/R.

We begin with a description of the selected case (the simultaneous ET/R of ex-hurricanes Danielle and Earl in September 1998), data, and model setup in section 5.2. Section 5.3 introduces  $PV_{mc}$  and provides a description of the  $PV_{mc}$  field in the model's initial conditions. Section 5.4 presents a description and analysis of a set of sensitivity tests designed to quantify the cyclogenetic importance of the remnant vortices of both Danielle and Earl. The paper concludes with a discussion of the findings in section 5.5.

## 5.2 Case Study and Model Description

The simultaneous ET/R of ex-hurricanes Danielle and Earl in September 1998 provides an excellent testbed for studies of the ET process. Both storms undergo significant periods of extratropical reintensification (each experiences a pressure fall of over 20 hPa in 36 hours), Earl on the upstream equatorward flank of the North At-

lantic jet, and Danielle on the downstream poleward side of the same feature. Not only does this case highlight a simultaneous ET/R event, but also it allows for the investigation of both baroclinic mode (Earl) and tropical mode (Danielle) redevelopments. A traditional synoptic diagnosis of the case is provided in Section 5.2.1, focusing on the observed and analyzed structures of the storms during the tropical phase of their respective lifecycles. The dataset and model used in this simulation study are described briefly in sections 5.2.2 and 5.2.3. A PV-focused diagnosis of the control simulation concludes this section (5.2.4).

### 5.2.1 Case Description

Although this study focuses on the extratropical phase of the lifecycles of hurricanes Danielle and Earl, a description of the tropical history of the TCs is necessary given the importance of the remnant tropical vortices to the processes under investigation. An understanding of the evolution of the circulation pattern and the moisture structure associated with each storm is of primary importance in conceptualizing the sensitivity tests presented in Section 5.4.

Hurricane Danielle began its lifecycle as a tropical wave over the west coast of Africa on 21 August 1998. The easterly wave began to organize convection southeast of the Cape Verde Islands on 24 August, and was classified as Tropical Storm Danielle by the National Hurricane Center (NHC) later that day. Progressing westward across the equatorial Atlantic, a tight eye was observed in satellite imagery on 25 August, and the storm was classified as a Category 1 hurricane (Saffir-Simpson hurricane scale, Simpson (1974)). Vertical shear associated with outflow from the powerful Hurricane Bonnie located near the western edge of the basin repeatedly disrupted Hurricane Danielle's structure, and caused precessions in the vortex which resulted in numerous intensity changes throughout the tropical phase of Danielle's lifecycle. Throughout, however, Danielle maintained a very tight structure with a radius of maximum wind estimated at approximately 100 km on 26 August, just before the hurricane's first intensity maximum ( $45 \text{ m s}^{-1}$  surface winds at 0600 UTC 26 August).

Hurricane Danielle continued to track west-northwestward until 31 August. Upon reaching 30°N, the hurricane abruptly completed recurvature under the influence of a strong upper-level trough over the North American continent. The storm tracked northeastward parallel to the eastern seaboard and approximately 500 km offshore, maintaining its intensity and reaching its lowest central pressure of 960 hPa on 3 September off the coast of Nova Scotia. Adopting an easterly track by 0000 UTC 4 September (hereafter 00/04), the system was declared extratropical by the NHC. Although subsequent analyses from the NHC, the Canadian Meteorological Centre (CMC), and the Canadian Hurricane Center (CHC) are inconsistent, it appears from satellite imagery (MGY03a) that the system continued to track eastward and weaken until approximately 00/05. Over the following 36 hours, the system intensified for a fifth and final time, reaching a minimum central pressure of 965 hPa (NHC) at 12/06. A marked cyclonic track change over the period of intensification left the system on a northeasterly heading which lead to its amalgamation with a pre-existing extratropical cyclone west of Scotland shortly after 00/08.

Hurricane Earl's lifecycle is somewhat less traditional than is that of Hurricane Danielle. Earl's formation also began with an easterly wave near the Cape Verde Islands; however, the proximity of the disturbance to the outflow from Hurricane Bonnie suppressed convection until the system had progressed into the Gulf of Mexico. It was designated Tropical Storm Earl by the NHC at 1800 UTC on 31 August. The ill-defined eye of the developing storm made tracking difficult over the following days, and Earl did not reach hurricane status until 12/02. Although briefly classed as a Category 2 hurricane, Earl made landfall in Panama City, Florida at 03/03 as a nominal Category 1 hurricane, although observed windspeeds never exceeded  $31 \text{ m s}^{-1}$  over the coast.

Earl tracked northeastward after landfall and rapidly began weakening from its 985 hPa peak intensity (estimated at 00/03 by the NHC). Declared extratropical by the NHC at 18/03 while still in eastern Georgia, the decaying storm exited the coast just north of Cape Hatteras at 15/04 and further weakened to 1004 hPa (CMC) by

00/05. At this time the remnant tropical vortex lay approximately 350 km east of New Jersey and was beginning to interact with an elongated baroclinic zone which ran parallel to the coast in advance of an approaching upper-level trough. Over the next 36 hours, the storm reintensified dramatically, and struck St. John's, Newfoundland with winds in excess of  $38 \text{ m s}^{-1}$  and a central pressure of 960 hPa (manual analysis by the CHC). Shortly thereafter, the storm took up an easterly heading and accelerated across the North Atlantic as it slowly weakened. By 00/09, Earl's structure had become indistinguishable from the system which resulted from the combination of Danielle and the pre-existing low.

### 5.2.2 Data Sources

The gridded data used for this study come from the CMC's regional analysis cycle. Three-dimensional grids are archived on 12 pressure levels from 1000 hPa to 50 hPa four times daily with a horizontal grid spacing of 24 km over the domain of interest. The regional analysis from 00/05 is used as the initial condition for the Mesoscale Compressible Community (MC2) model (described in section 5.2.3), and all subsequent analyses until 00/07 serve as model boundary conditions. For further information on the regional analysis cycle at the CMC, the reader is referred to Chouinard et al. (1994). Other datasets referred to in this text include NHC reports for the storms in question (including best track information) and surface manual analyses of ex-hurricane Earl's reintensification produced by the CHC. These sources, however, serve the present study only as diagnostic and verification resources.

### 5.2.3 Model Description

All simulations for this study are performed using version 4.9.5 of the Canadian MC2 model (Thomas et al. 1999; Benoit et al. 1997). The MC2 is a fully non-hydrostatic, limited area model that solves the elastic governing equations using semi-implicit timesplitting and semi-Lagrangian advection. This numerical scheme ensures model stability over a wide range of timesteps and spatial scales. A modified

Schär vertical coordinate is used with Takioka B grid staggering, and a Arikawa C grid is employed for horizontal distribution (Schär et al. 2002). An improved vertical advection formulation in this latest version of the MC2 provides enhanced accuracy in regions with steeply-sloping orography and in areas of strong vertical motion (Michel Desgagné 2003, personal communication).

Physical processes are parameterized using version 3.72 of the CMC Physics Library. Simple force-restore lower boundary conditions are sufficient for this study since both cyclones remain offshore over a model ocean whose temperature is temporally invariant. A kinetic energy closure scheme described by Benoit et al. (1989) is employed in the boundary layer to parameterize turbulent transports. The Kain-Fritsch (Kain and Fritsch 1990, 1992) deep-convective parameterization scheme is coupled with the Kong and Yau (1997) explicit microphysics scheme for the description of moist processes. No shallow convection parameterization is used.

#### 5.2.4 Control Simulation

All of the simulations for this study are initialized at 00/05 from the CMC regional analysis or a variant thereof, and are integrated for 48 hours with a 35 km grid spacing. At initialization time, both Earl and Danielle are at relatively weak stages in their intensity lifecycles. As shown in the track map and intensity plots of Fig. 5.2, ex-hurricane Danielle is located in the middle of the North Atlantic Ocean ( $45^{\circ}\text{N}$ ,  $34^{\circ}\text{W}$ ) with a minimum mean sea level pressure (MSLP) of 986 hPa and mean near-core winds (within 200 km of the MSLP center) of  $11 \text{ m s}^{-1}$  (not shown). Ex-hurricane Earl lies just off the eastern seaboard ( $37^{\circ}\text{N}$ ,  $72^{\circ}\text{W}$ ) with an MSLP of 1004 hPa and mean near-core winds of just over  $8 \text{ m s}^{-1}$ . A northward extension of the Bermuda high separates the two systems at lower levels and strengthens the northerly flow behind Danielle (Fig. 5.3a). An upper-level trough over Quebec is associated with a baroclinic zone that lies along the eastern seaboard and with which ex-hurricane Earl is just beginning to interact as the initial time of the simulation. A much weaker trough is evident upstream of Danielle at 00/05. A strong North Atlantic jet is evident

at 250 hPa, where windspeeds in the local maxima at the entrance and exit regions of the jet approach  $60 \text{ m s}^{-1}$  (Fig. 5.3b). Column-integrated water vapor (precipitable water) contents of over 50 mm are present in the vicinity of both centers, and bands of high precipitable water values extending into the tropics from both storms suggest that continued moisture channeling may be occurring as the simulation begins.

The control simulation proceeds in a very similar nature to that described in MGY03a. A traditional synoptic analysis of the results is presented in that paper, and will not be reproduced here. Instead, this analysis, and all analyses in this paper, will be presented under the “PV thinking” paradigm popularized by Hoskins et al. (1985). Dynamic tropopause analyses (Morgan and Nielsen-Gammon 1998) are combined with near-surface diagnostics to provide a full view of the atmosphere under the constraints of the Eady model (Eady 1949). The orography of the dynamic tropopause, represented by potential temperature distributions on the 1.5 PVU surface ( $1 \text{ PVU} = 10^{-6} \text{ m}^2 \text{ K kg}^{-1} \text{ s}^{-1}$ ), is intimately related to traditional synoptic features such as troughs, ridges, and jet streams, and has the advantage of highlighting all of these features simultaneously.

Over the first 24 hours of the simulation, the large cold pool on the dynamic tropopause associated with the upper-level trough above Quebec rotates slowly eastward across the east coast of North America (Fig. 5.4a,c). It intensifies gradually as it progresses, and a strengthening jet appears on its southeast flank. The smaller-scale trough feature upstream of Danielle undergoes a much more non-linear evolution over the first half of the simulation, as it filaments rapidly towards the southeast, and wraps cyclonically near  $15^\circ\text{W}$  by 24 hours. The large potential temperature gradient on the back side of this trough feature in Fig. 5.4c suggests that the North Atlantic jet bows anticyclonically and strengthens during the integration. Indeed, windspeeds on the 1.5 PVU surface exceed  $70 \text{ m s}^{-1}$  midway through the simulation. The 850 hPa potential temperature (taken as the approximate top of the maritime boundary layer) is presented with the mean low-level PV in Fig. 5.4b, d, and f. Both cyclones are initially seen as positive anomalies in the PV field, whose forms are modified rapidly by

the onset of frontal precipitation. The low-level evolutionary differences in the potential temperature structures of the storms are equally as dramatic as those occurring at upper levels. In ex-hurricane Earl's case, deformation of the existing baroclinic zone along the coast leads to the formation of strong potential temperature gradients after only 12 hours of simulation (not shown). In keeping with traditional baroclinic development, a warm sector and both cold and warm frontal features are evident 24 hours into the simulation, although the warm front is more pronounced at this time (Fig. 5.4d). Maximum precipitable water values, initially near the center of Earl's circulation, become concentrated along the developing cold-frontal region as the dry slot severs the initial moisture channel to the tropics (Fig. 5.3d). The near-surface fields associated with ex-hurricane Danielle evolve in a manner entirely unlike those near Earl. An intrusion of tropical air with high potential temperatures and large precipitable water contents wraps initially northward, and eventually westward ahead of the redeveloping system. Frontogenesis in the warm-frontal region is initially large, but by 12 hours of simulation, the area is predominantly frontolytic (not shown). No significant cold frontal development is observed, and the maximum in precipitable water remains fixed with the circulation center in Danielle's case (Fig. 5.3d).

The final 24 hours of the simulation display further developmental differences between the storms. The trough feature initially upstream of ex-hurricane Earl undergoes a rapid cyclonic rollup above the developing lower-level system (Fig. 5.4e). This LC2-type cyclonic wave-breaking process [for a description of cyclone lifecycle (LC) characteristics, see Thorncroft et al. (1993)] is indicative of the intense baroclinicity of this system. The depressed tropopause surrounding Danielle, however, expands outwards as more tropical air is wrapped into the immediate vicinity of the developing storm. A strong tropopause depression persists near the core of the system, the result of latent heat released by convection in the still-tropical local environment (MGY03a). The thermal wave associated with Earl's baroclinic redevelopment separates from the storm's center after 24 hours of simulation, and a warm-seclusion process appears to have occurred in Fig. 5.4f. Frontogenesis in the cold-frontal region

at 24 hours gives way to extensive frontolysis after 36 hours (not shown), although the pre-cold-frontal band of high precipitable water values is maintained throughout the simulation. The zone of warm potential temperatures surrounding Danielle's center continues to expand in size over the latter half of the simulation. No frontal signature is visible around the system by the end of the simulation in either the potential temperature or low-level potential vorticity fields (Fig. 5.4f). Associated with the tropical temperatures near the storm center are bands of high precipitable water contents (in excess of 30 mm) which have been wrapped into the local environment of the system.

Validation of the control simulation by MGY03a includes comparison with satellite observations and intensity analyses, and will not be repeated here since the simulations differ only slightly in evolution. Ex-hurricane Danielle's minimum MSLP drops to 964 hPa in this control integration, compared to 962 hPa in that of MGY03a. Similarly, Earl's minimum MSLP drops to within 5 hPa of the 960 hPa value obtained by MGY03a. In both cases, the values for storms in the updated control simulation are closer to those analyzed by the CMC than are their MGY03a counterparts. Further comparison of Earl's structure after 36 hours of simulation is made by MGY01 with a reanalysis of surface pressure and temperature distributions.

### 5.3 Moist Component PV

The use of PV as a diagnostic variable is desirable for two reasons. The first is that it is conserved for adiabatic, inviscid flows, and the second it that it is invertible given a balance equation, boundary conditions, and a background state (Hoskins et al. 1985). It is this second quality of PV that will prove most useful in the context of the current study, in that any distribution of PV can be inverted to obtain the corresponding balanced geopotential and streamfunction fields. Davis and Emanuel (1991) recast Ertel's PV equation (Ertel 1942) in component form, and couple it with different balance equations to yield insight into the nonlocal effects of PV anomalies on the surrounding flow. The technique of PV component isolation, inversion (using the

nonlinear balance equation, Charney (1955)), and removal has been used extensively (MGY01, Huo et al. (1998)) to test the sensitivity of modelled events to identifiable PV features in the initial fields. For example, MGY01 remove the dynamics associated with ex-hurricane Earl at 00/05, and find that intensification of a pre-existing low occurs in a very similar location to Earl in the control simulation. However, this PV modification techniques does not yield any insight into the influence of water vapor since the formulation of the equations takes place in a dry atmosphere.

To investigate the impact of water vapor on the instantaneous circulation, MGY03b develop the  $PV_{mc}$  diagnostic, which represents the component of the total PV field arising solely from the presence of atmospheric water. Here, as in MGY03b, only the effects of subsaturated water vapor are considered. Modifications to the initial-state  $PV_{mc}$  field can be made in the same way that modifications can be made to the dry PV associated with the remnant tropical vortex or upper-level trough. Inversion of the  $PV_{mc}$  field yields the balanced flow that results from the presence of the atmospheric water field, which is non-zero because of the difference in the partial pressures of water vapor and dry air. In this case, addition or removal of  $PV_{mc}$  allows for the balanced enhancement or destruction of the water vapor field associated with the flow surrounding the individual ex-tropical systems.

A full description of the derivation  $PV_{mc}$  is presented by MGY03b, as is a sample  $PV_{mc}$  inversion for a moisture maximum in a highly-simplified atmosphere. To make an analytic description of the  $PV_{mc}$  field possible, MGY03b assume geostrophic balance and work on an f-plane. These simplifying assumptions are relaxed in the current study through the use of a latitude-dependant Coriolis parameter and the application of the nonlinear balance equation (Charney 1955). The structures presented by MGY03b, however, remain qualitatively valid under these more realistic constraints. In general, a local maximum in the moisture field yields negative  $PV_{mc}$ . Because the effect on the geopotential field is additive with height (given a fixed lower boundary condition, all heights in a column are influenced by an increased thickness below), non-zero  $PV_{mc}$  values are present at all levels. Moist component PV is expected to

play a secondary role to dry PV in determining atmospheric dynamics. Although the existence of strong moisture gradients surrounding the remnant TC vortices result in absolute  $PV_{mc}$  values of up to 0.4 PVU at 700 hPa (e.g. Fig 5.5), they occur in regions where dry PV values are on the order of 1 to 2 PVU. The circulation resulting from these  $PV_{mc}$  structures does not exceed  $10 \text{ m s}^{-1}$  at 700 hPa, with corresponding geopotential height perturbations of less than 4 dam as will be shown in the Section 5.4.  $PV_{mc}$  therefore constitutes a small, albeit non-negligible, portion of the total PV field.

Figure 5.5, showing the  $PV_{mc}$  field at 700 hPa at 00/05, highlights important features in the dynamics and moisture fields. Ex-hurricane Earl is seen as a local minimum in the  $PV_{mc}$  field of -0.4 PVU, as is a moist region south of Newfoundland (-0.3 PVU). The circulation around the ex-tropical system can be seen to be drawing dry air off the coast as characterized by the elongated maximum in  $PV_{mc}$  extending northeastward from northern Florida. The maximum in  $PV_{mc}$  along the eastern seaboard is an indication of the dry air beneath the approaching trough. The moisture structure near Danielle's core is somewhat greater in extent than that surrounding Earl.  $PV_{mc}$  values exceed (negatively) -0.1 PVU in a broad region, and also highlight a moisture channel extending to the southwest of the system.

The identification of  $PV_{mc}$  anomalies associated with the ex-tropical systems allows for the isolation of the moisture associated with each storm individually. The role of  $PV_{mc}$  in the context of this research is therefore twofold. Firstly, the  $PV_{mc}$  field allows for the determination of the magnitude and areal extent of the impact that each ex-tropical system has on the water vapor field. Secondly, it provides a balanced method by which to remove the system's water vapor and associated dynamics, thereby completely removing the effects of tropical moisture values from the ensuing sensitivity testing simulations.

## 5.4 Sensitivity Tests

The objective of the set of sensitivity tests presented in this section is to quantify the importance of the remnant TC vortex to the ET/R process. Two features of the initial vortex structures at 00/05 are considered: dry dynamics, and moisture. Each test proceeds according to the formula,

- Identification of PV component anomaly (dry PV or  $PV_{mc}$ );
- Isolation and inversion of the PV anomaly;
- Balanced removal of the derived mass (heat or moisture) and wind fields from the initial conditions (00/05); and,
- Integration of the MC2 model for a 48 hour period with a setup identical to that described in section 5.2.3.

Anomaly fields of both dry PV and  $PV_{mc}$  are shown in Fig. 5.5. For each ex-tropical system, three sensitivity tests are undertaken. As shown in Table 5.1, the first involves the removal of the dry PV anomaly associated with the storm, the second consists of the removal of system's anomalous  $PV_{mc}$ , and the third comprises both of the previous modifications. Large differences between the control simulation and an individual sensitivity test indicate that the quantity removed (the remnant's circulation, the remnant's moisture, or both) is integral to the spin-up of the system over the period of integration. The sensitivity tests for ex-hurricane Earl are presented in section 5.4.1, and those for Danielle are described in section 5.4.2. Intensity indicators and track plots for each sensitivity test are included as Figs. 5.6 and 5.7 for reference. The plots in Fig. 5.6 display storm-relative quantities throughout the integration; however, model spin-up over the first 6 hours may influence the initial segments of these traces.

### 5.4.1 Ex-hurricane Earl

The ET/R of ex-hurricane Earl is classed as baroclinic mode by MGY03a. As presented in the description of the control simulation in section 5.25.2.4, the upper-level trough initially located over central Quebec plays a crucial role in determining the nature of the ET process. The quantitative impact of the trough is described by MGY01, who find its presence to be a necessary condition for reintensification. To what extent the remnant tropical circulation, and the moisture associated with it, further enhance the ET process is a question not fully addressed by MGY01. Their sensitivity test involving the removal of the ex-hurricane's vortex is repeated here for the updated control simulation (noEarl), followed by the removal of the moisture associated with the TC remnant (EarlDry). A final simulation proceeds following the removal of both the dry dynamics and the moisture associated with ex-hurricane Earl (noEarlDry) and represents the most complete removal possible of the initial TC feature.

#### Circulation removal (noEarl)

The removal from the model's initial conditions of the dry PV anomaly associated with the TC remnant will yield an estimate of the influence of ex-hurricane's circulation on the development processes occurring beneath the approaching upper-level trough. Figure 5.8a shows the region selected to contain only the PV anomalies associated with the remnant vortex, extending from the surface to 400 hPa. As discussed in MGY01, the results presented here are insensitive to small changes in the subjectively-chosen bounds of the removal area. This figure also shows the horizontal and vertical structure of the balanced height and wind fields associated with the anomaly. Removal of this mass and flow distributions from the initial conditions ensures the removal of the remnant tropical vortex at 00/05.

As shown in Fig. 5.8b, the removal of the ex-hurricane's circulation results in a reduction of the thermal anomaly along the eastern seaboard (compare with Fig. 5.4b). A cooling of over 2 K takes place primarily in the warm region to the east of the near-

coastal baroclinic zone, thus slightly reducing its intensity. No appreciable changes are evident on the dynamic tropopause since the bulk of the decaying anomaly is concentrated at lower levels (Fig. 5.8a).

The evolution of the upper-level features proceeds very similarly to that described in section 5.2.4 for the control simulation. The cyclonic rollup of the upper-level cold (trough) anomaly on the dynamic tropopause occurs over the latter half of the simulation, with the maximum tropopause depression phase-locking above the lower-level circulation (Fig. 5.9a). At lower levels, however, marked differences are observed between this simulation and the control. The incipient circulation in this case is initially located in east-central Quebec, ahead of the upper-level trough feature (Fig. 5.7a). This center strengthens slowly, reaching 998 hPa after the first 24 hours of integration (Fig. 5.6). Although there is a maximum in near-surface frontogenesis along the developing cold front between 12 and 24 hours (not shown), the warm-frontal zone is dominant in Fig. 5.9b despite large values of mean lower-level PV ahead of the approaching cold air. Although there is little suggestion of a frontal occlusion at this time, a mature “t-bone” structure is evident in the potential temperature field and the storm has intensified dramatically (Fig. 5.6) while tracking south of Newfoundland. The sudden increase in near-core precipitation accumulations observed in Fig. 5.6 at the time of the onset of rapid intensification is associated with stable moist ascent in the warm frontal region, and may be a result of the remnant tropical moisture not affected by the removal of the dry PV associated with the TC vortex.

### Moisture removal (EarlDry)

The objective of this simulation is to investigate the impact that tropical moisture values have on the reintensification of the remnant tropical vortex. Figure 5.10a shows ex-hurricane Earl’s  $PV_{mc}$ , which extends throughout the depth of the model atmosphere. The horizontal and vertical structures of the balanced mass and flow fields associated with this  $PV_{mc}$  distribution are also shown in the figure, and closely resemble the results of the idealized balanced flow for the analytic atmosphere dis-

played in MGY03b Fig. 7.

Removal of the local minimum in the  $PV_{mc}$  field near the core of the decaying vortex results in minor height falls at the surface, and an initial central pressure for ex-hurricane Earl of 1002 hPa at 00/05 (Fig. 5.6). As shown in Fig. 5.10b, the precipitable water values surrounding the remnant vortex have been decreased by as much as 30 mm (compare with Fig. 5.3b). A local minimum appears on the dynamic tropopause above the dry inflow region, but there is no change to the structure or to the intensity of the trough feature.

In all respects, the results of this integration are similar to those of the control. The LC2-type cyclonic rollup of the trough above the lower-level vortex takes place at the same time and in the same location as described in section 5.2.4 (Fig. 5.11a). The resulting storm intensity (Fig. 5.6) shows no marked sensitivity to the removal of the tropical moisture structure. Most surprising is the observation that despite an initial reduction in precipitation quantities, 3-hourly precipitation accumulations in this run exceed those obtained in the control between 12 and 24 hours. Similarly, the precipitable water field at after 36 hours of integration (Fig. 5.11b) bears striking similarities to that of the control (Fig. 5.3f).

The reason for this apparent contradiction becomes evident when one considers that both positive and negative  $PV_{mc}$  anomalies associated with the remnant TC are removed from the initial state. When the tropical moisture surrounding the system is removed, so too is the dry inflowing air from the southern United States. This result is entirely consistent with the complete removal of the moisture structure of the storm since the dry inflow is a consequence of the system's dynamics. It is the ingestion of this dry air into the southwestern quadrant of the storm in the control simulation, a commonly-observed feature during ET (Klein et al. 2000), that effectively severs the link between Earl and the tropics. Southwesterly mid-level flow along the coast ahead of the approaching upper-level trough advects moist air from the Gulf of Mexico towards the redeveloping system. This mid-level moisture ingestion increases lower-level convective stability and results in reduced convective activity as

shown in Fig. 5.6b(ii). The conveyor belt structure continues to pull moisture from the tropics until 18 hours into the simulation, when a dry inflow region is developed by the intensifying system. The cyclone in this test therefore had access to a tropical moisture source for almost 12 hours longer than did the control storm, and effectively replenished its moisture supply. This, combined with the primarily baroclinic nature of Earl's redevelopment process, results in very little sensitivity to the initial tropical moisture content.

### **Circulation and moisture removal (noEarlDry)**

This sensitivity test involves a combination of the dry PV anomaly removal made in noEarl, and the  $PV_{mc}$  anomaly removal made in EarlDry, and represents the complete removal of all moisture and dynamics associated with ex-hurricane Earl from the initial conditions (Fig. 5.12a).

As in the noEarl test, lower-level cooling in the tropical airmass near the ex-hurricane's center is again prevalent in the potential temperature field of Fig. 5.12b, again decreasing the intensity of the near-coastal baroclinic zone. Concurrently, the  $PV_{mc}$  removal results in a reduction of precipitable water values near the center and the elimination of the incipient dry slot as shown for the EarlDry test in Fig. 5.10b.

As suggested by the traces in Fig. 5.6a and the track in Fig. 5.7a, the evolution of the system during this integration is very similar to that of the storm in the noEarl simulation. The cyclonic rollup of the trough anomaly on the dynamic tropopause at 36 hours is virtually identical, although the fold on the southeastern flank of the trough feature is slightly less intense, and southwesterly flow in the region is reduced by  $8 \text{ m s}^{-1}$  (Fig. 5.13a). A typical mature baroclinic cyclone structure is once again evident in the low-level potential temperature field (Fig. 5.13b), although the PV associated with the warm-frontal cloud shield is less organized due to reduced diabatic generation by condensation over the first half of the simulation.

Rain rates near the core in this simulation again show a seemingly dichotomous sensitivity to the removal of the moisture field when compared to those of the noEarl

simulation. Specifically, rain rates during the latter half of this simulation are generally higher than those observed in the noEarl test. As for the EarlDry test, the explanation for this phenomenon stems from the amplitude of the upper-level trough responsible for the development. Once the vortex and its associated moisture have been removed, flow at all levels parallels the eastern seaboard from the southwest in advance of the upper-level trough. Large precipitable water values over the Gulf of Mexico are advected northeastward ahead of the trough, and are stretched to lie along the cold-frontal slope of the developing system (Fig. 5.11b). The moisture transport in this case is even more effective than in the EarlDry simulation since the storm's northeasterly flow at low levels along the coast is replaced by more moist southwesterly winds. The 3-6 hour delay in the development of the system (Fig. 5.6), and the reduced intensity of the warm front result from this delay in the ingestion of high precipitable water values towards the storm's center.

The baroclinic nature of the ex-hurricane Earl's ET/R leads to little sensitivity to the initial state of the tropical vortex. In the absence of any tropical forcing, an intense storm with mean winds in excess of  $15 \text{ m s}^{-1}$  develops off the east coast of North America. It can therefore be concluded that the trough initially over Quebec is both a necessary and a sufficient condition for cyclone development.

### 5.4.2 Ex-hurricane Danielle

Ex-hurricane Danielle's ET/R is classed as tropical mode by MGY03a. As outlined in section 5.2.4, a sharp upper-level PV anomaly upstream of Danielle filaments south-eastward and wraps cyclonically around the redeveloping circulation, entrapping a locally tropical environment near the system. The LC2-type vortex rollup is not present in this case, nor are the strong frontal features diagnosed for Earl's reintensification. As for ex-hurricane Earl's case, three sensitivity tests are undertaken in which individually the remnant circulation (noDan), the remnant moisture (DanDry) and both the remnant circulation and moisture (noDanDry) are removed.

**Circulation removal (noDan)**

The objective of this sensitivity test is to quantify the influence of the remnant tropical circulation on the ET/R process. The region identified to contain anomalous dry PV associated with Danielle is shown in Fig. 5.14a, and again extends from the surface to 400 hPa. The structures of the balanced fields associated with this anomaly are shown in the same figure.

Removal of the initial low-level PV anomaly associated with Danielle results in height rises at the surface, thickness reductions, and concomitant cooling in the column. As a hydrostatic result of reduced low-level thicknesses (inset Fig. 5.14a), a reduction in the thermal anomaly associated with Danielle can be seen in Fig. 5.14b (compare with Fig. 5.4b). Cooling on the order of 5 K occurs over a large area near the former remnant location. The structure of the dynamic tropopause remains essentially unchanged.

During the first 12 hours of simulation, a small incipient cyclone forms near 39°N, 26°W (Fig. 5.7b) and travels slowly eastward under the influence of a pre-existing extratropical cyclone over Ireland. Shortly thereafter, a second incipient vortex forms 500 km to the southwest of the original center, and begins to intensify gradually. At upper-levels, advective processes dominate in the trough feature responsible for Danielle's reintensification. After 36 hours of simulation (Fig. 5.15a), there is no evidence of the filamentation and wrapping processes that occur at upper levels in the control simulation. Elevated tropopause potential temperatures do not penetrate northwards to the east of the developing system since the low-level circulation responsible for the advection of tropical air ahead of the system has been removed. The tightly-rolled lower-level PV structures evident in the control simulation around Danielle are not developed in this simulation. Instead, a moderately-intense warm front extends northeastward from the cyclone's center, and a cold front reaches south to 30°N (Fig. 5.15b). Although the mean winds near the newly-developed center climb to almost 15 m s<sup>-1</sup> after 42 hours of simulation, its MSLP never drops below 988 hPa (Fig. 5.6a).

At all levels, the evolutionary differences between this simulation and the control integration are striking. Instead of the tropical mode reintensification diagnosed in the control, this system develops as a weak baroclinic cyclone with little support from the predominantly linear processes aloft.

### Moisture removal (DanDry)

Removal of the tropical moisture field associated with the remnant vortex allows for a quantification of the impact of the system's high humidity values on the ET/R process. Notable features in the  $PV_{mc}$  field of Fig. 5.16a include a negative maximum to the north of the center (-0.3 PVU) which corresponds to the storm's near-core moisture maximum, and a band of large negative  $PV_{mc}$  values that extends to the southwest and is indicative of a moisture channel connecting Danielle to the tropics. The corresponding mass and flow fields are of slightly larger magnitude than those for the EarlDry simulation.

The balanced removal of the tropical moisture field results in an initial vortex whose MSLP is 3 hPa lower than Danielle's remnant TC in the control (Fig. 5.6a). As shown in Fig. 5.16b, precipitable water contents surrounding the cyclone are dramatically reduced. The tropopause structure is once again not greatly altered from its initial state in the control simulation.

The trough anomaly initially upstream of the redeveloping vortex undergoes a similar filamentation and wrapping process to that of the control. The only notable difference between the feature in this simulation (Fig. 5.17a) and the control after 36 hours (Fig. 5.4e) is the absence of a central potential temperature minimum on the dynamic tropopause caused (in the control) by latent heat released by near-core convection. The distribution of precipitable water in the system (Fig. 5.17b) is different from the control, with higher values extending along the weak cold front instead of accumulating near the storm's core. The overall intensity of the system (as measured by mean near-core windspeeds) is reduced by almost 20%, and the MSLP of the DanDry storm never falls below 975 hPa (Fig. 5.6), compared to 965 hPa for

Danielle in the control (Fig. 5.2).

Although storm-total precipitation accumulations in this simulation are smaller than those of the control following model spin-up, convective totals over the latter half of the simulation are slightly larger. Because of the differing storm dynamics, the explanation in this case does not lie in the removed dry inflow and ingestion of non-local moisture as it does for Earl. Instead, it is locally-enhanced oceanic latent heat fluxes which are responsible for convectively destabilizing the dried region by injecting water vapor at low levels in a process analogous to dry continental outflow patterns which often result in cellular convection over the Gulf Stream. These fluxes exceed  $450 \text{ W m}^{-2}$  in this simulation after three hours, while fluxes in the control remain below  $325 \text{ W m}^{-2}$  (Fig. 5.18). Once the moistened boundary layer becomes potentially unstable beneath the dried air aloft, and an outbreak of convection occurs [Fig. 5.6b(iv)]. No such widespread latent heat flux enhancement is observed in either the EarlDry or noEarlDry simulations where the primary moistening process is advective. The surface flux-driven convective destabilization in this case, as compared to the stabilizing mid-level moisture transport in the Earl tests, results in oppositely-signed convective sensitivities in Figs. 5.6b(ii) and (iv) and again serves to highlight the important physical differences between the tropical and baroclinic transition modes.

The removal of the tropical moisture associated with ex-hurricane Danielle results in a weaker storm with fewer clearly-defined tropical characteristics such as the long-lived upright tower of near-core convection which appears in the control.

### **Circulation and moisture removal (noDanDry)**

Complete removal of the remnants of ex-hurricane Danielle requires the combined removal of the balanced dry PV and  $PV_{mc}$  anomalies described in the previous sections. This simulation will be used to determine the extent to which the structure and location of the remnant tropical vortex has an impact on cyclogenesis in the eastern North Atlantic over the period of interest.

The inversion of the PV and  $PV_{mc}$  distributions shown in Fig. 5.19a yields balanced mass and flow fields which allow for the complete removal of ex-hurricane Danielle's dynamical and moisture structures (Fig. 5.19b). The moisture channel, low-level warm perturbation, and cyclonic flow around the vortex are all removed from the initial state.

The incipient cyclone in this simulation is once again difficult to track over the initial 12 hours, as was the case for noDan. A weak center forms southwest of the extratropical cyclone over Ireland and progresses slowly eastward until a second vortex appears to its southwest (Fig 5.7b). This second incipient cyclone intensifies slightly more rapidly than its counterpart in the noDan simulation, but still only obtains an MSLP of 993 hPa after 24 hours of simulation (Fig. 5.6). The filamentation and wrapping of the upper-level trough anomaly is once again absent from the evolution of the dynamic tropopause during the integration. By 36 hours (Fig 5.20a) there is a hint of a vortex rollup at upper-levels, but no elevated tropopause indicative of tropical air in the region of cyclogenesis is observed. The evolution of lower-level PV is also dramatically different in this integration from that of the intensifying system in the control. None of the banded PV structures evident in the control simulation are reproduced in this simulation after 36 hours (Fig.5.17b). The lack of a broad region of high precipitable water contents near the storm center at this time (not shown) is responsible for the reduced total precipitation accumulations in the last 12 hours of the simulation (Fig. 5.6); however, the convective destabilization process described for the DanDry test produces noticeable convective bursts at 15 and 24 hours.

The cyclogenetic process in the eastern North Atlantic over the period of interest is at least partially dependent on the presence of a decaying TC vortex. The nonlinear evolution of the upper-level structure and the intensity of the resulting system both require access to the ex-hurricane's circulation and elevated moisture content.

## 5.5 Summary and Discussion

The objective of the current study is to determine the sensitivity of cyclogenesis during the reintensification phase of ET to the ex-tropical features themselves. Specifically, the impact of the remnant TC circulation and moisture structures on North Atlantic cyclogenesis is examined. The modelling study begins with the simulation of a well-studied simultaneous ET/R event involving ex-hurricanes Danielle and Earl (September 1998). A 48 hour simulation of the reintensification phase of both cyclones (initialized 00/05) yields storms that closely reproduce the observed systems in terms of track, intensity, and structure. As diagnosed by MGY03a, the evolutions of the two cyclones differ significantly from one another, with ex-hurricane Earl undergoing a baroclinic mode redevelopment, and ex-hurricane Danielle reintensifying in a tropical mode.

Identification and removal of the remnant TC features from the initial conditions of the model leads to a quantification of their impact on North Atlantic cyclogenesis over the period of interest. Removal of the remnant dynamics is accomplished using a piecewise PV inversion methodology developed by Davis and Emanuel (1991). Identification of the atmospheric moisture fields associated with the ex-hurricanes requires the development of an additional component under the piecewise PV framework ( $PV_{mc}$ ).  $PV_{mc}$  is used to diagnose and modify the initial water vapor fields in order to remove the moisture associated with the ex-tropical systems while maintaining overall atmospheric balance.

The successive application of dry PV and  $PV_{mc}$  anomaly removals allows for the development of a series of atmospheric states which are used as initial conditions for a set of sensitivity simulations, the results of which are summarized in table 5.2. Figure 5.6 provides a further summary of the characteristics of the systems developed in each of the sensitivity tests. The baroclinic mode cyclogenetic process responsible for Earl's reintensification is not critically dependent on the existence of the decaying TC. However, tropical mode cyclogenesis such as that experienced by Danielle during

its final reintensification phase depends on both the dynamics and moisture associated with the remnant TC. Both the structure and the intensity of the resulting system are affected by removal of either or both of the transitioning storm's dry PV and  $PV_{mc}$  anomalies.

The sensitivity of the ET/R process to the strength of the remnant TC depends on the mode of transition. The baroclinic mode event simulated in this study does not rely on any of the properties associated with the tropical vortex for cyclogenesis. The tropical mode ET/R of ex-hurricane Danielle is sensitive both to the vortex dynamics and to the accessibility of the storm's tropical moisture content.

feature removed	<b>Earl</b>	<b>Danielle</b>
dry dynamics	noEarl	noDan
moisture	EarlDry	DanDry
dry dynamics and moisture	noEarlDry	noDanDry

Table 5.1: Summary of initial condition modifications for each test.

feature removed	<b>Earl</b>	<b>Danielle</b>
dry dynamics	small effect	large effect
moisture	small effect	moderate effect
dry dynamics and moisture	small effect	large effect

Table 5.2: Summary of cyclogenetic sensitivity for each test.

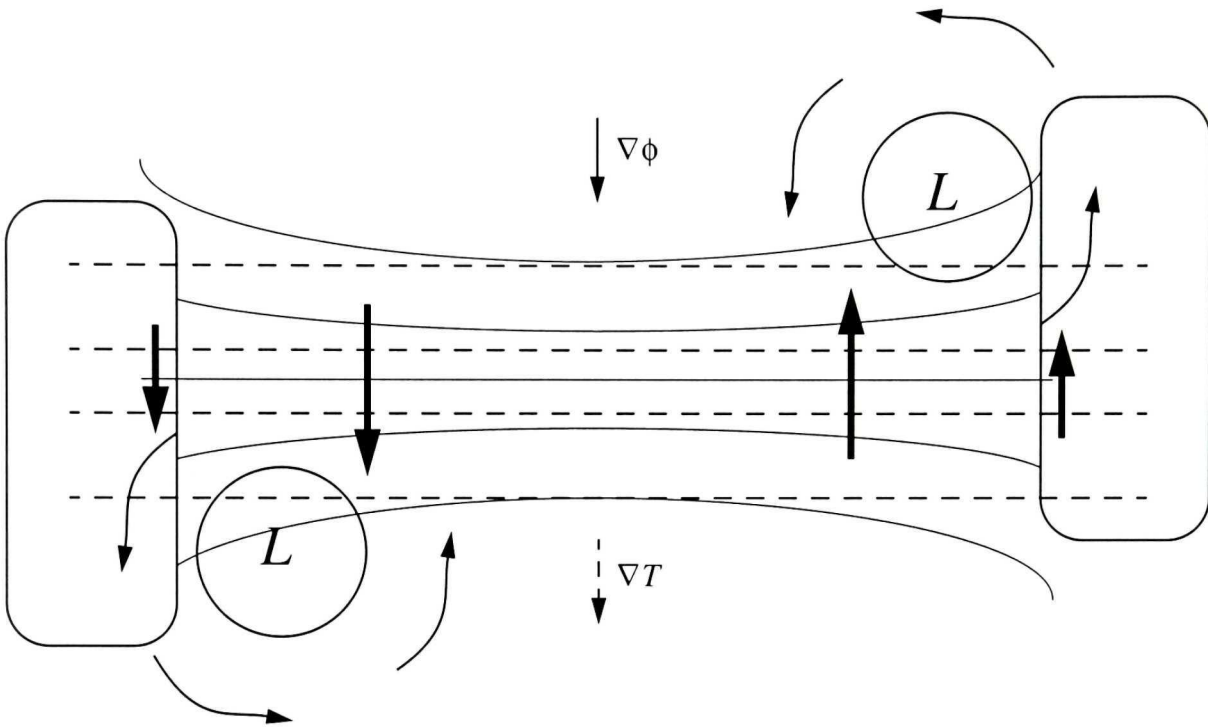


Figure 5.1: Schematic representation of a linear jet maximum. Light solid lines indicate upper-level height contours with the gradient oriented as indicated. Dashed lines represent lower-level isotherms, again with the gradient as shown. The horizontal secondary circulation at low levels generated by the jet is indicated by the heavy arrows. Two surface lows are superposed on the feature with cyclonic circulations as shown. Regions of enhanced cold and warm advection are shaded on the left and right sides of the figure, respectively. Reprinted from MGY03a.

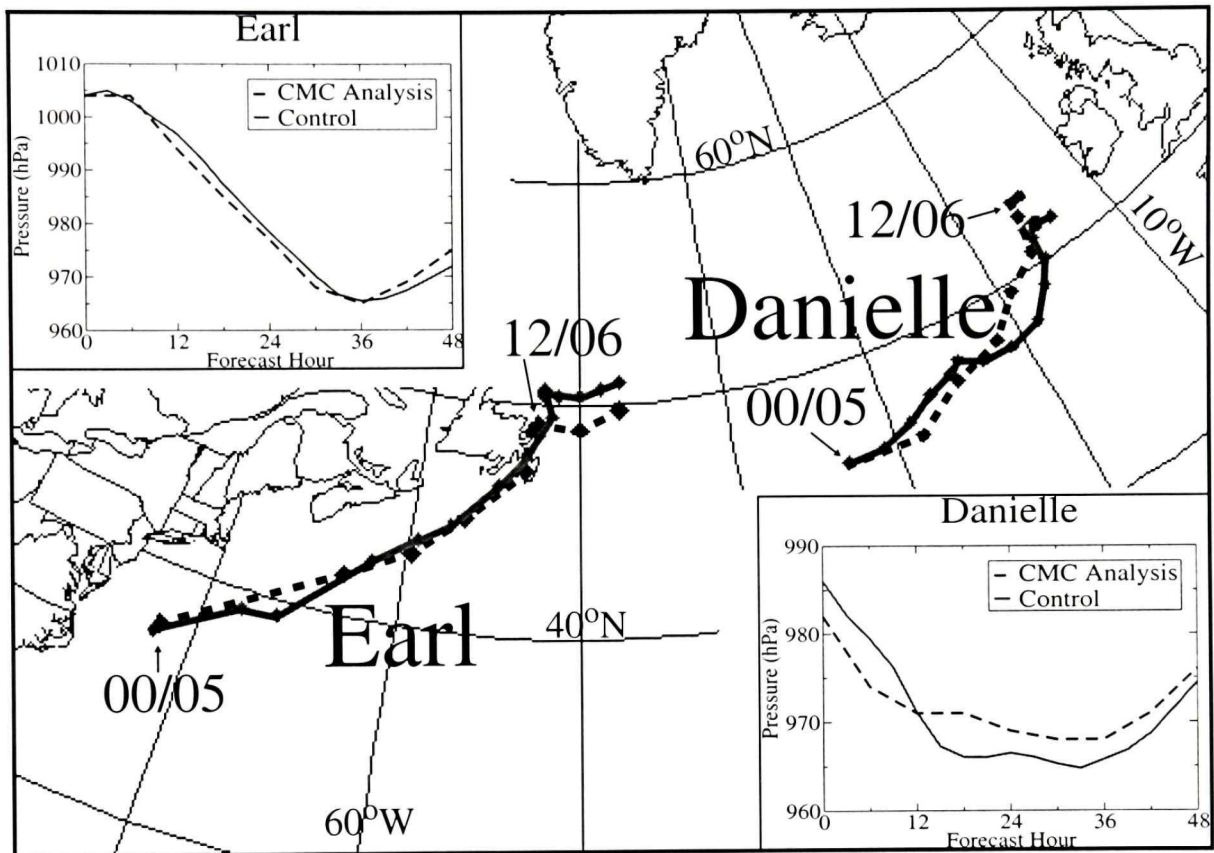


Figure 5.2: Analysis (dashed) and control simulation (solid) tracks and MSLP traces (inset) with locations plotted at 6 hour intervals.

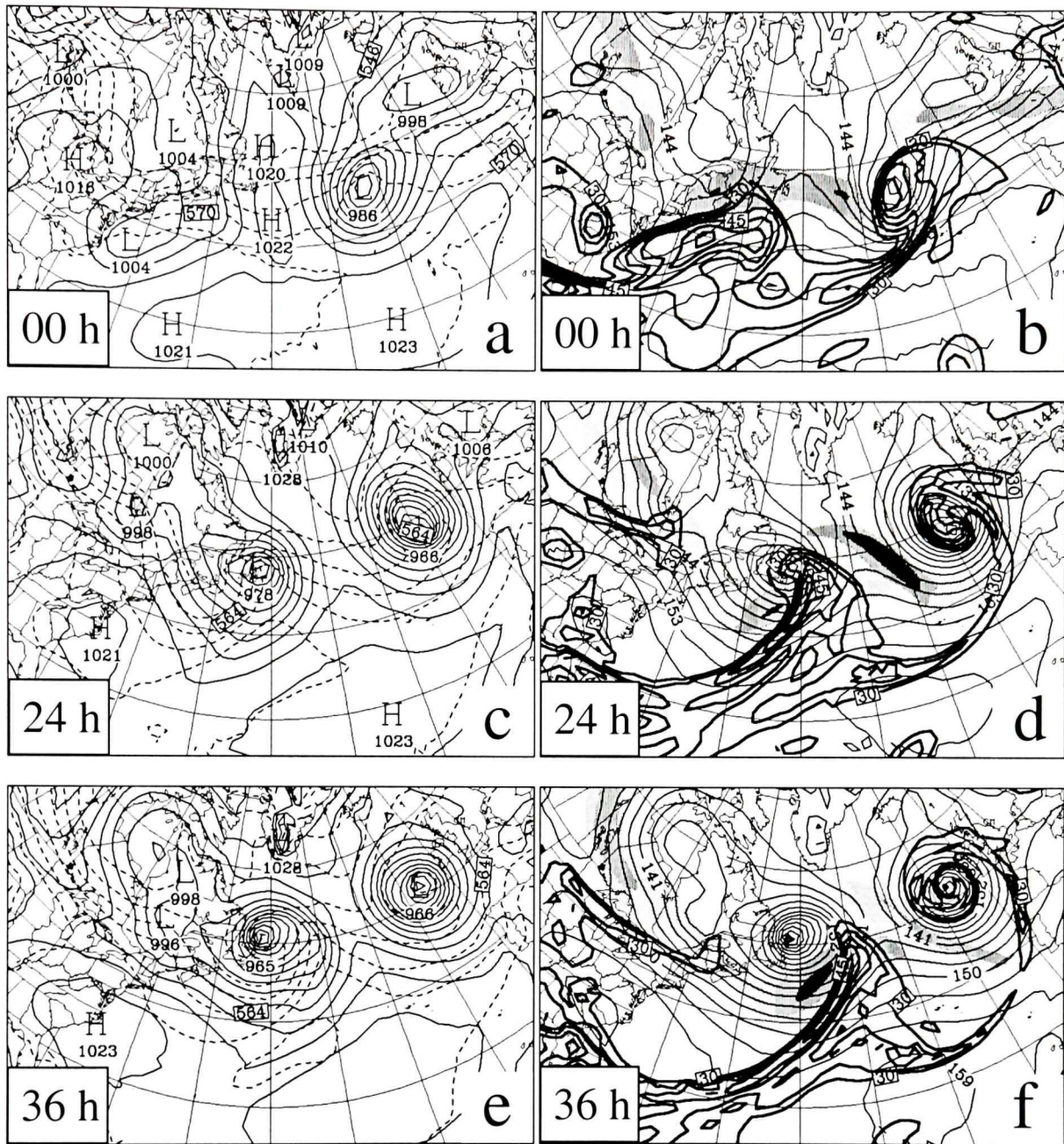


Figure 5.3: Left column: sea level pressure (solid, 4 hPa interval) and 1000-500 hPa thickness (dashed, 6 dam interval) in the initial conditions (panel a), and after 24 and 36 hours of simulation (panels c and e). Right column: 850 hPa height (light solid, 6 dam interval), column-integrated water vapor (precipitable water, heavy solid at 5 mm interval above 25 mm), and 250 hPa windspeed (shading for greater than 40, 50, and 60 m s<sup>-1</sup>) in the initial conditions (panel b), and after 24 and 36 hours (panels d and f).

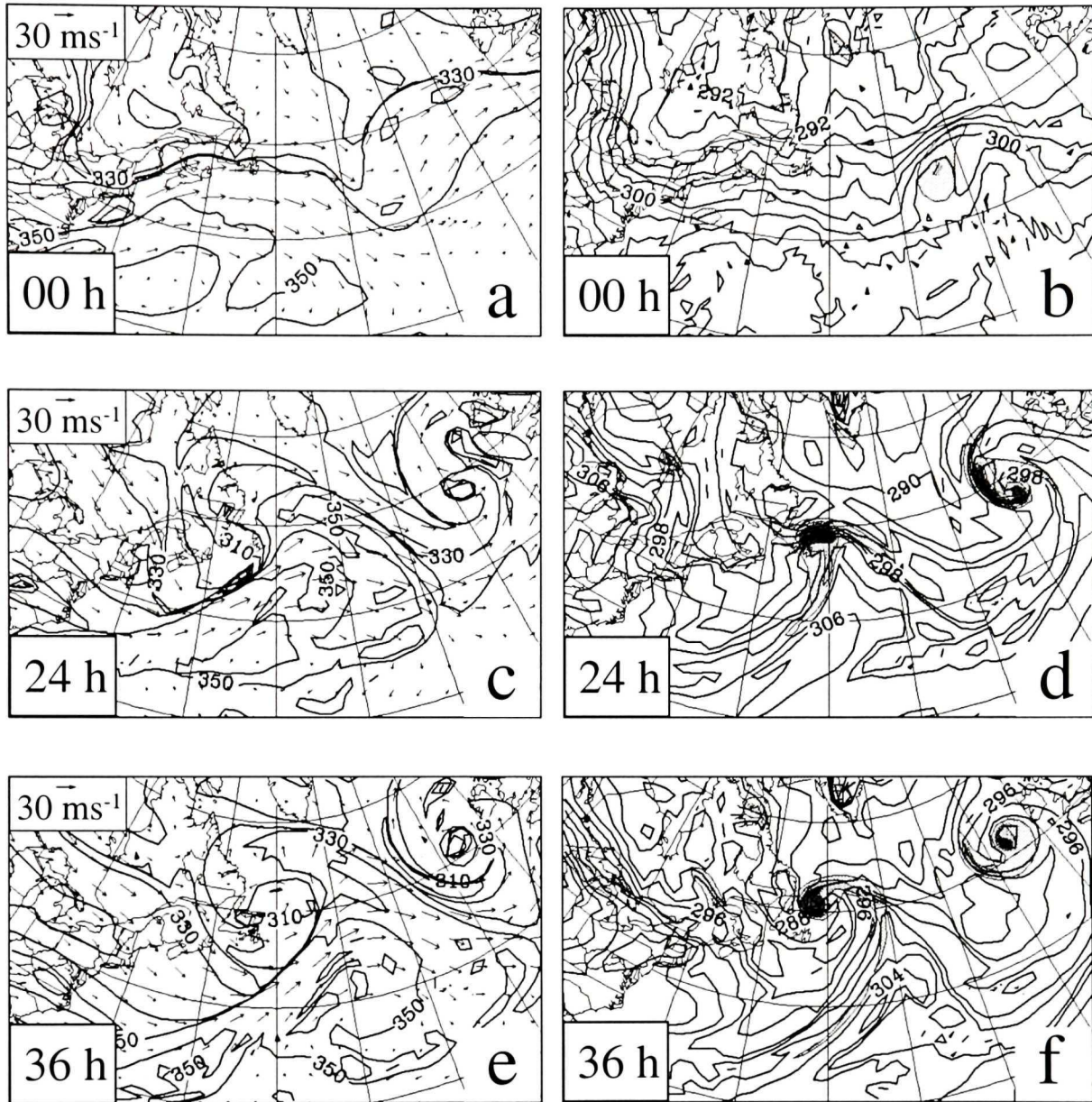


Figure 5.4: Left column: dynamic tropopause potential temperature (solid, 10 K interval) and winds in the initial conditions (panel a), and after 24 and 36 hours (panels c and e). Right column: 850 hPa potential temperature (solid, 2 K interval) and mean 1000-700 hPa PV (shading for absolute values greater than 1, 1.5, and 2 PVU) for the initial time (panel b), and after 24 and 36 hours (panels d and f).

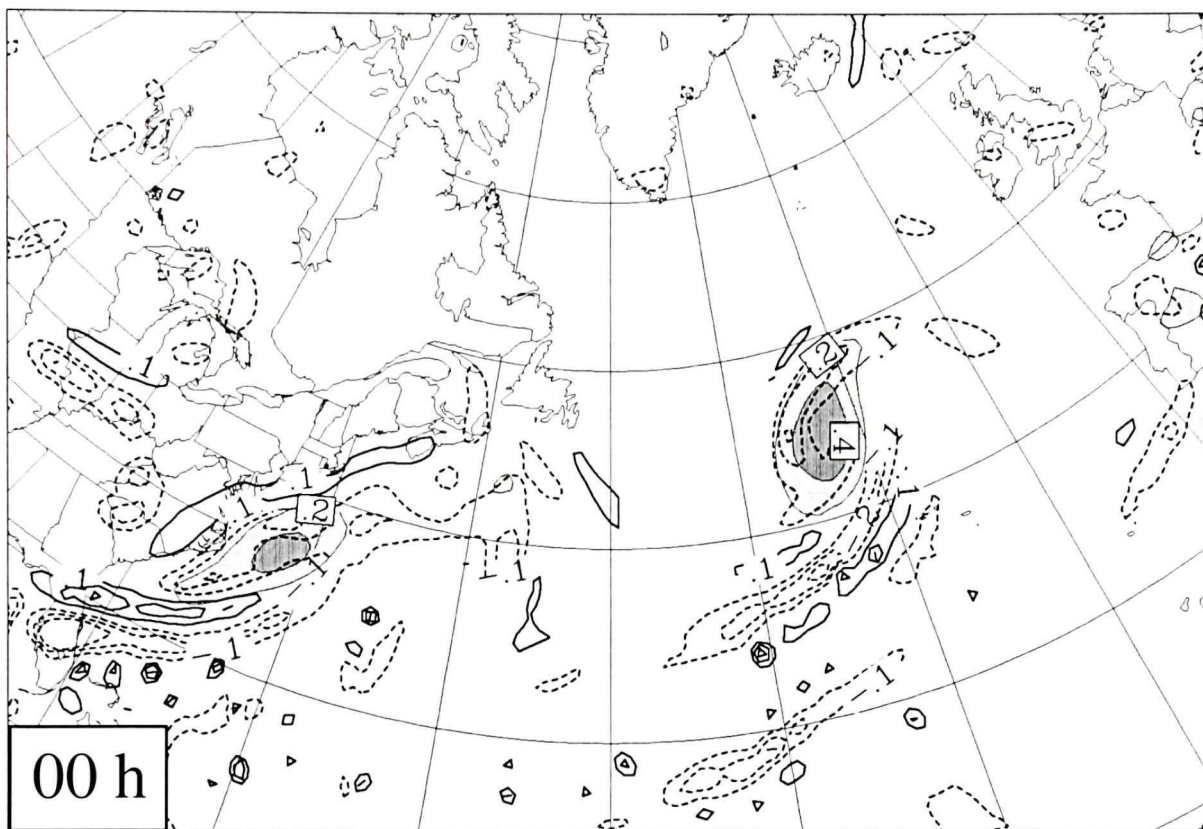


Figure 5.5: Moist component PV anomaly (heavy solid, 0.1 PVU interval, dashed negative, no zero) and dry PV anomaly (light solid and shading, 0.2 PVU interval) at 700 hPa in the initial state.

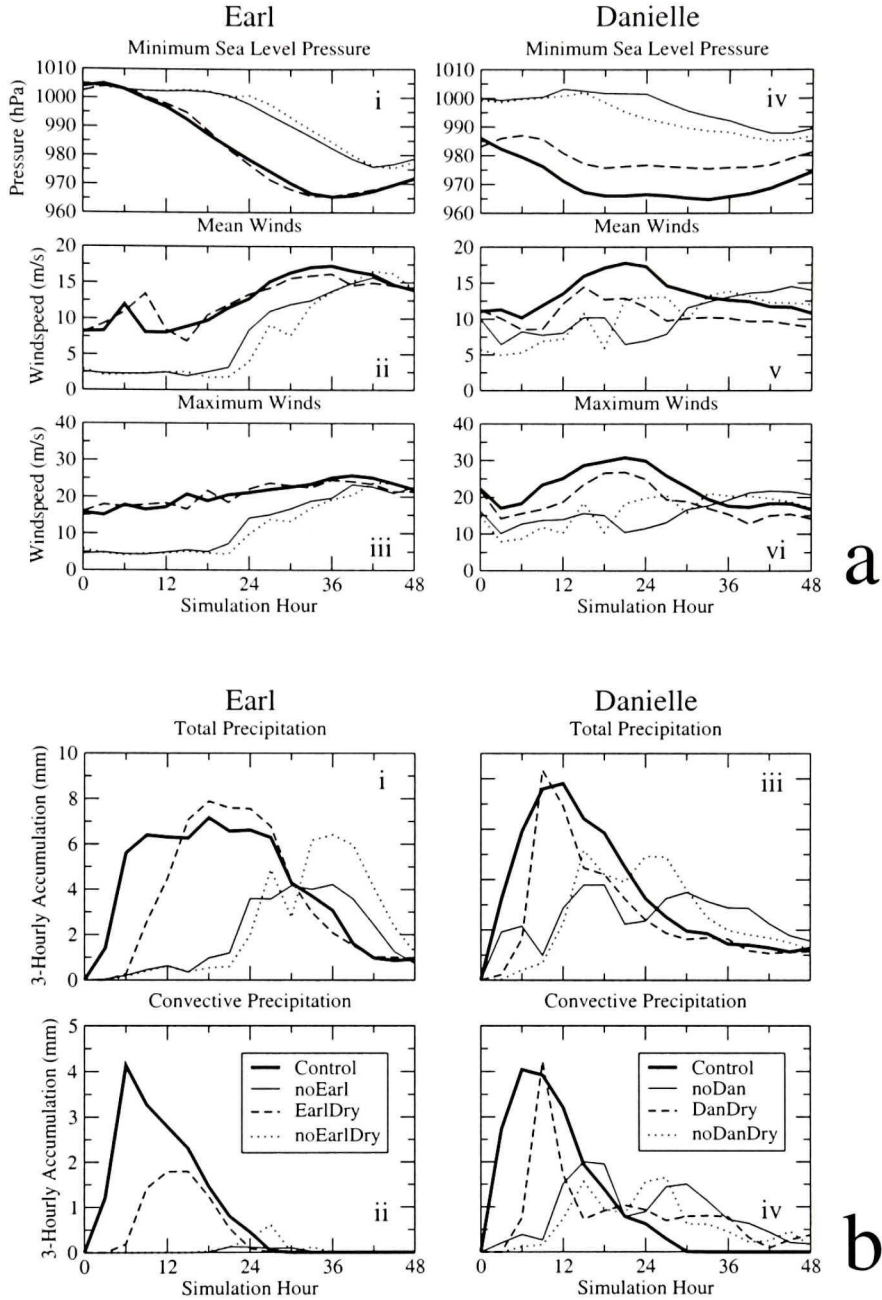


Figure 5.6: Mean sea level pressure and 10 m windspeed intensity indicators [panel a(i) to a(vi)] within 200 km of the MSLP center for the western North Atlantic cyclone (Earl, left column) and the eastern North Atlantic cyclone (Danielle, right column) for control simulation (heavy solid), circulation removal (light solid), moisture removal (heavy dashed) and both circulation and moisture removal (light dotted). Near-core (within 400 km) 3-hourly precipitation accumulations are shown in panel b(i) to b(iv), with column and test references as for panel a. The legends shown in panels b(ii) and b(iv) apply to all plots in the figure.

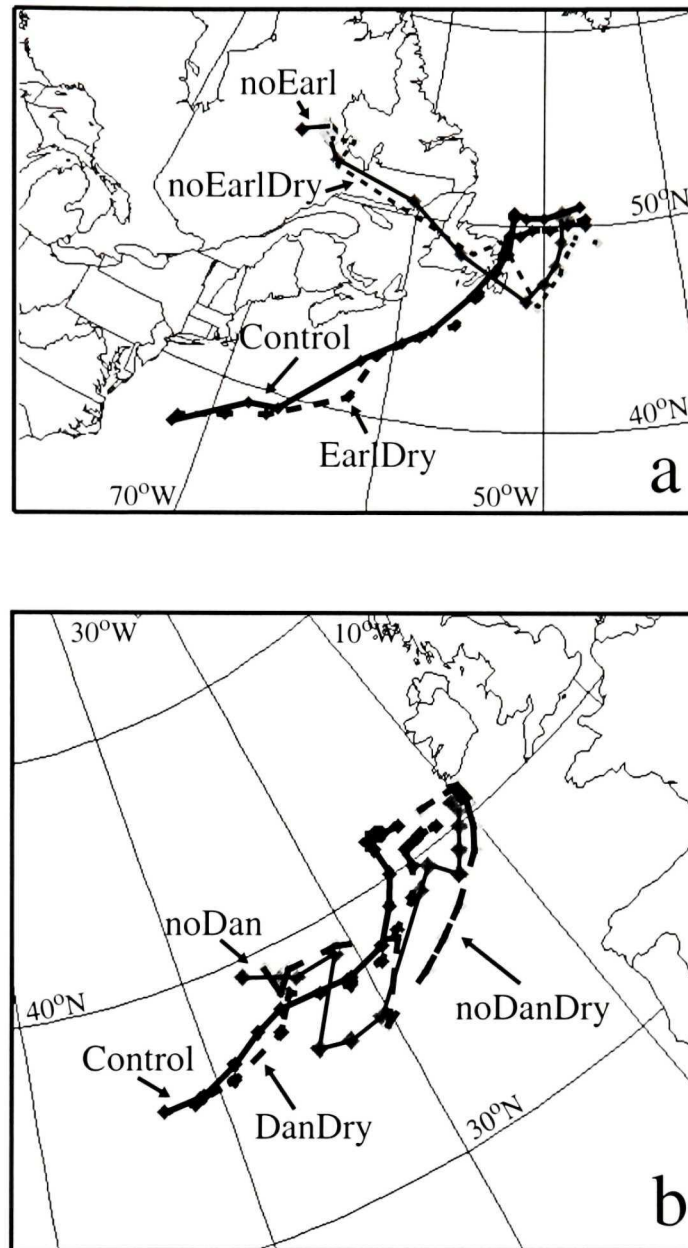


Figure 5.7: Storm tracks for Earl simulations (panel a) and Danielle simulations (panel b). Positions are plotted at 3 hour intervals with a heavy solid line for Control simulations, a dashed line for moisture removals, a light solid line for circulation removals, and a dotted line for both removals of both circulation and moisture (as for Fig. 5.6).

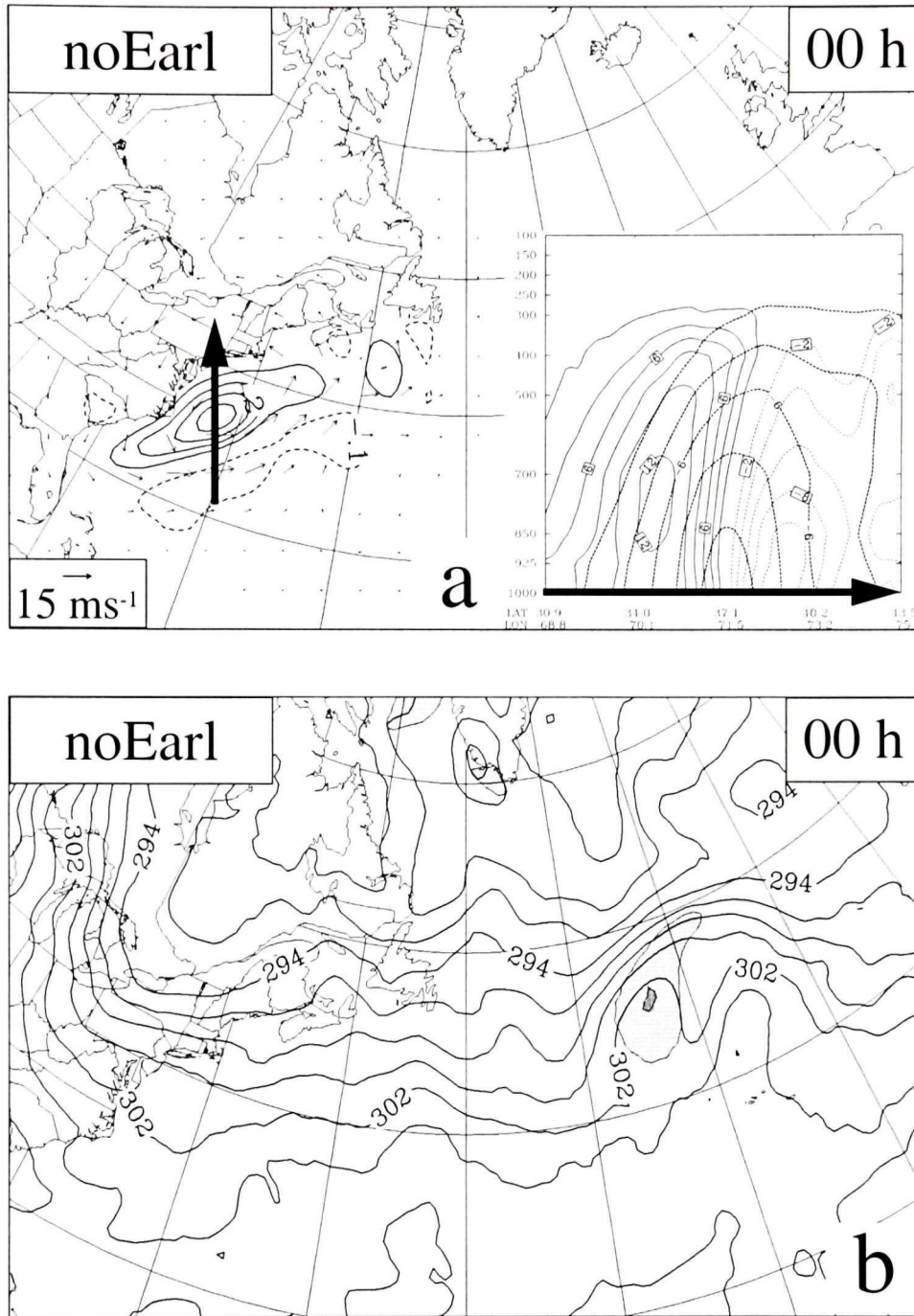


Figure 5.8: Dry PV at 700 hPa associated with the ex-tropical feature is shown in panel a (0.1 PVU contour interval, no zero) with the balanced inverted wind field at 700 hPa. Inverted height (heavy dashed, 2 dam intervals) and wind ( $2 \text{ m s}^{-1}$  intervals) perturbation structure is shown in the inset for a cross-section as indicated by the arrow. Panel b shows potential temperature (solid, 2 K interval) and mean 1000-700 hPa PV (shading for absolute values greater than 1, 1.5, and 2 PVU) for the initial time.

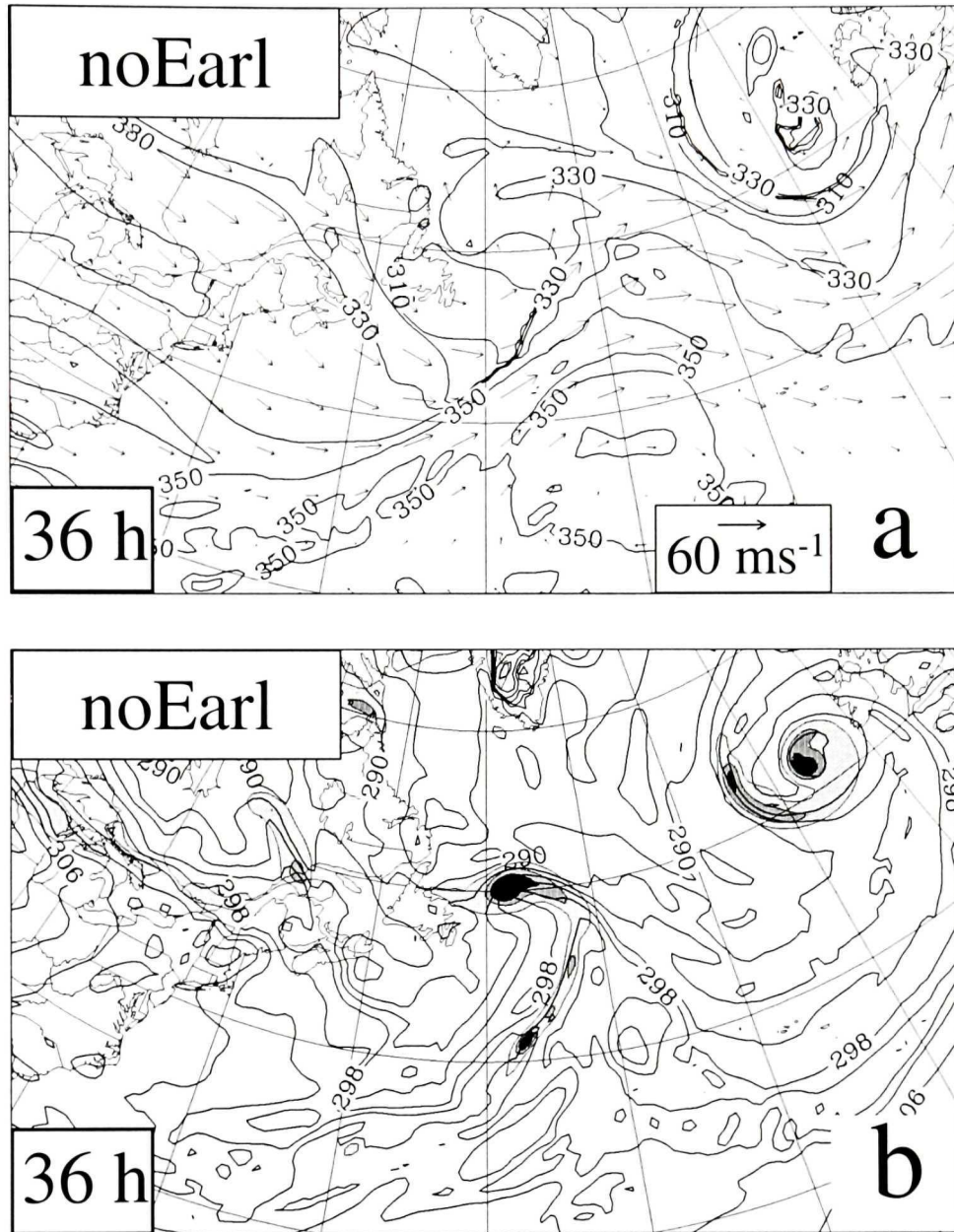


Figure 5.9: Dynamic tropopause potential temperatures and winds (panel a) after 36 hours of simulation, as plotted in Fig. 5.4e. Potential temperature at 850 hPa and lower-level mean PV (panel b) after 36 hours plotted as in Fig. 5.4f.

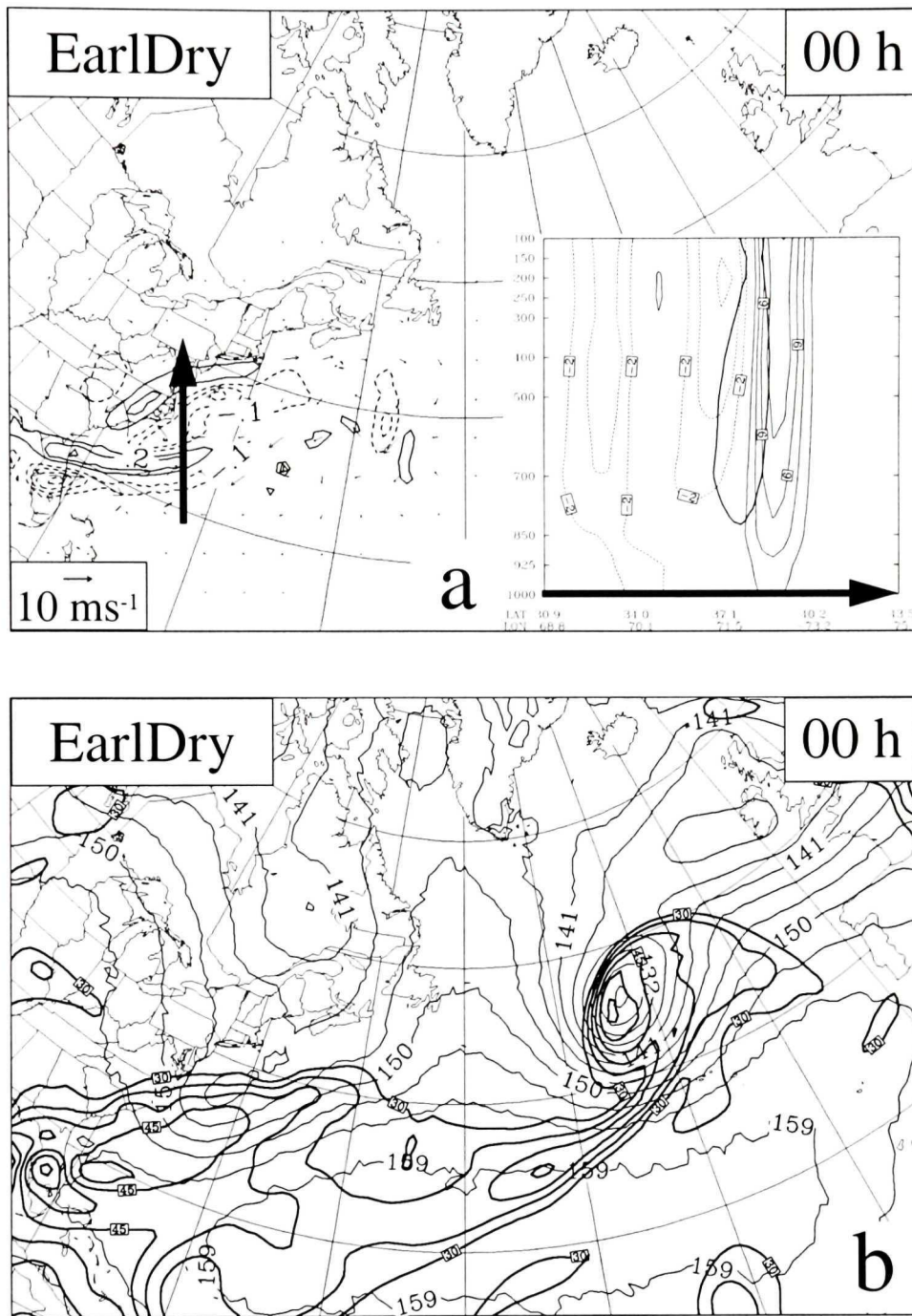


Figure 5.10: Moist component PV and inverted winds at 700 hPa in the initial conditions, plotted as in Fig. 5.8a, are shown in panel a. Heights at 850 hPa and precipitable water contents (panel b) are plotted as in Fig. 5.3b, without windspeeds.

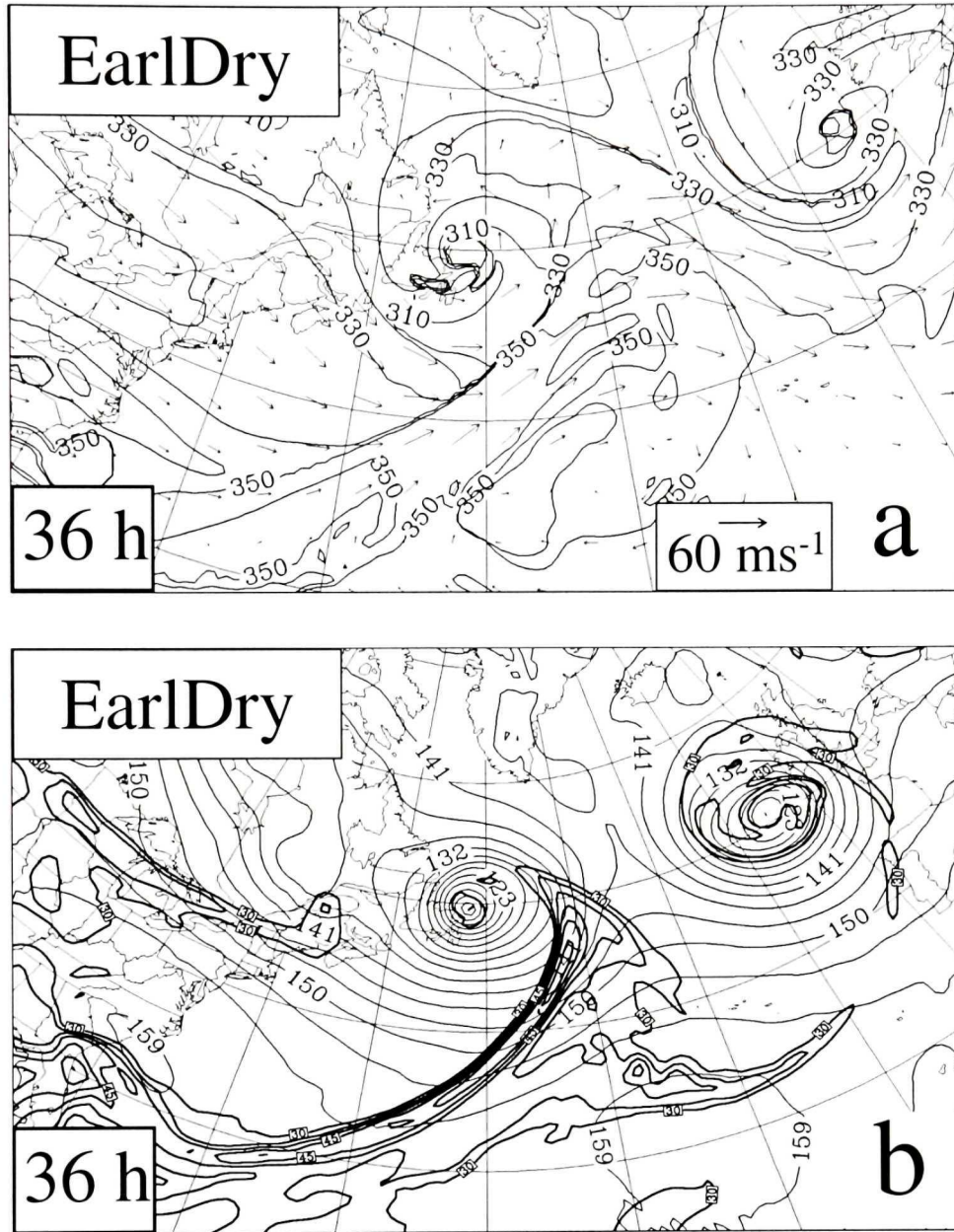


Figure 5.11: Panel a is as for Fig. 5.9a, but for EarlDry simulation. Panel b is as for Fig. 5.10, but after 36 hours of simulation.

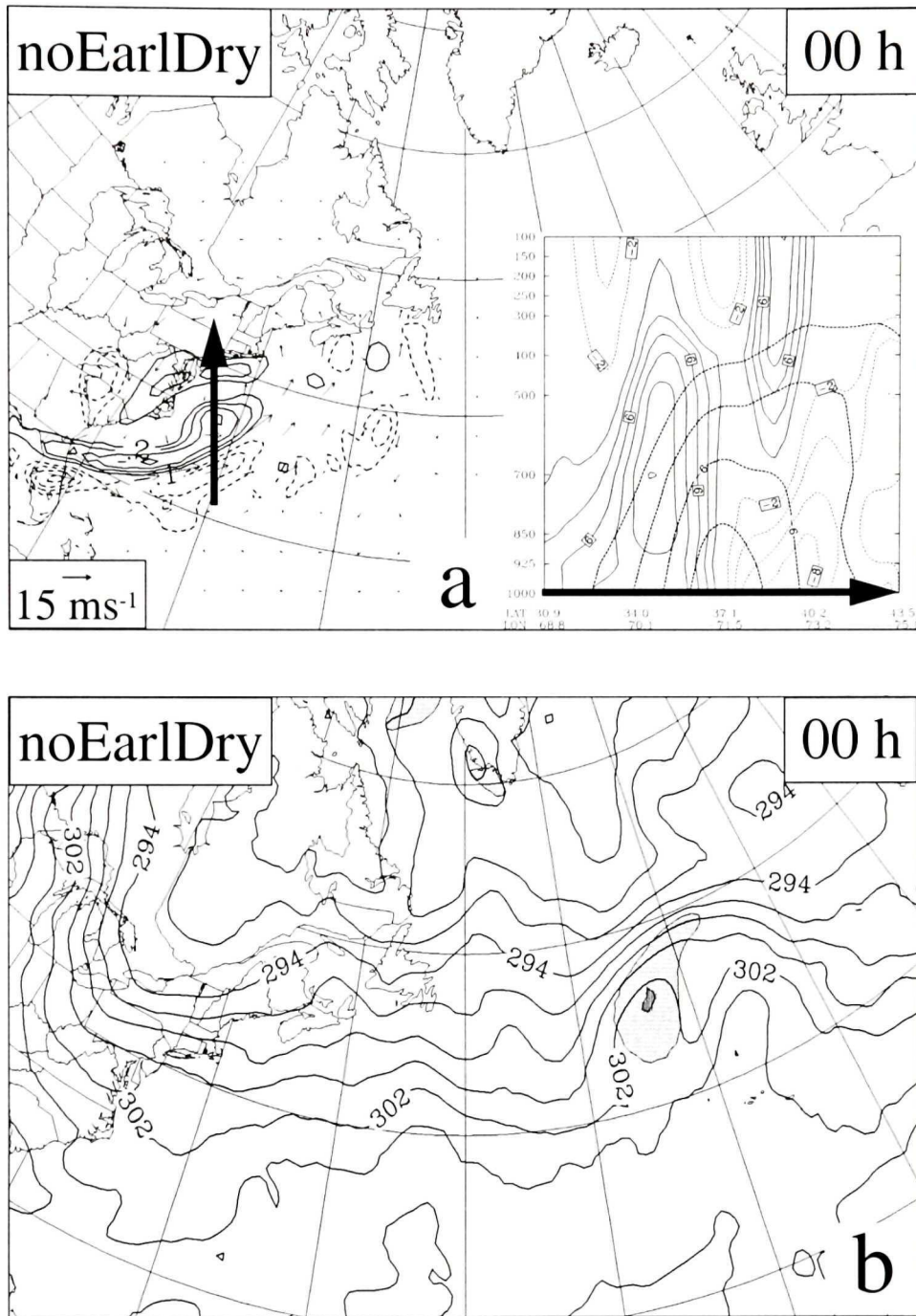


Figure 5.12: Panel a is as for Fig. 5.8a, but includes both dry PV and  $PV_{mc}$  anomalies. Panel b is as for Fig. 5.8b, but for the noEarlDry simulation.

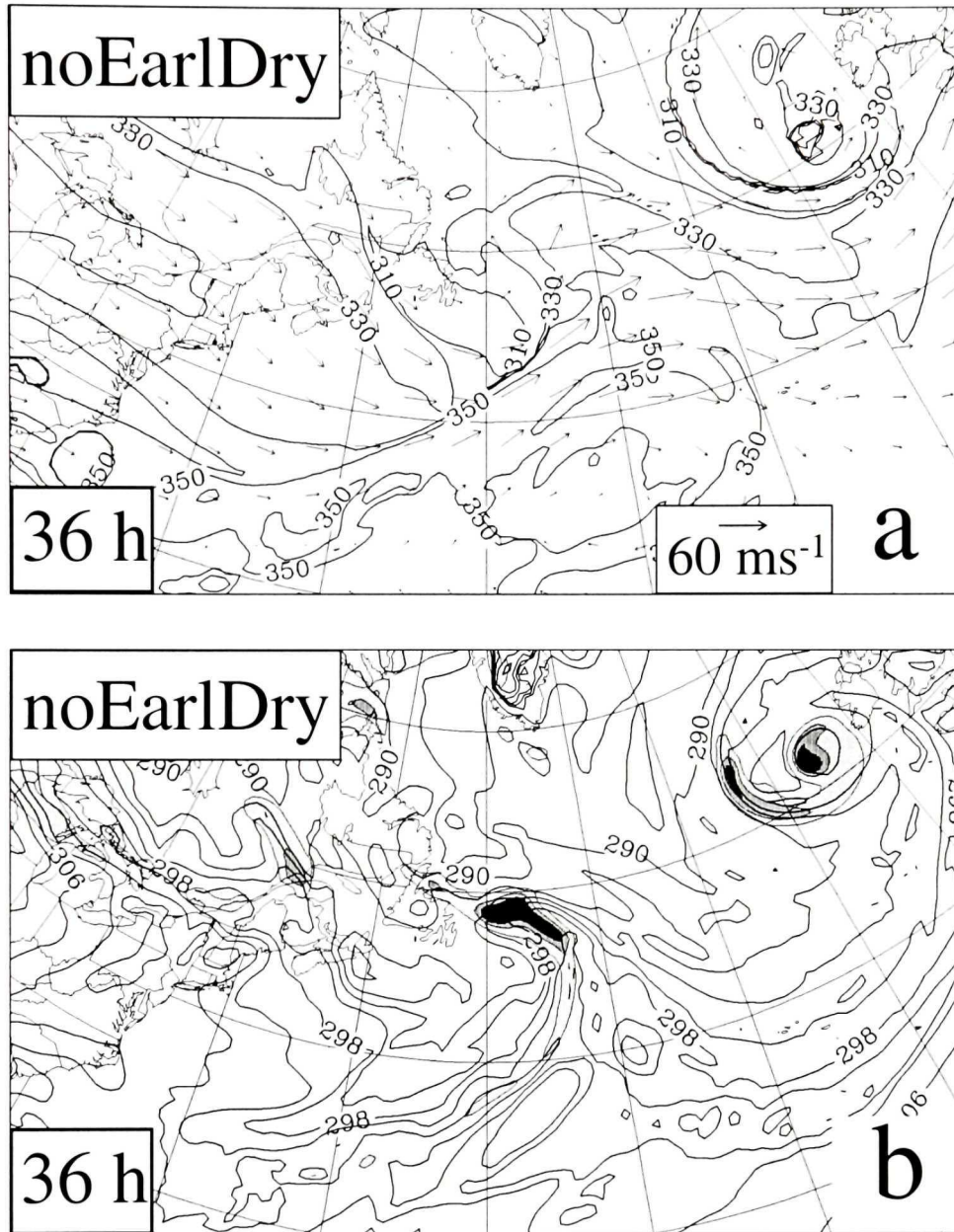


Figure 5.13: Panels are as for Fig. 5.9, but for the noEarlDry simulation.

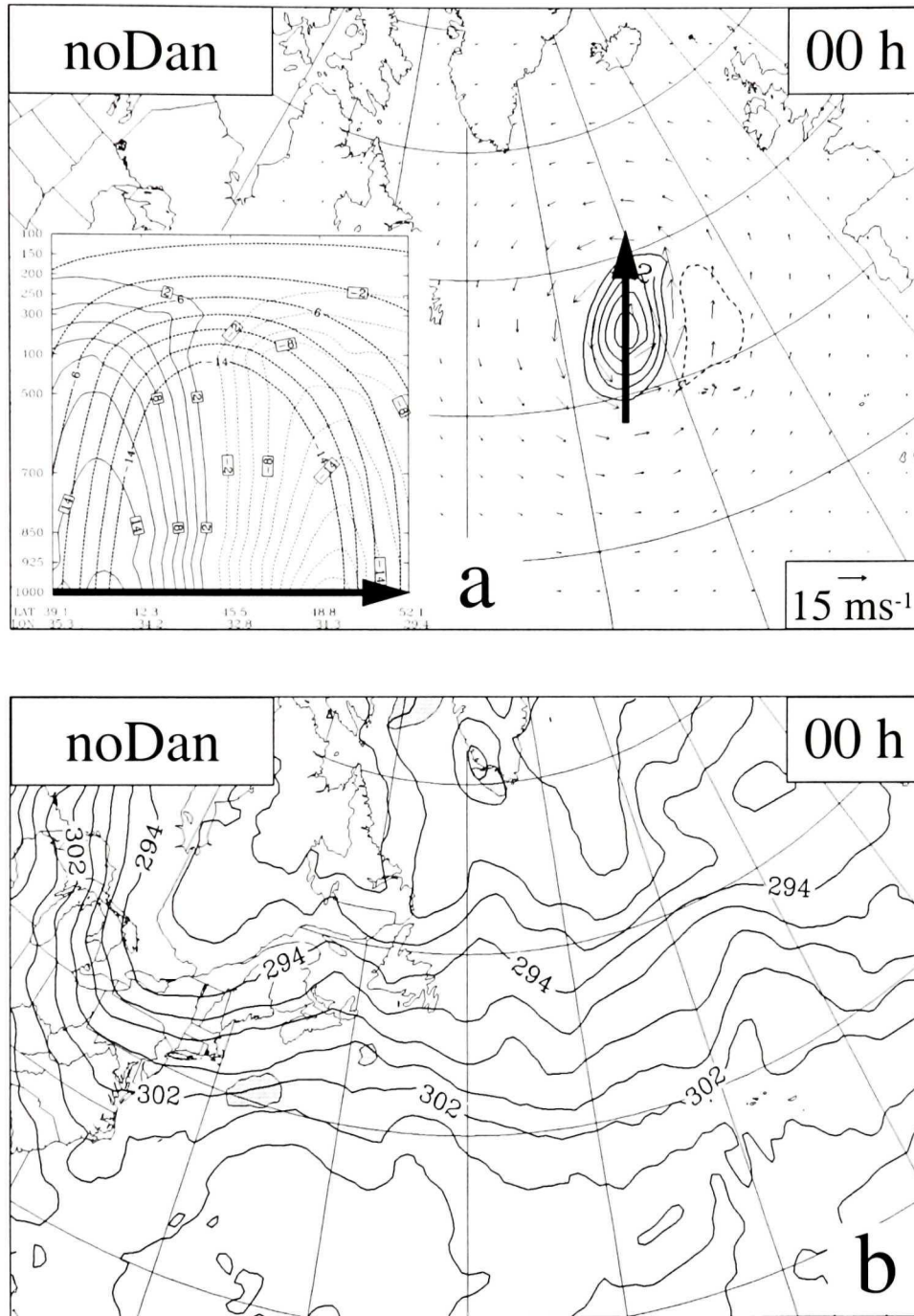


Figure 5.14: Panels are as for Fig. 5.8, but for the noDan simulation.

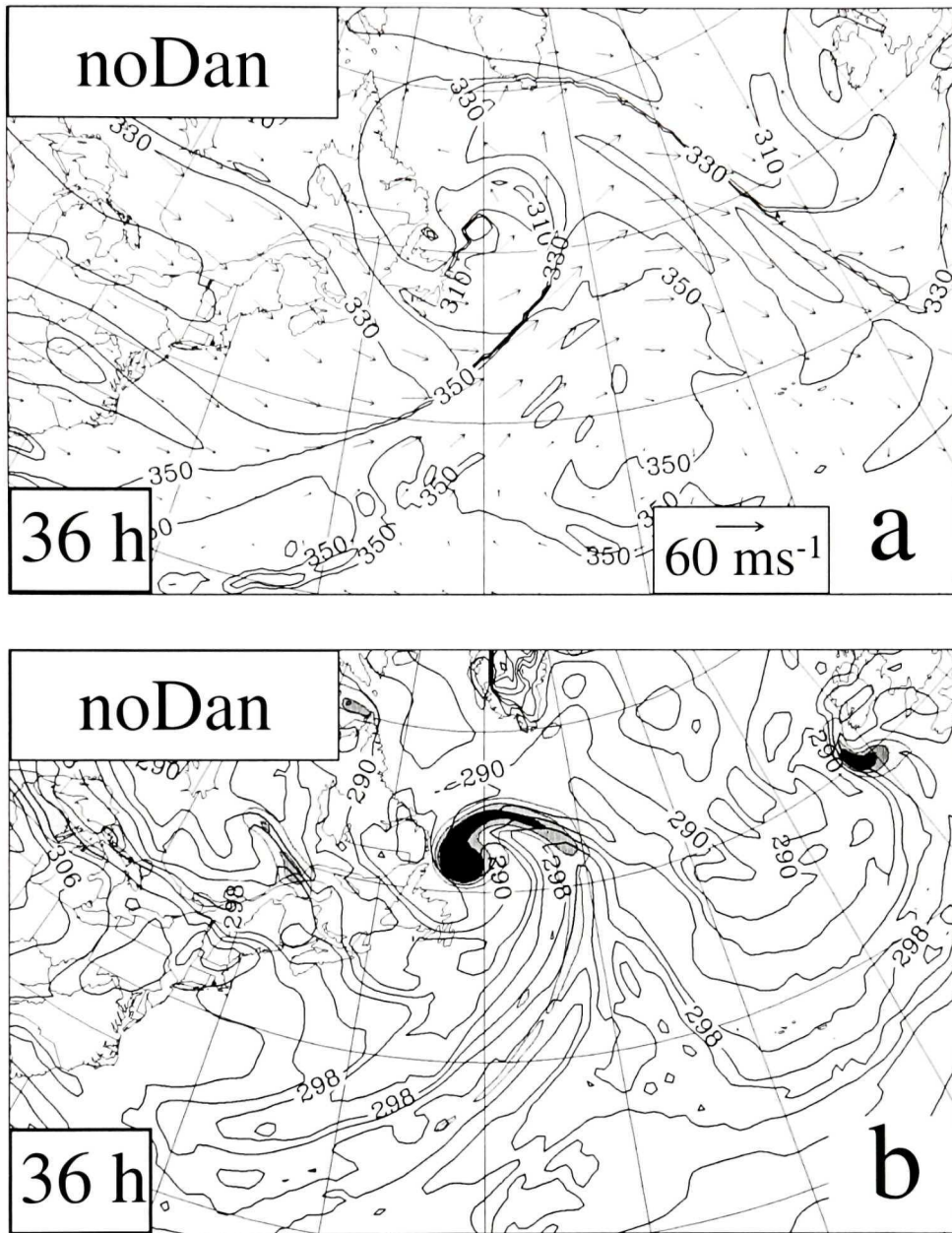


Figure 5.15: Panels are as for Fig. 5.9, but for the noDan simulation.

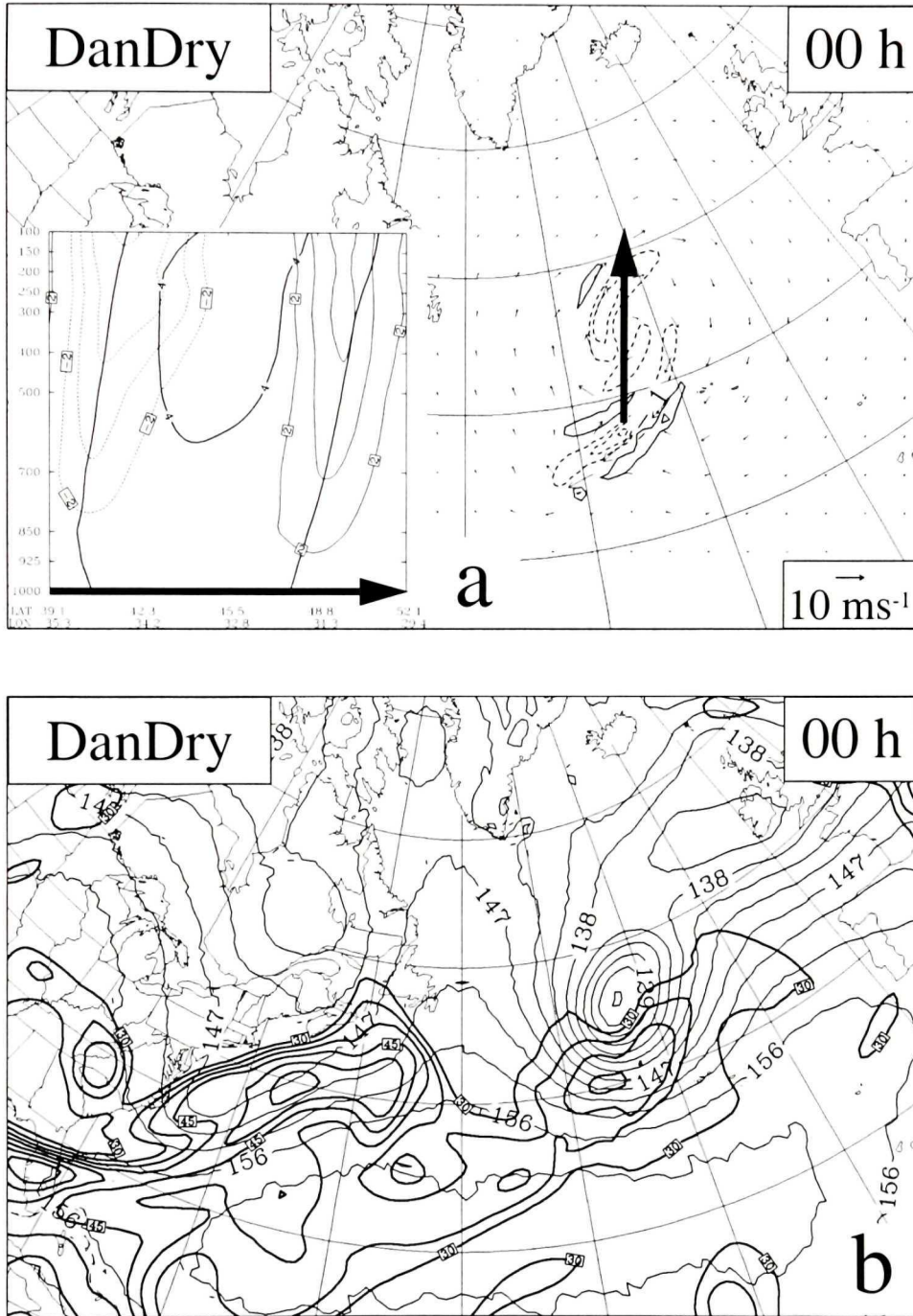


Figure 5.16: Panels are as for Fig. 5.10, but for the DanDry simulation.

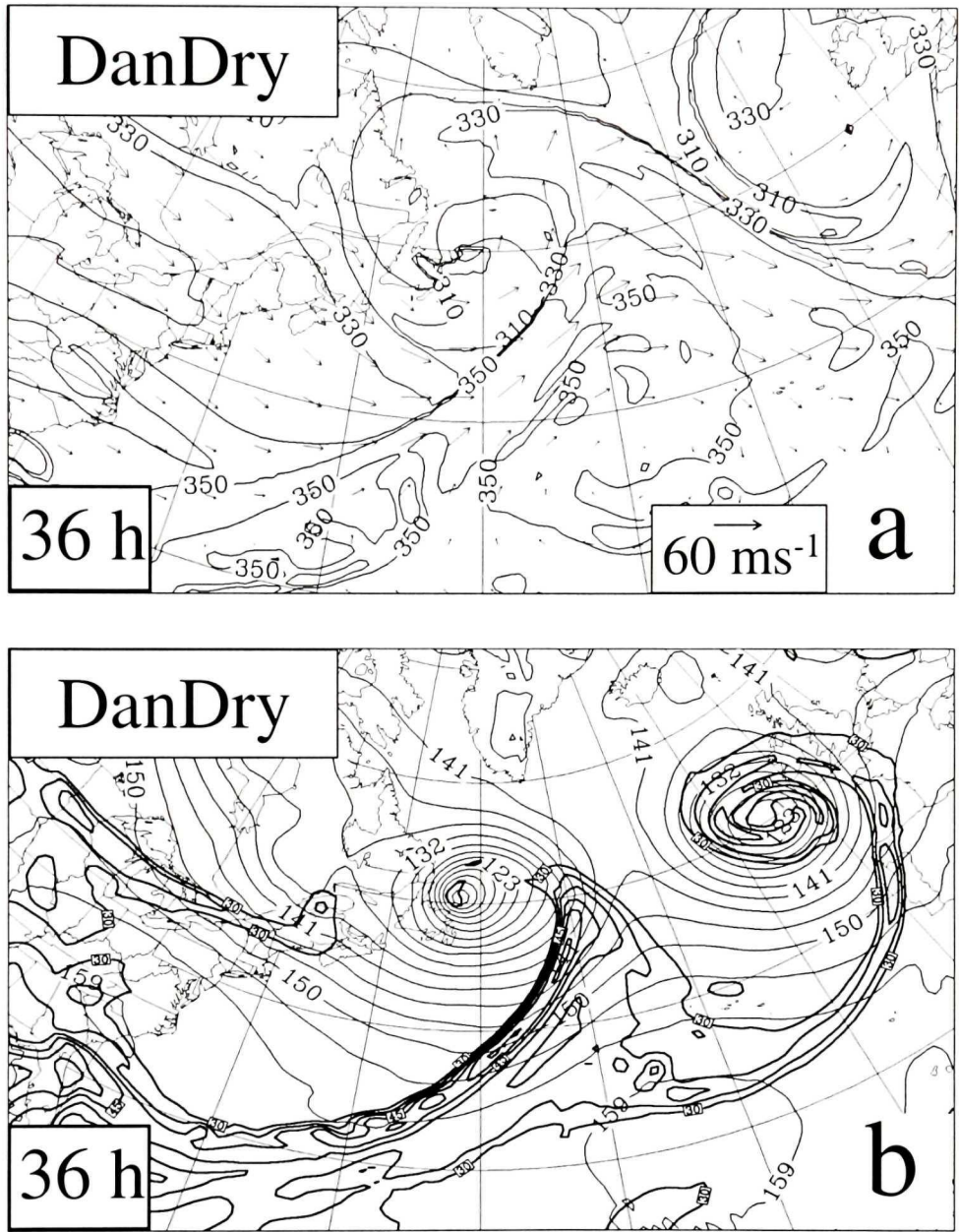


Figure 5.17: Panels are as for Fig. 5.11, but for the DanDry simulation.

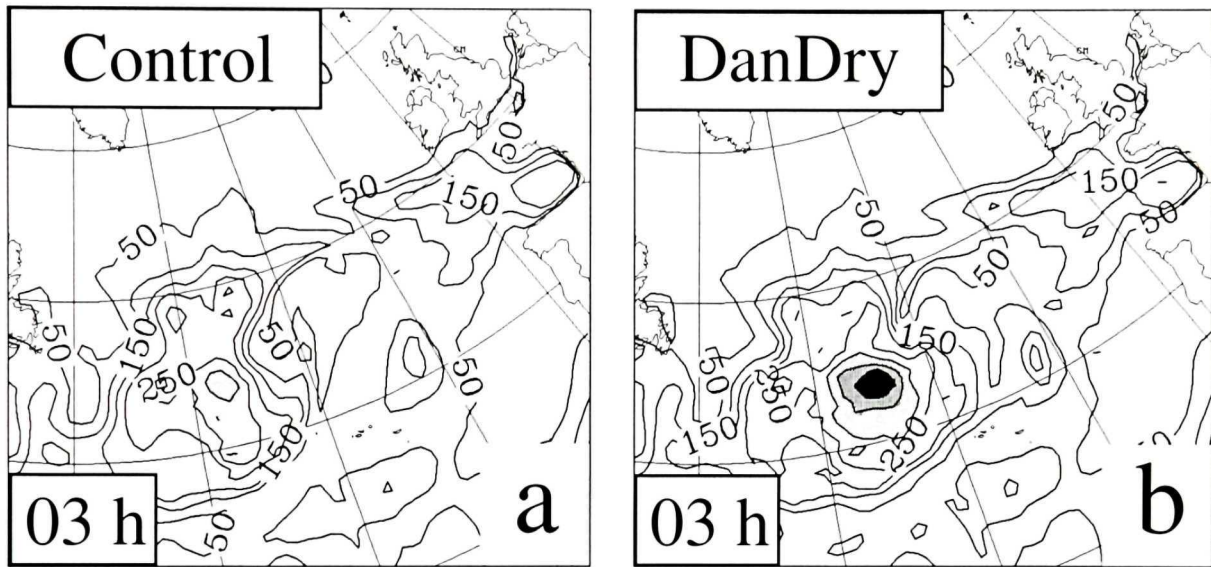


Figure 5.18: Oceanic latent heat fluxes after 3 hours in the control simulation (panel a) and DanDry sensitivity test (panel b). Contours are plotted every 50 W/m<sup>2</sup>, with shading above 300, 350, and 400 W/m<sup>2</sup>.

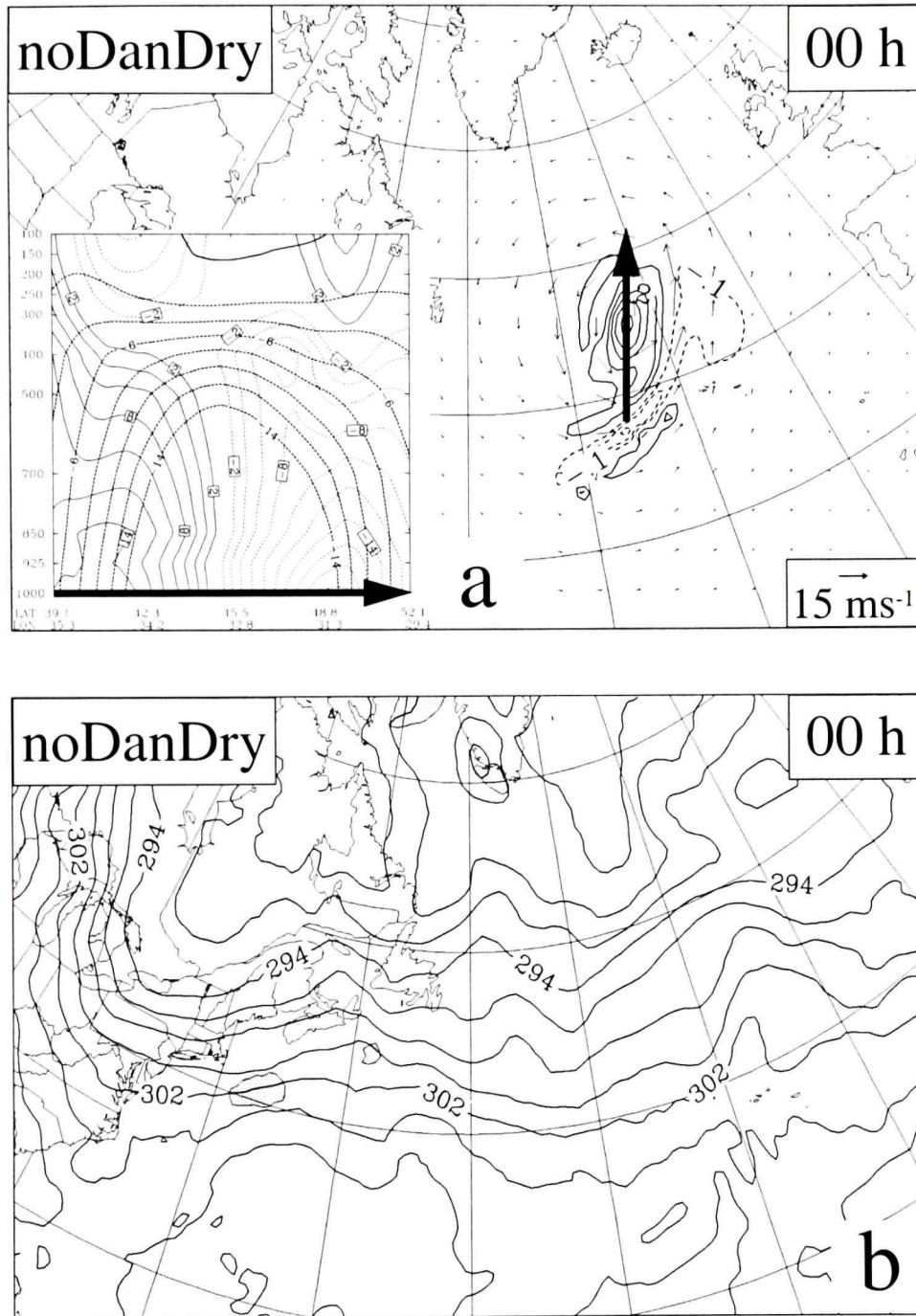


Figure 5.19: Panels are as for Fig. 5.12, but for the noDanDry simulation.

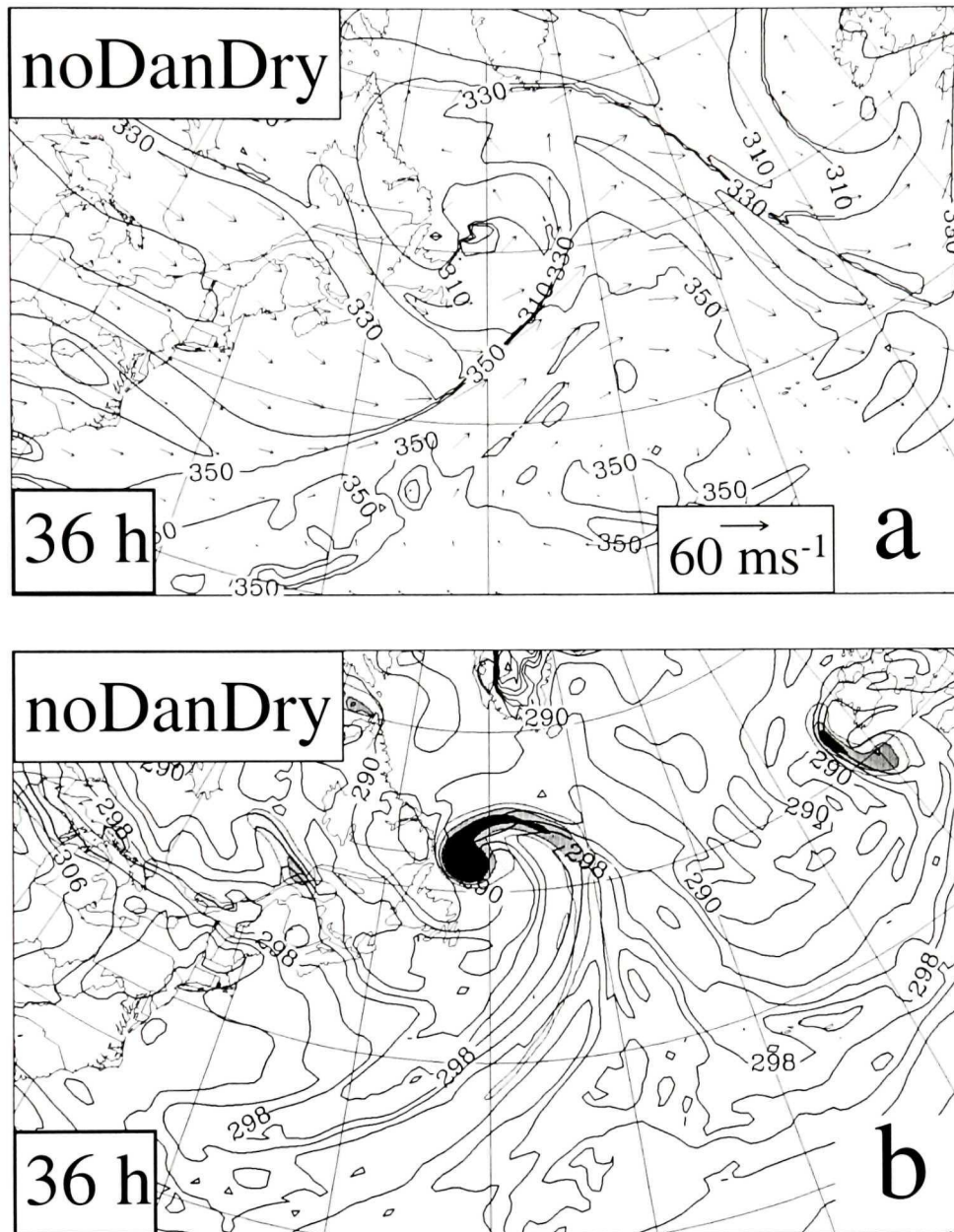


Figure 5.20: Panels are as for Fig. 5.13, but for the noDanDry simulation.

# Chapter 6

## Summary, Discussion, and Future Research

The goal of this thesis is to evaluate the sensitivity of the ET/R process to identifiable tropical and midlatitude features present at the onset of the reintensification phase of ex-hurricanes Danielle and Earl (1998). The work presented in the preceding chapters is summarized here in order to clarify the results of the multiple sets of control simulations and sensitivity tests that are required to address many degrees of freedom of this problem.

### 6.1 Utility of PV and $PV_{mc}$

Throughout this study, PV-based diagnostics and PV modification and inversion procedures are used extensively. For analysis, the conservative nature of PV in frictionless, inviscid flows makes it the ideal quantity by which to define the dynamic tropopause, the orography of which has important dynamical consequences throughout the atmosphere. Diagnosis of a second conservative quantity, such as the potential temperature, on the dynamic tropopause provides dynamical insight beyond that obtained through traditional analysis techniques. Moreover, the invertibility of PV under the constraints of a balance equation allows for the derivation of the complete dry atmospheric state from the three dimensional PV field. Piecewise PV inversion is employed extensively throughout the present study as a way to identify the structure

of the mass and flow fields associated with individual, anomalous PV patterns.

The extension of the PV decomposition framework presented in Chapter 4 allows for the diagnosis and inversion of  $PV_{mc}$ , defined as the portion of the total PV field that is directly attributable to the presence of atmospheric water. Although the isolation and modification of the anomaly-correlated water vapour field is not necessary for the dry upper-tropospheric PV modifications and inversions presented in Chapter 2, it is of paramount importance in subsequent work involving the removal of the remnant tropical vortices (Chapter 5).

The development of  $PV_{mc}$  is an important result of this study and the full extent of its value as a diagnostic variable remains to be determined. The  $PV_{mc}$  fields shown in Chapter 5 highlight dynamically and thermodynamically important structures in the TC remnants. Dry inflow regions and extended conveyor belt circulations are clearly visible in both storms, as are the tropical moisture values contained within the vortices themselves. The mass and flow fields corresponding to the TC-related  $PV_{mc}$  anomalies clearly show regions in which the inverted flow acts to reinforce these observed features. Furthermore, removal of both the dry PV and  $PV_{mc}$  associated with the remnant TC circulations is necessary for the complete removal of the extratropical feature as studied in Chapter 5.

## 6.2 Case Summary

The simultaneous ET/R of two Atlantic hurricanes (Danielle and Earl, 1998) form an ideal testbed in which to simulate and analyse the myriad of tropical/extratropical interactions that are involved in the ET/R process. Earl, a Gulf of Mexico Category 2 landfalling hurricane, undergoes rapid extratropical reintensification in the 36 h following 00/05 as the storm's minimum MSLP falls from 1004 hPa to approximately 960 hPa. A Category 2 hurricane that completes recurvature well off the eastern seaboard, Danielle also enters the reintensification phase at 00/05 and experiences a central pressure drop of approximately 20 hPa (from 985 hPa at 00/05) over the subsequent 36 h period.

Although both storms are located in the North Atlantic basin at 00/05, the dynamics associated with the individual ET/R events display marked differences. Beginning its extratropical spin-up just off the east coast of the United States of America north of Cape Hatteras, Earl interacts strongly with a baroclinic zone that lies along the western edge of the North Atlantic basin. The associated upper-level trough PV feature rolls cyclonically above the developing baroclinic surface cyclone. Danielle, already more than half of the way across the North Atlantic by 00/05, redevelops in a near-tropical environment created by strong northward advection of warm, moist air in advance of the system. The initially-weak trough feature upstream of Danielle extends rapidly southward, filaments, and wraps around the perimeter of the quasi-tropical airmass surrounding the storm's central circulation. In both cases, the warm core structures of the tropical vortices are maintained, Earl's through a frontal seclusion process and Danielle's through continued deep convection. Although each of the forcings listed here undoubtedly play at least a minor role in the ET/R process, the object of this research is to determine which features are absolutely critical to the observed nature and intensity of the rapid reintensification of the storms.

### 6.3 Upstream Features - Ex-hurricane Earl

A set of upper-level trough PV anomalies, described in detail in Chapter 2, lie upstream of Earl's remnant circulation at 00/05. Each of these is removed individually using the dry PV modification and inversion techniques summarized earlier in this chapter. The depth of the 500 hPa trough is found to be of secondary importance to Earl's ET/R when compared to the north-south amplitude of the trough feature. With a reduced meridional circulation, increased westerly shear destroys the tropical vortex and a secondary cyclogenesis mechanism is found to be responsible for initiating the subsequently-intensifying circulation. The complete removal of all anomalous PV associated with the trough results in virtually no reintensification (the lowest central MSLP obtained in the NOTR simulation is 989 hPa after 48 h) and a storm track with a greatly enhanced easterly component, consistent with the zonal flow

aloft. It is concluded that the large-amplitude trough upstream of Earl at 00/05 is absolutely crucial to the ET/R process.

## 6.4 Downstream Features

The sensitivity of ET/R to identifiable features in the downstream atmospheric state is of a drastically different nature from that which attends upstream perturbations. Throughout the sensitivity tests conducted for upstream investigations of ex-hurricane Earl, the evolution of the transitioning system retains the same qualitative form. In all but the NOTR trough removal simulation, the rapid cyclonic rollup of the remaining trough PV features is ubiquitous, and the resulting system consistently displays strong frontal development. The ET/R of ex-hurricane Danielle, as described earlier in this chapter, occurs in a weakly baroclinic environment surrounded by a filamenting upper-level trough. The possibility of a bimodality in the ET/R process (“baroclinic” and “tropical” redevelopment modes) is explored using a set of sensitivity tests composed of various idealized initial states downstream of ex-hurricane Earl. The complete removal of downstream structure (IDEALLAT) and the downshear extension of Earl’s local environment (EXT) both result in systems that undergo tropical mode redevelopment, similar to Danielle in the control. The retention of an idealized form of the North Atlantic jet/front structure is required for the induction of a baroclinic mode of ET/R similar to that experienced by Earl in the control. Linear jet theory and superposition arguments are used to suggest that ET/R processes occurring in the equatorward entrance region of a jet maximum are likely to be of baroclinic mode, whereas those occurring in the poleward jet exit region will in general display tropical mode ET/R characteristics. This modulating quality of the midlatitude jet make it another key feature in the ET/R process.

## 6.5 Vortex Structure

The importance of the tropical properties of the remnant TC to ET/R seems intuitively unquestionable. However, the work of Sinclair (2002) and Thorncroft and Jones (2000) suggests that the strongest TCs do not necessarily represent the optimal seed vortices for ET/R. A quantification of the role in ET of the remnant circulation and the moisture structure of the decaying tropical feature is therefore one of the primary goals of the study. A three-step modification and removal process is undertaken in order to construct a set of sensitivity tests for both Danielle and Earl. It is found that the baroclinic mode of ET/R (Earl) displays very little sensitivity to the structure or even to the existence of the TC remnant. In the absence of ex-hurricane Earl's dry PV and PV<sub>mc</sub> structure, pure extratropical cyclogenesis results in the development of a storm of a strength almost equal to that of Earl in the control, and in a similar location. Removal of Danielle's cyclonic circulation results in a reduction of the southward extension and filamentation in the upper-level PV structure, which thereafter produces very little cyclogenetic forcing at the surface. Removal of the tropical moisture contained in the remnant TC also results in a weakened reintensification and leads to the reduction of the warm core perturbation. The tropical mode of ET/R is therefore sensitive to both the dynamic and thermodynamic structures of the transitioning TC.

## 6.6 General Conclusions

Through a series of simulations of the simultaneous ET/R events of ex-hurricanes Danielle and Earl, a list of the key ingredients for dramatic reintensification has been obtained. The necessity of some form of upper-level trough upstream of the transitioning TC is unquestionable, and the larger the north-south amplitude of this feature, the stronger the ET/R process will be. Redevelopment of the tropical vortex in the divergent equatorward entrance region of a midlatitude jet maximum will likely result in a baroclinic mode reintensification that is insensitive to the structure of the

remnant TC. However, ET/R events occurring in the poleward exit region of a jet streak will generally undergo a tropical mode of reintensification whose nature and intensity is highly dependent both on the strength of the remnant circulation and on the existence of large precipitable water contents in the tropical air surrounding the transitioning cyclone. This description of the North Atlantic ET/R process, as diagnosed for ex-hurricanes Danielle and Earl, provides an indication of the ingredients necessary for the rapid redevelopment of a TC vortex. The author hopes that the sensitivities discovered over the course of this research will provide insight and guidance to those who continue to pursue the study of the ET/R process as well as to those who make crucial forecasts and decisions based on our still-evolving understanding of these extreme events.

## 6.7 Future Research Directions

The limitations of case-based research are well known, and may only be dismissed following the application of case-derived conceptual models to numerous events of similar and differing structure to that which originally prompted the theory. With the goal of developing a general description of ET/R in mind, studies similar to the one presented here should be carried out for other ET events, some of which resulted in reintensification, and others of which did not. Already, the works of Thorncroft and Jones (2000) and Browning et al. (1998) in part support the findings of this study; however, a much larger dataset must be collected before any level of statistical significance for the results can be achieved.

Further study of the utility of the  $PV_{mc}$  variable is warranted given its success in isolating the moisture structures of the ex-tropical vortices in this study. The ability of this variable to couple dynamics and thermodynamics may make it a valuable diagnostic tool once its properties are fully understood. The ability to modify atmospheric moisture fields in a dynamically meaningful sense and without introducing either hydrostatic or dynamic imbalance could prove useful in fields such as ensemble forecasting, where the use of  $PV_{mc}$  could provide an extra dimension in the sampling

of atmospheric state space.

The issue of phasing between the upper-level trough and the TC remnant is one which remains unaddressed in this study. Ma et al. (2003) stress the importance of the rapidly-decreasing horizontal displacement of the upper- and lower-level PV anomalies during ex-hurricane Earl's evolution. A simulation-based study of multiple ET/R events by Klein et al. (2002) further shows that the reintensification process is highly sensitive to the relative location of the PV features. Rigorous investigation of the sensitivity of the ET/R events of Danielle and Earl to the phasing of the upstream trough features would represent a logical continuation of the current study.

Finally, the need for an observational program focused on the study of ET/R is continually increasing. Sinclair (2002) notes that there has never been a major field campaign devoted to ET. The observations presented by Browning et al. (1998), and data collected by Environment Canada for ex-hurricane Michael in 2000 (Jim Abraham 2000, personal communication) are not adequate given the increasing pace of ET/R research. Validation and diagnostic datasets containing observations of complete TC lifecycles are required in order to verify or reject the conceptual models of ET proposed over the last two decades. A Canadian ET field study involving multiple aircraft and enhanced surface-based observing systems will help to address this issue during the 2003 hurricane season.

# Bibliography

- Abraham, J., G. Parkes, and P. Bowyer, 1999: The transition of the "Saxby Gale" into an extratropical storm. *3rd Conference on Hurricanes and Tropical Meteorology (Volume II)*. American Meteorological Society, 795-798 .
- Alaka, M.A., 1962: On the occurrence of dynamic instability in incipient and developing hurricanes. *Mon. Wea. Rev.*, **90**, 49–58.
- Anthes, R.A., 1972: The development of asymmetries in a three-dimensional numerical model of the tropical cyclone. *Mon. Wea. Rev.*, **100**, 461–476.
- Anthes, R.A., 1990: Advances in the understanding and prediction of cyclone development with limited-area fine-mesh models. Newton, C.W., and E.O. Holopainen, editors, *Extratropical Cyclones, Palmén Memorial Volume*, pages 211–253. American Meteorological Society.
- Benoit, R, J. Cote, and J. Mailhot, 1989: Inclusion of a TKE boundary layer parameterization in the Canadian regional finite-element model. *Mon. Wea. Rev.*, **117**, 1726–1750.
- Benoit, R., M. Desgagné, P. Pellerin, S. Pellerin, S. Desjardins, and Y. Chartier, 1997: The Canadian MC2: a semi-Lagrangian, semi-implicit wide-band atmospheric model suited for fine-scale process studies and simulation. *Mon. Wea. Rev.*, **125**, 2382–2415.
- Bjerknes, J., and H. Solberg, 1922: Life cycle of cyclones and the polar front theory of atmospheric circulation. *Geofys. Publ.*, **3**, 1–18.

- Black, P.G., and R.A. Anthes, 1971: On the asymmetric structure of the tropical cyclone outflow layer. *J. Atmos. Sci.*, **28**, 1348–1366.
- Bosart, J.L., 1981: The President's Day snowstorm of 18-19 February 1979: A subsynoptic-scale event. *Mon. Wea. Rev.*, **109**, 1542–1566.
- Bosart, L.F., and J.A. Bartlo, 1991: Tropical storm formation in a baroclinic environment. *Mon. Wea. Rev.*, **119**, 1979–2013.
- Bosart, L.F., and G.M. Lackmann, 1995: Postlandfall tropical cyclone reintensification in a weakly baroclinic environment: A case study of Hurricane David (September 1979). *Mon. Wea. Rev.*, **123**, 3268–3291.
- Browning, K., G. Vaughan, and P. Panagi, 1998: Analysis of an ex-tropical cyclone after its reintensification as a warm-core extratropical cyclone. *Quart. J. Roy. Meteor. Soc.*, **124**, 2329–2356.
- Browning, K.A., S.P. Ballard, and C.S.A Davitt, 1997: High-resolution analysis of frontal fracture. *Mon. Wea. Rev.*, **125**, 1212–1230.
- Carr, F., and L.F. Bosart, 1978: A diagnostic evaluation of rainfall predictability for Tropical Storm Agnes, June 1972. *Mon. Wea. Rev.*, **106**, 363–374.
- Carrera, M.L., J.R. Gyakum, and D.L. Zhang, 1999: A numerical case study of secondary marine cyclogenesis sensitivity to initial error and varying physical processes. *Mon. Wea. Rev.*, **127**, 641–660.
- Charney, J., 1955: The use of the primitive equations of motion in numerical prediction. *Tellus*, **VII**, 22–26.
- Charney, J.G., 1947: The dynamics of long waves in a baroclinic westerly current. *J. Meteor.*, **4**, 135–162.

- Chien, H.H., and P.J. Smith, 1977: Synoptic and kinetic energy analysis of Hurricane Camille (1969) during transit across the southeastern United States. *J. Geophys. Res.*, **105**, 67–77.
- Chouinard, C., J. Maillhot, H. L. Mitchell, A. Staniforth, and R. Hogue, 1994: The Canadian regional data assimilation system: operational and research applications. *Mon. Wea. Rev.*, **122**, 1306–1325.
- Davis, C., 1992a: A potential-vorticity diagnosis of the importance of initial structure and condensational heating in observed extratropical cyclogenesis. *Mon. Wea. Rev.*, **120**, 2409–2428.
- Davis, C., 1992b: Piecewise potential vorticity inversion. *J. Atmos. Sci.*, **49**, 1397–1411.
- Davis, C., and K. Emanuel, 1991: Potential vorticity diagnosis of cyclogenesis. *Mon. Wea. Rev.*, **119**, 1929–1953.
- Davis, C., E. Grell, and M. Shapiro, 1996: The balanced dynamical nature of a rapidly intensifying oceanic cyclone. *Mon. Wea. Rev.*, **124**, 3–26.
- DiMego, G.J., and L.F. Bosart, 1982a: The transformation of Tropical Storm Agnes into an extratropical cyclone. Part I: the observed fields and vertical motion computations. *Mon. Wea. Rev.*, **110**, 385–411.
- DiMego, G.J., and L.F. Bosart, 1982b: The transformation of Tropical Storm Agnes into an extratropical cyclone. Part I: The observed fields and vertical motion computations. *Mon. Wea. Rev.*, **110**, 385–411.
- DiMego, G.J., and L.F. Bosart, 1982c: The transformation of Tropical Storm Agnes into an extratropical cyclone. Part II: moisture, vorticity, and kinetic energy budgets. *Mon. Wea. Rev.*, **110**, 412–433.
- Eady, E., 1949: Long waves and cyclone waves. *Tellus*, **1**, 33–52.

- Emanuel, K.A., 1988: The maximum intensity of hurricanes. *J. Atmos. Sci.*, **45**, 1143–1155.
- Ertel, H., 1942: Ein Neuer hydrodynamischer Wirbelsatz. *Met. Z.*, **59**, 271–281.
- Evans, J.L., and R.E. Hart, 2003: Objective indicators of the life cycle evolution of extratropical transition for Atlantic tropical cyclones. *Mon. Wea. Rev.*, **131**, 909–925.
- Gal-Chen, T., and R.C. Sommerville, 1975: On the use of a coordinate transformation for the solution of Navier-Stokes. *J. Comput. Phys.*, **17**, 209–228.
- Gyakum, J.R., 1983a: On the Evolution of the *QE II* Storm. I: Synoptic Aspects. *Mon. Wea. Rev.*, **111**, 1137–1155.
- Gyakum, J.R., 1983b: On the Evolution of the *QE II* Storm. II: Dynamic and thermodynamic structure. *Mon. Wea. Rev.*, **111**, 1156–1173.
- Gyakum, J.R., P. Roebber, and T.A. Bullock, 1992: The role of antecedent surface vorticity development as a conditioning process in explosive cyclone intensification. *Mon. Wea. Rev.*, **120**, 1465–1489.
- Harr, P.A., and R.L. Elsberry, 2000a: Extratropical transition of tropical cyclones over the western North Pacific. Part I: Evolution of structural characteristics during the transition process. *Mon. Wea. Rev.*, **128**, 2613–2633.
- Harr, P.A., and R.L. Elsberry, 2000b: Extratropical transition of tropical cyclones over the Western North Pacific. Part I: evolution of structural characteristics during the transition process. *Mon. Wea. Rev.*, **128**, 2613–2633.
- Harr, P.A., and R.L. Elsberry, 2000c: Extratropical transition of tropical cyclones over the Western North Pacific. Part II: the impact of midlatitude circulation characteristics. *Mon. Wea. Rev.*, **128**, 2634–2653.

- Hart, R.E., 2003: A cyclone phase space derived from thermal wind and thermal asymmetry. *Mon. Wea. Rev.*, **131**, 585–616.
- Hart, R.E., and J.L. Evans, 2001: A climatology of the extratropical transition of Atlantic tropical cyclones. *J. Climate*, **14**, 546–564.
- Holland, G.J., 1983: *Tropical cyclones in the Australian/southwest Pacific region*. Colorado State University, Fort Collins, CO, 264 pp.
- Holland, G.J., and R.T. Merrill, 1984: On the dynamics of tropical cyclone structural changes. *Quart. J. Roy. Meteor. Soc.*, **110**, 723–745.
- Hoskins, B., M. M<sup>c</sup>Intyre, and A. Robertson, 1985: On the use and significance of isentropic potential vorticity maps. *Quart. J. Roy. Meteor. Soc.*, **111**, 877–946.
- Hughes, L.A., G.E. Baer, and R.E. Kaylor, 1955: Hurricane Hazel and a long-wave outlook. *Bull. Amer. Meteor. Soc.*, **36**, 528–533.
- Huo, Z., D. Zhang, and J. Gyakum, 1998: An application of potential vorticity inversion to improving the numerical prediction of the March 1993 Superstorm. *Mon. Wea. Rev.*, **126**, 424–436.
- Kain, J.S., and J. M. Fritsch, 1992: The role of the convective ‘trigger’ function in numerical forecasts of mesoscale convective systems. *Meteor. Atmos. Phys.*, **49**, 93–106.
- Kain, J.S., and J.M. Fritsch, 1990: A one-dimensional entraining /detraining plume model and its application in convective parameterization. *J. Atmos. Sci.*, **47**, 2784–2802.
- Keyser, D., M.J. Reeder, and R.J. Reed, 1988: A generalization of Pettersen’s frontogenesis function and its relation to the forcing of vertical motion. *Mon. Wea. Rev.*, **116**, 762–780.

- Keyser, D., and M.A. Shapiro, 1986: A review of the structure and dynamics of upper-level frontal zones. *Mon. Wea. Rev.*, **114**, 452–499.
- Kitade, T., 1980: Numerical experiments of tropical cyclones on a plane with variable Coriolis parameter. *J. Meteor. Soc. Japan*, **58**, 471–488.
- Klein, P., 1997: Extratropical transition of western North Pacific tropical cyclones. Master's thesis, Naval Postgraduate School, 1 University Circle, Monterey, CA, 93943.
- Klein, P.M., P.A. Harr, and R.L. Elsberry, 2000: Extratropical transition of Western North Pacific tropical cyclones: and overview and conceptual model of the transformation stage. *Wea. Forecasting*, **15**, 373–395.
- Klein, P.M., P.A. Harr, and R.L. Elsberry, 2002: Extratropical transition of western North Pacific tropical cyclones: midlatitude and tropical cyclone contributions to reintensification. *Mon. Wea. Rev.*, **130**, 2240–2259.
- Kleinschmidt, 1951: Grundlagen einer Theorie der tropischen Zyklonen. *Arch. Meteor. Geophys. Bioklimatol.*, **A4**, 53–72.
- Knox, J.L., 1955: The storm "Hazel", synoptic resume of its development as it approached southern Ontario. *Bull. Amer. Meteor. Soc.*, **36**, 877–946.
- Kong, F.Y., and M.K. Yau, 1997: An explicit approach to microphysics in MC2. *Atmosphere-Ocean*, **35**, 257–291.
- Kornegay, F.C., and D.G. Vincent, 1976: Kinetic energy budget analysis during interaction of tropical storm Candy (1968) with an extratropical frontal system. *Mon. Wea. Rev.*, **104**, 849–859.
- Krishnamurti, T.N., 1968: A diagnostic balance model for studies of weather systems at low and high latitudes, Rossby number less than 1. *Mon. Wea. Rev.*, **96**, 197–207.

- Kuo, H.L., 1974: Further studies of the parameterization of the influence of cumulus convection on large scale flow. *J. Atmos. Sci.*, **31**, 1232–1240.
- Kurihara, Y., and R.E. Tuleya, 1974: Structure of a tropical cyclone developed in a three-dimensional numerical simulation model. *J. Atmos. Sci.*, **31**, 893–919.
- Ma, S., H. Richie, J.R. Gyakum, J. Abraham, C. Fogarty, and R. McTaggart-Cowan, 2003: A study of the extra-tropical re-intensification of former Hurricane Earl using Canadian Meteorological Centre regional analyses and ensemble forecasts. *Mon. Wea. Rev.*, **131**, in press.
- Mailhot, J., S. Bélair, R. Benoit, B. Bilodeau, Y. Delage, L. Fillion, L. Garand, C. Girard, and A. Tremblay, 1998: Scientific description of RPN physics library - Version 3.6. Technical report, Atmospheric Environment Service, 2121 TransCanada Hwy., Montreal, QC H9P 1J3 Canada.
- Mailhot, J., and R. Benoit, 1982: A finite-element model of the atmospheric boundary layer suitable for use with numerical weather prediction models. *J. Atmos. Sci.*, **39**, 2249–2266.
- Matano, H., and M. Sekioka, 1971: Some aspects of extratropical transformation of a tropical cyclone. *J. Meteor. Soc. Japan*, **49**, 736–743.
- Matano, J., 1958: On the synoptic structure of Hurricane Hazel, 1954, over the eastern United States. *J. Meteor. Soc. Japan*, **36**, 23–31.
- McTaggart-Cowan, R., J.R. Gyakum, and M.K. Yau, 2001: Sensitivity testing of extratropical transitions using potential vorticity inversions to modify initial conditions: Hurricane Earl case study. *Mon. Wea. Rev.*, **129**, 1617–1636.
- McTaggart-Cowan, R., J.R. Gyakum, and M.K. Yau, 2003a: The influence of the downstream state on extratropical transition: Hurricane Earl (1998) case study. *Mon. Wea. Rev.*, **131**, in press.

- McTaggart-Cowan, R., J.R. Gyakum, and M.K. Yau, 2003b: Moist component potential vorticity. *J. Atmos. Sci.*, **60**, 166–177.
- Milbrandt, J., and M.K. Yau, 2001: A mesoscale modeling study of the 1996 Saguenay flood. *Mon. Wea. Rev.*, **129**, 1419–1440.
- Molinari, J., S. Skubis, and D. Vollaro, 1995: External influences on hurricane intensity. Part III: Potential vorticity structure. *J. Atmos. Sci.*, **52**, 3593–3606.
- Montgomery, M.T., H.D. Snell, and Z. Yang, 2001: Axisymmetric spindown dynamics of hurricane-like vortices. *J. Atmos. Sci.*, **58**, 421–435.
- Morgan, M.C., and J.W. Nielsen-Gammon, 1998: Using tropopause maps to diagnose midlatitude weather systems. *Mon. Wea. Rev.*, **126**, 2555–2579.
- Nielsen, John W., and Randall M. Dole, 1992: A survey of extratropical cyclone characteristics. *Mon. Wea. Rev.*, **120**, 1156–1168.
- Palmen, E., 1958: Vertical circulation and release of kinetic energy during the development of hurricane Hazel into an extratropical cyclone. *Tellus*, **10**, 1–23.
- Parkes, G.S., L.A. Ketch, C.T. O'Reilly, J. Shaw, and A. Ruffman, 1999: The Saxby Gale of 1869 in the Canadian maritimes. *3rd conference on Hurricanes and tropical meteorology Volume II*. American Meteorological Society, 791-794 .
- Petterssen, S., and S. Smebye, 1971: On the development of extratropical storms. *Quart. J. Roy. Meteor. Soc.*, **97**, 457–482.
- Pierce, C.H., 1939: The meteorological history of the New England hurricane of Sept. 21, 1938. *Mon. Wea. Rev.*, **67**, 237–285.
- Rappaport, E.N., and J.J. Fernandez-Partagas, 1997: History of the deadliest Atlantic tropical cyclones since the discovery of the New World. Chapter 5. Diaz, H.F., and R.S. Pulwarty, editors, *Hurricanes: Climate change and socioeconomic impacts*, pages 93–108. Springer-Verlag, New York.

- Rappaport, E.N., and A. Ruffman, 1999: The catastrophic 1775 hurricane(s): the search for data and understanding. *3rd conference on Hurricanes and tropical meteorology Volume II*. American Meteorological Society, 787-790 .
- Riehl, H., 1950: A model for hurricane formation. *J. Atmos. Phy.*, **13**, 949–965.
- Ritchie, E.A., and R.L. Elsberry, 2001: Simulations of the transformation stage of extratropical transition of tropical cyclones. *Mon. Wea. Rev.*, **129**, 1462–1480.
- Robert, A., T. Yee, and H. Ritchie, 1985: A semi-Lagrangian and semi-implicit numerical integration scheme for multilevel atmospheric models. *Mon. Wea. Rev.*, **113**, 388–394.
- Rossby, C.G., 1939: Relation between variations in the intensity of the zonal circulation of the atmosphere and the displacements of the semi-permanent centers of action. *J. Mar. Res.*, **2**, 38–55.
- Ruffman, A., 1999: A multi-disciplinary and inter-scientific study of the Saxby Gale: an October 4-5 1869 hybrid hurricane and record storm surge. *CMOS Bulletin*, **27(3)**, 67–75.
- Schär, C., D. Leuenberger, O. Fuhrer, D. Lüthi, and C. Girard, 2002: A new terrain-following vertical coordinate formulation for atmospheric prediction models. *Mon. Wea. Rev.*, **130**, 2459–2480.
- Schubert, W.H., S.A. Hausman, M. Garcia, K.V. Ooyama, and H. Kuo, 2001: Potential vorticity in a moist atmosphere. *J. Atmos. Sci.*, **58**, 3148–3157.
- Shapiro, M.A., and D. Keyser, 1990: Fronts, jet streams and the tropopause. Newton, C.W., and E.O. Holopainen, editors, *Extratropical Cyclones*, pages 167–191. American Meteorological Society, Boston, Mass.
- Simpson, R.H., 1974: The hurricane disaster potential scale. *Weatherwise*, **27**, 169–186.

- Sinclair, M., 1993a: A diagnostic study of the extratropical precipitation resulting from tropical cyclone Bola. *Mon. Wea. Rev.*, **121**, 2690–2707.
- Sinclair, M., 1993b: Synoptic-Scale Diagnosis of the Extratropical Transition of a Southwest Pacific Tropical Cyclone. *Mon. Wea. Rev.*, **121**, 941–960.
- Sinclair, M., 2002: Extratropical transition of Southwest Pacific tropical cyclones. Part I: climatology and mean structure changes. *Mon. Wea. Rev.*, **130**, 590–609.
- Sinclair, M., and M. Revell, 2000: Classification and composite diagnosis of extratropical cyclogenesis events in the Southwest Pacific. *Mon. Wea. Rev.*, **128**, 1089–1105.
- Tanguay, M., A. Robert, and R. Laprise, 1990: A semi-implicit semi-Lagrangian fully compressible regional forecast model. *Mon. Wea. Rev.*, **118**, 1970–1980.
- Tannehill, I.R., 1938: Hurricane of September 16-22, 1938. *Mon. Wea. Rev.*, **66**, 286–288.
- Thomas, S.J., C. Girard, R. Benoit, Desgagné M., P. Pellerin, and A.V. Malevsky, 1999: A new dynamics kernel for the MC2 model. *Atmosphere-Ocean*, **36**, 241–270.
- Thomson, W., 1852: On the dynamical theory of heat, with numerical results deduced from Mr. Joule's equivalent of a thermal unit, and Mr. Regnault's observations on steam. *Philosophical Magazine*, **4**, 1–14.
- Thorncroft, C.D., B.J. Hoskins, and M.E. McIntyre, 1993: Two paradigms of baroclinic-wave life-cycle behaviour. *Quart. J. Roy. Meteor. Soc.*, **119**, 17–55.
- Thorncroft, C.D., and S.C. Jones, 2000: The extratropical transitions of hurricanes Felix and Iris in 1995. *Mon. Wea. Rev.*, **128**, 947–971.